

Greening, Browning or Drowning?

Permafrost – Vegetation – Climate Interactions
in the Siberian Lowland Tundra



Rúna Í. Magnússon

Propositions

1. Spectral greening and browning trends of tundra ecosystems are determined more by the temporal and spatial scale of observation than by environmental processes (this thesis)
2. The current suite of global climate models used by the IPCC is not suitable for quantification of permafrost carbon emissions (this thesis)
3. Suspension of institutional scientific collaboration with Russia impedes the quantification of realistic carbon emission budgets
4. Experiences are a more effective tool than facts to communicate the urgency of climate change to the general public
5. If we would abolish industrial livestock farming today, then practically nobody would miss it in a few decades
6. The covid pandemic is a missed opportunity to implement a universal basic income

Propositions belonging to the thesis, entitled:

Greening, Browning or Drowning? Permafrost – Vegetation – Climate Interactions in the Siberian Lowland Tundra

Rúna Íris Magnússon
Wageningen, 28 September 2022 (defense date)

Greening, Browning or Drowning?

**Permafrost – Vegetation – Climate Interactions in the Siberian Lowland
Tundra**

Rúna Íris Magnússon

Thesis committee

Promotor

Prof. Dr D. Kleijn
Professor of Plant Ecology and Nature Conservation
Wageningen University & Research

Co-promotors

Dr M. M. P. D. Heijmans
Assistant professor, Plant Ecology and Nature Conservation Group
Wageningen University & Research

Dr J. Limpens
Associate professor, Plant Ecology and Nature Conservation Group
Wageningen University & Research

Other members

Prof. Dr W. Peters, Wageningen University & Research

Dr I. H. Myers-Smith, University of Edinburgh, Scotland

Dr J. E. Vonk, Vrije Universiteit Amsterdam

Prof. Dr J. H. C. Cornelissen, Vrije Universiteit Amsterdam

This research was conducted under the auspices of the Graduate School for Socio-Economic and Natural Sciences of the Environment (SENSE)

Greening, Browning or Drowning?

Permafrost – Vegetation – Climate Interactions in the Siberian Lowland
Tundra

Rúna Íris Magnússon

Thesis

submitted in fulfilment of the requirements for the degree of doctor
at Wageningen University
by the authority of the Rector Magnificus,
Prof. Dr A.P.J. Mol,
in the presence of the
Thesis Committee appointed by the Academic Board
to be defended in public
on 28 September 2022
at 4 p.m. in the Omnia Auditorium

Rúna Íris Magnússon

Greening, Browning, or Drowning? Permafrost – Vegetation – Climate interactions in the Siberian Lowland Tundra

220 pages.

PhD thesis, Wageningen University, Wageningen, the Netherlands (2022)

With references, with summary in English & Dutch

ISBN: 978-94-6447-358-2

DOI: <https://doi.org/10.18174/575129>

Table of Contents

1.	General Introduction	p. 6
2.	Chapter 2 – Rapid vegetation succession and coupled permafrost dynamics in Arctic thaw ponds in the Siberian lowland tundra	p. 24
3.	Chapter 3 – Shrub decline and expansion of wetland vegetation revealed by very high resolution land cover change detection in the Siberian lowland tundra	p. 46
4.	Chapter 4 – Extremely wet summer events enhance permafrost thaw for multiple years in Siberian tundra	p. 68
5.	Chapter 5 – Precipitation variability differentially affects growth and temperature response of <i>Betula nana</i> across topographical gradients in a Siberian lowland tundra site	p. 84
6.	Chapter 6 – Tundra browning in the Indigirka Lowlands (North-eastern Siberia) explained by drought, floods and small-scale vegetation shifts	p. 108
7.	General Discussion	p. 130
8.	Supplementary Materials	p. 146
9.	References	p. 174
10.	Summaries & End Matter	p. 201
	Summary (English)	p. 202
	Samenvatting (Dutch)	p. 206
	Affiliations of Co-authors	p. 210
	About the Author	p. 112
	Acknowledgements	p. 214
	List of Artwork	p. 217
	Graduate School Diploma	p. 218
	Funding	p. 220

‘[...] the claim of the Arctic on our imagination has been inverted. A landscape that once symbolized the sublime indifference of nature will, for future generations, come to symbolize its tragic vulnerability.’

Elizabeth Kolbert - The Arctic: An Anthology.

1.

General Introduction



1.1 Environmental change in a warming Arctic: a problem of global concern

Arctic environments have traditionally occupied our imagination as the harshest and most untouchable regions on earth. In recent decades this perspective is shifting as Arctic environments show drastic changes in a warming climate, the impacts of which may be felt far beyond the Arctic itself. The Arctic is now warming three times faster than the global average (AMAP 2021). As a result, Arctic ecosystems are showing fundamental changes in hydrology, snow and ice dynamics and vegetation (Notz and Stroeve 2016, Box et al. 2019, Richter-Menge et al. 2020, AMAP 2021). Apart from gradual temperature increases, the occurrence of extreme conditions is increasing, including heavy precipitation, drought spells and heat waves (AMAP 2021, IPCC 2021). These changes have far-reaching consequences for ecosystems, infrastructure and the livelihoods and safety of Arctic communities (Crate et al. 2017, Box et al. 2019, Ksenofontov et al. 2019, Meredith et al. 2019, Hjort et al. 2022). Arctic warming affects global climate through several feedback mechanisms, such as the loss of reflective sea ice (Screen and Simmonds 2010), the release of greenhouse gases from thawing soils and wildfires (Schuur et al. 2015, Natali et al. 2021, Miner et al. 2022) and shifts in vegetation composition and carbon cycling (Pearson et al. 2013, Box et al. 2019). Two of the main manifestations of climate warming in the terrestrial Arctic are widespread thawing and degradation of frozen ground (permafrost) (Biskaborn et al. 2019, Meredith et al. 2019), associated with release of greenhouse gases (Schuur et al. 2015, Turetsky et al. 2019, Miner et al. 2022), and increased productivity and biomass of Arctic tundra ecosystems in warmer and longer growing seasons (Elmendorf et al. 2012a, Bjorkman et al. 2018, Myers-Smith et al. 2020, Frost et al. 2021b). The latter mainly manifests as expansion of shrub vegetation (Elmendorf et al. 2012a, Bjorkman et al. 2018) and may result in carbon uptake in biomass and soils (Chapin et al. 2005, McGuire et al. 2018). The balance between permafrost degradation, associated with landscape changes and carbon losses, and increased tundra productivity, associated with carbon uptake, is a core knowledge gap in Arctic climate change studies (McGuire et al. 2018, Box et al. 2019, Meredith et al. 2019, Turetsky et al. 2020).

The consequences of carbon losses resulting from permafrost degradation are not limited to the Arctic itself. Permafrost is ground that remains frozen for at least 2 consecutive years, of which only the topmost layers thaw in summer (Shur et al. 2011). Apart from mineral soil and ice, permafrost may contain varying amounts of carbon. The upper three meters of all Arctic and boreal permafrost combined is estimated to contain 1400-1700 Gt of soil organic carbon (SOC) in total (Meredith et al. 2019, Miner et al. 2022). This is approximately double the amount of carbon currently in the atmosphere and comprises approximately half of the total terrestrial SOC store (Tarnocai et al. 2009, Hugelius et al. 2014, Schuur et al. 2015, Meredith et al. 2019). Thawing of permafrost enhances decomposition of previously frozen SOC into greenhouse gases (GHGs) (Schuur et al. 2008, Koven et al. 2011, Schuur et al. 2015, Voigt et al. 2017). The potential decomposition of such a large carbon pool may result in significant additional climate warming (Schuur et al. 2015, Comyn-Platt et al. 2018, Natali et al. 2021, Miner et al. 2022). Estimated additional greenhouse gas emissions resulting from permafrost degradation range from tens to hundreds GtC by 2100 under a high emission scenario (Meredith et al. 2019). Other studies have found estimates of roughly 10% increase in global GHG emissions or 0.13 to 0.27°C additional global warming by the end of this century (Schuur et al. 2015, Comyn-Platt et al. 2018). While there is high confidence that this “permafrost carbon feedback” (PCF) will lead to carbon emissions high enough to require consideration in remaining carbon budgets, the exact magnitude and timing of permafrost carbon emissions are currently poorly quantified (IPCC 2021, Natali et al. 2021, Miner et al. 2022).

Beside uncertainties in the degree of carbon emissions from permafrost itself, there is considerable uncertainty regarding future carbon uptake of Arctic vegetation under changing climatic conditions (Abbott et al. 2016, McGuire et al. 2018, Meredith et al. 2019). Recent model-based evidence and

expert assessments suggest that increased carbon uptake by Arctic vegetation under climate warming is unlikely to compensate for all permafrost carbon emissions, especially under high emissions scenarios (Schuur et al. 2015, Abbott et al. 2016, Turetsky et al. 2020, Natali et al. 2021). However, the model estimates of the extent to which the carbon sink function of Arctic vegetation is modelled to partially mitigate the carbon source dynamics of permafrost thaw vary substantially (McGuire et al. 2018, Meredith et al. 2019). This balance depends strongly on emission scenarios, models' process-detail in the numerical representation of permafrost thaw and vegetation, the level of landscape spatial variability and timescales considered (McGuire et al. 2018, Meredith et al. 2019, Nitzbon et al. 2020, Turetsky et al. 2020). Additional uncertainty arises from incomplete understanding of future changes in biogeophysical processes such as drought and wildfire dynamics, aquatic carbon transport and wetland dynamics under changing temperature and precipitation (Abbott et al. 2016, Vonk et al. 2019, Natali et al. 2021, Miner et al. 2022). Spatially distributed long-term observational records are needed to inform earth surface models with respect to the dynamics of permafrost degradation and vegetation change, interactions between the two, and the spatial and temporal scales on which they occur (Turetsky et al. 2019, Heijmans et al. 2022). However, holistic and long-term records of coupled permafrost degradation, vegetation changes and carbon cycling are scarce across the Arctic, which makes assessment of the future carbon balance of permafrost ecosystems a complex challenge (Box et al. 2019, Turetsky et al. 2019). Within this context, this thesis contributes to the mechanistic understanding of coupled permafrost and vegetation dynamics in Arctic ecosystems and their temporal and spatial scales through integrated, field-based assessment of permafrost development, climate drivers, vegetation and hydrology in the understudied Siberian lowland tundra.

1.2 Changes in the Arctic climate

1.2.1 Temperature trends

The Arctic is warming at an increasing rate. Researchers shifted from reporting a trend that is “twice as fast as the global average” to “more than twice as fast” and recently to “three times as fast” as the global average (Stocker et al. 2013, AMAP 2017, 2021, IPCC 2021). Over 1971 to 2019, annual average temperatures in the Arctic increased by 3.1°C on average, with a range from approximately 0 to 8°C (AMAP 2021). Warm spells are occurring more frequently throughout the Arctic, while the number of cold spells shows a decline (AMAP 2021). Recent heat waves in Siberia with temperature anomalies of up to 6°C and subsequent permafrost degradation, wildfire and pest outbreaks have made international headlines (Overland and Wang 2021). Increasing Arctic air temperatures (fig. 1.1a-c) drive feedback processes such as the loss of Arctic sea ice, thawing of permafrost, melting of glaciers and reductions in spring snow cover. Such changes promote further warming of Arctic surface temperatures (Box et al. 2019, Meredith et al. 2019, Richter-Menge et al. 2020), and make the Arctic less resilient to future climate warming and more prone to climatic extremes (Overland 2020).

1.2.2 Precipitation trends

Due to intensification of the hydrological cycle in a warming Arctic, Arctic precipitation has increased by 9% over the period 1971-2019 (AMAP 2021). An increase of 27% to 50% in total annual Arctic precipitation is expected by 2100 depending on emission scenarios (see also fig. 1.1d-f), of which most increases will occur in autumn and winter (Bintanja and Andry 2017). Due to the combined effect of temperature and precipitation increases, the percentage of Arctic precipitation that falls as rain rather than snow may increase from 35% to 60% of total precipitation by 2100 (Bintanja and Andry 2017). The extent of spring (May-June) snow cover has decreased by 27% over 1971-2020 (AMAP 2021), with large potential impacts on ecosystem energy balances, carbon balance and phenology of tundra species (Box et al. 2019). On a panarctic scale, a general reduction in snow cover duration is observed, but trends in snow depth are regionally diverse (AMAP 2017). These large changes to precipitation regimes are likely to affect both permafrost and vegetation dynamics (Callaghan et al. 2011). There is currently

less quantitative data on the occurrence of precipitation extremes and floods (Walsh et al. 2020, AMAP 2021), as precipitation dynamics are highly local and rain gauge undercatch is a common problem in cold and windy environments (Yang et al. 2005). Similarly, the effects of precipitation extremes and their timing and duration on Arctic ecosystems is poorly understood. Extreme rainfall may become increasingly common, since the annual variability of Arctic precipitation is observed and expected to increase (Fischer and Knutti 2015, IPCC 2021), and particularly in summer (Bintanja et al. 2020). However, observational data of the effects of single, extreme precipitation events are rare and a better understanding is urgently needed, especially since their impact may be felt for multiple years or trigger irreversible changes (Iijima et al. 2010, Christensen et al. 2020, Douglas et al. 2020).

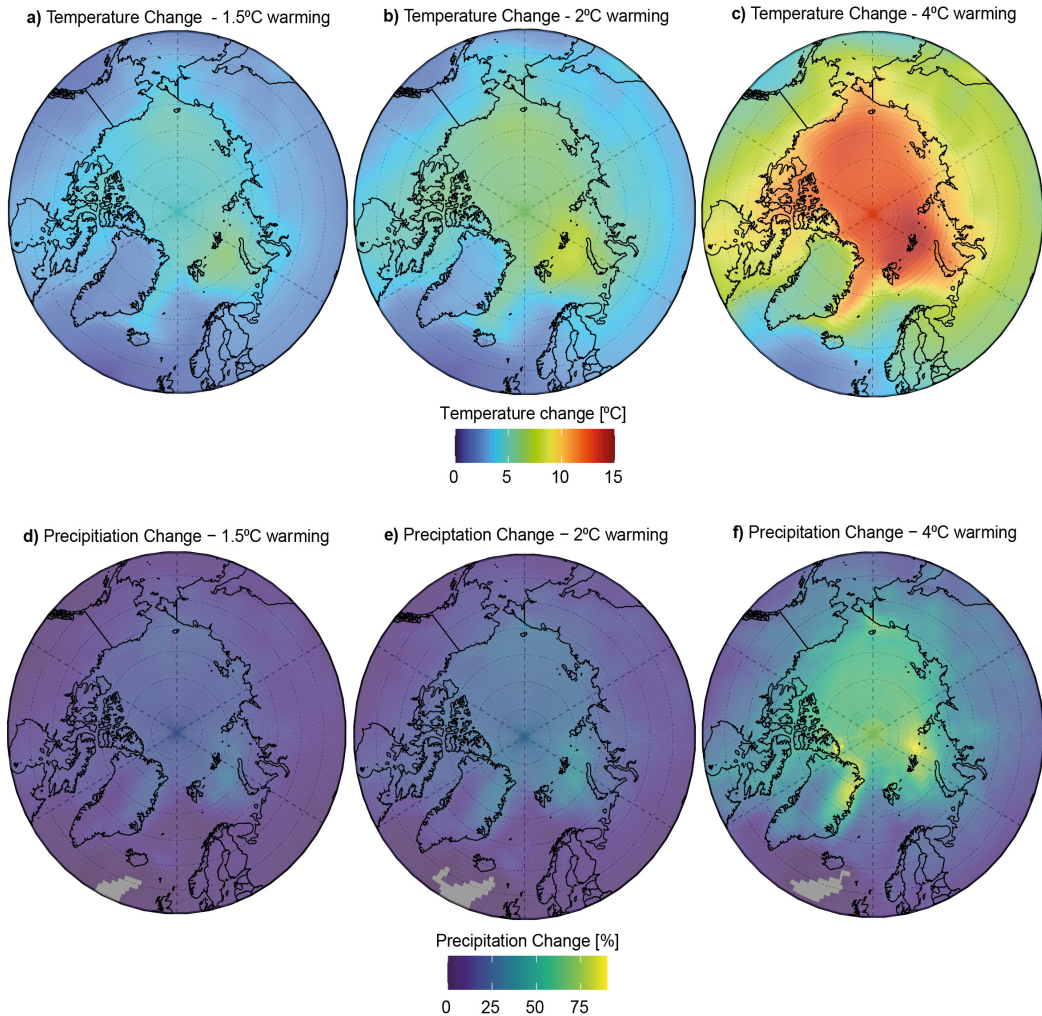


Figure 1.1) Projected temperature and precipitation increases across the Arctic, as reported in the IPCC's sixth assessment report (IPCC 2021). Top row shows local projected temperature increase under a 1.5°C (a), 2°C (b) and 4°C (c) global warming scenario. Bottom row shows local projected precipitation increase under a 1.5°C (d), 2°C (e) and 4°C (f) global warming scenario. Trends are derived from earth surface models of the 6th Coupled Model Intercomparison Project (CMIP6) under the SSP5 scenario and are reported as changes relative to 1850-1900 baseline conditions. Gray colours indicate areas with uncertain trends. Data retrieved from the IPCC Interactive Atlas (<https://interactive-atlas.ipcc.ch/>, 24-02-2022).

1.3 Pan-arctic trend of permafrost degradation

1.3.1 Permafrost and its characteristics

Degradation of permafrost is one of many manifestations of climate change in the Arctic (Box et al. 2019). Permafrost is defined as ground that stays below 0°C for at least 2 consecutive years (Shur et al. 2011). Permafrost may be found under 19-24% of the global land surface (Brown et al. 1997, Shur et al. 2011, van Huissteden 2020) and varies in thickness from several meters to a maximum of about 1500m (Yershov 2004). Typically, permafrost terrain is classified into continuous (> 90% areal coverage), discontinuous (50-90%), sporadic (10-50%) or isolated (0-10%) permafrost based on areal extent of permafrost within a region (fig. 1.2a) (Brown et al. 1997). The “active layer” is the upper ground layer in permafrost soils that thaws seasonally (Shur et al. 2011, van Huissteden 2020). Permafrost temperatures and the depth of seasonal thaw (“active layer thickness”) are recognized as “essential climate variables” of the Global Climate Observing System (GCOS n.d.). As permafrost soils thaw and warm up, an increasing share of organic matter in permafrost soils is subjected to decomposition into greenhouse gases, mainly CO₂ and CH₄ (Schuur et al. 2008, Koven et al. 2011, Schuur et al. 2015, Voigt et al. 2017, Miner et al. 2022).

1.3.2 The importance of ground ice in permafrost thaw dynamics

The dynamics of permafrost thaw are strongly determined by ground ice volume (fig. 1.2b), which affects its sensitivity and response to thaw. A permafrost soil is considered “ice-rich” if it contains excess ground ice, indicating that the total volume of water resulting from the melting of ground ice exceeds the available pore space of the soil in an unfrozen state (van Everdingen 2005). Loss of ground ice volume causes soil subsidence (Kokelj and Jorgenson 2013, van Huissteden 2020). Since ground ice volumes can vary on small spatial scales, differential subsidence and subsequent local feedbacks can cause a distinct land surface with local depressions called “thermokarst” (Kokelj and Jorgenson 2013). Opposed to gradual deepening of the active layer, thawing of ice-rich permafrost can occur on very short timescales (days to decades) and affect meters of permafrost on short timescales (Grosse et al. 2011, Kokelj and Jorgenson 2013). Through the combined effect of subsidence and deepening of the active layer, the net amount of previously frozen soil that thaws and becomes subject to biogeochemical processes is substantially higher than in case of active layer deepening alone (Rodenhizer et al. 2020). This so-called “abrupt thaw” trajectory generally causes dramatic changes in soil properties, local hydrology and vegetation composition (Schuur and Mack 2018). Climatic extremes and wildfires may additionally trigger abrupt thaw to occur over large areas and result in large carbon emissions (Natali et al. 2021). Earth surface models only consider the impact of gradual deepening of the active layer (“gradual thaw”) on carbon cycling (Turetsky et al. 2019, Natali et al. 2021) as they generally lack the spatial resolution and vertical detail in soil depth to represent abrupt thaw processes (Turetsky et al. 2019, Burke et al. 2020). However, it is exactly through the combination of abrupt thaw events and local feedbacks that Arctic landscapes and their carbon sink/source behaviour can change most dramatically (Jorgenson et al. 2015, Nauta et al. 2015, Natali et al. 2021). As such, model projections of permafrost-associated greenhouse gas emissions based only on gradual thaw processes are expected to underestimate future permafrost carbon emission (Turetsky et al. 2020, IPCC 2021, Natali et al. 2021).

1.3.3 Trends in permafrost degradation

Recent global and circumpolar climate models all predict continued warming of Arctic soils and deepening of active layers. The magnitude of thaw and resulting decrease in areal extent of near-surface permafrost in response to climate warming varies substantially among models (Koven et al. 2013, Slater and Lawrence 2013, Chadburn et al. 2017, McGuire et al. 2018, Meredith et al. 2019). Near-complete disappearance of permafrost may occur by 2300 under high emission scenarios, whereas losses in the area of permafrost in the range of 30 – 40% would occur under stabilization of global warming below 2 degrees Celsius (fig. 1.2c-e) (Chadburn et al. 2017, McGuire et al. 2018). Much of

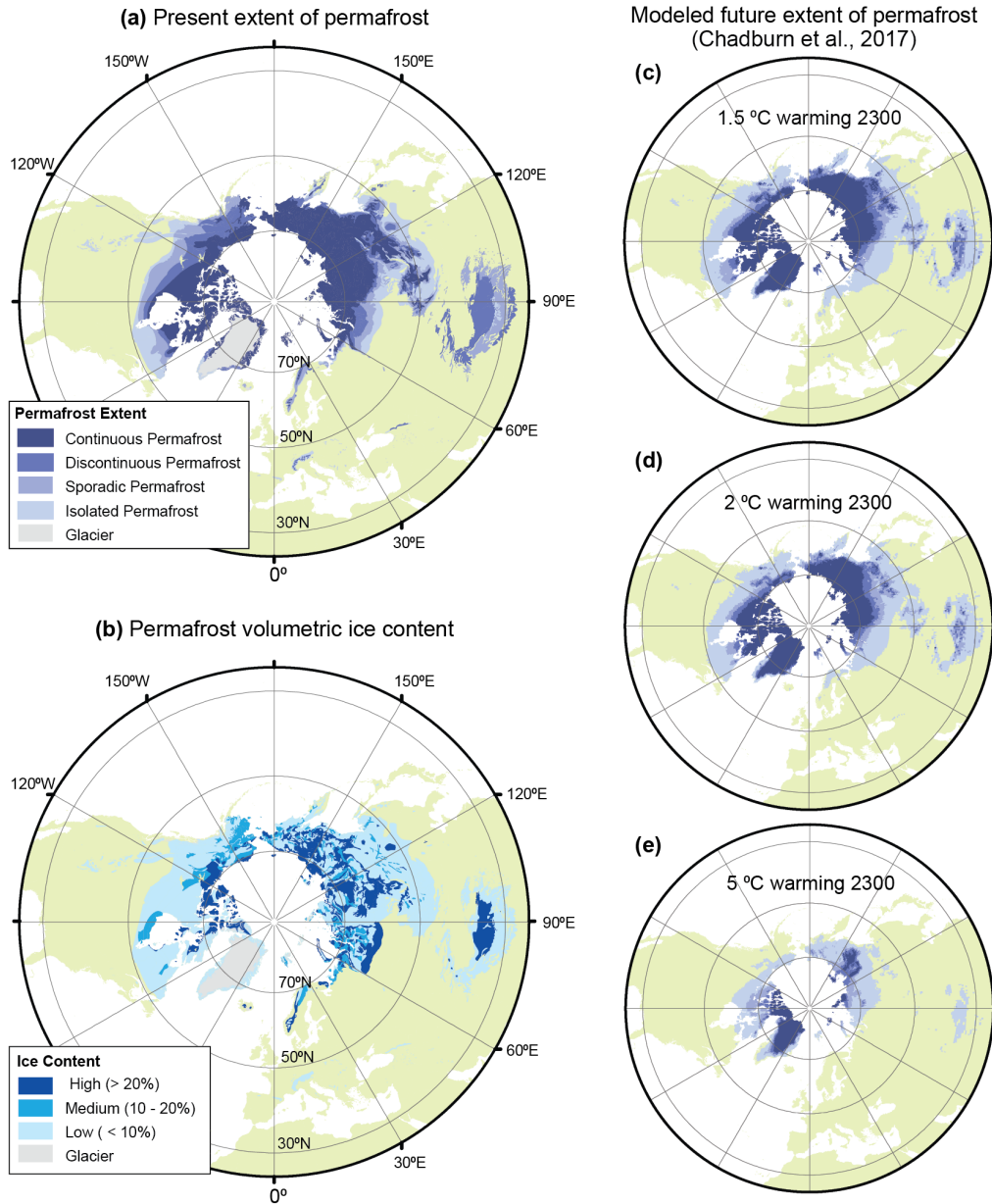


Figure 1.2) a) Current distribution of continuous, discontinuous, sporadic and isolated permafrost (Brown et al. 1997). b) Volumetric content of visible ground ice in the upper 10-20m of permafrost (Brown et al. 1997). (c-e) Modelled future extent of permafrost based on air temperature projections (Chadburn et al. 2017), using the permafrost classes from Brown et al. (1997) (glaciers not depicted). c) Modelled extent of permafrost in 2300 under stabilization at 1.5°C climate warming. d) Modelled extent of permafrost in 2300 under stabilization at 2°C climate warming. e) Modelled extent of permafrost in 2300 under stabilization at 5°C climate warming.

these losses are anticipated to already occur by 2100 (McGuire et al. 2018, Meredith et al. 2019). These model projections are generally corroborated by ground observations, which show ubiquitous warming and thawing of permafrost soils at regionally variable rates (AMAP 2017, Biskaborn et al. 2019, Miner et al. 2022, Smith et al. 2022).

For abrupt thaw processes, circumpolar trends have only recently been quantified for the first time and were estimated to affect 8.8% of the total permafrost region (1.6 million km²) by 2100 and 13.9% (2.5 million km²) by 2300, relative to a baseline area 5% (0.9 million km²) in 1900 (Turetsky et al. 2020). Under a pessimistic global warming scenario this may add 80 Pg of carbon emissions (or 40%) relative to recent multi-model mean estimated emissions of 208 Pg C based on gradual thaw alone by 2300 (McGuire et al. 2018, Turetsky et al. 2020). Recent field and remote sensing studies confirm widespread increase in the number of small thermokarst features such as ponds, pits and troughs across Arctic ecosystems (Jorgenson et al. 2006, Reynolds et al. 2014, Liljedahl et al. 2016). Because abrupt thaw processes are very likely to occur more frequently in a warmer future Arctic (Natali et al. 2021, Miner et al. 2022) and have a more dramatic effect both on carbon emissions and on landscapes, infrastructures and livelihoods than gradual thaw (Turetsky et al. 2019), there is an urgent need for incorporation of these processes into global climate projections, climate policy and emissions budgets (Natali et al. 2021). This in turn strongly depends on the availability of field records to inform numerical representation of the triggers and evolution of abrupt thaw features (Turetsky et al. 2019, Turetsky et al. 2020, Natali et al. 2021).

1.4 Changes in Arctic Vegetation

1.4.1 Arctic Vegetation from tall shrub to polar desert

Arctic vegetation covers approximately 5 million km² (or 3.4% of the earth's land surface, excluding glaciers) (Walker et al. 2005). Vegetation in the Arctic is adjusted to a cold climate with short growing seasons through numerous adaptations in growth form, reproduction, phenology and chemistry (Billings and Mooney 1968). Arctic vegetation communities show strong latitudinal contrasts. In the northernmost Arctic regions, summer temperatures below zero and permanent ice cover limit plant growth, whereas towards the treeline Arctic tundra ecosystems transition to boreal forest biomes (fig. 1.3b) (CAVMTeam 2003, Walker et al. 2005). Along this north to south gradient with increasing summer temperature, ecosystem composition changes from sparse cover of mosses, lichens and decumbent dwarf shrubs ("polar desert") to progressively higher cover and taller canopies of graminoids, wetlands and shrubs (fig. 1.3b) (CAVMTeam 2003, Walker et al. 2005). On a local scale however, vegetation composition is mostly determined by microgradients in topography and wetness (Peterson and Billings 1980). With ongoing changes in the Arctic climate, these vegetation zones are expected to become subject to range shifts (Pearson et al. 2013). Due to limited potential for range expansion beyond the Arctic coast, the northernmost Arctic vegetation types are expected to decline while trees and taller shrubs continue to expand northwards (Pearson et al. 2013, Meredith et al. 2019). Such large-scale vegetation shifts may have far-reaching consequences for permafrost dynamics and climate feedback (Pearson et al. 2013, Heijmans et al. 2022). Currently however, most Arctic vegetation change is expressed on small spatial scales and often related to thermokarst and local successional development, which complicates pan-Arctic assessment of range shifts in Arctic communities over larger scales under continuing future warming (Reynolds et al. 2019).

1.4.2 Arctic greening - on the ground and from the air

In response to climate warming and longer growing seasons, a significant proportion of the Arctic has shown increases in photosynthetically active biomass in recent decades (Tape et al. 2006, Elmendorf et al. 2012a, Myers-Smith et al. 2015a, Bhatt et al. 2017, Frost et al. 2021b), generally referred to as "Arctic greening". Greening may be observed on the ground as increases in the biomass, extent or

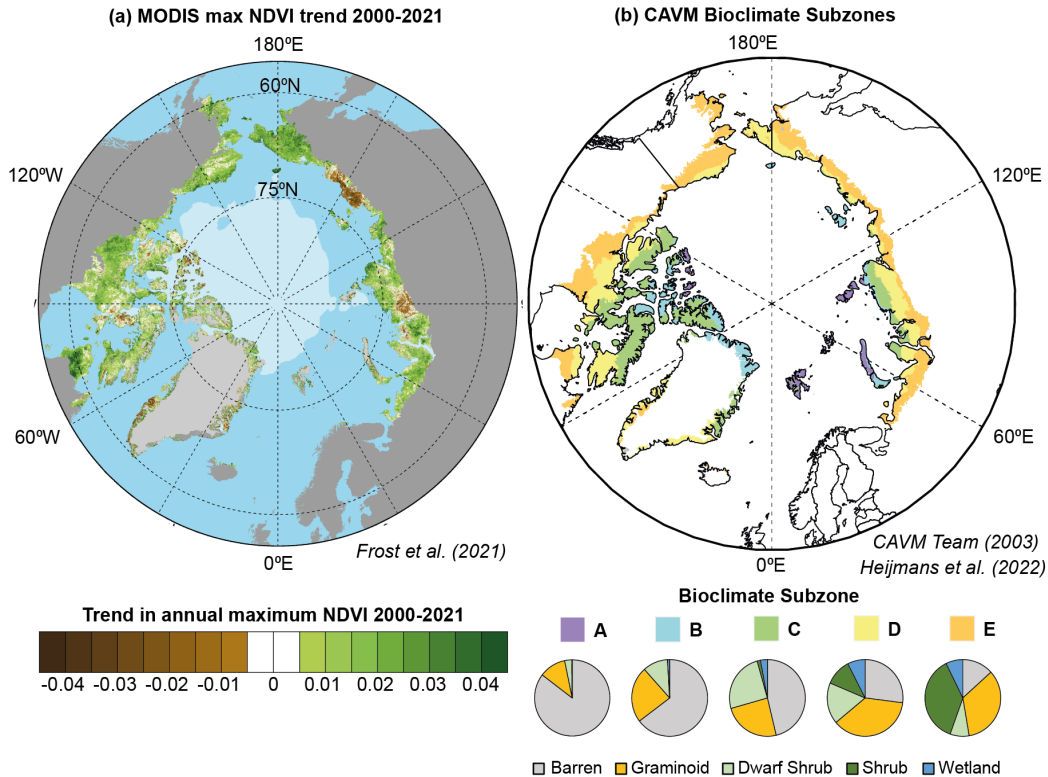


Figure 1.3) Main Arctic biomes and greening trends. a) Trend in annual maximum NDVI derived from the MODIS MCD43A4 product. Source: Frost et al. (2021b). b) Main Arctic vegetation subzones, as defined in the Bioclimate Subzones of the Circumpolar Arctic Vegetation Map (CAVM). Map is based on the 2003 shapefile version of the CAVM (CAVM Team, 2003). Pie charts of vegetation composition from Heijmans et al. (2022). Subzones A-E may be roughly described as “High Arctic” / “Polar Desert” (A) - “Northern Arctic Tundra” (B) - “Middle Arctic Tundra” (C) - “Southern Arctic Tundra” (D) - “Subarctic tundra” / “Shrub tundra” / “Low Arctic” (E). These zones are roughly equivalent with temperature ranges of 0-3°C (A), 3-5°C (B), 5-7°C (C), 7-9°C (D) and 9-12°C (E) (CAVMTeam 2003, Heijmans et al. 2022).

morphology of Arctic vegetation (Hudson and Henry 2009, Elmendorf et al. 2012a, Elmendorf et al. 2012b, Bjorkman et al. 2018, Bjorkman et al. 2020, Ercan et al. 2021). Warming experiments have generally resulted in increases in the abundance of shrubs and graminoids and decreases of lichens and bryophytes (Walker et al. 2006, Elmendorf et al. 2012b, Bjorkman et al. 2020). In addition, greening can be observed from satellite image timeseries using spectral vegetation indices (Berner et al. 2020, Frost et al. 2021b) such as the Normalized Difference Vegetation Index (NDVI) (Tucker 1979). These different types of greening are also referred to as “ecological greening” and “spectral greening” (Myers-Smith et al. 2020). Field studies monitoring greening under ambient climatic change generally find that the most common trend in Arctic vegetation composition is one of “no change” (Bjorkman et al. 2020, Callaghan et al. 2021). However, in sites where vegetation composition does change, it often manifests as an expansion of biomass or abundance of shrubs and graminoids (Elmendorf et al. 2012a, Elmendorf et al. 2012b, Hobbie et al. 2017, Bjorkman et al. 2020, Heijmans et al. 2022). While shrub expansion is generally regarded as the most common change in Arctic vegetation (Elmendorf et al. 2012a, Bjorkman et al. 2020, Heijmans et al. 2022), opposing trends in vegetation composition are evident across sites (Bjorkman et al. 2020) and exact mechanisms of vegetation change likely differ locally (Heijmans et al. 2022).

Similarly, NDVI trend analysis shows that the majority of the Arctic shows no significant trend in NDVI. Increases in NDVI (spectral greening) may be observed in 20-40% of the Arctic biome and significant decreases in NDVI (spectral browning) in 1-8% of the Arctic biome, depending on the timespan and satellite used (fig. 1.3a) (Berner et al. 2020, Myers-Smith et al. 2020, Frost et al. 2021b). Changes in NDVI can be explained by ecological processes such as encroachment of vegetation in previously non-vegetated sites, changing vegetation community composition or changes in plant characteristics such as canopy height and leaf area (Myers-Smith et al. 2020). Spectral greening has frequently been attributed to the expansion of shrub vegetation in particular (Forbes et al. 2010, Macias-Fauria et al. 2012, Epstein et al. 2013, Myers-Smith et al. 2020). Spectral browning (i.e., a decrease in NDVI) is often related to a reversal of such processes (Phoenix and Bjerke 2016, Myers-Smith et al. 2020). Ecological drivers of browning include loss of foliar vegetation due to for instance disruptions in protective winter snow layer over shrub vegetation (e.g. winter warming, rain-on-snow events and reduced thermal insulation under low snow cover), pathogen outbreaks, herbivory and thermokarst (Phoenix and Bjerke 2016, Bjerke et al. 2017). Increased surface water presence, soil moisture and persistence of snow patches can manifest as a direct decrease in NDVI irrespective of vegetation due to the sensitivity or near-infrared reflection to water (Goswami et al. 2011, Gamon et al. 2013, Reynolds and Walker 2016, Myers-Smith et al. 2020). Due to the large amount of potential influences on NDVI, non-linearity in the response of NDVI to biomass and the influence of spatial and temporal scale on NDVI trends, attributing greening and browning dynamics to particular mechanisms without proper resolution data and ground truthing is very challenging (Phoenix and Bjerke 2016, Assmann et al. 2020, Beamish et al. 2020, Myers-Smith et al. 2020).

1.5 Mixing it up: Exploring the Permafrost – Vegetation – Climate Interface

It is evident that local weather patterns as well as permafrost thermal state and vegetation composition are responding to global temperature increases (Box et al. 2019, Meredith et al. 2019, AMAP 2021). Interactions among these components are numerous (fig. 1.4) and influential for the future Arctic and global climate as well as local vegetation composition and ground temperatures (Jorgenson et al. 2010, Loranty et al. 2018a, Heijmans et al. 2022). While research is beginning to unravel complexities on the interface of climate drivers, permafrost thermal processes and vegetation changes, numerous knowledge gaps persist that currently limit the extent to which we can assess the future state of Arctic ecosystems (Loranty et al. 2018a, Heijmans et al. 2022, Smith et al. 2022). Below (fig. 1.4, Box 1.1), I summarize current perspectives on permafrost – vegetation – climate interactions and their role in the future state of Arctic ecosystems. This thesis will mainly focus on interactions between abrupt permafrost thaw and vegetation dynamics in ice-rich lowland tundra systems, and how both components are affected by climate change. With respect to climate effects, I particularly focus on the relatively understudied role of summer rainfall and rainfall extremes. More complete reviews of vegetation - permafrost interactions in a changing climate can be found in Heijmans et al. (2022) and Loranty et al. (2018a). Paragraph 1.7 summarizes the key knowledge gaps within this context and how this thesis will address them.

Box 1.1 - Vegetation - Permafrost Interactions in a warming Arctic

Warmer conditions are generally expected to increase vegetation biomass, and particularly that of shrubs (1) (paragraph 1.4.1) as summer temperatures explain most of the variance in spectral greening of tundra ecosystems (Berner et al. 2020) and in shrub growth (Myers-Smith et al. 2015a) on panarctic scales. Shrub expansion and greening are often found to be stronger when temperature increases are met with sufficient moisture availability (Myers-Smith et al. 2015a, Ackerman et al. 2017, Gamm et al. 2018, Buchwal et al. 2020). But interestingly, there isn't always a straightforward relation between the magnitude of climatic change and changes in vegetation, suggesting strong local controls on vegetation composition and potentially an important role of climatic thresholds (Callaghan et al. 2021). Temperature responses of shrub traits, growth, abundance or biomass and NDVI show considerable spatial and temporal variability (Martin et al. 2017, Bjorkman et al. 2018, Lara et al. 2018, Ercan et al. 2021) and increasing decoupling from warming trends (Martin et al. 2017). Drought stress, increases in disturbances such as thermokarst (KG1), plagues and loss of protective snow cover in winter along with numerous other local factors (Bokhorst et al. 2009, Bjerke et al. 2014, Buchwal et al. 2020, Callaghan et al. 2021, Mekonnen et al. 2021a) may contribute to heterogeneity in shrub - temperature response.

Warming affects permafrost through heat transport from the atmosphere to the soil, increasing the depth of the active layer in summer (2). Apart from air temperature (AMAP 2017, Biskaborn et al. 2019, Smith et al. 2022), permafrost temperatures are generally strongly related to snow depth in winter due to thermal insulation of permafrost against cold air by the snowpack (Stieglitz et al. 2003, Zhang 2005). The role of summer rainfall in permafrost degradation is less straightforward (KG2) (Smith et al. 2022). Several studies find increases in permafrost thaw depth or temperatures as a result of infiltration of rainwater and increased conductive heat transport (Iijima et al. 2010, Neumann et al. 2019, Douglas et al. 2020, Mekonnen et al. 2021b), but other studies report colder soils due to increased latent heat requirement for phase transitions (Clayton et al. 2021) or evaporative cooling (Zhu et al. 2017, Luo et al. 2020). The role of water in the ground thermal regime is also strongly governed by (micro)topography and vegetation (Loranty et al. 2018a, Hamm and Frampton 2021), which makes it difficult to establish straightforward relations between precipitation and permafrost degradation.

Permafrost dynamics, and particularly thermokarst, can strongly determine local vegetation changes in Arctic ecosystems. On the one hand, gradual permafrost thaw can promote nutrient availability and rooting space (3) (Keuper et al. 2012, Keuper et al. 2017, Wang et al. 2017), thereby enhancing potential for Arctic greening. On the other hand, abrupt thaw generally manifests as a disturbance and critical re-organization of the local ecosystem (Heijmans et al. 2022), often resulting in declines in green vegetation biomass (Phoenix and Bjerke 2016). Abrupt thaw tends to critically reorganise hydrological connectivity, with divergent effects across (micro)topographical gradients (Christensen et al. 2004, Baltzer et al. 2014, Chasmer et al. 2014, Walvoord and Kurylyk 2016). In lowland systems, thaw subsidence tends to result in local ponding due to concentration of lateral flow (4) and trapping of snow (5) (Woo and Young 2006, Nauta et al. 2015, Loranty et al. 2018a). Waterlogging in turn can induce shrub mortality and shifts towards aquatic vegetation communities (6) (Jorgenson et al. 2015, Nauta et al. 2015, Li et al. 2017). Counter-intuitively, continued active layer deepening and melting of ground ice structures can eventually result in drainage of surface water features, effectively constituting a drying effect (7) (Liljedahl et al. 2016, Walvoord and Kurylyk 2016, Kreplin et al. 2021). While thermokarst causes an initial disturbance of vegetation, re-colonization of thermokarst features can lead to momentary shrub expansion and greening (Frost et al. 2013, Huebner and Bret-Harte 2019, Verdonen et al. 2020), although timescales associated with these processes are still poorly quantified across heterogeneous permafrost ecosystems (KG3).

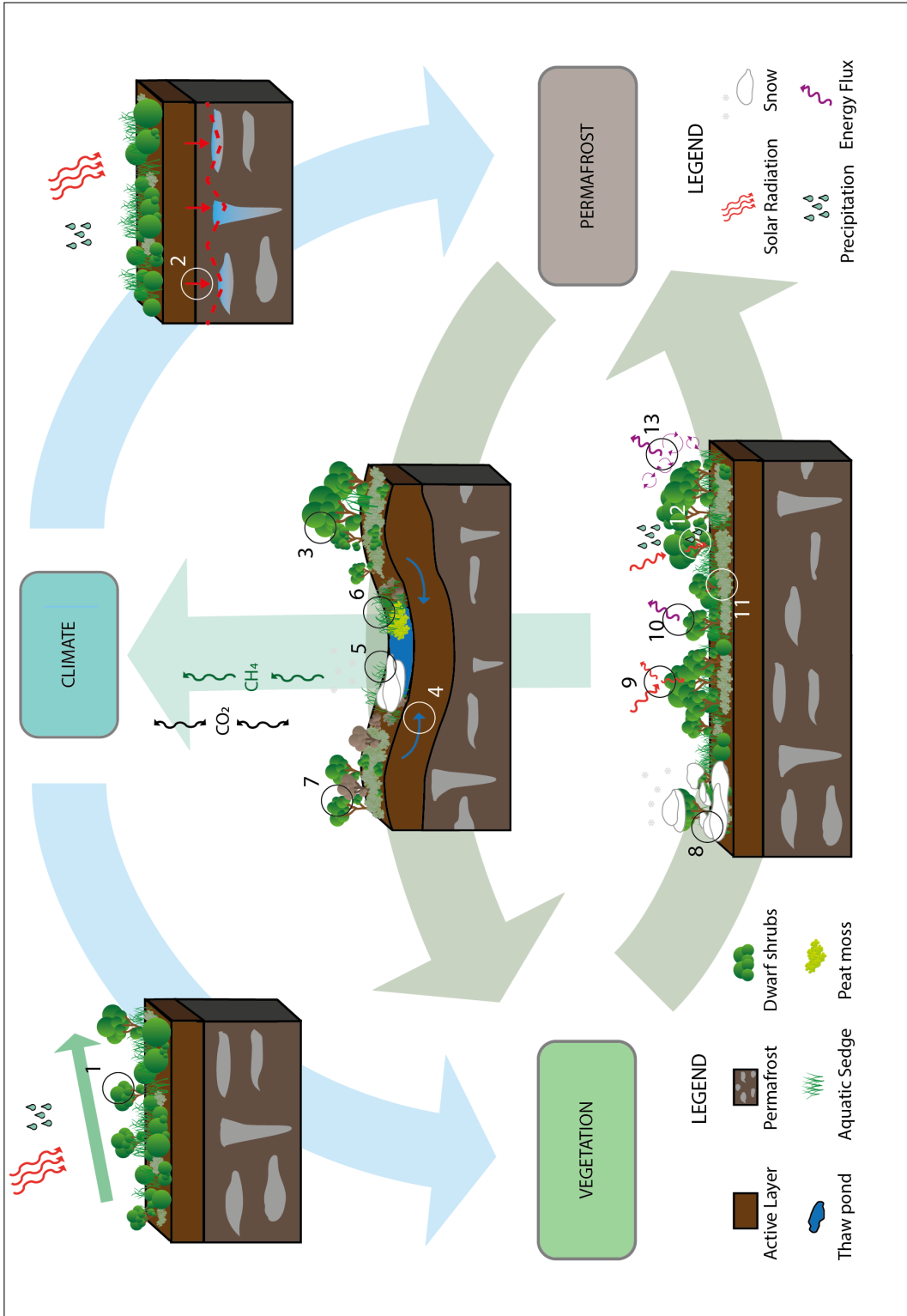


Figure 1.4) Diagram of the Permafrost – Vegetation – Climate interface on which research for this thesis takes place. Changes in the Arctic climate affect growing conditions for Arctic vegetation. Numbers 1-13 indicate several key processes on this interface, which are introduced in Box 1.1. KG1- KG3 indicate three specific knowledge gaps in permafrost – vegetation – climate interaction that this thesis addresses (paragraph 1.7).

In turn, vegetation changes can affect permafrost temperatures. Taller canopies, most notably those of tall shrubs, can trap and accumulate snow in winter. This affects timing of snowmelt (Domine et al. 2016, Wilcox et al. 2019), enhances insulation of the soil surface and increases permafrost temperatures (8) (Kropp et al. 2021). In summer, changes in vegetation composition, for instance between light coloured lichens and darker coloured shrubs, may alter the surface albedo and thereby regulate the amount of incoming shortwave radiation absorbed or reflected by the canopy surface (9) (Beringer et al. 2005, Juszak et al. 2016). Vegetation characteristics further affect energy partitioning within the canopy and thereby determine the amount of incoming radiation that can enter the soil (Loranty et al. 2018a, Heijmans et al. 2022). Taller and denser vegetation canopies as well as organic soil surface layers tend to decrease heat penetration into the ground (Myers-Smith and Hik 2013, Heijmans et al. 2022). This can result from loss of latent heat fluxes through increased evapotranspiration rates (10) (Eugster et al. 2000, Beringer et al. 2005, van Huissteden 2020), canopy interception of rainfall (12) (Zwieback et al. 2019), insulation of the soil by dry moss and organic layers (11) (Jorgenson et al. 2010, Soudzilovskaia et al. 2013), shading of the ground surface by interception of radiation higher up in the canopy (12) (Blok et al. 2010, Myers-Smith and Hik 2013) and turbulent heat exchange between the canopy and surrounding air, regulated by canopy height and physical structure (13) (Bonan 2015, van Huissteden 2020). Previous studies have identified snow trapping in winter and canopy shading in summer as the most influential processes in vegetation effects on permafrost (Myers-Smith and Hik 2013, Loranty et al. 2018a, Heijmans et al. 2022). This leads to a divergent effect of soil warming in winter and cooling in summer, the net effect of which on permafrost degradation is still poorly understood (Heijmans et al. 2022). This poses the question to what extent cooling effects of recolonizing vegetation in summer may assist permafrost recovery (KG3).

The multitude of interactions between vegetation and permafrost in a changing climate illustrated in fig. 1.4 and Box 1.1 have diverse consequences for the greenhouse gas balance and climate of the future Arctic. Changes in vegetation composition and resulting changes in the albedo and surface energy balance may further increase temperature and moisture content of Arctic air masses (Chapin et al. 2005, Bonfils et al. 2012, Loranty et al. 2018a). Gradual deepening of active layers can expose increasing amounts of soil carbon to decomposition into greenhouse gases (Schuur et al. 2015, Natali et al. 2021, Miner et al. 2022), but also provide rooting space and nutrients for enhanced vegetation growth (Keuper et al. 2012, Keuper et al. 2017, Wang et al. 2017). On a pan-arctic scale, model assessments of biomass offsets on permafrost carbon emissions are generally based on an assumption of such gradual thaw alone (McGuire et al. 2018, Meredith et al. 2019), but these offsets may be nullified once abrupt thaw is taken into account (Turetsky et al. 2020). Abrupt thaw is generally associated with strong GHG release (Turetsky et al. 2020, Natali et al. 2021, Miner et al. 2022). Formation of water bodies as a result of thermokarst in particular reduces CO₂ uptake and increases CH₄ emissions (Nauta et al. 2015, Beckebanze et al. 2022), which enhances climate feedback due to the stronger long-term warming potential of CH₄ compared to CO₂ (Miner et al. 2022). The relative contribution of CH₄ and CO₂ is further regulated by surface aeration, vegetation composition and microbial communities (Sundh et al. 1995, Ström et al. 2005, Parmentier et al. 2011a, Kwon et al. 2017). Such characteristics are regulated by vegetation succession following permafrost disturbance. Vegetation succession can further affect the longer-

term greenhouse gas balance through accumulation of peat and other biomass (Turetsky et al. 2007, O'Donnell et al. 2011, Van Huissteden and Dolman 2012). The balance between net emissions during degradation and net uptake during recovery of thermokarst features determines the net greenhouse gas emission of thermokarst features over their lifespan (Van Huissteden and Dolman 2012, Turetsky et al. 2020). Estimates of timescales associated with recovery of permafrost, vegetation and carbon stocks following abrupt thaw are essential to inform models of carbon emissions from abrupt thaw processes, but vary from several decades to hundreds of thousands of years (Jorgenson and Shur 2007, Turetsky et al. 2007, Jorgenson et al. 2015, Kanevskiy et al. 2017, Turetsky et al. 2020). These highly variable estimates of timescales involved in degradation and recovery of permafrost landforms in different Arctic environments suggest that timescales depend strongly on the local setting as well as the type and magnitude of abrupt thaw events (Kanevskiy et al. 2017). Among other factors, such as hydrological transport of permafrost carbon and the role of wildfire, poor understanding of degradation-recovery dynamics of abrupt thaw features across heterogeneous permafrost environments in a rapidly changing climate currently limits our understanding of the relative magnitude of permafrost carbon emissions and biomass offsets (Abbott et al. 2016, Turetsky et al. 2020).

1.6 The final frontier? High potential for climate feedback in the Russian Arctic.

The Russian Arctic harbours a large proportion of the world's Arctic ecosystems (fig. 1.3b) (Raynolds et al. 2019). However, the majority of Arctic vegetation monitoring data is available from the Alaskan Arctic, with relatively few publications available from the North-Eastern Siberian Arctic in international scientific literature (Elmendorf et al. 2012a, Martin et al. 2017, Bjorkman et al. 2020, Kirpotin et al. 2021). Interestingly, the Indigirka Lowlands region in North-Eastern Siberia currently shows one of the most pronounced browning trends across the Arctic based on MODIS and Landsat NDVI time series (Frost et al. 2021b, Mekonnen et al. 2021a). Literature on the mechanisms underlying such pronounced local browning is lacking (at least in English) (Callaghan et al. 2021, Kirpotin et al. 2021) and it is unknown how it relates to permafrost dynamics and recent extremes such as heat waves (Overland and Wang 2021) and flooding (Tei et al. 2020, Haverkamp et al. 2022). Better representation of Arctic ecosystems in North-Eastern Siberia would likely shed more light on drivers of Arctic greening and browning and lead to improved assessment of vegetation changes and associated carbon and permafrost dynamics.

The Russian Arctic also contains more than half of the global area of permafrost, and especially ice-rich, continuous permafrost is highly concentrated in North-Eastern Siberia (fig. 1.2a) (Brown et al. 1997). Permafrost temperatures in this area have shown the largest increases of all Arctic regions (Miner et al. 2022). Permafrost monitoring sites in North-Eastern Siberia in particular have historically shown relatively large increases in active layer thickness in recent decades compared to Western Siberia, Alaska and Scandinavia (Shiklomanov et al. 2012, Smith et al. 2022). North-Eastern Siberian permafrost generally has a relatively high ice content (fig. 1.2b), and can locally have high carbon content due to the prevalence of wetlands and Yedoma deposits (Schirrmeister et al. 2013, Olefeldt et al. 2016, Nitzbon et al. 2020). Due to poor drainage in flat lowland terrain (Woo and Young 2006, Schuur and Mack 2018), these ecosystems are prone to local feedbacks where thermokarst and soil subsidence leads to local accumulation of snow and surface water, small-scale ponding and associated methane emissions (Morgenstern et al. 2011, Nauta et al. 2015, Olefeldt et al. 2016, Nitzbon et al. 2020, Beckebanze et al. 2022). Lastly, the North-Eastern Siberian lowland tundra region has a continental climate with relatively high summer temperatures compared to other Arctic regions (Van der Molen et al. 2007). These characteristics give the North-Eastern Siberian tundra high potential for rapid thaw, methane emissions and climate feedback (Nitzbon et al. 2020) and illustrate this region's potentially substantial contribution to the PCF. The need for ecosystem and permafrost monitoring in this underrepresented region is urgent.

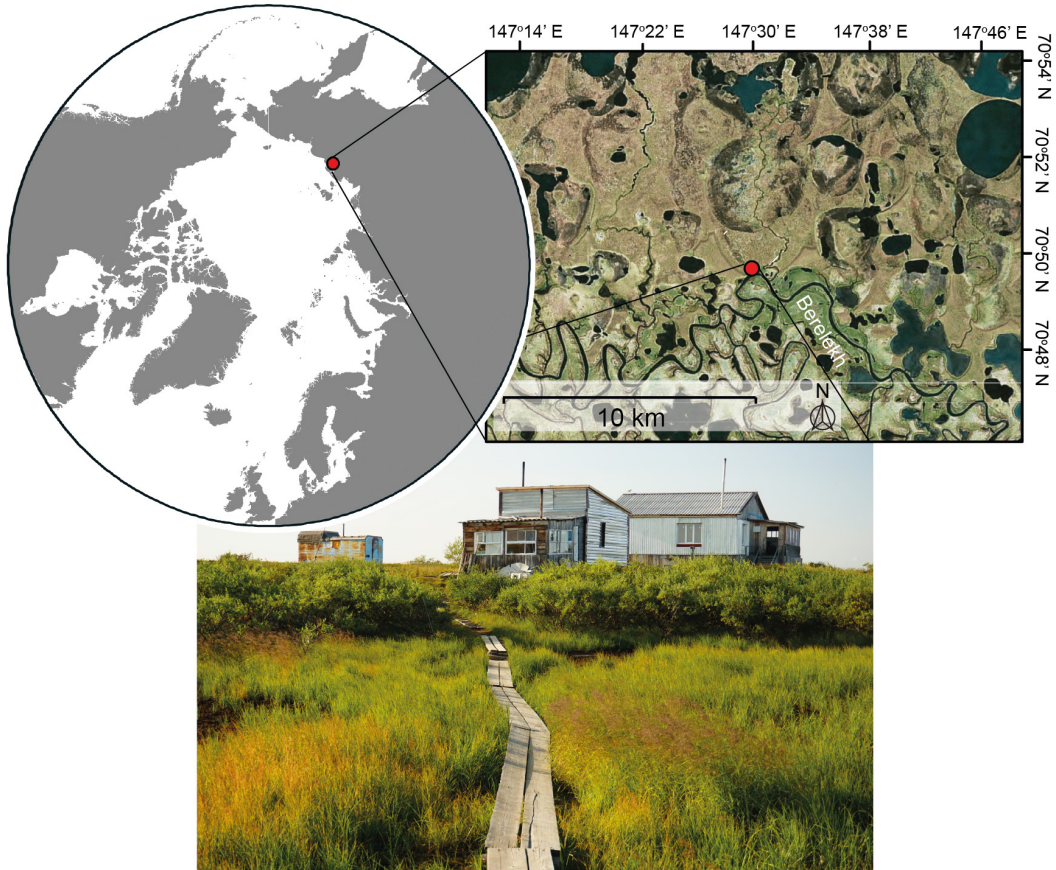


Figure 1.5) Location of the Chokurdakh Scientific Tundra Station; the focus area of this thesis. The photograph of the station is taken from the floodplain of the river Berelekh, which means “full of wolves” in Yakutian.

1.7 Aim and objectives of this thesis

The global risk of future Arctic carbon emissions and the intricate interactions between climatic change, permafrost and vegetation dynamics that determine these emissions illustrate the need for field data to accurately assess net changes and interactions of permafrost and vegetation over time across heterogeneous permafrost ecosystems. Such data and knowledge are particularly scarce in Russian Arctic ecosystems. This thesis responds to this need by quantifying interactions between abrupt permafrost degradation, vegetation development and precipitation in the North-Eastern Siberian lowland tundra. All field research for this thesis was carried out at the Chokurdakh Scientific Tundra Station in the Kytalyk reserve in northern Yakutia (fig. 1.5). This is one of few active environmental research stations representing the North-Eastern Siberian lowland tundra region (Virkkala et al. 2019).

Specifically, this thesis focuses on 3 specific knowledge gaps regarding the development of North-eastern Siberian lowland tundra ecosystems:

(1) The extent to which the Siberian lowland tundra ecosystem displays shrub expansion or decline and how this is related to abrupt thaw processes

The Russian Arctic remains underrepresented in field studies of vegetation changes and shrub expansion even though this region has shown very strong local browning in recent decades (paragraph 1.6). In ice-rich lowlands, ponding due to abrupt permafrost thaw may occur at the expense of shrubs and potentially other vegetation types, with negative implications for tundra greenness and the local greenhouse gas balance. Whether such a mechanism occurs, or whether other factors may underlie recent browning trends, would shed further light on the extent to which carbon uptake in vegetation biomass may be expected in various Arctic environments. Based on local observations of shrub mortality in thaw ponds in the Kytalyk site, recent heat waves and flooding, I expect that abrupt thaw, soil subsidence and waterlogging can lead to rapid and local shrub mortality in this landscape, potentially causing tundra browning on a larger scale.

(2) The influence of summer precipitation on permafrost dynamics

The influence of summer rainfall is an emerging research topic in permafrost studies (Box 1.1) and its effect on permafrost degradation is still poorly quantified. Potential interactive effects between summer rainfall and summer temperature and the duration of the effects of rainfall extremes remain significant knowledge gaps. I expect that extreme rainfall events in summer may substantially enhance permafrost thaw through increased advection and conduction of heat into the soil, and that these effects may be stronger if accompanied by warm air temperatures. In addition, I expect that these effects may last for multiple years due to the role of positive feedbacks. If excessive rainfall and permafrost warming cause soil subsidence, accumulation of snow and surface water in later years may continue to enhance permafrost degradation. Precipitation extremes may additionally affect vegetation composition and greenness dynamics.

(3) Development of small-scale thermokarst features in the Siberian Lowland tundra

Quantification of net carbon emissions resulting from abrupt thaw processes is currently limited by uncertainties in the timescales associated with degradation and recovery of permafrost and vegetation communities (paragraph 1.5). In this respect, the ubiquitous small-scale thermokarst features (< 1 ha) that are abundant in the Siberian Arctic have been largely overlooked. I expect that degradation of permafrost and shifts in vegetation communities in the ice-rich Siberian lowland tundra may be strongly dominated by negative feedbacks following warming, such as subsidence, waterlogging and shrub mortality. However, upon establishment of wetland species, I expect that progressive vegetation succession and accumulation of organic layers may facilitate thermal insulation of underlying permafrost in summer and allow for permafrost aggradation. Due to their small size, vegetation succession and recovery may occur rapidly compared to other thermokarst landforms. Ongoing vegetation succession into a peat moss dominated state may provide a suitable substrate for re-establishment of previously dominant dwarf shrub tundra.

By providing new research data and insights into these sources of uncertainty in the response of permafrost and Arctic vegetation to a changing climate, I hope to support larger scale modelling efforts and quantification of Arctic greening and future permafrost carbon emissions. In addition, I hope to aid local policymakers and communities in anticipating future changes in the North-eastern Siberian lowland tundra ecosystem.

1.8 Structure of this thesis: a multi-disciplinary approach to quantify complex environmental interactions

To improve our understanding of the complex local interactions that regulate the response of ice-rich permafrost of the North-Eastern Siberian lowland tundra to a changing climate, I adopted a multi-disciplinary approach. I studied climatic, soil physical, hydrological and biological developments integrately in a single lowland tundra site. Five chapters address the knowledge gaps described under 1.7 using analysis of time series of very high resolution satellite images, field measurements in chronosequences of thermokarst features, tree-ring, climate and NDVI time series analysis, field experiments or combinations thereof. Through the use of these various angles of approach, new perspectives emerged on the development of the ice-rich North-Eastern Siberian lowland tundra in a rapidly changing climate. The specific questions addressed by each chapter, and how they relate to the identified knowledge gaps (fig. 1.4, paragraph 1.7), are discussed below.

Chapter 2 describes field-measured vegetation composition and abiotic conditions in a chronosequence of thermokarst features (“thaw ponds”), supported by a dendrochronological analysis of re-establishment of shrubs after permafrost degradation. The chronosequence of thaw ponds is derived from a time series of satellite imagery, showing the expansion and terrestrialization dynamics of ponds. These data are used to characterize the development of small thaw ponds (knowledge gap 3) on decadal timescales and assess how they may contribute to permafrost greenhouse gas emissions and Arctic vegetation change over the course of their lifespan.

Chapter 3 describes changes in land cover classes representing different functional groups of vegetation as determined from a time series of very high resolution satellite imagery. Apart from determining whether the studied area displays expansion or decline of shrub vegetation (knowledge gap 1), the results are used to identify vegetation succession mechanisms and to assess the development of thermokarst features over time (knowledge gap 3) on a landscape scale. We compare identified vegetation cover changes to coarser scale MODIS greenness products and Landsat-derived surface water dynamics to assess the representability of the studied site for the larger Indigirka Lowlands ecosystem.

Chapter 4 describes the result of a unique tundra irrigation experiment in which plots of dwarf shrub dominated vegetation received 100 mm of additional precipitation in July 2018 to mimic an extremely wet summer. Using this controlled setup, effects of precipitation on soil thermal properties and permafrost thaw depth were assessed. A fully coupled 1D thermal hydrology model conditioned using field data, is used to reproduce the observed effects and extend the analysis to various precipitation and temperature scenarios. The response of permafrost thaw depths is used to assess the effect of increasing summer rainfall on permafrost degradation (knowledge gap 2).

Chapter 5 describes the response of one of the main Arctic shrub species, *Betula nana*, to a changing climate using dendrochronological (tree ring) analysis. Samples of *B. nana* were gathered from various (micro)topographical positions to assess whether *B. nana* responds differently to long term climate records depending on microsite conditions. In addition, we study changes in sensitivity of this circumarctic shrub species to climate over time. These findings are used to assess the future potential for shrub expansion or decline for this site and potential heterogeneity thereof in the future under a changing climate (knowledge gap 1) and provides complimentary insight into effects of recent rainfall extremes (knowledge gap 2) on shrub growth.

Chapter 6 evaluates whether recent tundra browning (decline in NDVI) may be explained by recent variability in climate and hydrology and vegetation shifts at our Siberian tundra site. We quantify associations between Landsat peak summer NDVI, weather observations and changes in vegetation

General Introduction

composition (Chapter 3) across landforms to gain an understanding of the relative impact of vegetation change, hydrology and annual weather variability on NDVI in this ecosystem. This also provides insight into how larger scale, openly available satellite indices like NDVI can reflect field-measured changes in shrub dynamics and permafrost degradation (knowledge gaps 1 and 3). This will aid interpretation of pan-Arctic NDVI trends and hopefully shed light on the mechanisms behind the pronounced recent browning observed in the North-eastern Siberian tundra region.

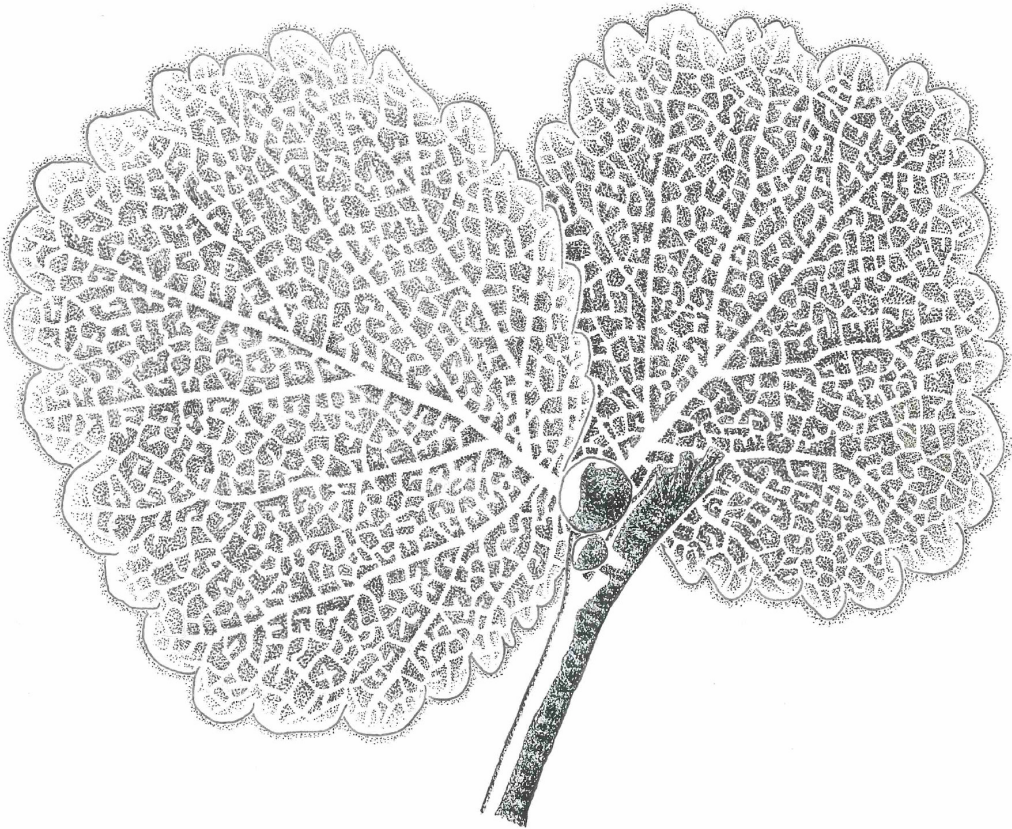
Lastly, Chapter 7 reflects on the results from individual chapters 2-6 and their implications for the identified knowledge gaps and for the broader context of permafrost degradation and vegetation change in the Siberian lowland tundra.

2.

Rapid Vegetation Succession and Coupled Permafrost Dynamics in Arctic Thaw Ponds in the Siberian Lowland Tundra

Rúna Í. Magnússon, Juul Limpens, Ko van Huissteden, David Kleijn,
Trofim C. Maximov, Ronny Rotbarth, Ute Sass-Klaassen, Monique
M. P. D. Heijmans

Published in *Journal of Geophysical Research: Biogeosciences*, 125,
e2019JG005618 (2020).



2.1 Abstract

Thermokarst features, such as thaw ponds, are hotspots for methane emissions in warming lowland tundra. Presently we lack quantitative knowledge on the formation rates of thaw ponds and subsequent vegetation succession, necessary to determine their net contribution to greenhouse gas emissions. This study set out to identify development trajectories and formation rates of small-scale ($< 100 \text{ m}^2$), shallow arctic thaw ponds in north-eastern Siberia. We selected 40 ponds of different age classes based on a time-series of satellite images and measured vegetation composition, microtopography, water table and thaw depth in the field and measured age of colonizing shrubs in thaw ponds using dendrochronology. We found that young ponds are characterised by dead shrubs, while older ponds show rapid terrestrialization through colonization by sedges and *Sphagnum* moss. While dead shrubs and open water are associated with permafrost degradation (lower surface elevation, larger thaw depth), sites with sedge and in particular *Sphagnum* display indications of permafrost recovery. Recruitment of *Betula nana* on *Sphagnum* carpets in ponds indicates a potential recovery towards shrub dominated vegetation, although it remains unclear if and on what timescale this occurs. Our results suggest that thaw ponds display potentially cyclic vegetation succession associated with permafrost degradation and recovery. Pond formation and initial colonization by sedges can occur on sub-decadal timescales, suggesting rapid degradation and initial recovery of permafrost. The rates of formation and recovery of small-scale, shallow thaw ponds have implications for the greening/browning dynamics and carbon balance of this ecosystem.

2.2 Introduction

The Arctic is warming twice as fast as the global average. It is expected that by the end of the 21st century, the global area of near-surface permafrost will decrease by $24 \pm 16\%$ (IPCC scenario RCP2.6) to $69 \pm 20\%$ (IPCC scenario RCP8.5) (Meredith et al. 2019). This thawing of permafrost exposes previously frozen soil organic carbon to microbial decomposition, resulting in the release of greenhouse gases. This constitutes a positive feedback to climate change (Schuur et al. 2015). The expected release of greenhouse gases (GHG) from thawing permafrost is in the order of 10s to 100s gt carbon by the end of the 21st century (Meredith et al. 2019). There is, however, considerable uncertainty about the exact magnitude of this “permafrost carbon feedback” (Schuur et al. 2015, Meredith et al. 2019). Part of this uncertainty revolves around the relative importance of two thawing mechanisms: gradual versus abrupt thaw. Gradually increasing thaw depths and higher temperatures have resulted in increased vegetation cover and productivity (Tape et al. 2006), most notably in shrubs (Myers-Smith et al. 2015a), which may partly offset GHG emissions from thawing permafrost (Euskirchen et al. 2009). Satellite monitoring of the Normalized Difference Vegetation Index (NDVI), a measure of vegetation greenness and photosynthetic capacity, confirms that the Arctic has shown a greening trend over most of the past decades (Epstein et al. 2018). In contrast, abrupt permafrost thaw occurs when excess ground-ice in the permafrost melts, causing a collapse of the soil surface (thermokarst) (Schuur et al. 2015). Such processes may counteract the widely observed Arctic greening trend (Abbott et al. 2016, Phoenix and Bjerke 2016, Reynolds and Walker 2016). Since 2011, local browning (a decrease in NDVI) has diminished or even halted the overall Arctic greening trend (Epstein et al. 2018). Abrupt rather than gradual thaw may predominate in large parts of the Arctic (Schuur et al. 2015, Olefeldt et al. 2016) and has been found to occur increasingly throughout Arctic regions (Walter et al. 2006, Fedorov et al. 2014, Reynolds et al. 2014, Jorgenson and Grosse 2016, Liljedahl et al. 2016, Frost et al. 2018b, Farquharson et al. 2019). Abrupt thaw can lead to formation and expansion of surface water in continuous permafrost (Jorgenson et al. 2006, Reynolds et al. 2014) and is expected to increase the area of small lakes by 50% by 2100 under IPCC scenario RCP8.5 (Meredith et al. 2019). It thereby enhances GHG emission through increased wetting and disturbance of the existing vegetation (Abbott et al. 2016). However, most studies on permafrost carbon dynamics have focused on gradual thaw, and abrupt thaw processes are currently

not considered in climate models (Van Huissteden and Dolman 2012, Schuur et al. 2015, Meredith et al. 2019).

Thaw ponds are an example of features resulting from abrupt thaw of which we have limited understanding. Thaw ponds are isolated depressions of less than one hectare which form due to local melting of ground-ice. In these local depressions, snow and water accumulate, posing a positive feedback on thawing (Nauta et al. 2015). Thaw ponds are demonstrated sources of methane, as opposed to shrub dominated tundra vegetation (Van Huissteden et al. 2005, 2009, Van Huissteden and Dolman 2012, Nauta et al. 2015). Thaw ponds are abundant throughout ice-rich lowland tundra, but small waterbodies often go undetected in remote sensing analysis of thermokarst features (Grosse et al. 2008, Campbell et al. 2018, Reynolds et al. 2019). In contrast to the deep, ditch-shaped ponds resulting from ice-wedge degradation, melting of various other types of ground ice (e.g. ice lenses) may result in shallow, irregular shaped thaw ponds (van Huissteden 2020). Smaller, shallow ponds may be especially vulnerable to climate induced changes in hydrological regimes (Wolfe et al. 2011, Campbell et al. 2018). Such thaw ponds have received little scientific attention compared to other abrupt thaw features (e.g. thaw lakes, ice-wedge degradation, retrogressive thaw slumps). This warrants research into trends in shallow thaw pond area, the processes that trigger formation of such thaw ponds and their long-term fate.

Several studies have focused on long-term development of thermokarst features related to ice-wedge degradation (Jorgenson et al. 2015, Liljedahl et al. 2016, Kanevskiy et al. 2017) or thermokarst bogs in subarctic regions (Robinson and Moore 2000, Payette et al. 2004, Turetsky et al. 2007, Myers-Smith et al. 2008). These studies suggest the existence of a coupled vegetation succession and permafrost degradation-recovery mechanism, described by Kanevskiy et al. (2017) as “quasi-cyclic” succession. Such successions are characterized by soil subsidence due to melting of ground ice, followed by formation of open water features, which are in turn colonized by wetland vegetation (e.g. graminoids and peat mosses). Vegetation succession, especially colonization by peat mosses (*Sphagnum*), may improve insulation of the permafrost, which allows for permafrost recovery (Zoltai and Tarnocai 1975, Seppala 1988).

We investigate whether shallow arctic thaw ponds in north-eastern Siberia, a large and understudied lowland tundra region, follow the quasi-successional succession model described above. As a novel aspect, we apply dendrochronological dating to assess the presence of Arctic dwarf shrubs across stadia of thaw pond development and to assess timespans of formation and recovery. Specifically, we explored (i) whether thaw ponds in lowland tundra display a dominant vegetation succession trajectory, (ii) if permafrost degradation and recovery are coupled to vegetation dynamics and (iii) on which timescales vegetation succession and permafrost degradation and recovery in thaw ponds occur. We hypothesized that the following vegetation succession occurs: following soil subsidence and ponding of water in the new depressions, the initially dominant dwarf shrub vegetation drowns and is replaced by open water. Sedges are expected to be the first species to re-colonize such open water areas, followed by formation of *Sphagnum* moss carpets. Additionally, we expect *Sphagnum* moss to be associated with permafrost recovery and to be an important micro-site for the re-establishment of dwarf shrubs. Thus, we expect to find a (quasi-)cyclic succession mechanism similar to that described for ice-wedge degradation.

2.3 Methods

2.3.1 Study Site

Vegetation composition and associated abiotic conditions in shallow thaw ponds of various ages were studied in the “Kytalyk” Nature Reserve in north-eastern Siberia (70°49'N, 147°29'E) approximately 30 km north-west of the town of Chokurdakh. This area is situated in a region that displays frequent indications of browning rather than greening between 1982 and 2018 (Epstein et al. 2018). North-eastern Siberia is a region with high abundance of thermokarst wetlands and lakes (Olefeldt et al. 2016).

Our study site is characterized by a shallow active layer overlying continuous permafrost of over 300 m thickness (Van Huissteden et al. 2005, 2009). Mean annual temperature is -13.4 °C, with an average July temperature of 10.3 °C (1981-2010). Mean annual precipitation is 196 mm, with 76 mm falling in June to August (1981-2010) (Trouet and Van Oldenborgh 2013). Our study location is situated in a drained thaw lake basin or “alas”, surrounded by remnants of Pleistocene yedoma deposits, floodplains and thaw lakes. Our site represents an older episode of lake drainage, evident from the multiple levels of alases in the area (fig. 2.1a). Paleoecological data suggest that peat accumulation has taken place in this lakebed for at least 4000 years (Telteuvsokoi et al. 2016). Holocene alases are abundant throughout coastal eastern Siberia (Morgenstern et al. 2013, Fedorov et al. 2018) and cover approximately 111,000 km² in coastal Yakutia alone (Fedorov et al. 2018). The lakebed vegetation is characterized by slightly elevated shrub patches dominated by *Betula nana*, lichens and mosses, interspersed with waterlogged depressions characterized by *Eriophorum angustifolium*, *Carex* spp. and *Sphagnum* spp. (Siewert et al. 2015). The Circumpolar Arctic Vegetation Map classifies this site as a mix of tussock-sedge tundra, erect dwarf shrub tundra and sedge-moss wetland. These vegetation classes are typically found in low elevation areas with relatively high summer temperatures and are representative of a major part of coastal north-eastern Siberia (Raynolds et al. 2019). Around Chokurdakh, ground ice content is high (75 vol-% on average in the top 1 to 2 m of soil) (Iwahana et al. 2014, Wang et al. 2019), and in recent decades a doubling in area of thaw ponds at the Kytalyk site has been observed (van Huissteden et al. 2017). Apart from these shallow, irregular shaped thaw ponds (fig. 2.1d), polygonal thermokarst features related to ice-wedge degradation (fig. 2.1e) and diffuse drainage gullies (fig. 2.1c) also occur in the study area.

2.3.2 Thaw pond selection

For our research we selected isolated non-polygonal thaw ponds (< 100 m²) surrounded by dwarf shrub vegetation (see fig. 2.1f). Thaw ponds were identified based on a series of commercial high-resolution satellite images (GeoEye I from 2010, WorldView II from 2015 and 2017 and WorldView III from 2018; specifications in table S2.1) and inspected in the field. We observed both recently formed and older ponds. The latter frequently showed indications of terrestrialization. To represent temporal variability in thaw pond formation, we selected thaw ponds from three age classes based on their presence and extent in satellite images from previous years. Ponds that were not present yet in 2010 were labelled “Young ponds” (Y, n = 12). Ponds that were present in 2010 and showed an increase in the extent of open water from 2010 to 2018 were labelled “Old Increasing ponds” (OI, n = 13). Ponds that were present in 2010 and showed a decrease in the extent of open water from 2010 to 2018 were labelled “Old Decreasing ponds” (OD, n = 15). We assumed that these Pond Age Classes represent successional stages from young ponds resulting from recent soil subsidence due to permafrost degradation to older ponds in which the open water area is decreasing due to terrestrialization. Table S2.22 contains an overview of the expansion trends of the 40 selected ponds. All thaw ponds were situated within a matrix of shrub vegetation with shallow thaw depths (\pm 20 cm) to exclude external hydrological influences such as drainage. Satellite images were co-registered based on manually selected control points using the geo-referencing toolbox and pan-sharpened with the Gram-Schmidt algorithm in ArcMap 10.3.1 (ESRI 2019). Pond boundaries were mapped manually as polygons based on visual distinction between open water and vegetated pixels in the pansharpened satellite images. While this manual delineation introduces a degree of subjectivity, we expect the effects of pond expansion and terrestrialization on the spectral data to exceed variation resulting from differences in interpretation (table S2.22). Approximate lateral expansion rates of ponds were calculated based on changes in bounding box geometry of pond polygons.

Rapid Vegetation Succession and Coupled Permafrost Dynamics

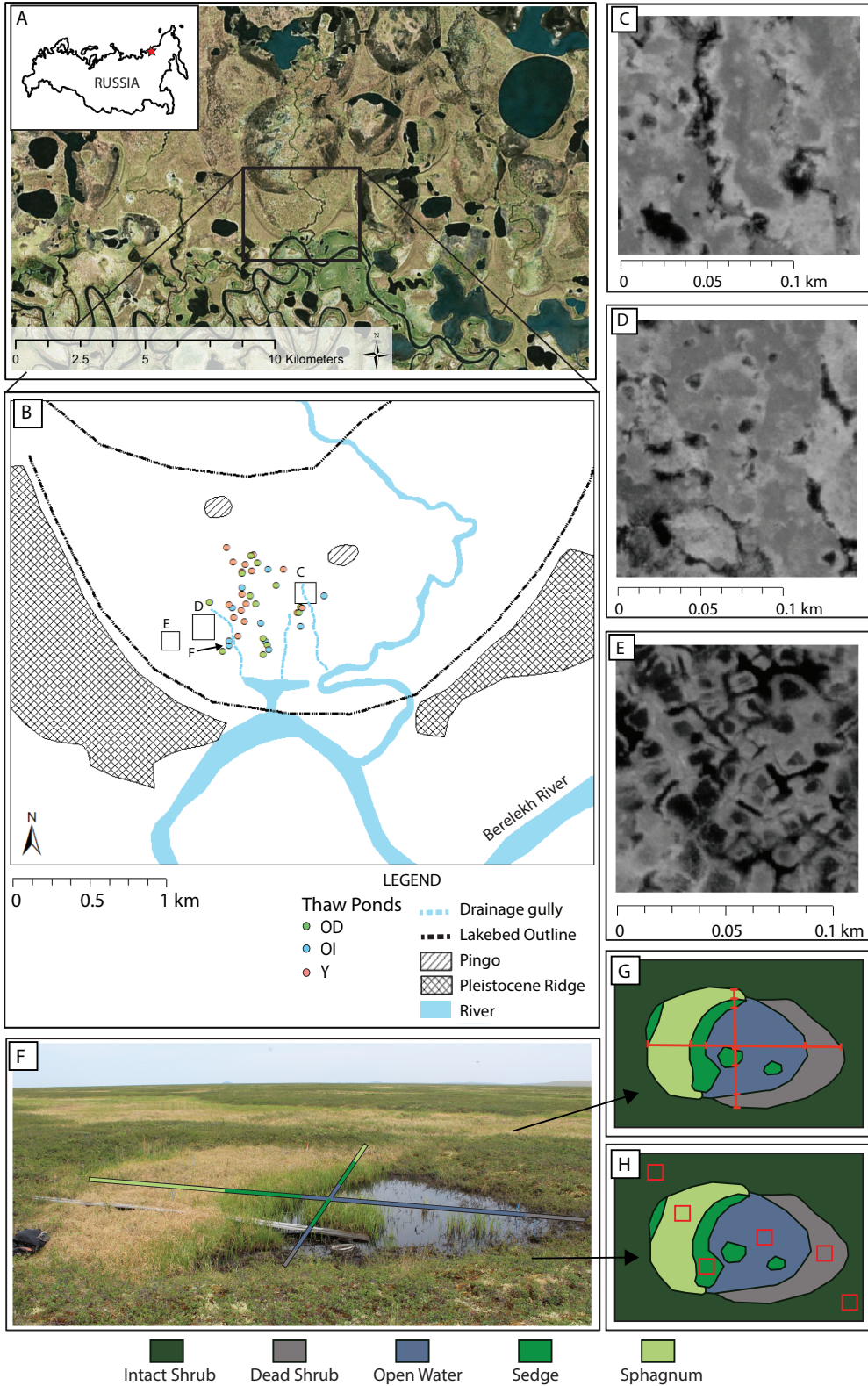


Figure 2.1) Schematic overview of the transect layout over thaw ponds. a) Location of the site. Image courtesy of ESRI/ Digital Globe. b) Overview of the study site and locations of the selected thaw ponds. Y = Young thaw ponds; OI = Old Increasing thaw ponds; and OD = Old Decreasing thaw ponds. c) Panchromatic image (WorldView © 2019 MAXAR) of a drainage gully. d) Panchromatic image (WorldView © 2019 MAXAR) of an example of the studied isolated, small scale thaw ponds. e) Panchromatic image (WorldView © 2019 MAXAR) of polygonal tundra features. f) Photograph of isolated, small scale thaw pond. g) Placement of transects and pickets over thaw ponds, indicated as red lines. h) Placement of quadrats within and around thaw ponds, indicated as red squares.

Table 2.1) Plant Functional Type (PFT) Classes Distinguished for the Purposes of This Study. In order of hypothesized succession

Group	PFT	Description
Shrubs	Intact Shrubs	Dwarf shrub-dominated vegetation, mainly <i>Betula nana</i> and some <i>Salix pulchra</i> . Understory dominated by non- <i>Sphagnum</i> mosses (<i>Polytrichum</i> spp., <i>Dicranum</i> spp.) and lichens.
	Drowning Shrubs	Same as above, but dwarf shrubs show clear indications of compromised growth (small, discolored leaves).
	Dead Shrubs	Same as intact shrubs, but dwarf shrubs and understory are dead (brown without any green leaves). Shrubs are not completely submerged.
Graminoids	Grass	Vegetation dominated by tall grasses, e.g., <i>Arctagrostis latifolia</i> .
Open Water	Open Water	Standing water without living vegetation. Where present, dead shrubs are completely submerged or decomposed.
Graminoids	Sedge	Sedge dominated vegetation, mostly <i>Eriophorum angustifolium</i> and in some cases <i>Eriophorum vaginatum</i> and <i>Carex aquatilis</i> .
Mosses	<i>Sphagnum</i>	Carpet-forming peat moss (<i>Sphagnum</i> spp., mostly <i>S. obtusum</i> and <i>S. squarrosum</i>) dominated vegetation. Some sedges present on <i>Sphagnum</i> carpet.
	Other Mosses	Vegetation dominated by other mosses, e.g., <i>Aulacomnium turgidum</i> .

2.3.3 Field Measurements

2.3.3.1 Vegetation Composition

To be able to identify dominant vegetation succession mechanisms, vegetation composition in ponds from the three age classes (Young, Old Increasing and Old Decreasing) was studied. In all 40 selected thaw ponds, two perpendicular transects were laid out over the pond perimeter (fig. 2.1f). Transect directions were selected to most accurately represent vegetation composition of the pond. The total length of the transect was measured as the distance from one pond margin with intact, *Betula nana* dominated vegetation to another (i.e., intact shrub vegetation outside the pond perimeter was not considered). Transitions in vegetation composition along the transect were marked with pickets (fig. 2.1g). A vegetation transition is defined here as a transition from one dominant plant functional type (PFT) class to the other (table 2.1). Boundaries were distinguished based on dominance of either of the PFT classes defined in table 2.1 determined by visual cover estimates. Using this set-up, vegetation composition was quantified as total length between pickets for each class present within the thaw pond, expressed as a percentage of the total length of the transects. Measurements were conducted over the course of several days in late July 2018.

2.3.3.2 *Abiotic Conditions*

To assess the coupling of vegetation succession with the development of permafrost degradation and recovery, abiotic variables (microtopography, height of the water table above the permafrost and thaw depth) were measured under various PFTs in thaw ponds of the three age classes. In a subset of 21 thaw ponds, 50 x 50 cm quadrats were placed on sites reflecting the PFT classes from table 2.1 (fig. 2.1h), with the exception of “grass”, “other moss” and “drowning shrubs”, which were either only present in small and narrow areas (< 0.5 m width) or in few ponds ($n < 5$). The dominant PFT was determined by visual cover estimates. In the centre of each of the 112 quadrats, thaw depth (referred to hereafter as TD), was measured using a pointed metal probe with cm scale indication. TD was defined as the distance between the moss surface and frozen soil as measured in early August, before maximum thaw at the end of the summer season. In our study site, temperatures typically fall below zero again in late August – early September (Van der Molen et al. 2007, Parmentier et al. 2011b). As such, reported values should be interpreted as instantaneous thaw depths rather than an active layer thickness, which is generally defined as the top soil layer subject to annual freezing and thawing (Shur et al. 2011) or the depth of maximum seasonal penetration of the 0°C isotherm (Muller 1947). The water table (hereafter: WT) was measured as the height of the water table above the frozen soil. In non-inundated sites, a peat corer was used to determine whether there was a water table above the permafrost. No WT was recorded in absence of a water table. Thickness of the organic layer (OLT) was measured as the distance between the moss or soil surface and mineral soil in a peat core. No OLT was recorded in case no mineral soil was visible (i.e. $OLT > TD$). Lastly, relative surface elevation (hereafter: RSE) of a quadrat was measured as millimetre elevation relative to a local reference level using an optical leveller (Kompensator-Nivellier NI 025, VEB Carl Zeiss, Jena, Germany). The reference level was calculated as the average elevation of four positions outside the pond perimeter on intact shrub vegetation, at 2 m distance of the pond margin. The permafrost position (PP) was calculated as $RSE - TD$, representing the depth at which frozen soil occurs (before maximum end-of-summer thaw) relative to the reference level. Measurements were conducted once per quadrat over the course of several days in early August 2018, except OLT, which was measured in early August 2019.

2.3.3.3 *Shrub distribution*

To assess whether vegetation succession can lead to re-establishment of dominant dwarf shrub vegetation, an inventory was made of presence of living dwarf shrubs (yes/no) in all quadrats inside the pond perimeter.

2.3.3.4 *Dendrochronological analysis*

To gain an insight in the timescales associated with degradation of permafrost, vegetation succession and re-establishment of shrub vegetation, the ages of shrubs, their year of establishment and death were determined using dendrochronology. In a subset of 15 thaw ponds (five from each age class), stem samples of *Betula nana* were taken for tree-ring analysis. Three types of *Betula nana* shrubs were sampled: (i) living shrubs from shrub vegetation surrounding the thaw pond, (ii) dead shrubs from within the thaw pond (including terrestrialized areas) and (iii) living shrubs (established from seeds or ramets) from within the thaw pond (including terrestrialized areas, e.g. on a moss carpet or other substrate). For each shrub type, two replicates per pond were sampled, if present, resulting in a total of 66 samples (30 living, outside ponds, 24 dead, inside ponds and 12 living, inside ponds). From all sampled shrubs, three stem sections of 2 cm length were clipped at the field site and preserved in a 3:1 mixture of vodka and glycerol. Sections were cut at the root-shoot interface, at the moss surface, and above the moss surface just below the first branch (Li et al. 2016). The root-shoot interface was identified as a slight thickening in the stem diameter, often followed by a bend in the belowground stem (see also fig. S2.1).

Ages of shrubs were determined by tree ring analysis on 20 to 30 μm micro-thin sections prepared by a sliding microtome (GSL1, WSL, Birmensdorf, Switzerland) from each stem cross section using CooRecorder v. 9.0 (Cybis, 2019b). A hierarchical cross-dating approach based on serial sectioning (Hallinger et al. 2010, Wilmking et al. 2012, Myers-Smith et al. 2015a, Myers-Smith et al. 2015b) was used to correct for missing rings (Kolischuk 1990, Myers-Smith et al. 2015b) and to determine the year of shrub establishment and death based on the individual stem disks. Initially visual cross-dating was carried out in WinTSAP v. 4.70d (Rinntech 2017). Afterwards, cross-dating accuracy was evaluated statistically using COFECHA v. 6.02p (Holmes 1983) and ring width series were adjusted to maximize correlation among cross-sections. A full protocol of the dendrochronological analysis is available in text S2.1.

2.3.4 Data analysis

2.3.4.1 Vegetation Composition

Differences in PFT composition among thaw ponds of various age classes were assessed using multivariate analysis of variance. Cover percentages of both transects (fig. 2.1c) were averaged per pond. Since the assumption of normality was violated and percentage data was zero-inflated, PERMANOVA using Bray-Curtis distance was used to test for differences in the covers of the PFTs among the three Pond Age Classes (Anderson 2001). Prior to PERMANOVA analysis, a betadisper test using the average distance of group members to the group spatial median (Anderson 2006) followed by Tukey's Honest Significant Difference analysis was used to confirm multivariate homogeneity of dispersion among Pond Age Classes. To correct for an unbalanced design with small sample sizes, a $\sqrt{(n(n-1))}$ correction (Stier et al. 2013) was used for the betadisper test. Pairwise PERMANOVAs for each pair of Pond Age Classes were conducted as a post-hoc comparison, using Bonferroni adjustment of p-values to correct for multiple testing. Lastly, SIMPER analysis (Clarke 1993) was used to assess contribution of specific PFTs to difference in overall PFT composition among Pond Age Classes. SIMPER analysis was restricted to 1000 permutations and used Bray-Curtis distance.

2.3.4.2 Abiotic Conditions

Differences in TD, WT, RSE and PP among the PFTs in thaw ponds of the three age classes were analysed using Linear Mixed Effects Models (LMMs) using Restricted Maximum Likelihood (REML). "Pond Age Class" and a quadrat's "PFT Class" were used as categorical predictor variables. Since a water table was absent in 95% of the Intact Shrub quadrats (no water table above the permafrost), observations of WT in this PFT Class were omitted from analysis. TD was log-transformed prior to analysis to improve residual diagnostics. All models were checked for significance of PFT Class, Pond Age Class and their interaction term and for random slope and/or intercept for individual ponds. First, the optimal random structure was determined using Likelihood Ratio tests (LRTs) on a full (or as full as feasible) model. Then, the optimal fixed structure was determined using backwards selection. P-values of predictor variables were calculated on nested models, using F-tests with Kenward-Roger approximation for fixed effects and likelihood ratio tests (LRTs) for random effects. Models were selected based on predictor p-values, Akaike's Information Criterion (AIC), normality and homoscedasticity of residuals and absence of patterns of residuals against grouping factors and fitted values. Normality of residuals for LMMs was determined visually. As a post-hoc test, Tukey contrasts and Bonferroni adjusted p values were calculated. Lastly, the root mean square error (RMSE) of the candidate models derived from leave-one-out cross validation (LOOCV) was compared to check for overfitting.

2.3.4.3 Shrub Distribution

A binomial GLMM with Laplace Approximation of Maximum Likelihood was used to model presence (yes/no) of shrubs as a function of PFT Class and Pond Age Class, with Pond ID as a random factor. Observations in "Intact Shrub" and "Open Water" quadrats were omitted from statistical analysis due

to complete presence or absence of living shrubs. The same procedure for model selection as described for Abiotic Data was adopted. Success rates for the prediction of presence of *Betula nana* were calculated from confusion matrices based on LOOCV.

2.3.4.5 Shrub Ages

Differences in age among shrub types (living & inside the thaw pond perimeter, living & outside the thaw pond perimeter and dead & inside the thaw pond perimeter) were assessed using a Poisson GLMM with Laplace Approximation of Maximum Likelihood, using Pond Age Class and shrub type as fixed effects and Pond ID as a random effect. To correct for age differences resulting from the time elapsed since drowning of dead shrubs relative to living shrubs, the GLMM was performed on year of establishment of the shrub, expressed as number of years since the earliest year of establishment found in the dataset. The same procedure for model selection as described in paragraph 2.3.4.2 was adopted.

All analyses were carried out in R version 3.5.1 (R Development Core Team 2019). The `adonis2`, `betadisper`, `TukeyHSD` and `simper` functions from the `vegan` package (Oksanen et al. 2015) were used for vegetation composition analysis. The `lme4` package (Bates et al. 2014) was used for (G)LMMs. For F-tests with Kenward-Rogers approximation, the `KRmodcomp()` function from the `pbkrtest` package (Halekoh and Højsgaard 2014) was used. LRTs were implemented using the base R `anova()` function. The `emmeans()` function from the `emmeans` package (Lenth 2018) was used for pairwise contrasts. Residuals of GLMMs were transformed to standardized space prior to visual inspection and tested for overdispersion, uniformity and zero-inflation using the `DHARMA` package (Hartig 2017).

2.4 Results

2.4.1 Selected ponds

Based on the time series of satellite images, we selected ponds of contrasting age, size and expansion dynamics. 12 young ponds were selected, which were assumed to be at most 8 years old during time of sampling (since the satellite image of 2010 showed no indication of disturbance of the original vegetation). Most young ponds were visible in 2015 and thus at least 3 years old. Several young ponds already showed a decline in open water extent between 2015 and 2018. Of the 28 ponds that were older than 8 years (i.e., open water was visible in the satellite image of 2010), 13 were expanding in open water extent, and 15 were declining. However, inspection of satellite images indicated that ponds did not necessarily decline or expand uniformly and could display expansion of open water on one side of the pond, and terrestrialization on the other side (table S2.22). We found slightly higher lateral expansion rates of open water area for Young ponds (mean = 0.52 ± 0.28 m / yr) than for Old Increasing ponds (mean = 0.33 ± 0.26 m / yr). Old decreasing ponds showed shrinking trends of similar magnitude, albeit more variable (mean = -0.43 ± 0.39 m / yr) (fig. 2.2). Mean field transect lengths, including terrestrialized areas with sedge and *Sphagnum* dominated vegetation, were 3.61 ± 1.26 m for Young ponds, 6.41 ± 2.57 m for Old Increasing ponds and 7.79 ± 3.26 m for Old Decreasing ponds. Figure 2.2a suggests that ponds may reach highly variable open water extent before starting to terrestrialize.

2.4.2 Vegetation composition

Vegetation composition as derived from transect distances differed among thaw ponds of the three age classes and showed a progression over time from dead shrubs towards sedge and *Sphagnum* dominated vegetation. Pond Age Class explained 31% of variance in vegetation composition compared to variance among individual ponds (Pond Age Class: $F = 8.18$, $df = 2$, $p = 0.001$, PERMANOVA). Pairwise PERMANOVAS showed that all pairwise combinations of ponds differed significantly in vegetation composition (Young vs. Old Increasing: $F = 5.26$, $p = 0.012$, Young ponds vs. Old Decreasing ponds: $F = 17.15$, $p = 0.003$, Old Increasing vs. Old Decreasing: $F = 4.43$, $p = 0.003$). Young ponds were characterised by a relatively high cover of dead shrub vegetation, low cover of sedges and in most cases

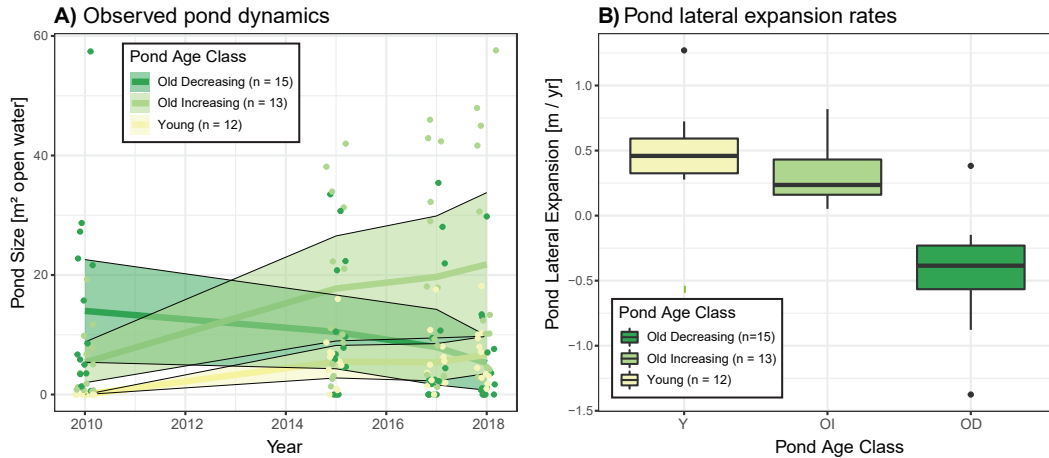


Figure 2.2) Observed dynamics of selected thaw ponds. a) Observed trends in open water area per pond age class (see table S2.22 for images of individual ponds per year). Y = Young ponds; OI = Old Increasing ponds; and OD = Old Decreasing ponds. Shaded areas represent 95% confidence interval per pond age class. b) Observed lateral expansion rates of open water area per pond age class. One decreasing pond displayed a positive lateral expansion while its net area decreased, due to development of a complex shape.

absence of *Sphagnum* moss. Old Increasing ponds contained open water more frequently, increased cover of sedges and *Sphagnum* and decreased cover of dead shrubs compared to Young ponds. Old Decreasing ponds contained the highest cover of *Sphagnum*, and low cover of drowning shrubs (fig. 2.3a-b). The difference between Young and Old Increasing ponds was mostly determined by dead shrubs (diff. Y – OI = 42.70%, $p = 0.002$, SIMPER) and open water (diff. OI – Y = 13.79%, $p = 0.009$). The contrast between Young and Old Decreasing ponds was mostly determined by dead shrubs (diff. Y – OD = 52.30%, $p = 0.001$) and *Sphagnum* cover (diff. OD – Y = 39.52%, $p = 0.001$). Old Decreasing ponds had significantly more *Sphagnum* (diff. OD – OI = 25.45%, $p = 0.008$) and less open water (diff. OI – OD = 17.12%, $p = 0.015$) than Old Increasing ponds. See table S2.3-S2.5 for all SIMPER results analysis.

Detailed visual cover estimates in quadrats indicated that dwarf shrub vegetation consisted mainly of *Betula nana* and occasionally *Salix pulchra* and *Vaccinium vitis-idaea* with a dense moss and lichen layer. Sedge vegetation consisted mainly of *Eriophorum angustifolium*. Sparse sedge cover was also present on *Sphagnum* dominated sites and especially *Carex aquatilis* was often found in association with *Sphagnum* (table S2.21, fig. S2.3). *Sphagnum* species were almost exclusively *S. obtusum* and *S. squarrosum*, with incidental presence of *S. subsecundum* and *S. balticum* (Magnússon, pers. obs.). Sedges and *Sphagnum* were generally absent in intact shrub quadrats (table S2.21).

2.4.3 Shrub Distribution & Ages

Analysis of shrub distribution and ages indicated that young *Betula nana* individuals are found in thaw ponds, predominantly on *Sphagnum* carpets. Out of 66 shrubs sampled, 43 were cross-dated with sufficient statistical certainty (see text S2.1) to determine their age and the year of establishment. Correlation of ring-width series among these 43 shrubs was strong (average correlation coefficient = 0.52 ± 0.10). Ages of living shrubs from outside the pond perimeter and dead shrubs inside the pond perimeter ranged from 30 to 84 years (mean = 46.23 ± 13.00 , $n = 30$) and did not significantly differ ($p = 0.058$), suggesting that pond formation occurred in intact shrub vegetation. Living shrubs from inside the pond perimeter ranged from 2 to 18 years in age (mean = 7.83 ± 4.76 , $n = 13$) and hence were significantly younger than dead shrubs or living shrubs from outside the pond perimeter ($p < 0.001$ for

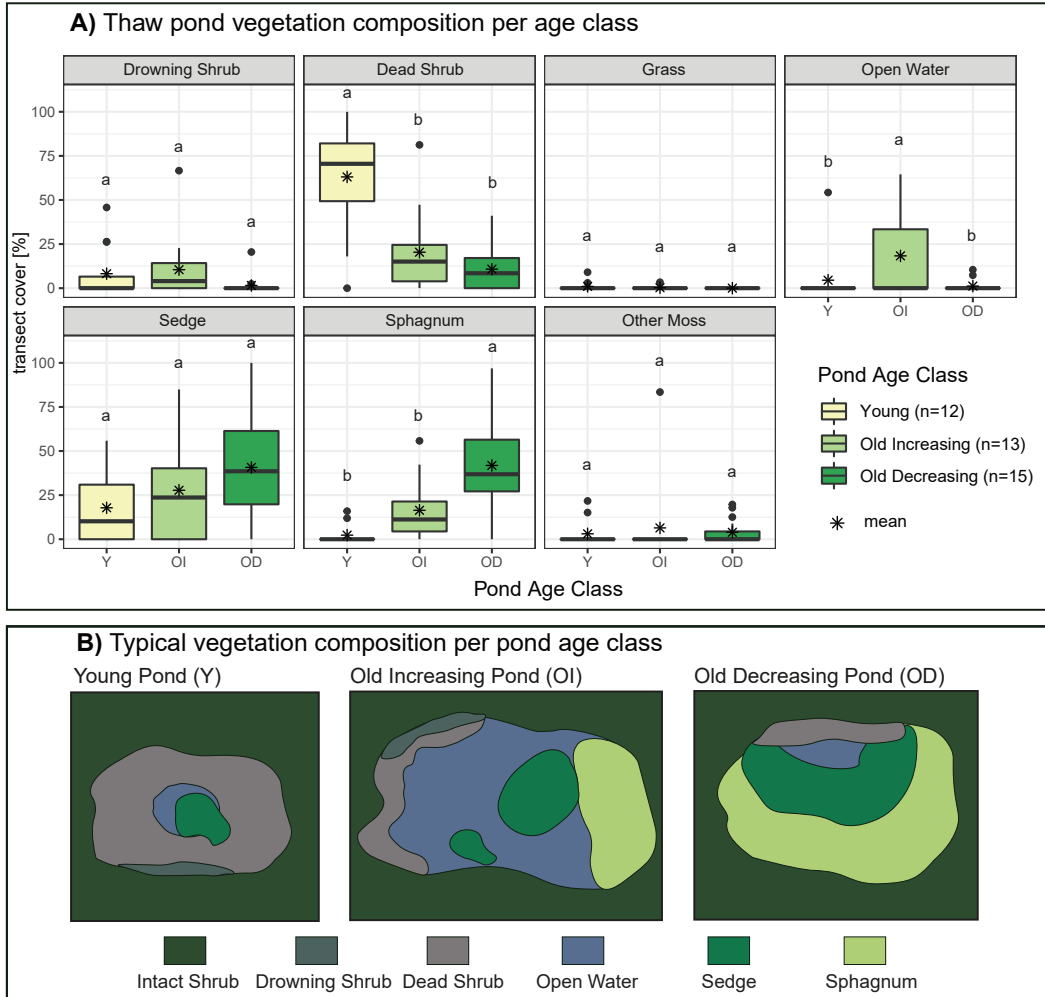


Figure 2.3) Vegetation Composition of Thaw Ponds. a) Boxplots of averaged transect cover of PFT classes in various pond age classes. Y = Young ponds; OI = Old Increasing ponds; and OD = Old Decreasing ponds. Asterisks indicate group mean. Small letters above bars indicate significance ($p < 0.050$) of pairwise contrasts (bars sharing a letter show no significant contrast), as determined by SIMPER analysis (see table S2.3 – S2.5). Order of vegetation classes (top left to bottom right) follows hypothesized order of succession. b) Visualization of typical vegetation composition per pond age class.

both contrasts), suggesting they established after pond formation (fig. 2.4a). As expected, dead shrubs in Young Ponds generally died more recently than those in Older ponds (fig. 2.4a). See table S2.9 - S2.10 for model specifications and pairwise contrasts.

Analysis of shrub distribution (recorded per quadrat), showed that living dwarf shrubs inside the pond perimeter were predominantly found in quadrats dominated by *Sphagnum*, and occasionally also in quadrats dominated by sedges and dead shrubs (fig. 2.4b). Pairwise contrasts indicated that they were more likely to be found on *Sphagnum* than on sedge (diff. = 0.46 ± 0.18 , $p = 0.035$), other contrasts were not significant. See table S2.6 - S2.8 for model specifications, RMSEs and pairwise contrasts. Where present, dwarf shrubs had sparser cover inside the pond perimeter (mean = 1.23 ± 3.89 %) than in the intact tundra vegetation surrounding the pond (mean = 41.11 ± 18.46 %) (table S2.21).

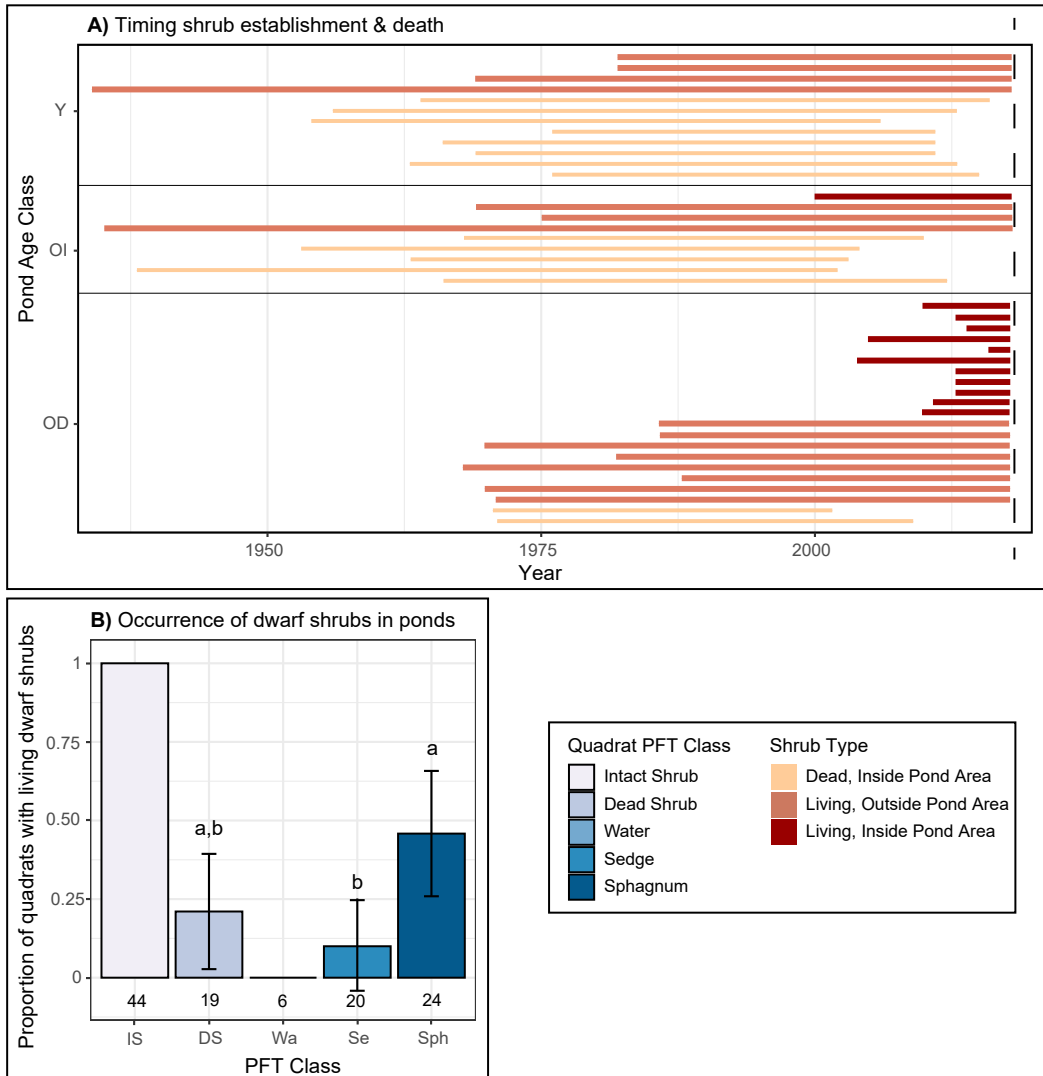


Figure 2.4) Shrub Distribution & Ages in Thaw Ponds. a) Presence of the three shrub types in Young ponds (Y), Old Increasing ponds (OI), and Old Decreasing ponds (OD). Bars represent an individual shrub’s life span (left end = year of establishment, right end = year of death). Dashed line represents moment of sampling (summer 2018). b) Proportion of quadrats per PFT class in which *B. nana* shrubs occurred. Error bars represent 95% CI. Small letters above bars indicate significance ($p < 0.050$) of pairwise contrasts (bars sharing a letter show no significant contrast). No error bars or pairwise contrasts are shown for Intact Shrub and Open Water due to complete presence/absence of *B. nana*. Numbers under bars represent number of samples per class.

2.4.4 Abiotic Conditions

We found that abiotic conditions in thaw ponds are significantly related to the dominant vegetation type (PFT Class) in the pond. When we ordered dominant vegetation types according to their association with the three pond age classes (fig. 2.3), this resulted in a clear pattern of permafrost degradation and subsequent recovery (fig. 2.5). Pond Age Class explained only a small additional amount of variance in Thaw Depth (TD), Water Table (WT) and Permafrost Position (PP). Relative Surface Elevation (RSE) and PP decreased progressively from intact shrub to dead shrub to open water (fig. 2.5a & 2.5g), coinciding with an increase in WT and TD (fig. 2.5c & 2.5e). Under *Sphagnum* vegetation, and to some

Rapid Vegetation Succession and Coupled Permafrost Dynamics

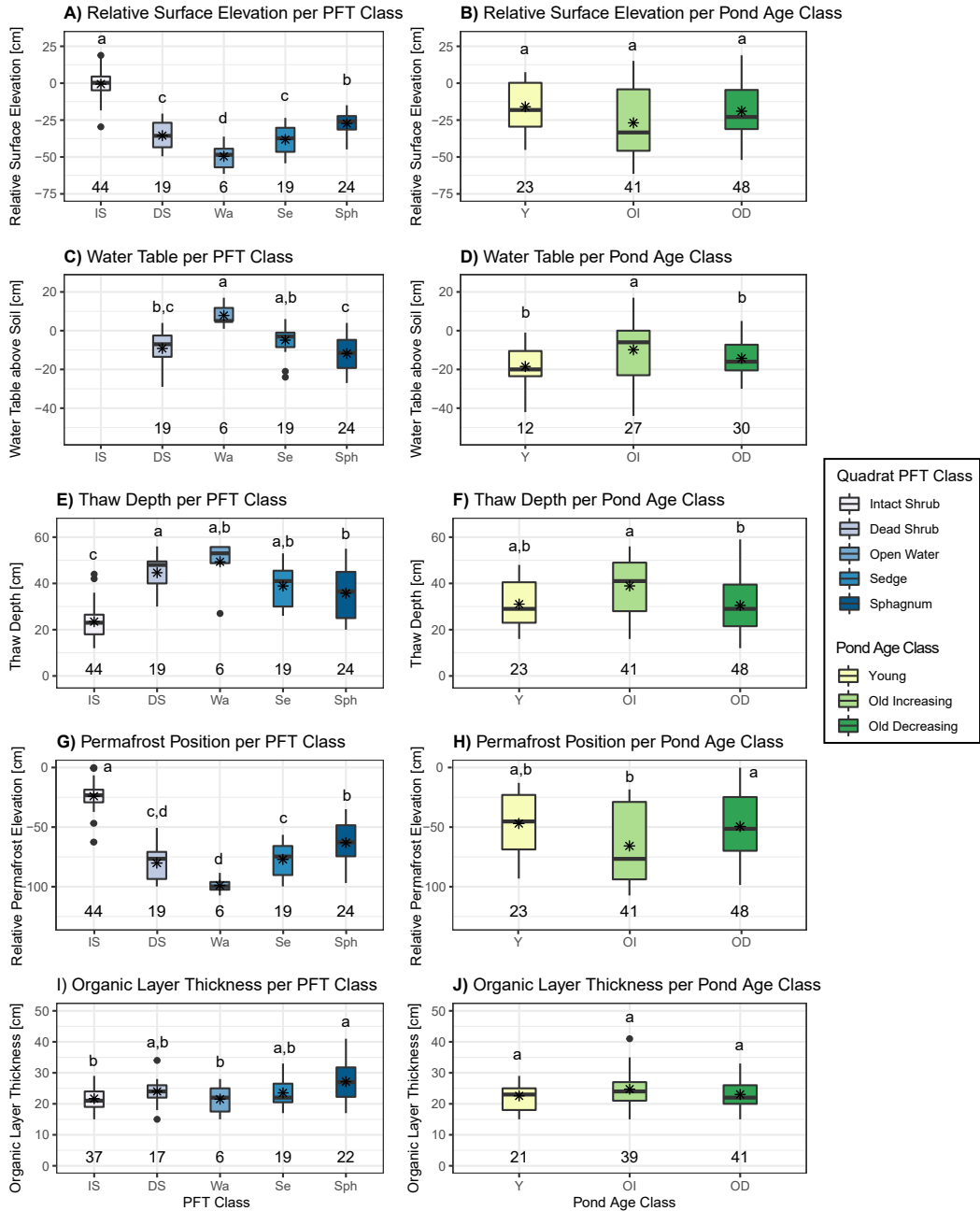


Figure 2.5) Abiotic conditions in quadrats of different PFT classes in ponds of different age classes. a) Relative Surface Elevation per PFT Class. b) Relative surface elevation per Pond Age Class. c) Water Table per PFT. d) Water Table per Pond Age Class. e) Thaw depth per PFT. f) Thaw depth per Pond Age Class. g) Permafrost position per PFT. h) Permafrost position per Pond Age Class. i) Organic layer thickness per PFT. j) Organic layer thickness per Pond Age Class. Small letters above boxes indicate significance ($p < 0.050$) of pairwise contrasts (boxes sharing a letter show no significant contrast). Numbers below the bars indicate number of quadrats per class. Number of observations differs for panels i and j due to limitations in peat core depths (i.e., TD < OLT). Y = Young ponds; OI = Old Increasing ponds; and OD = Old Decreasing ponds. IS = Intact Shrub; DS = Dead Shrub; Wa = Open water; Se = Sedge; Sph = *Sphagnum*.

extent sedges, RSE, PP and Organic Layer Thickness (OLT) increased again, whereas TD and WT decreased. No large differences were observed along the pond age class gradient (from Young to Old Increasing to Old Decreasing), however, in Old Increasing ponds PP was lower (fig. 2.5h) and WT and TD were higher (fig. 2.5d & 2.5f) compared to the other pond age classes. Pairwise contrasts indicate that relative to intact shrubs, PP is 56 cm lower under dead shrubs and 71 cm lower under open water ($p < 0.001$ for both contrasts). Compared to open water, PP lies 18 cm and 32 cm higher under sedge and *Sphagnum* respectively ($p = 0.021$ & $p = 0.003$ respectively). However, under both types of aquatic vegetation, PP remains significantly lower than under intact shrub vegetation ($p < 0.001$ for both contrasts). Pairwise contrasts for OLT indicate a significantly higher OLT under *Sphagnum* vegetation compared to intact shrubs (diff. = 5.63 cm, $p < 0.001$) and open water (diff. = 5.85 cm, $p = 0.038$). Table S2.11 - S2.18 contain model specifications, RMSEs and pairwise contrasts for all abiotic variables.

2.5 Discussion

The aim of this study was to determine whether thaw ponds display quasi-cyclic successional vegetation development linked to permafrost degradation and recovery and to provide a preliminary estimate of the timescales associated with thaw pond formation and recovery. Overall, our results from three lines of evidence (vegetation composition in thaw ponds of various age classes, abiotic conditions related to various PFT classes and dendrochronology on dwarf shrubs), suggest that formation and terrestrialization of thaw ponds can occur rapidly in shrub dominated tundra. Colonization by sedges was already observed in young ponds with ages of up to 8 years. Though a vegetation succession trajectory towards *Sphagnum* dominated vegetation in older, decreasing ponds was observed and recruitment of shrubs on *Sphagnum* carpets was demonstrated, it remains uncertain whether the previously dominant shrub vegetation can fully re-establish in thaw ponds and on what timescale. In the paragraphs below, we will elaborate on this interpretation of our findings.

2.5.1 Permafrost degradation

Our results suggest that thaw ponds may form and develop rapidly in the north-eastern Siberian lowland tundra. Young thaw ponds (up to 8 years in age, see table S2.22) were found to be mostly composed of dead shrubs (fig. 2.3). Presence of open water (fig. 2.3) and associated deeper thaw depths (fig. 2.5) were most common in older but still expanding ponds. Interestingly, we found that several of the young ponds already started declining again in open water extent between 2015 and 2018 (fig. 2.2, table S2.22). This suggests that complete degradation (the transformation from intact shrub vegetation to open water with dead shrubs) can occur within a time span of under eight years but may continue towards more advanced degradation on longer timescales. Similarly, formation of ponds was observed by Nauta et al. (2015) and Li et al. (2017) within 5 years following removal of shrubs. However, some degree of interannual variability in the open water extent of ponds cannot be ruled out, as the water level in thaw ponds also depends on specific weather conditions (Plug et al. 2008, Jones et al. 2009, Wolfe et al. 2011, Campbell et al. 2018). We found elevation differences in thaw ponds of around 50 cm compared to intact tundra vegetation, which is relatively low compared to elevation differences reported for thermokarst troughs (i.e. ice wedge degradation) by Kanevskiy et al. (2017), ranging from 50 to 110 cm. Li et al. (2017) found an even smaller elevation difference of up to 30 cm within a time span of 8 years after thaw pond formation following removal of shrubs. Existing data on the time span of degradation in the case of ice-wedges indicate that for 50 cm soil subsidence to occur, about ten years would be required (Jorgenson et al. 2015, Kanevskiy et al. 2017). In the case of ice-wedge degradation, such initial degradation may continue into advanced degradation on timescales of up to hundreds of years with soil subsidence of over 3 meters (Kanevskiy et al. 2017). We did not find evidence of such magnitudes of subsidence in thaw ponds, indicating that rates and magnitudes of subsidence associated with thaw pond formation may be comparable to shallow or initial forms of ice wedge degradation. Lateral expansion rates of ponds suggest that initial expansion of Young thaw ponds (mean = 0.52

m / yr) exceeds that of Old Increasing ponds (mean = 0.33 m / yr). For a mean observed transect diameter of 7.79 m for Old Decreasing ponds (including already terrestrialized areas), a time span of pond formation of approximately 20 years would be required based on observed pond lateral expansion rates. However, ponds were observed to attain highly variable sizes before starting to terrestrialize (fig. 2.2). Observed variability in soil subsidence and degradation rate may be attributed to different initial ground ice content. The amount and configuration of ground ice may also differ between the observed shallow, irregular shaped thaw ponds (ice lenses) and thermokarst troughs (ice wedges) (van Huissteden 2020). Interestingly, dead shrubs that died recently still occur in older decreasing ponds (fig. 2.4a). This confirms our observation that thaw ponds may not grow and decline uniformly (table S2.22). Overall, our results for thaw pond degradation in this lowland tundra ecosystem correspond well with reported rates of shallow ice-wedge degradation, indicating that they form on relatively short timescales compared to thermokarst troughs. However, this claim would need to be validated by longer term monitoring.

Dendrochronology on dead shrubs was used to more accurately identify the onset of thaw pond formation. Evaluating the year of death of dead shrubs, it became evident that in many cases, timing of thaw pond formation (as derived from satellite imagery, e.g. before 2010 or before 2015) predated the year of drowning of shrubs. This indicates that dead shrubs identified in older thaw ponds in this study likely represent more recent expansions of older thaw ponds. It is likely that the oldest parts of an older thaw pond are currently overlain by moss carpets, overgrowing remains of dead shrubs. Therefore, the years of death of the sampled dead shrubs may not represent the earliest onset of permafrost degradation, unless woody material is preserved and can be recovered from the oldest parts of a thaw pond. In addition, Arctic dwarf shrubs, especially in older individuals, may show extremely narrow or completely absent rings due to reduced growth activity (Hallinger et al. 2010, Wilmking et al. 2012, Myers-Smith et al. 2015b). Our study demonstrates that cross-dating of dead *Betula nana* shrubs is feasible. However, the detected year of death of dead shrubs should be considered a minimum estimate.

2.5.2 Aquatic vegetation succession in thaw ponds

Results from vegetation composition analysis confirm the hypothesized quasi-cyclic vegetation succession in our shallow thaw ponds. Older ponds are colonized by wetland vegetation, most notably *E. angustifolium* and *Sphagnum* mosses (fig. 2.3, table S2.21). *Sphagnum* mosses, in particular, were clearly associated with shrinking ponds (fig. 2.3). Earlier studies confirm this association between encroaching vegetation and a decline in pond or lake area (Andresen and Lougheed 2015, Jorgenson et al. 2015, Frost et al. 2018a). We found mean lateral shrinkage rates of Old Decreasing ponds of 0.43 m / yr, indicating that terrestrialization of ponds occurs at similar rates as their formation (an estimated 20 years based on observed transect diameters). This suggests a rapid transition of thaw ponds towards bog vegetation, despite highly variable shrinkage rates (fig. 2.2b). This observed succession and associated abiotic development correspond well to the initial degradation (dead shrubs), advanced degradation (open water), initial stabilization (sedges) and advanced stabilization (*Sphagnum*) phases reported by Jorgenson et al. (2015) and Kanevskiy et al. (2017) for ice-wedge degradation, and with vegetation successions derived from peat stratigraphy in boreal thermokarst ecosystems (Kuhry et al. 1993, Robinson and Moore 2000, Payette et al. 2004, Turetsky et al. 2007, Myers-Smith et al. 2008).

Observed sedge vegetation consisted mainly of *Eriophorum angustifolium* (table S2.21). *E. angustifolium* is known as a rapid colonizer of disturbed, waterlogged sites (Phillips 1954). Occasional presence of tussock sedge *E. vaginatum* in ponds (table S2.21) may be interpreted as a relic of pre-thaw vegetation. Seven out of 12 of our young thaw ponds contained varying amounts of *E. angustifolium* dominated sedge vegetation (fig. 2.3, table S2.21), which indicates that initial colonization by sedges can occur within a time span of eight years or less (the time difference between the earliest satellite images and the field measurements). In the case of ice-wedge degradation, such initial colonization and associated increase

in surface elevation in a thermokarst trough may occur within a decade after degradation (Jorgenson et al. 2015). Li et al. (2017) found establishment of sedges in thaw ponds resulting from the removal of *B. nana* shrubs within several years of thaw pond initiation. Additionally, narrow zones of grass vegetation, predominantly *Arctagrostis latifolia*, were found in Young and Old Increasing thaw ponds, often in association with dead shrubs and subsiding soil. This indicates that grasses may represent a short interval in the thaw pond vegetation succession. The early presence of grasses can be explained by their ability to utilize nutrients from recently thawed permafrost through deeper roots (Wang et al. 2017), while their lower tolerance to water explains the temporary character of the grass vegetation.

Sphagnum was most clearly associated with old decreasing ponds (fig. 2.3). Observed *Sphagnum* species in our study site are almost exclusively *S. obtusum* and *S. squarrosum* (Magnússon, pers. obs.), see also Iturrate-García et al. (2016). Both species are associated with relatively wet and mesotrophic to eutrophic sites (Daniels and Eddy 1990). Occasional presence of *S. subsecundum* and *S. balticum* was observed mainly in old decreasing ponds (Magnússon, pers. obs.), which may indicate a shift towards mesotrophic to oligotrophic conditions (Daniels and Eddy 1990, Kuhry et al. 1993). Earlier studies of peat stratigraphy in boreal thermokarst bogs indicate distinct succession of *Sphagnum* species associated with wetter conditions such as *S. angustifolium* and *S. riparium* upon degradation towards increasingly oligotrophic species associated with drier conditions such as *S. fuscum* (Kuhry et al. 1993, Zoltai 1993, Robinson and Moore 2000, Camill et al. 2009) and subsequent re-establishment of woody vegetation (Zoltai 1993, Robinson and Moore 2000, Camill et al. 2009, Routh et al. 2014, Treat et al. 2016). In our study region, *Sphagnum* species associated with oligotrophic, drier sites such as *S. lenense* and *S. rubellum* (Daniels and Eddy 1990) may be found in polygonal tundra (fig. 2.1e) but were not observed in the shallow, non-polygonal thaw ponds analysed in this study (Magnússon, pers. obs.). This suggests that the studied thaw ponds are in an early stage of *Sphagnum* bog succession. Our results correspond with an observed trend of replacement of woody vegetation by *Sphagnum* vegetation upon permafrost degradation in boreal ecosystems (Myers-Smith et al. 2008, Jorgenson et al. 2010, Jones et al. 2017). The relatively high summer temperatures (paragraph 2.3.1) of the study area due to a strongly continental climate and the relatively shallow nature of the studied ponds could explain the rapid terrestrialization of ponds in this ecosystem and similarity to processes described in boreal ecosystems. High summer temperatures have been associated with enhanced vegetation encroachment in thaw lakes (Roach et al. 2011) and succession from sedge to *Sphagnum* dominated vegetation in thermokarst bogs (Myers-Smith et al. 2008). In addition, high summer temperatures may enhance evaporation in shallow, isolated ponds (Wolfe et al. 2011, Campbell et al. 2018), further promoting vegetation encroachment through a lowering of the water table (Payette et al. 2004, Roach et al. 2011).

2.5.3 Permafrost recovery

Our results suggest that vegetation succession in thaw ponds is strongly related to permafrost dynamics. Sites characterized by colonizing wetland vegetation showed an increase in surface elevation and decrease in thaw depth and water table relative to sites with dead shrubs and open water, indicating initial recovery of permafrost. This effect was more pronounced under *Sphagnum* than under sedges. Differences in abiotic conditions among PFTs have also been described in polygonal tundra in the vicinity of the Kytalyk reserve by Minke et al. (2009) and Donner et al. (2007). Although the presence of PFTs can be interpreted as the result of abiotic gradients (Donner et al. 2007), changes in surface elevation and permafrost position can also be a result of vegetation development and peat formation (Minke et al. 2009, Shur et al. 2011). For instance, *Sphagnum* growing above the water remains dry during the summer, providing insulation to the permafrost below (Seppala 1988). Low thermal conductivity of dry *Sphagnum* mosses was demonstrated by Van Breemen (1995) and Soudzilovskaia et al. (2013). This improved insulation can lead to refreezing of thawed soil, as well as aggradation of ground ice resulting in frost heave (Shur et al. 2011). Frost heave further contributes to terrain rise above the water table and thereby to insulation (Seppala 1988). Our results confirm the tight coupling between

permafrost status and vegetation cover and indicate that vegetation succession, most notably towards a *Sphagnum* dominated stage, may play a key role in recovery of permafrost and microtopography. However, manipulation experiments would be necessary to demonstrate causal effects. The proposed thaw pond succession mechanism is visualized in figure 2.6.

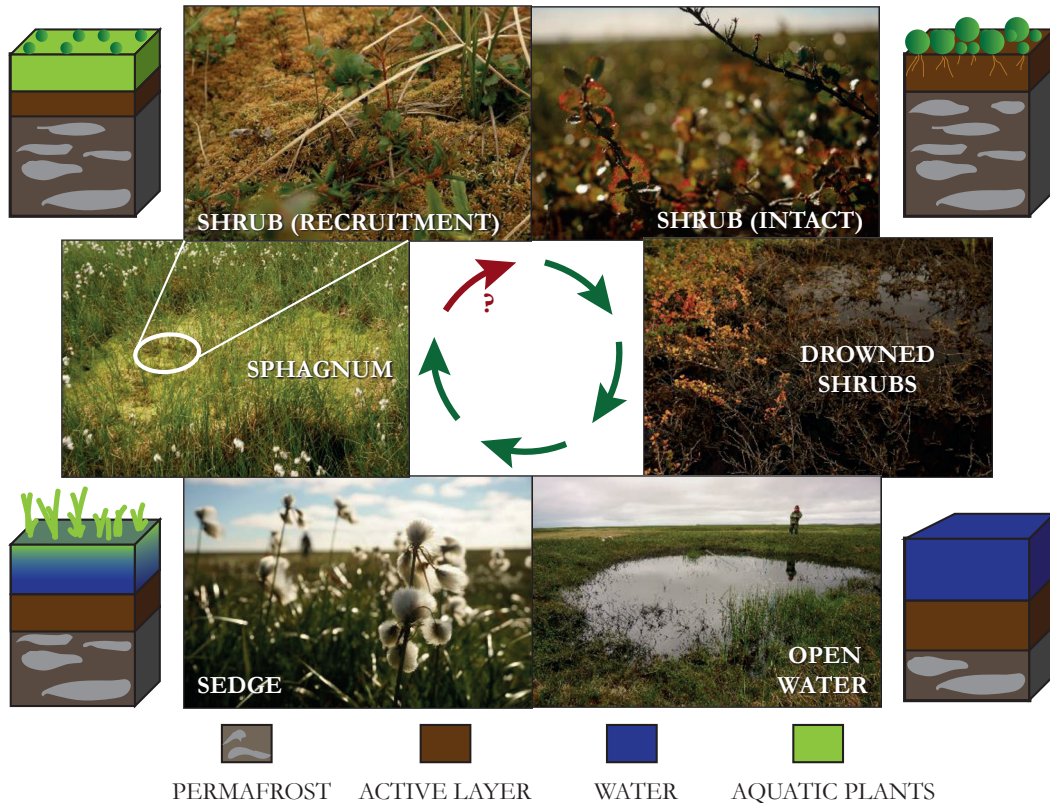


Figure 2.6) Schematic representation of our proposed mechanism of thaw pond formation (degradation) followed by vegetation succession (recovery). Through melting of ice-rich permafrost, local depressions are formed in which the initially dominant dwarf shrub vegetation drowns due to waterlogging. This is associated with soil subsidence, increased thaw depths, and formation of open water. The open water can be colonized by water-tolerant species such as sedges, which is associated with slight decreases in water table and thaw depth and slight increases in surface elevation. Colonization by *Sphagnum* mosses is associated with larger decreases in water table and thaw depth, and an increase of the surface elevation, resulting from organic matter accumulation and permafrost recovery. *Sphagnum* carpets can provide a substrate for reestablishment of dwarf shrubs, although it is presently unclear whether this initial reestablishment also leads to complete reestablishment of the former shrub-dominated vegetation.-

We found changes in permafrost position of +18 cm under sedge vegetation and +32 cm under *Sphagnum* vegetation, although the permafrost position remains significantly deeper than under intact shrub vegetation (fig. 2.5g). Quantification of ice content would be a valuable topic of future research to determine the relative influence of ground ice aggradation and frost heave as opposed to refreezing of previously thawed soil during successional development. Comparison of the increase in the relative surface elevation over the successional gradient from open water to *Sphagnum* (+23 cm) and the increase in organic layer thickness (+6 cm) would suggest that peat accumulation constitutes a relatively small component of surface heave, and that frost heave due to ice aggradation below the organic layer may play an important role in the recovery of the terrain. This is corroborated by Wang et al. (2019), who

observed a positive relation between ground ice content in the top 20 cm of permafrost and moss layer thickness and relative surface elevation in the Kytalyk lakebed site. An observed decrease in thaw depth (-9 cm) over the successional gradient from open water to *Sphagnum*, despite the increase in organic layer thickness, could suggest the formation of an ice rich intermediate permafrost layer (Shur et al. 2011). Detailed soil stratigraphical data may provide clearer insights into the relative role of peat accumulation, refreezing and ice aggradation.

The recovery rates observed in our shallow ponds seem high compared to those reported for thermokarst ponds formed after ice-wedge degradation. Complete recovery of permafrost after ice-wedge degradation has been reported to take tens to hundreds of years (Jorgenson et al. 2015, Kanevskiy et al. 2017). The fast recovery rates observed in our study may be related to the limited subsidence compared to thermokarst troughs (see paragraph 2.5.1). Early colonization by sedges and associated changes in abiotic conditions indicate that initial recovery of permafrost can already be initiated within sub-decadal timescales. Shrinking rates of older decreasing ponds suggest that complete terrestrialization of ponds can occur within 20 years (see paragraph 2.5.2) However, timescales associated with the full recovery of the permafrost underneath, if this occurs at all, remain uncertain. In addition, pond dynamics depend on pond characteristics such as size and depth and hydrological influences such as drainage, precipitation and evaporation (Jones et al. 2009, Campbell et al. 2018). Small, shallow ponds in particular may be prone to evaporative loss of surface water in a warming climate (Wolfe et al. 2011, Campbell et al. 2018). Lastly, it is unclear to what extent degradation or recovery of permafrost in thaw ponds is entirely cyclic. Kanevskiy et al. (2017) propose the use of the term “quasi-cyclic” development for ice-wedges, since recovery of ice-wedges often leads to a complete re-arrangement of ground ice patterns and accumulation of organic matter which in turn affects the ice-wedges’ susceptibility to future thaw. It is unclear whether such re-arrangements also occur in thaw ponds.

2.5.4 Re-establishment of dwarf shrub vegetation?

Our study is the first to explicitly look at re-establishment of dwarf shrubs in thaw ponds. At our study site, the living shrubs (both established from seeds or from ramets) found within thaw ponds were significantly younger than living shrubs outside of the thaw pond in intact shrub vegetation. This indicates that recruitment of dwarf shrubs, both through sexual reproduction and clonally, occurs in thaw ponds. Similarly, Huebner and Bret-Harte (2019) found increased shrub recruitment on bare soil in retrogressive thaw slumps compared to undisturbed tundra vegetation, which was attributed to reduced competition by surrounding vegetation and creation of suitable conditions for germination. However, whereas Huebner and Bret-Harte (2019) found the highest recruitment densities on more recently disturbed sites (1-10 years since disturbance), we found the majority of recruitment on *Sphagnum* carpets in older, decreasing thaw ponds. This may be explained by the ability of *Sphagnum* species to grow above the water table, generating the moist but unsaturated substrate needed for recruitment of dwarf shrubs (Bell and Bliss 1980, Huebner and Bret-Harte 2019). Frost heave may contribute substantially to the generation of unsaturated conditions (Seppala 1988).

It remains unclear however to what extent this recruitment can lead to a full recovery of the original shrub-dominated vegetation. The year of establishment of recruiting *Betula nana* within the thaw pond perimeter provides insight into the timescales associated with this potential recovery of shrubs. Most recruiting shrubs were up to nine years in age, with outliers of up to 18 years. This age range (2 – 18 years) of recruiting shrubs and their low cover compared to intact shrub quadrats (table S2.21) indicate that a potential full recovery likely may require multidecadal timescales after terrestrialization, although no reliable estimate can be made based on available data. It may also indicate an underrepresentation or absence of sites in an advanced state of vegetation recovery. Additionally, recruitment rates of most Arctic species, including *Betula nana*, may strongly depend on climatic pulses, and mortality among recruiting shrubs is high (Büntgen et al. 2015). This indicates that presence of young recruitment

does not necessarily mean successful recolonization of a thaw pond. Often, the year of establishment of recruiting *Betula nana* predates the death of dead shrubs from another site within the same pond, indicating again that both processes may occur simultaneously within the same thaw pond. Further tree-ring analysis of recruiting shrubs in thaw ponds may provide clearer insight into the timescales associated with the potential re-establishment of dwarf shrubs.

2.5.5 Implications for the Arctic greening trend and carbon balance

The balance between formation and recovery of thaw ponds on a landscape scale may have profound implications for the vegetation composition and greenhouse gas balance of lowland tundra ecosystems. Our results seem to suggest that thaw pond formation may occur very rapidly, whereas no sites in advanced state of recovery of the original dwarf shrub vegetation were observed. Such an imbalance could provide a potential explanation for local tundra browning observed around the study region by Epstein et al. (2018). Formation of open water features and subsequent death of shrub vegetation (Li et al. 2017) is associated with decreased NDVI (Raynolds and Walker 2016). As such, thermokarst has been suggested as a driver of Arctic browning (Phoenix and Bjerke 2016, Raynolds and Walker 2016). Conversely, colonization of a pond by aquatic vegetation may cause a local increase in NDVI (Zona et al. 2010) or other greenness indices such as Tasseled Cap Components (Raynolds and Walker 2016). Thus, the balance between thaw pond formation and recovery over a larger spatial scale may affect Arctic greening/browning dynamics.

The balance between permafrost degradation and recovery also affects the carbon balance of the lowland tundra ecosystem. Earlier research at the Kytalyk site has indicated that thaw pond formation can shift the lowland tundra ecosystem from a methane sink to a methane source (Nauta et al. 2015). Methane emissions were found to be higher for *Eriophorum* dominated sites than for drier, *Sphagnum* dominated sites (Van Huissteden et al. 2005, 2009). *Eriophorum* spp. and *Carex* spp. enhance methane emissions through gas exchange via aerenchyma (Ström et al. 2005, Ström et al. 2012). Conversely, *Sphagnum* may reduce methane emissions directly through methane oxidation facilitated by symbiosis with endophytic methane-consuming bacteria and presence of aerated surface peat (Sundh et al. 1995, Parmentier et al. 2011a). Presence of *Sphagnum* above the water table may further reduce GHG emissions by facilitating permafrost recovery through its insulation capacity (Seppala 1988, Soudzilovskaia et al. 2013). Lastly, *Sphagnum* may act as an ecosystem engineer during peat growth, enhancing soil carbon stocks (Van Breemen 1995, Robinson and Moore 2000, Myers-Smith et al. 2008, Siewert et al. 2015). Increasing organic layer thickness from open water to sedge to *Sphagnum* mosses (fig. 2.5i) suggests that peat accumulation occurs during the observed succession. While there is considerable debate about the carbon source/sink dynamics of thermokarst features over the long term (Robinson and Moore 2000, Turetsky et al. 2007, Van Huissteden and Dolman 2012), studies from boreal peatlands suggest that a full recovery of pre-thaw carbon stocks through peat accumulation may require centuries (Turetsky et al. 2007, Jones et al. 2017). Lastly, pond dynamics and associated greenhouse gas dynamics may depend on weather patterns determining precipitation and evapotranspiration (Plug et al. 2008, Jones et al. 2009) and drainage processes (Gorham 1991, Zona et al. 2010, Regmi et al. 2012). This may also explain the observed variability of expansion and terrestrialization rates of the studied ponds across different time intervals (table S2.22). Overall, thaw pond formation results in the release of methane, whereas advanced vegetation succession, especially colonization by peat-building *Sphagnum* mosses, is associated with lower methane emissions and net carbon storage.

To estimate the net contribution of thaw ponds to GHG emissions over the course of their development it is necessary to (i) determine net amounts of carbon emission and uptake associated with permafrost degradation and recovery respectively (Van Huissteden and Dolman 2012), (ii) determine whether there is a net trend of thaw pond formation and associated shrub decline or recovery and associated shrub expansion and lastly, (iii) how the rates of these two processes relate to climate. Additionally, efforts

should be made to determine exactly how abundant small-scale thaw ponds are across the Arctic since small waterbodies tend to be overlooked in remote sensing inventories (Grosse et al. 2008, Reynolds et al. 2019).

2.6 Conclusion

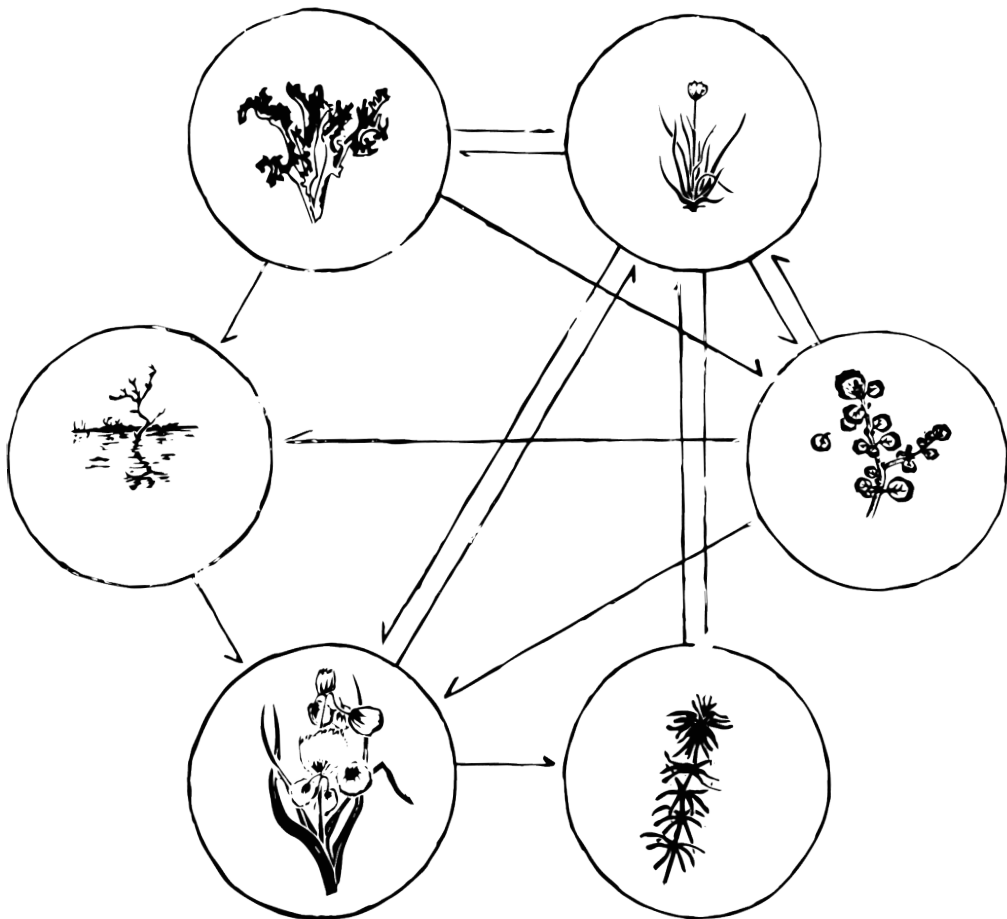
Our study is the first to characterize vegetation successions in thaw ponds in the Siberian Arctic. In this lowland tundra ecosystem, thaw ponds can develop in shrub-dominated lowland tundra within sub-decadal to decadal timescales, resulting in depressions with dead shrubs, standing water and thawing permafrost. Early colonizers such as sedges can establish within several years of formation and complete terrestrialization may occur within 20 years. Especially colonization by *Sphagnum* moss is associated with permafrost recovery, and *Sphagnum* carpets are important microsites for the re-establishment of dwarf shrubs. The succession mechanisms identified in shallow, irregular shaped thaw ponds in the Siberian lowland tundra correspond well with earlier work on ice-wedge degradation and boreal thermokarst bogs, although degradation and initial colonization seem to occur on relatively short timescales and thaw ponds show relatively shallow subsidence compared to ice-wedge degradation. Main challenges for future research will be to assess whether the relative rates of thaw pond formation and recovery will result in a net trend of tundra wetting and to determine the net greenhouse gas emission of thaw ponds over the course of their formation and recovery. The balance of tundra greening and wetting will have profound implications for the contribution of Arctic lowland tundra areas to greenhouse gas emissions.

3.

Shrub decline and expansion of wetland vegetation revealed by very high resolution land cover change detection in the Siberian lowland tundra

Rúna Í. Magnússon, Juul Limpens, David Kleijn, Ko van Huissteden, Trofim C. Maximov, Sylvain Lobry, Monique M. P. D. Heijmans

Published in *Science of the Total Environment*, 782, 146877 (2021).



3.1 Abstract

Vegetation change, permafrost degradation and their interactions affect greenhouse gas fluxes, hydrology and surface energy balance in Arctic ecosystems. The Arctic shows an overall “greening” trend (i.e. increased plant biomass and productivity) attributed to expansion of shrub vegetation. However, Arctic shrub dynamics show strong spatial variability and locally “browning” may be observed. Mechanistic understanding of greening and browning trends is necessary to accurately assess the response of Arctic vegetation to a changing climate. In this context, the Siberian Arctic is an understudied region. Between 2010 and 2019, increased browning (as derived from the MODIS Enhanced Vegetation Index) was observed in the Eastern Siberian Indigirka Lowlands. To support interpretation of local greening and browning dynamics, we quantified changes in land cover and transition probabilities in a representative tundra site in the Indigirka Lowlands using a timeseries of three very high resolution (VHR) (0.5m) satellite images acquired between 2010 and 2019. Using spatiotemporal Potts model regularization, we substantially reduced classification errors related to optical and phenological inconsistencies in the image material. VHR images show that recent browning was associated with declines in shrub, lichen and tussock vegetation and increases in open water, sedge and especially *Sphagnum* vegetation. Observed formation and expansion of small open water bodies in shrub dominated vegetation suggests abrupt thaw of ice-rich permafrost. Transitions from open water to sedge and *Sphagnum*, indicate aquatic succession upon disturbance. The overall shift towards open water and wetland vegetation suggests a wetting trend, likely associated with permafrost degradation. Landsat data confirmed widespread expansion of surface water throughout the Indigirka Lowlands. However, the increase in the area of small water bodies observed in VHR data was not visible in Landsat-derived surface water data, which suggests that VHR data is essential for early detection of small-scale disturbances and associated vegetation change in permafrost ecosystems.

3.2 Introduction

The Arctic is warming twice as fast as the global average, resulting in release of greenhouse gases (GHG) from thawing permafrost (Schuur et al. 2015, Meredith et al. 2019) and widespread vegetation change (Pearson et al. 2013). Shrubs in particular have been observed to expand across the Arctic, resulting in an overall greening trend (i.e. an increase in Normalized Difference Vegetation Index, NDVI) as evident from remote sensing studies (Tape et al. 2006, Epstein et al. 2013, Myers-Smith et al. 2015a, Bhatt et al. 2017, Epstein et al. 2018). Increased carbon uptake in shrub biomass may partially mitigate greenhouse gas (GHG) emissions from thawing permafrost (Epstein et al. 2012, McGuire et al. 2018). However, shrubs do not expand everywhere and show divergent responses to climatic drivers (Naito and Cairns 2011, Lin et al. 2012, Epstein et al. 2013, Martin et al. 2017, Bjorkman et al. 2020). Browning (i.e., a decrease in NDVI) is increasingly observed in various locations across the Arctic (Bhatt et al. 2017, Frost et al. 2020). The Russian Arctic is an underrepresented region in the context of ground studies and high-resolution remote sensing of Arctic shrub expansion in English scientific literature (Elmendorf et al. 2012a, Martin et al. 2017, Bjorkman et al. 2020), despite harboring approximately half of the total circumpolar area of shrub and tussock-shrub dominated tundra ecosystems (Raynolds et al. 2019). Dendrochronological studies in the Russian Arctic have shown a positive response of dwarf shrubs to climate warming (Forbes et al. 2010, Blok et al. 2011b), supported by several remote sensing studies that report increased NDVI and shrub expansion (Forbes et al. 2010, Lin et al. 2012, Frost et al. 2014, Nitze and Grosse 2016). However, browning related to permafrost degradation (Nitze and Grosse 2016) and increases in open water and wetland vegetation (Lin et al. 2012) have also been reported locally in the Russian Arctic. Mechanistic understanding of the drivers and impacts of browning is necessary to predict the response of this understudied region to a warming climate.

The lowland tundra of north-eastern Siberia is of particular interest in the context of Arctic climate change, due to its high ground ice content (Iwahana et al. 2014, Olefeldt et al. 2016, Nitzbon et al. 2020) and distinctly continental climate with high summer temperatures (Van der Molen et al. 2007), giving it the potential for rapid permafrost degradation (Nitzbon et al. 2020). This can result in disturbance of vegetation (Abbott et al. 2016), particularly in poorly drained lowland sites (Loranty et al. 2018a). As such, surface wetting as a result of abrupt thaw has been suggested as a potential cause of local Arctic browning (Phoenix and Bjerke 2016, Reynolds and Walker 2016), among other drivers such as wildfires, outbreaks of insects and pathogenic fungi and increased variability in winter temperature and precipitation (Phoenix and Bjerke 2016, Bjerke et al. 2017). An estimated 20% of the total circumpolar area contains ice-rich permafrost and is sensitive to abrupt thaw (Olefeldt et al. 2016). These findings illustrate the need to take abrupt thaw in ice-rich permafrost into consideration as a potential control on shrub dynamics and the Arctic greening trend. Earlier research in the Siberian lowland tundra suggests that shrub vegetation can be replaced rapidly by graminoids and peat moss vegetation through formation of small-scale, waterlogged permafrost collapses in previously dwarf shrub dominated vegetation (Nauta et al. 2015, Li et al. 2017, Magnússon et al. 2020). Comparable successions towards sedge and peat moss dominated vegetation have been observed as a response to ice-wedge degradation (Jorgenson et al. 2015, Kanevskiy et al. 2017). Such successions affect the GHG balance (Turetsky et al. 2020) and surface energy balance (Loranty et al. 2018a) of permafrost ecosystems.

Acquisition of satellite images in the Arctic is often limited by low sun-angles, short growing seasons, high cloud frequencies and logistic challenges in the acquisition of ground reference data (Beamish et al. 2020, Myers-Smith et al. 2020). Furthermore, greening dynamics derived from satellite-based vegetation indices such as NDVI are influenced by the spatial scale of satellite images and timing of acquisition, as well as non-vegetation related terrain properties such as water and snow dynamics. As a result, it remains a challenge to relate large scale greening dynamics to actual vegetation processes in Arctic ecosystems (Myers-Smith et al. 2020) and vegetation indices do not always capture actual vegetation cover dynamics (Loranty et al. 2018b). Increasing availability of very high resolution (VHR) satellite images have substantially advanced monitoring studies of Arctic ecosystems and interpretation of local greening dynamics, but are subject to similar heterogeneity in optical properties and seasonal timing (Beamish et al. 2020). This limits the potential for traditional change detection based on post-classification comparison, as misclassifications in individual images and spectral inconsistencies among images introduce false positives and negatives in change detection (Singh 1989, Aspinall and Hill 1997, Serra et al. 2003). Markov Random Field (MRF) regularization, introduced in computer vision by Geman and Geman (1984), is a potential remedy for false positives and false negatives in change detection using heterogeneous image time series. This method uses the inherent spatial relations between pixels in an image to enhance consistency of classification and can be extended to include temporal relations between pixels to improve classification consistency in timeseries (Solberg et al. 1996, Cai et al. 2014, Wang et al. 2015, Wehmann and Liu 2015, Gómez et al. 2016).

To advance our process-based understanding of Arctic greening and browning dynamics, we relate larger scale trends in vegetation greenness and surface water area to high resolution land cover changes of typical tundra vegetation types. Based on field observations and earlier studies, we expected coarse resolution browning trends in the Indigirka Lowlands to be associated with expansion of surface water bodies at the expense of shrub vegetation, followed by succession of aquatic species (Nauta et al. 2015, Li et al. 2017, Magnússon et al. 2020). First, we derived trends in vegetation greenness as measured by the Enhanced Vegetation Index (EVI) from the MODIS record and trends in surface water area from the Landsat-based Global Surface Water Map (Pekel et al. 2016) for the entire Indigirka Lowlands region. For a smaller study area, we classified a time series (2010 – 2019) of three VHR (0.5 m) GeoEye-1 and WorldView-2 satellite images into land cover classes representing distinct types of tundra vegetation (a.o. shrub-dominated vegetation). Our approach based on the use of VHR data has the

advantage that small-scale disturbances on shorter timescales can be captured that may not be evident from moderate (e.g. Landsat) to coarse resolution (e.g. MODIS) data (Grosse et al. 2008, Muster et al. 2013). We applied the Potts model (Potts 1952), a simple and widely used MRF regularization method, supported by validation data of areas of known change or no change in land cover. This allowed us to optimize and quantify accuracy of change detection using satellite images from different sensors and phenological stages. By explicitly quantifying not only net changes but also rates and potential trajectories of vegetation change, we contribute to process-based knowledge on shrub dynamics. We thereby improve our understanding of underlying mechanisms of vegetation change and greening in this understudied Arctic region.

3.3 Data & Methods

3.3.1 Study area

We studied greening and browning trends and surface water dynamics in the Indigirka Lowlands region (108,786 km²) in North-Eastern Siberia. Its main landscape units are drained thaw lake basins or “alases”, river floodplains, inter-alas Yedoma ridges and coastal marshlands (Fedorov et al. 2018). Vegetation in this low elevation region consists primarily of tundra vegetation, transitioning to taiga vegetation in the south (fig. 3.1a). We quantified land cover change in a focus area consisting of a single alas in the “Kytalyk” Nature Reserve in the Indigirka Lowlands in north-eastern Siberia (70°49'N, 147°29'E) near the town of Chokurdakh (fig. 3.1). This area is characterized by a shallow active layer overlying continuous permafrost of over 300 m thickness (Van Huissteden et al. 2005). Mean annual temperature is -13.4 °C, with an average July temperature of 10.3 °C (1981-2010). Mean annual precipitation is 196 mm, with 76 mm falling in June to August (1981-2010) (Trouet and Van Oldenborgh 2013). The Circumpolar Arctic Vegetation Map (CAVM) classifies this site as a mix of tussock-sedge tundra (type G4), erect dwarf shrub tundra and sedge-moss wetland, which are typical vegetation classes for low elevation areas with relatively high summer temperatures and high NDVI (Raynolds et al. 2019). This combination of landform, climate and vegetation types is representative for a major part of coastal north-eastern Siberia (Fedorov et al. 2018, Raynolds et al. 2019). Ground ice content around the study site is high (75 vol-% on average in the top 1 to 2 m of soil) (Iwahana et al. 2014, Wang et al. 2019) and the studied alas shows both ice-wedge degradation and formation of shallow, irregularly shaped thaw ponds most likely resulting from degradation of lenticular ground ice (Magnússon et al. 2020, van Huissteden 2020). Within the study area, elevated Yedoma remnants and pingos are characterized by tussock-sedge (*Eriophorum vaginatum*) vegetation. Lower elevation areas such as alases are characterized by slightly elevated shrub patches dominated by *Betula nana*, lichens and mosses, interspersed with waterlogged depressions characterized by *Eriophorum angustifolium*, *Carex* spp. and *Sphagnum* spp. In the study area, these waterlogged depressions tend to be orientated perpendicular to the local terrain slope, forming wide diffuse drainage lines of irregular width (see e.g. linear patterns in figure 3.1c directed towards the river). Lastly, floodplains are characterized by willow vegetation, grasslands and bare ground (Siewert et al. 2015). We selected our study site as a single, older (fig. 3.1b) alas, excluding rivers, human infrastructure, surrounding inter-alas Yedoma ridges and areas subject to occasional flooding due to high river discharge. This resulted in a total area of 2.33 km² (see fig. 3.1c).

3.3.2 Regional dynamics of vegetation greenness and surface water

To inventory greening/browning trends and surface water dynamics in the wider Indigirka lowlands region, we evaluated Terra and Aqua MODIS Enhanced Vegetation Index (EVI) products for 2000 to 2019 (products MOD13Q1 and MYD13Q1 v.006) (Didan 2015b, a). Similar to NDVI, EVI uses the ratio of red and near infrared reflectance, but applies corrections for variable aerosol concentrations and soil brightness (Didan 2015a). For each year, we selected all 16-day composite 250m resolution EVI images in June, July and August and calculated the annual maximum EVI to represent the peak growing season over the entire Indigirka Lowlands region (fig. 3.1a). Using the MODIS pixel

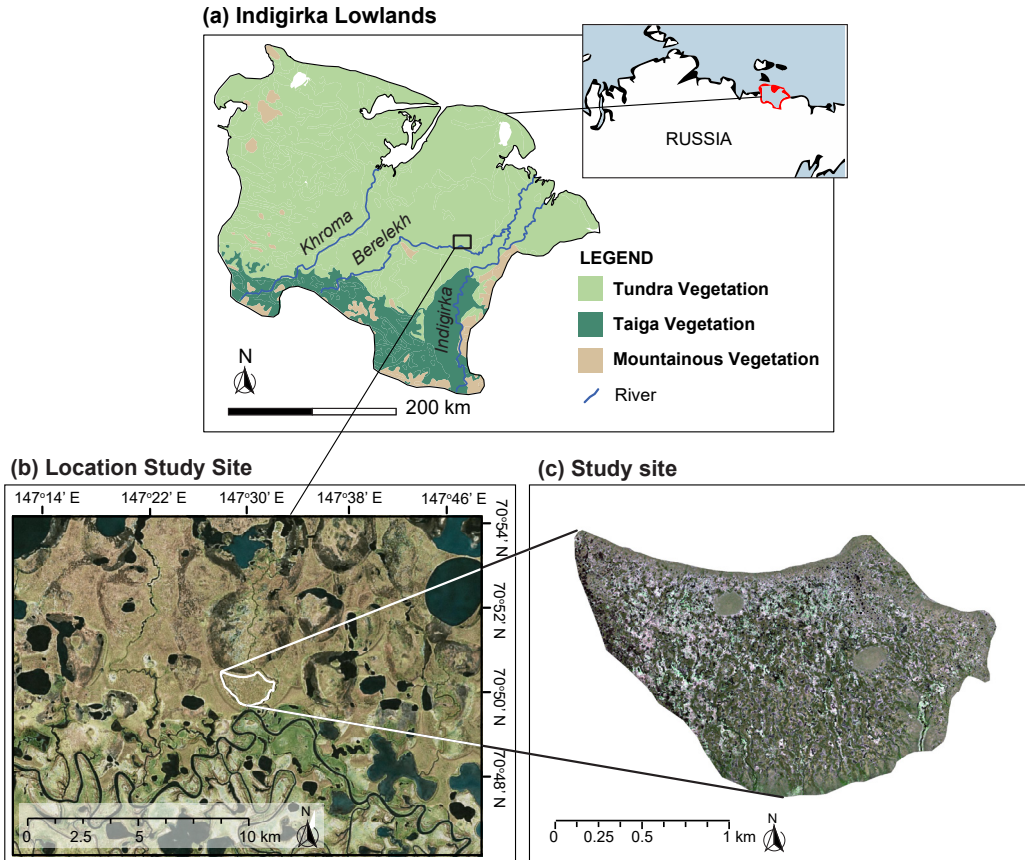


Figure 3.1) Location of the study area. a) Location of the Indigirka Lowlands and main vegetation zones and rivers as defined in Fedorov et al. (2018) b) Landsat image of the study region, which contains numerous small lakes, streams and alases, as well as larger lakes in the north. The selected alas represents an older episode of thaw lake drainage. The bottom half of the image shows the meandering Berelekh river and its floodplain. The study area is bordered by Pleistocene yedoma ridges in the southeast and southwest. Image courtesy of ESRI/DigitalGlobe. c) WorldView-2 satellite image of the study area. Worldview © MAXAR 2019. Light colours represent *Sphagnum* carpets, darker spots are surface water features. The two circular features are pingos with tussock vegetation. Numerous small ponds, areas with polygonal tundra and several diffuse drainage lines are visible.

reliability product we selected only “high” and “useful” quality pixels. Maximum EVI generally fell in late July. We calculated linear trends in maximum EVI over time for the entire MODIS observation period (2000-2019) as well as the period (2010 - 2019) that was used for land cover change analysis. Trends were quantified as slope coefficients over time using ordinary least squares linear regression. To assess significance of trends, slope coefficients were estimated using an ordinary bootstrap method with replacement ($n = 100$). We used the adjusted bootstrap percentile (Davison and Hinkley 1997) to calculate the 95% confidence interval (CI) of the slope estimate. EVI trends were reported as significant if the 95%-CI did not include zero. We then compared EVI trends within the smaller study area to those in the entire Indigirka lowlands region. Used software and packages are listed in text S3.2. In addition, we quantified the dynamics of various types of surface water (permanent, seasonal and ephemeral) for the Indigirka Lowlands as derived from the Global Surface Water Map (GSWM). The GSWM contains 30m resolution data on the presence and change dynamics of surface water as derived from the Landsat record between the 1984-1999 and 2000-2019 periods (Pekel et al. 2016).

3.3.3 Satellite data and distinguished land cover classes

To assess recent changes in land cover at our site in high spatial detail, we used three VHR, cloud-free satellite images from different sensors with different timing of acquisition within the growing season. We used a GeoEye-1 image from mid-August 2010, a WorldView-2 image from early July 2015 and a WorldView-2 image from early August 2019, with comparable resolution and bandwidths (see table S3.1). All three images were pan-sharpened to 0.5m resolution using the Gram-Schmidt algorithm in ArcMap 10.6.1 (ESRI 2019). Images were georeferenced manually, using permanent and recognizable features in the landscape. All three images achieved subpixel (0.5 m) georeferencing accuracy. Correction to top-of-atmosphere reflectance was performed for all three products according to Podger et al. (2011) for GeoEye-1 and Updike and Comp (2010) for WorldView-2. Since training data were available for each individual year, atmospheric correction was not deemed necessary for classification purposes (Song et al. 2001).

To study land cover dynamics, we distinguished six specific land cover classes (table 3.1). Similar distinctions for this study area have been used by Siewert et al. (2015) and Li et al. (2017). Distinctions were made between vegetation dominated by woody plants (dwarf shrubs), aquatic sedge communities (sedges), tussock sedge communities (tussock), peat mosses (*Sphagnum*) and lichens (lichen), with open water areas representing a final land cover class. The “open water” class included areas of mud with no considerable amount of living vegetation, since fluctuations in water level may cause large differences in open water extent in alases (Jones et al. 2009, Desyatkin et al. 2014, Fedorov et al. 2014).

3.3.4 Ground reference data









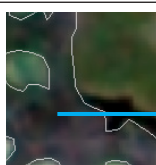



We used training, validation and test data for our classification workflow, which were created as polygon shapefiles in ArcMap 10.6.1 (ESRI 2019). Training sites were selected based on visual interpretation of satellite images by researchers familiar with the area. Wherever possible (i.e. sites showed no vegetation change), we selected the same pixels for all images to minimize inconsistencies in initial classification due to differences in training site selection. In support of classification, we calculated Bhattacharyya distance (Bhattacharyya 1946) as a metric of class separability based on the spectral data of training sites.

Validation sites were selected based on repeated photographs of plots with known coordinates from previous experiments in the study area (Li 2017), including both areas with known changes in vegetation composition and areas with no change (fig. S3.22). Photographs from the summer of 2011 were used for the 2010 image, while photographs from the same summer were available for 2015 and 2019. The same pixels were used in each year as validation sites. About 15% of pixels in the validation data showed a change in land cover class.

Test sites for 2019 were located in the field in August 2019 using a Real-Time Kinematic Global Navigation Satellite System (Hiper HR, TopCon, Tokyo, Japan) in a base and rover set-up using GPS and GLONASS satellites. The perimeter of 171 patches representing the land cover classes in table 3.1 was recorded with sub-centimeter accuracy. Test sites for 2015 and 2010 were copied from the test sites for 2019 if visual inspection of the images showed no indication of land cover change. The same pixels were used for the test set in all three years to avoid inconsistency of accuracy assessment due to the use of different sets of pixels. Wherever possible, validation and test sites were selected as adjacent patches including patch borders to avoid validating and testing only against highly representative patch centers. Boundaries between land cover classes in the validation and test sites were assigned based on visual interpretation of species composition in the field or from reference photographs. The amount of area covered by training, validation and test sites is summarized in table S3.2.

Shrub decline and expansion of wetland vegetation

Table 3.1) Land cover classes used for this study. Examples are fragments (1:1,500) of the 2015 WorldView-2 image to illustrate the appearance of the distinguished land cover classes. Fragments are pan-sharpened true color composites (red, green and blue band) of top-of-atmosphere reflectance values. Worldview © MAXAR, 2019. Photographs by Rína Magnússon.

Name	Description	Main Species	Example	Field Photograph
Shrub	Dwarf shrubs with moss and lichen understory, occurring on slightly elevated patches. Green shades in satellite images.	<i>Betula nana</i> , <i>Salix pulchra</i> , <i>Polytrichum</i> spp., <i>Dicranum</i> spp., <i>Flavocetraria cucullata</i> , <i>Cladonia</i> spp., <i>Peltigera</i> spp.		
Tussock	Mixed vegetation of tussock sedges, dwarf shrubs, mosses and lichens. Visible as light greyish areas in satellite images.	<i>Eriophorum vaginatum</i> , <i>Rhododendron tomentosum</i> , <i>Vaccinium vitis-idaea</i> , <i>Flavocetraria cucullata</i> , <i>Betula nana</i> , <i>Salix pulchra</i> , <i>Cladonia</i> , <i>Polytrichum</i> and <i>Dicranum</i> spp.		
Lichen	Lichen rich areas with little to no shrubs and/or tussock sedges. Visible as light yellow-green areas in satellite images.	<i>Flavocetraria cucullata</i> , <i>Cetraria</i> spp., <i>Cladonia</i> spp., <i>Vaccinium vitis-idaea</i> , occasionally <i>Betula nana</i> and <i>Salix pulchra</i> .		
Open Warer	Areas with open water or mud with no considerable amount of living vegetation. Visible as dark areas in satellite images.	None. Occasionally with dead vegetation (mostly shrubs).		
Sedge	Wet areas dominated by sedges. Visible as dark green areas in satellite images.	Aquatic sedges, predominantly <i>Eriophorum angustifolium</i> , and <i>Carex aquatilis</i> .		
<i>Sphagnum</i>	Peat moss carpets. Visible as light white to green areas in satellite images.	<i>Sphagnum</i> mosses, predominantly <i>Sphagnum obtusum</i> and <i>Sphagnum squarrosum</i> , often with partial cover of dried out aquatic sedges.		

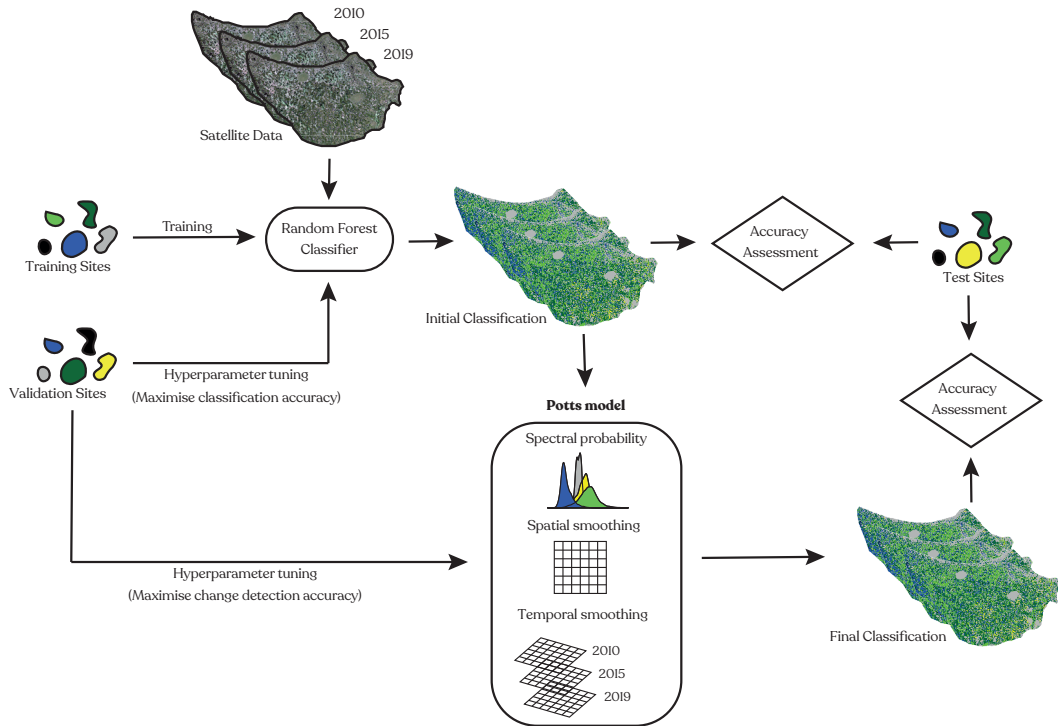


Figure 3.2) Schematic representation of workflow used for satellite data classification. Initial classification was derived from a random forest classifier using the training data. The validation data were used to tune the random forest based on overall classification accuracy, and to select the hyperparameters for the Potts model based on accuracy of change detection. The accuracy of the resulting final classification and the initial classification were calculated from the test data.

3.3.5 Classification and change detection

Image classification was performed in R version 3.6.2 (R Development Core Team 2019). Images were co-registered using bilinear interpolation and classified based on the training data with a Random Forest (RF). The hyperparameters of the RF classifier (number of trees and the number of variables randomly sampled as candidates at each split) were empirically set to 500 and 2 respectively for maximum overall accuracy of classification using the validation data.

In support of land cover classification of spectrally and seasonally heterogeneous images we used a spatiotemporal implementation of the Potts model (Potts 1952). Apart from class probabilities based on spectral data, the Potts model introduces a smoothing term based on the correspondence of a pixel's class with the classes of spatially adjacent pixels. We included an additional smoothing term representing the degree of correspondence of a pixel's class with the class values of temporally adjacent pixels (i.e., the same pixel in an earlier or later image). This way, the probability for a pixel belonging to a class that is different from its spatial neighbors, or different from the class it was assigned to in the previous or following image was reduced. After adjusting probabilities for each pixel in this way, the class of a pixel was set to that which then had the highest probability. This process was repeated using Iterated Conditional Modes (ICM) (Besag 1986) optimization until a stable classification was reached. A detailed description of the classification algorithm is provided in text S3.1. Used software and packages are listed in text S3.2.

We set the weights assigned to the spatial and temporal smoothing terms (β_0 and β_1) for optimal change detection using the validation data. Classification was performed for a range of potential values for the spatial ($\beta_0 = 0 - 2$ with steps of 0.2) and temporal ($\beta_1 = 0 - 3$ with steps of 0.5) smoothing weights. For the resulting suite of optimized classifications, change detection performance indicators described in paragraph 3.3.6 were calculated to select the final, optimal classification. Our workflow is summarized visually in figure 3.2.

3.3.6 Accuracy Assessment

Change detection accuracy was determined from change detection confusion matrices (Macleod and Congalton 1998) per combination of two images using the areas of known change and no-change from the validation data. Similar to conventional confusion matrices, these tabulate the predicted class transitions against the observed class transitions for each combination of two images. To assess the degree to which chosen parameters lead to over- or underestimation of change, we calculated Matthew's Correlation Coefficient (MCC) (Matthews 1975) from a confusion matrix for a binary reclassification into change/no-change areas. The MCC is a more reliable metric than overall accuracy in case of binary classification of unbalanced datasets (Chicco and Jurman 2020) and is calculated from the relative number of true positives (TP), true negatives (TN), false positives (FP) and false negatives (FN) in the confusion matrix. An MCC of +1 indicates perfect prediction, 0 represents no better than random prediction and -1 represents a perfect negative correlation between the prediction and the ground truth (eq. 3.1).

$$MCC = ((TP*TN)-(FP*FN)) / \sqrt{((TP+FP)*(TP+FN))*(TN+FP)*(TN+FN)} \quad \text{eq. 3.1}$$

In addition, from the change / no change confusion matrix we calculated the false discovery rate (FDR) of change detection as $FP/(FP+TP)$ and the false omission rate (FOR) as $FN/(FN+TN)$.

Final classification accuracy per individual image was calculated using a confusion matrix based on the predicted and observed class values for the test sites (Congalton 1991). For reference, baseline accuracies for the initial RF classifications without Potts model regularization were determined in the same manner. We calculated the total area of land cover classes per year as well as net transitions for both time periods (2010-2015 and 2015-2019). Class transition probabilities were calculated according to Muller and Middleton (1994) per combination of two images.

3.4 Results

3.4.1 Trends in vegetation greening and terrain wetting in the Indigirka Lowlands

Over the entire MODIS observation period (2000 – 2019), the Indigirka Lowlands region showed no pronounced overall greening/browning (mean trend = $0.67e^{-3} \text{ yr}^{-1} \pm 2.09e^{-3} \text{ yr}^{-1}$). Of all pixels for which trends could be calculated, 12.29% showed significant greening and 2.26% showed significant browning. However, distinct spatial differences related to landscape heterogeneity were evident (fig. 3.3b): mountainous vegetation (fig. 3.1a) east of the Indigirka river and coastal tundra showed relatively strong greening. Particularly strong and divergent EVI trends were found around lakes and in alases. The Landsat-derived GSWM indicates a widespread increase in surface water between the periods 1984-1999 and 2000-2019, although not in the study area (fig. 3.3a). The extent of permanent water features showed a relative increase of 9.96% and the extent of seasonal surface water increased more than eightfold (+846.70%). Increases in surface water appear concentrated in flood plains of major rivers and in alas terrain north of the river Berelekh and west of the river Khroma. Although no clear EVI trends were observed in the study area over the MODIS observation period (mean trend = $-0.86e^{-3} \text{ yr}^{-1} \pm 0.79e^{-3} \text{ yr}^{-1}$, fig. 3.3b), intensified browning was observed over the study period 2010 – 2019 (mean trend = $-8.77e^{-3} \text{ yr}^{-1} \pm 2.57e^{-3} \text{ yr}^{-1}$) and EVI decreased steadily (fig. S3.26e). Similar increases in browning

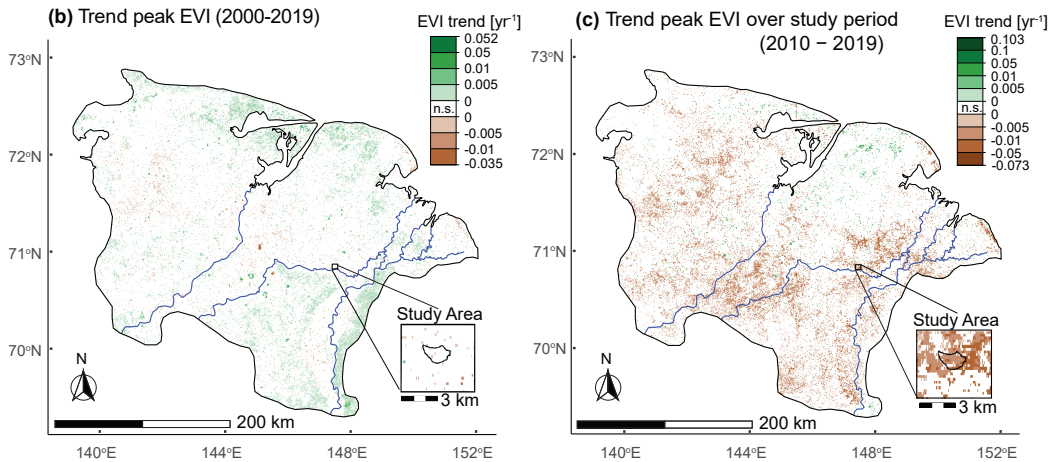
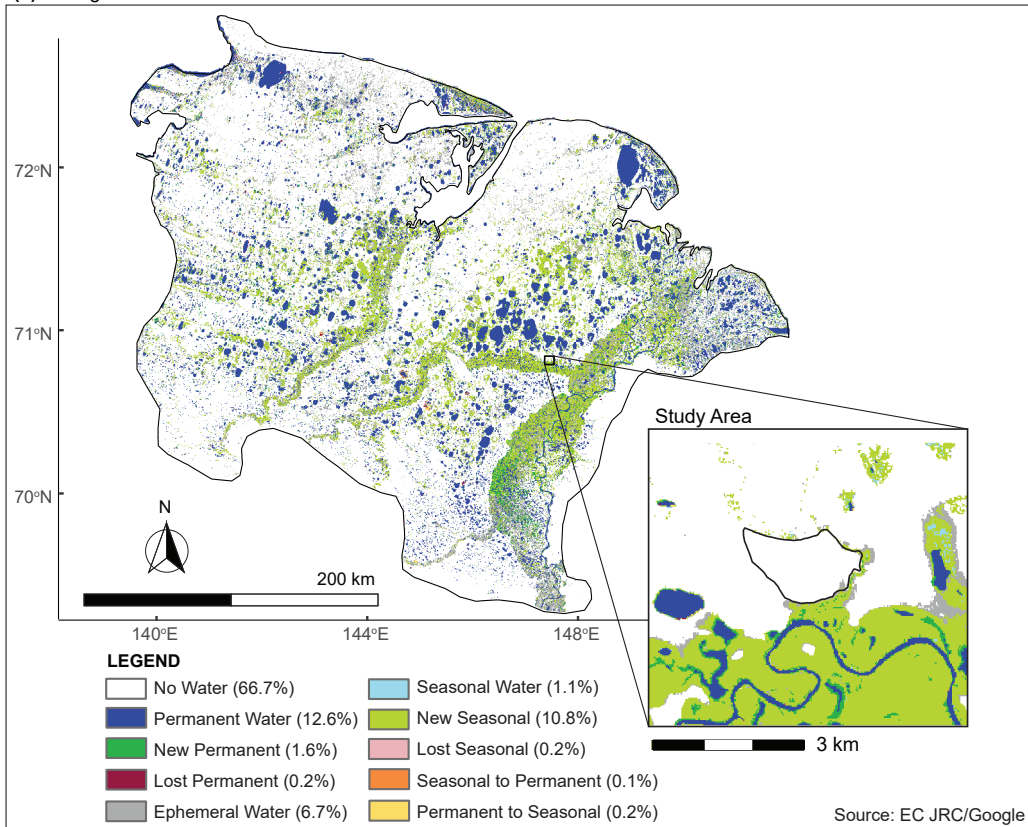
(a) Changes in Surface Water Presence between 1984-1999 and 2010-2019

Figure 3.3) Dynamics of MODIS peak growing season. Enhanced Vegetation Index and surface water presence in the Indigirka Lowlands. a) Surface water transitions between the periods 1984-1999 and 2000-2019. Numbers in legend indicate the percentage of the total area of the Indigirka Lowlands subject to that particular transition. GSWM data retrieved from <https://global-surface-water.appspot.com/map>, accessed 04-09-2020. b) Trend in MODIS maximum growing season EVI over the MODIS observation period (2000-2019). c) Trend in MODIS maximum growing season EVI over the high resolution land cover change analysis period (2010-2019). Larger versions of maps a – c are available in fig. S23-S25.

Table 3.2) Classification and change detection accuracy for baseline RF and Potts model classification. The overall classification accuracy is determined for each image separately using the class labels of the test data. The change detection accuracy is determined from class labels of the validation data for each combination of two images. Net predicted change in area per class is given for both the baseline RF classification and RF + Potts model classification.

	Baseline RF	RF + Potts Model
Overall Accuracy 2010	78%	91%
Overall Accuracy 2015	91%	93%
Overall Accuracy 2019	82%	91%
Change Detection Accuracy 2010 - 2015	69%	79%
Change Detection Accuracy 2015 - 2019	69%	76%
Change Detection Accuracy 2010 - 2019	63%	75%
Net Change Area Shrubs	-16%	-11%
Net Change Area Tussock	-18%	-16%
Net Change Area Lichen	-11%	-6%
Net Change Area Open Water	+34%	+49%
Net Change Area Sedge	+19%	+11%
Net Change Area <i>Sphagnum</i>	+29%	+22%

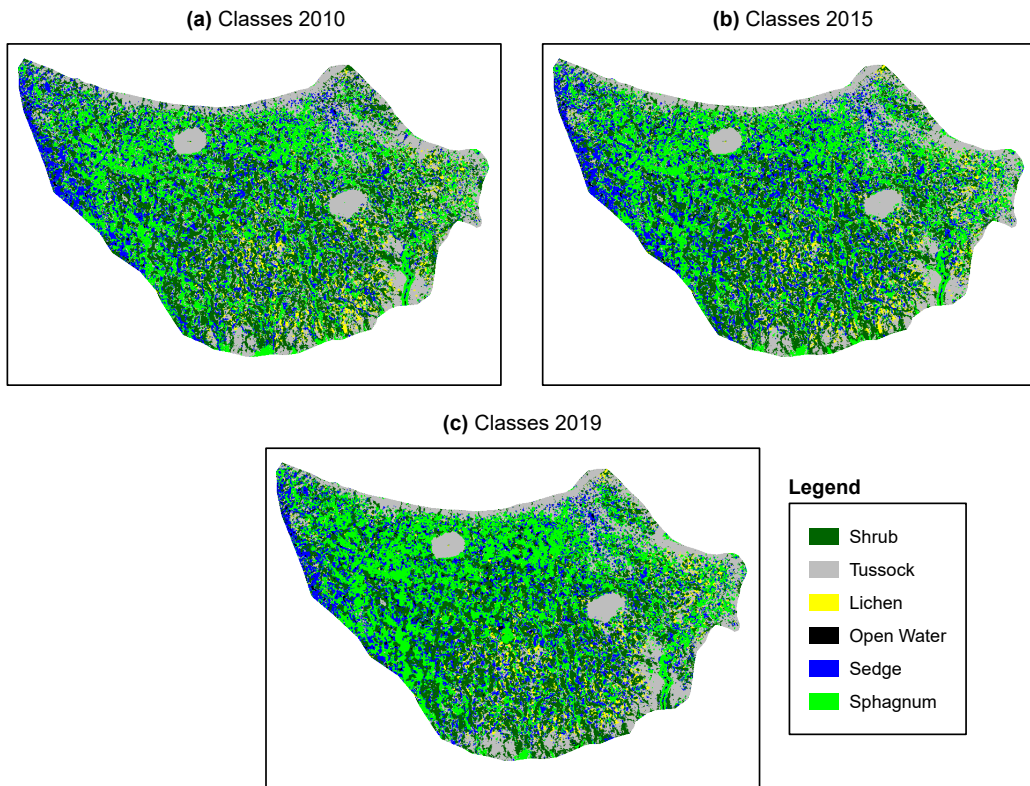


Figure 3.4) Classified images using optimized weights for the Potts model. a) Vegetation class map 2010. b) Vegetation Class Map 2015. c) Vegetation Class Map 2019. A substantial expansion of *Sphagnum* was visible, especially between 2015 and 2019. Higher elevation areas (edges of the alas, pingos) feature stable homogeneous tussock vegetation. The round tussock areas in the middle of the study area are pingos.

after 2010 were found across the Indigirka Lowlands (mean trend = $-1.99e^{-3} \text{ yr}^{-1} \pm 4.96e^{-3} \text{ yr}^{-1}$). 1.60% of pixels showed significant greening while 14.16% showed significant browning between 2010 and 2019. Variability in trends was high and particular sites, such as northern coastal lowlands, continued greening (fig. 3.3c).

3.4.2 Optimization of very high resolution image classification

VHR image classification accuracy and change detection accuracy were improved substantially after Potts model regularization. Initial RF classifications achieved overall classification accuracies of 78% (2010), 91% (2015) and 82% (2019). Change detection accuracies were between 62% and 68% per image pair. MCCs were 0.27 (2010 – 2015), 0.26 (2015 – 2019) and 0.30 (2010 – 2019) (table S3.8). Confusion matrices for baseline RF classifications (table S3.6) and spectral separability plots (fig. S3.1 -S3.3, table S3.3 - S3.5) indicate that the extent to which particular classes could be distinguished using only spectral data varied among images as well as classes. *Sphagnum* and shrub had high spectral separability and accuracy across images, whereas misclassifications were relatively frequent for lichen and for sedge in 2010 and for sedge and open water in 2019.

Potts model regularization with spatial smoothing weight $\beta_0 = 1.2$ and temporal smoothing weight $\beta_1 = 3$ converged within the set limit of 30 iterations and achieved change detection accuracies of 75% - 79% per image pair, an improvement of 7- 12% relative to the baseline RF classification. This resulted in final overall accuracies of over 90% in each year, an improvement of 2 – 13% relative to the baseline RF classification (table 3.2). MCCs improved substantially to 0.66 (2010 – 2015), 0.45 (2015 – 2019) and 0.66 (2010 – 2019). In particular, false positives in change detection, as evident from the FDR, were reduced substantially from 58% to 25% over the period 2010 – 2019 with Potts model regularization. This indicates that the baseline RF classification likely substantially overestimates change, confirmed by the generally higher net changes evident from the baseline classification (table 3.2). Further increase of the spatial and temporal smoothing weights did not improve change detection or MCC or change detection accuracy anymore (table S3.8 – S3.10, fig. S3.16 – S3.18). All accuracies, MCCs, convergences and other assessment criteria are visualized as heatmaps per unique combination of β_0 and β_1 in fig. S3.4 – S3.18. All results shown hereafter are for a Potts model classification with $\beta_0 = 1.2$ and $\beta_1 = 3$.

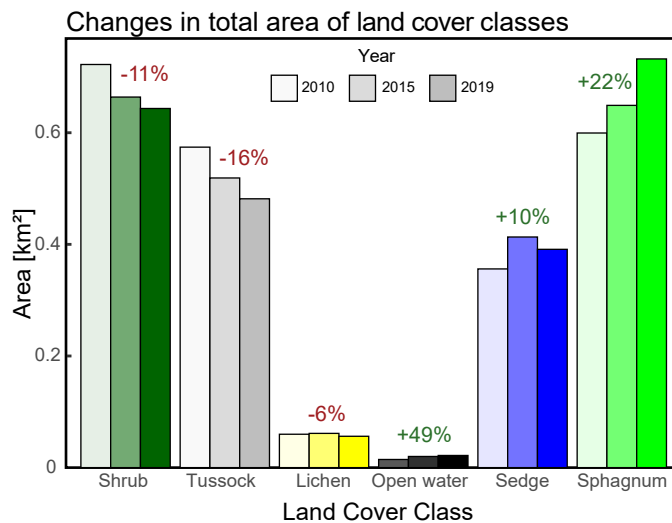


Figure 3.5) Total area of each land cover class in each year for the selected Potts model classification. Numbers above sets of bars represent change in total area over 2010 – 2019 relative to the total area in 2010.

3.4.3 Final Classifications

Final classifications in figure 3.4 showed several larger areas of stable tussock vegetation, especially on slightly elevated pingos, levees of small streams and edges of the lakebed. Two larger zones of sedge dominated vegetation were identified at the left and top right of the study area. In the center of the alas, patches of aquatic species (sedge and *Sphagnum*) as well as open water increased at the expense of shrub, tussock and lichen vegetation. *Sphagnum* showed the most pronounced expansion. Confusion matrices for classified data and test data indicated that after implementation of the Potts model with the selected parameters, most land cover classes achieved user's and producer's accuracies of > 80% (table 3.2). Lichen remained relatively poorly separable from shrub and tussock, potentially explained by the overlap in species composition between these three classes (table 3.1). In the 2019 image, open water was frequently misclassified as sedge, despite high separability of open water and sedge in the other images. This indicates year-to-year variability in class separability, potentially related to hydrological conditions (the early summer of 2019 was relatively dry and warm, fig. S3.26).

3.5 Observed land cover change

Comparison of the total area of each class in the three images indicated that shrub and tussock vegetation decreased whereas open water, sedge and *Sphagnum* increased (fig. 3.5), to an extent that the dominant class changed from shrub to *Sphagnum* by 2019. *Sphagnum* increased consistently, whereas open water and sedge increased mostly between 2010 and 2015, potentially related to the earlier date (early July) of the 2015 image compared to 2010 and 2019 (early August). Tussock vegetation showed a larger percent decline than shrubs and lichen, although similar to shrub in terms of total area affected (fig. S3.19).

In terms of total area affected, the most prominent transitions were from shrub to tussock, shrub to sedge, tussock to shrub, tussock to sedge, tussock to *Sphagnum* and sedge to *Sphagnum*. In addition, open water had a high transition rate to sedge, and lichen had a high transition rate to tussock, although these changes amounted to a small net area (fig. S3.19). Such transitions from open water to sedge to *Sphagnum* were also evident in the validation sites (fig. S3.21), and the validation sites displayed a similar tendency of shrub decline and increase of sedge and *Sphagnum* (fig. S3.20). Of all areas transitioning to open water between 2010 and 2019, 74% formed in shrub vegetation, 13% in sedge vegetation and 8% in tussock, indicating that dwarf shrub vegetation in this area may be especially prone to formation of open water features.

3.4.5 Transition probabilities

Figure 3.6 shows that transition probabilities were similar across the different time periods. Shrubs, sedge and *Sphagnum* were relatively stable classes, whereas tussock, lichen and open water showed a higher probability of transitioning to another class. The transition from open water to sedge was most prominent, with a probability of 45% over 2010 - 2019. Shrub and tussock also showed high transition probabilities to sedge, whereas lichen showed a high probability of transitioning to tussock. Sedge and tussock tended to transition to *Sphagnum*, whereas *Sphagnum* is a relatively stable class. Tussock had structurally high transition probabilities, except to and from open water. For 2015-2019 we found a lower probability of open water transitioning to sedge and higher probability of sedge transitioning to *Sphagnum* than for 2010-2015.

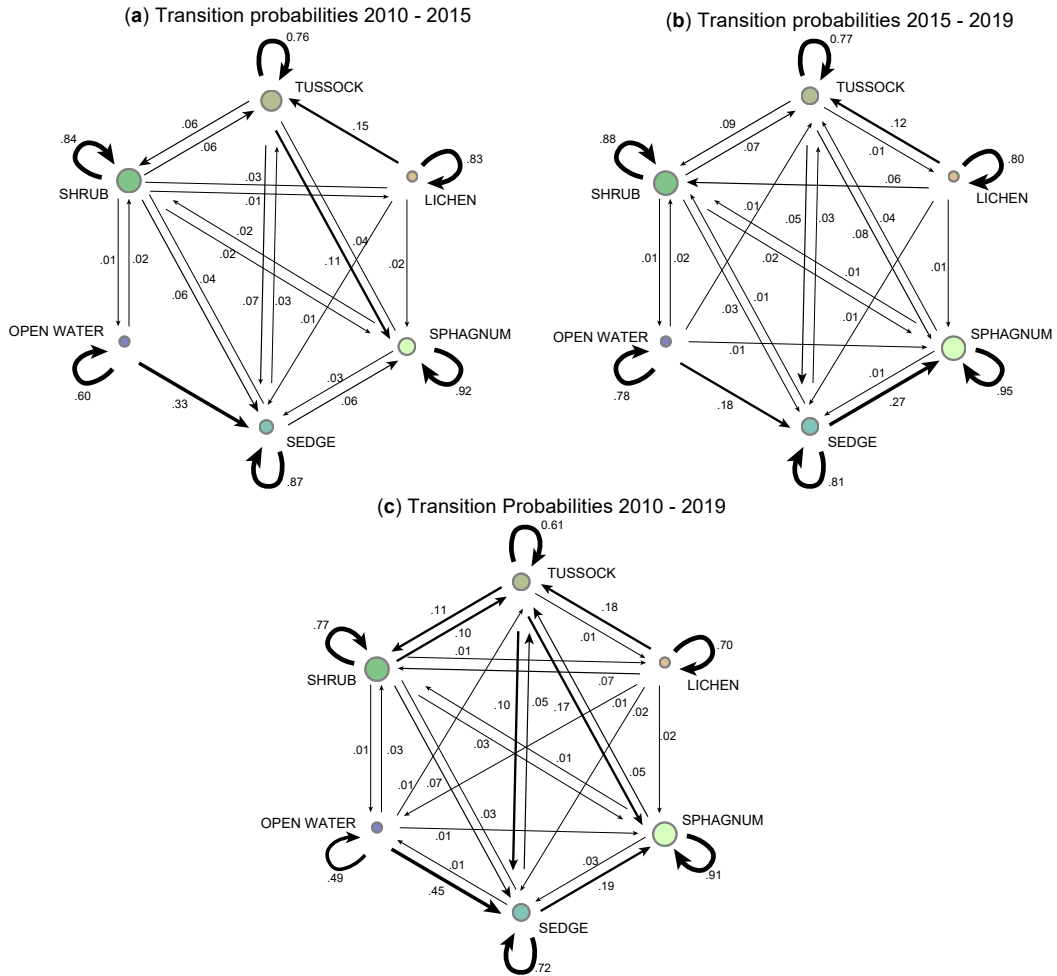


Figure 3.6) Markov Chain diagrams for observed transition probabilities (0 – 1). Separate diagrams were generated for a) 2010 – 2015, b) 2015 – 2019 and c) 2010 – 2019. The sizes of the circles representing each land cover class are proportional to the total area of that class. The thickness of arrows is proportional to the transition probability they represent (i.e. from one class to another). Probabilities < 0.01 are not shown.

3.5 Discussion

3.5.1 Regional trends in vegetation greening and surface water dynamics

3.5.1.1 Dynamics of surface water and vegetation greenness in the Indigirka Lowlands

The Landsat-derived GSWM (Pekel et al. 2016) shows large increases in the extent of permanent surface water and particularly in the extent of seasonal surface water. The floodplains of major rivers were identified as hotspots of surface water increase and showed local browning, particularly in the taiga zone along the Indigirka south of the study site (fig. 3.3b-c). This may be (partially) explained by recent flood events after years with anomalously high snowmelt (fig. S3.26d), resulting in detrimental effects on local vegetation (Tei et al. 2020). 2017 in particular showed extensive flooding (Tei et al. 2020) and record low regional EVI (fig. S3.26e). Shkolnik et al. (2018) predicted a 2 – 5% increase in annual flooded area for Siberian rivers for the coming decades, with increases up to 10% in the Indigirka Lowlands. This

suggests a continuation of the observed wetting trend and associated browning events observed in floodplains, with potential implications for local ecosystems and their carbon balance.

Trends in MODIS EVI indicate that greening and browning dynamics vary over space and time in the Indigirka Lowlands. Recent browning was common in floodplains and in alas terrain north of the rivers Berelekh and Khroma, while greening was more commonly observed in the coastal tundra areas and on inter-alas terrain (*sensu* Fedorov et al. 2018) and mountainous terrain along the floodplains of the Indigirka (fig. 3.3b, fig. 3.1). This hints at a divergent development of browning in lowland terrain vs. greening in upland and coastal terrain. Individual alases and thaw lake margins also show particularly pronounced changes in opposing direction, often in concert with lake expansion or drainage (fig. 3.3 & S3.23-S3.24). This suggests an important role of lake hydrology in local greening dynamics, as observed earlier in coastal Alaska and in the Lena delta. Here recently drained lakes showed rapid increases in biomass and NDVI (Zona et al. 2010, Regmi et al. 2012, Nitze and Grosse 2016), whereas browning was observed on wetting terrain such as margins of expanding thaw lakes, eroding coasts and areas affected by ice-wedge degradation (Raynolds et al. 2014, Nitze and Grosse 2016, Raynolds and Walker 2016). Such events may also be a direct result of terrain wetting rather than an indication of vegetation changes, as vegetation indices based on infrared reflectance are sensitive to water (Goswami et al. 2011, Lin et al. 2012, Raynolds and Walker 2016, Myers-Smith et al. 2020).

Temporal dynamics of EVI across the Indigirka Lowlands suggest a trend break, with intensified local browning and high year-to-year variability in EVI after 2010 (fig. 3.3b-c, fig. S3.26e). Similar trend breaks and increased variability are observed in other Arctic regions, as climate extremes and other browning causes increase in frequency (Phoenix and Bjerke 2016, Frost et al. 2020). Accordingly, increased variability in EVI and intensified browning in the Indigirka Lowlands was accompanied by a period with high variability in weather conditions, including extreme summer precipitation and snow height and spring heatwaves (fig. S3.26). Increases in height and duration of snow cover in particular may have contributed to browning by delaying the onset of vegetation growth (Bieniek et al. 2015, Phoenix and Bjerke 2016), potentially amplified by subsequent flooding (Tei et al. 2020) or thermokarst activity (Phoenix and Bjerke 2016, Lara et al. 2018). Observed land cover changes in the study area support this potential explanation (see paragraph 3.5.1.2 below).

3.5.1.2 Comparison of VHR land cover change and MODIS derived trends

Analysis of MODIS-derived Enhanced Vegetation Index indicated that our study area is representative for the Indigirka Lowlands in terms of range and dynamics of vegetation greenness but shows relatively strong browning in the past decade (fig. 3.3c & S3.26e). Relating large scale trends in EVI to local vegetation processes remains challenging, due to mismatches between the spatial scale of satellite data and small-scale vegetation patterns and confounding influences such as local hydrological dynamics (Myers-Smith et al. 2020). Despite the small spatial scale on which changes in plant functional type were expressed (fig. 3.4), observed land cover change (fig. 3.5) would be consistent with the observed browning trend. A decline in shrub cover was evident from high resolution change analysis, which is generally strongly related to spectral indices of vegetation greenness (Tape et al. 2006, Forbes et al. 2010, Epstein et al. 2013, Myers-Smith et al. 2015a, Raynolds and Walker 2016). Additionally, local small-scale wetting may have reduced EVI, both directly (Goswami et al. 2011, Lin et al. 2012, Raynolds and Walker 2016, Myers-Smith et al. 2020) and through shrub mortality and shifts towards aquatic vegetation types upon inundation (Nauta et al. 2015, Magnússon et al. 2020). Alternative potential browning causes include event-based disturbances such as outbreaks of pathogens, increased herbivory, coastal erosion, salt inundation, structural changes to surface hydrology and fires (Phoenix and Bjerke 2016, Bjerke et al. 2017, Myers-Smith et al. 2020). Lastly, browning can be related to gradual changes such as a reversal of greening causes and gradual deterioration of growing conditions (Bieniek et al. 2015, Phoenix and Bjerke 2016, Myers-Smith et al. 2020). As EVI decreases in the study area were fairly consistent between

2010 and 2019 despite variability in weather conditions (fig. S3.26e) and no obvious alternative browning mechanisms (e.g. observed fires, pathogen outbreaks or increased herbivory) were observed during the study period, wetting and associated land cover changes seem a likely explanation of observed recent browning. This raises the question whether the processes observed in the study area (small-scale thermokarst, shrub decline and transition towards wetter vegetation types) may also have contributed to larger scale intensified browning in the Indigirka Lowlands over the past decade (fig. 3.3c).

Although the GSWM confirmed widespread surface wetting throughout the Indigirka Lowlands, it indicated practically no occurrence of permanent or seasonal surface water in the study area (fig. 3.3a), despite the pronounced increase in open water evident from VHR images (fig. 3.5). Magnússon et al. (2020) found that thaw ponds in the study area are generally very small ($< 100 \text{ m}^2$) and show rapid terrestrialization. Other manifestations of thermokarst (ice-wedge degradation, expansion of diffuse drainage gullies) were also observed on much smaller spatial scales (fig. 3.7b,d) than the resolution of the GSWM. Underdetection of abundant smaller ponds in thermokarst ecosystems is a known phenomenon (Grosse et al. 2008, Muster et al. 2013), which implies that surface water expansion in the Indigirka Lowlands may be larger than Landsat-derived GSWM suggests. Multi-scale analysis of vegetation greenness and surface water presence in thermokarst ecosystems, e.g. using WorldView, Landsat/Sentinel and MODIS data, is a promising direction for further research. Our results suggest that moderate to coarse resolution analysis of changes in surface spectral properties do not accurately reflect the effects of abundant small-scale thermokarst processes on shorter timescales and highlight the importance of high-resolution data for early detection and monitoring of these potentially influential phenomena.

3.5.2 Identified land cover change trajectories and implications for Arctic vegetation dynamics

3.5.2.1 Abrupt permafrost thaw as driver of shrub decline?

We found a decrease in the total area of shrubs, which is in contrast with the panarctic trend of shrub expansion. Formation and expansion of water bodies predominantly took place in shrub vegetation. Spatially, open water expansion was mostly expressed as formation of small, isolated ($< 100 \text{ m}^2$) water bodies in shrub patches (see fig. 3.7c, video S3.1) and expansion of open water and sedge area into the edges of shrub patches (fig. 3.7a-b, video S3.1), often along the margins of diffuse drainage lines. As a result, most shrub patches in our study area diminished in size (fig. 3.4). Shrubs in the study area show a relative enrichment in near-surface (top 0 – 20 cm of permafrost) ground ice content (Wang et al. 2019), making abrupt thaw due to loss of ground ice a likely explanation for the observed expansion of open water at the expense of shrub patches. Abrupt thaw occurs when excess ground ice is exposed to above zero temperatures due to a deepening of the active layer and melts, causing subsidence of the soil surface (Jorgenson et al. 2006, Schuur et al. 2015, Olefeldt et al. 2016) and pond formation in poorly drained, flat terrain (Nauta et al. 2015). The resulting net area displaying a transition from shrub to open water over nine years was small compared to that of other transitions (fig. S3.19), but transitions from shrub to water were relatively accurately classified and somewhat underdetected (table S3.11-S3.13). This suggests that surface water expansion in shrub patches may be more pronounced than what is evident from our final classification. Transition of shrub vegetation to open water and sedge vegetation along the margins of diffuse drainage lines likely also represents degradation of permafrost as a result of advective heat transfer from seasonal water flow. Osterkamp et al. (2009) observed similar expansion of thermokarst features (thermokarst gullies and thermokarst pits) along diffuse water tracks in tussock-shrub tundra in interior Alaska. Our results indicate that formation and expansion of small water bodies, likely as a result of small-scale permafrost degradation, can contribute to local shrub decline and thereby potentially contributed to recent browning observed in this site. This corroborates the importance of high spatial resolution data in the context of Arctic shrub dynamics to identify such mechanisms.

3.5.2.2 *Aquatic succession*

Analysis of transition probabilities identified a distinct change trajectory from open water to sedge to *Sphagnum*. Within the 9-year time span of our satellite images, 45% of open water transitioned to sedge dominated vegetation and 19% of sedge dominated areas transitioned to *Sphagnum* (fig. 3.6). Such a succession mechanism from open water to sedges to *Sphagnum* confirms earlier findings of vegetation succession in thermokarst features (Jorgenson et al. 2015, Kanevskiy et al. 2017, Magnússon et al. 2020) and development of thermokarst bogs in boreal ecosystems (Kuhry et al. 1993, Robinson and Moore 2000, Payette et al. 2004, Turetsky et al. 2007, Myers-Smith et al. 2008). In our study site, Magnússon et al. (2020) found that colonization of thermokarst features by sedges and *Sphagnum* mosses may occur on subdecadal to decadal timescales. Transitions from open water to sedge and from sedge to *Sphagnum* were also very pronounced in the validation data in both time intervals (fig. S3.21) and relatively accurately detected (table S3.11-S3.13), lending further credibility to this observed trajectory. Our results suggest a succession towards bog vegetation following ponding, although the 9-year observation period likely mostly captures the rapid (aquatic) succession processes. Potential transitions towards climax vegetation, such as dwarf shrubs or tussock sedges, may require longer monitoring periods to be accurately quantified.

3.5.2.3 *Increase in area of wetland species*

Apart from aquatic successions, land cover change analysis demonstrated frequent transitions from tussock vegetation to sedge and *Sphagnum*, from lichen vegetation to tussock and from shrub vegetation to sedge or tussock (fig. 3.6 & S3.19). The former implies an expansion of wetland species, whereas the latter implies an expansion of graminoids into lichen and shrub dominated areas. This could be explained by gradual increases in active layer thickness and surface wetting. Sedges and *Sphagnum* are associated with wetter microsites (Iturrate-Garcia et al. 2016), and graminoids can profit from nutrient release at the thaw front in mixed vegetation tundra plots whereas shrubs acquire nutrients from upper soil layers (Wang et al. 2018).

Tussock vegetation showed relatively poor spectral separability in most years (fig. S3.1-S3.3), which may be explained by the inherently mixed nature of tussock vegetation found in this ecosystem (i.e. it contains graminoids as well as shrub and *Sphagnum* species, see table 3.1). It may therefore both be more prone to false positives in change detection and more prone to gradual changes in relative species abundance. The tussock sites in the validation set mostly did not display vegetation change in reality, complicating the accuracy assessment of observed changes to and from tussock. The slow growth rate of tussock sedges (McGraw and Chapin III 1989) makes a complete transition towards tussock sedge dominated vegetation unlikely on the observed timescale. As such, transitions to tussock may represent gradual transitions towards a more mixed species composition. Class transitions related to gradual changes in dominant vegetation species often occur in both directions (Gómez et al. 2016), which is also evident in our site (fig. 3.6). It is possible that gradual changes in the relative abundance of different species are more common than rapid, most likely disturbance-driven successions (paragraph 3.5.2.1), although these cannot be quantified with certainty with a 9-year observation period. Extended monitoring supported by repeated vegetation inventories is recommended.

3.5.2.4 *Inter-annual and seasonal variability in land cover*

The area of open water in alases can be highly variable (Desyatkin et al. 2014) and is driven both by precipitation (Desyatkin et al. 2014, Fedorov et al. 2014) and melting of local ground ice (Fedorov et al. 2014). High amounts of precipitation may enhance ponding (Nauta et al. 2015) and promote further permafrost degradation through enhanced thermal conductivity in wet soils (Hinkel et al. 2001, Jorgenson et al. 2010). The anomalously high summer precipitation in 2011 (fig. S3.26c) may have contributed to the relatively large increase in open water area between 2010 and 2015. The smaller increase in open water between 2015 and 2019 may be explained by exceptionally warm conditions in

the early summer of 2019 (fig. S3.26a), causing open water features to fall dry and manifest as patches of wet, bare ground (Magnússon & Heijmans, pers. obs.). Accordingly, confusion matrices indicate underestimation of the area of open water in 2019 (table S3.7, table S3.13). Similarly, the area of open water may be highest during the early summer period and decrease gradually due to evaporative loss (Jones et al. 2009), which may have contributed to the pronounced increase in open water between 2010 and 2015 (the image for 2015 was taken in July, whereas the images for 2010 and 2019 were taken in August). It is striking that despite the later acquisition date, summer drought in 2018 and early 2019 (fig. S3.26a-c), open water area still increased from 2015 to 2019 (fig. 3.5). This suggests a net trend of abrupt permafrost degradation, rather than influence of hydrological variability.

We found better baseline classification accuracy (table S3.6) and class separability (fig. S3.1 - S3.3) for the early summer 2015 image than for the late summer 2010 and 2019 images. This could be explained by differences in the temporal development of biomass of different vegetation types, affecting their spectral separability. For instance, Wang et al. (2016) found a difference in the timing of peak biomass between graminoids and dwarf shrubs in this site. Accordingly, spectral separability between shrub and sedge differed between the early season image and late season images (fig. S3.1 - S3.3, table S3.3 - S3.5). In addition, the spectral appearance of vegetation changes naturally over the season, for instance through discoloration of leaf material over the season or changes in soil moisture. The classification accuracy of the 2015 image also improved least with spatiotemporal regularization, suggesting that regularization may be particularly helpful in cases where class spectral separability differs seasonally among images.

3.5.2.5 Microtopographical controls on land cover change

In comparison to shrub vegetation, very little formation of open water features was observed in tussock vegetation (fig. S3.19), despite the roughly equal area of tussock and shrub. In contrast, widespread thermokarst has been reported in other tussock sedge ecosystems (Osterkamp et al. 2009, Jorgenson et al. 2010). In our study area, tussock vegetation was primarily found on slightly elevated or sloping terrain such as pingos, polygon rims, levees of small rivers and slightly elevated edges of the lakebed. Such areas showed few class transitions (fig. 3.4 & fig. 3.7d-e). Microtopographical gradients may promote drainage and decrease accumulation of water and ice (Wang et al. 2019) in the soil profile at higher elevation. In contrast, water accumulation in ice rich shrub patches in poorly drained lower areas and along the margins of diffuse drainage lines may result in soil subsidence and ponding as a result of heat transport and increased thermal conductivity (Iijima et al. 2010, Jorgenson et al. 2015, Nauta et al. 2015). This provides a likely explanation for the formation and expansion of open water in shrub patches (fig. 3.4, in detail in fig. 3.7a-c). A tight association between vegetation composition and dynamics and microtopography is confirmed by earlier studies (Siewert et al. 2015, Iturrate-García et al. 2016, Anderson et al. 2019).

3.5.3 Implications of identified land cover change for the lowland tundra ecosystem

The changes in vegetation composition we identified imply net trends of terrain wetting and permafrost degradation, with implications for greenhouse emissions. In Arctic ecosystems, *Betula nana* and to some extent *Eriophorum vaginatum* are associated with drier, upland microsites (Wein 1973, McGraw and Chapin III 1989, Walker et al. 1989, Walker et al. 1994, De Groot et al. 1997). In contrast, the main aquatic sedge and *Sphagnum* species in our study area (*Eriophorum angustifolium*, *Sphagnum obtusum* and *Sphagnum squarrosum*) are associated with distinctly wet to waterlogged habitats (Phillips 1954, Daniels and Eddy 1990, Iturrate-García et al. 2016). Hence, observed decreases in shrub, tussock and lichen versus increases in open water, aquatic sedges and *Sphagnum* strongly suggest a wetting trend.

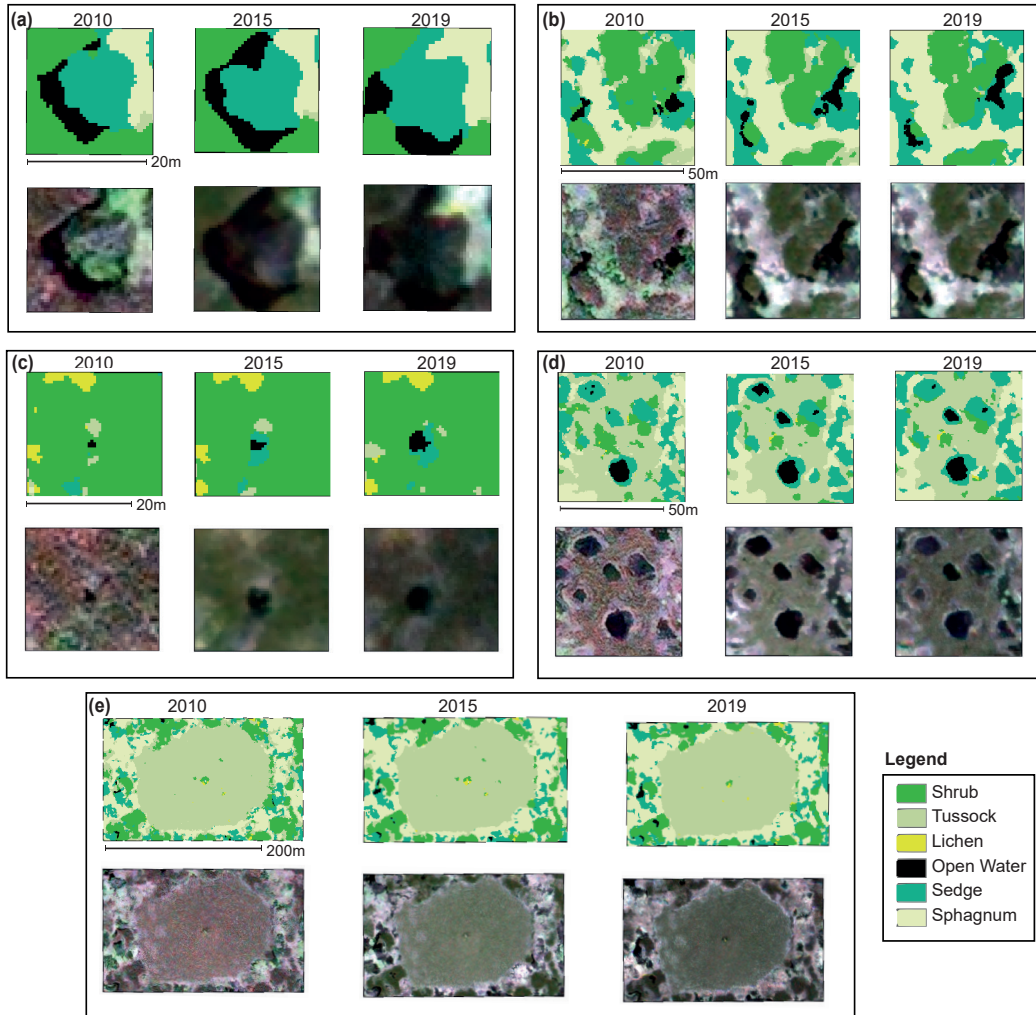


Figure 3.7) Snapshots of typical vegetation change phenomena. For each panel, the top row images contain classified vegetation maps and the bottom row are pansharpened, true color composites (red, green and blue band) of top-of-atmosphere reflectance values (GeoEye © MAXAR, 2019, Worldview © MAXAR, 2019). a) Edges of shrub patches tend to subside, especially along diffuse drainage lines. These subsided areas are colonized by sedges and in turn by *Sphagnum* carpets. b) Same as a, over a larger area. *Sphagnum* expands into previously sedge dominated areas. c) Within shrub patches, small thaw ponds may appear. d) Polygonal tundra appears relatively stable, although the relative amounts of sedge and open water in low center polygons seem to vary. Also, some variation in the relative amount of shrub and tussock is evident, without very visible changes in the satellite images. e) A small, few meters high pingo, which shows stable tussock vegetation. In the bottom left, a thaw pond appears in a shrub patch. Video S1 contains a dynamic visualization of vegetation change and permafrost dynamics.

These observed vegetation changes and related changes in terrain wetness go hand in hand with permafrost degradation. Increases in soil moisture and surface water expansion can promote permafrost degradation through increased heat conductivity (Jorgenson et al. 2010, Jorgenson et al. 2015, Iijima et al. 2017). Formation of open water features in elevated shrub patches strongly suggests the occurrence of abrupt permafrost thaw. In this ecosystem in particular, aquatic sedge and *Sphagnum* vegetation are associated with deeper thaw depths than shrub and tussock vegetation (Van Huissteden et al. 2005, Magnússon et al. 2020). In addition, observed changes in vegetation cover may affect the tundra surface

energy balance (Lorantý et al. 2018a). The relatively low albedo of shrubs compared to graminoids has for instance been suggested to lead to accelerated thaw upon shrub expansion (Bonfils et al. 2012), whereas *Sphagnum* moss may have a relatively high albedo (Juszak et al. 2017), especially in summer. Both dwarf shrubs and their associated moss understory (Blok et al. 2010, Blok et al. 2011a) and *Sphagnum* mosses (Seppala 1988, Soudzilovskaia et al. 2013) can provide a direct insulating effect to the permafrost, especially when dry (Seppala 1988). In this ecosystem thaw depths are generally larger under *Sphagnum* carpets than under dwarf shrub dominated vegetation (Van Huissteden et al. 2005, Magnússon et al. 2020), indicating that the observed vegetation changes (fig. 3.5) are likely associated with a net deepening of the active layer. Expansion of *Sphagnum* in previously waterlogged or sedge-dominated sites indicates potential for permafrost recovery (Magnússon et al. 2020).

Degradation of permafrost results in exposure of previously frozen soil organic carbon to microbial decomposition and potential release of greenhouse gases. This is anticipated to further increase climate warming, especially in cases where surface wetting favors anaerobic decomposition into methane (Schuur et al. 2015, Meredith et al. 2019). The observed increase in area of open water and wetland species and shrub decline thereby also implies an increase in methane emissions (Van Huissteden et al. 2005, Nauta et al. 2015). In contrast, accumulation of peat in thermokarst areas can facilitate storage of large amounts of carbon, especially in *Sphagnum* bogs (Robinson and Moore 2000, Myers-Smith et al. 2008, Gao and Couwenberg 2015, Siewert et al. 2015). In addition, *Sphagnum* growth may directly suppress methane emissions (Sundh et al. 1995, Van Huissteden et al. 2005, Parmentier et al. 2011a). This implies an eventual increase in carbon sequestration through peat accumulation, which may partially mitigate high initial emissions in thermokarst wetlands (Turetsky et al. 2020). To assess resulting net changes in the greenhouse gas balance of this ecosystem, a systematic survey of greenhouse gas fluxes associated with different vegetation classes is necessary.

3.5.4 Recommendations for future monitoring of Arctic vegetation change

3.5.4.1 Use of spatiotemporal regularization to mitigate satellite image inconsistency

Satellite data consistency in terms of seasonal timing and sensor properties is an important remaining challenge in remote sensing of Arctic vegetation change (Beamish et al. 2020). We found that MRF techniques such as the Potts model can substantially improve the quantification of vegetation change in VHR satellite data from different sensors and phenological stages. Repeated field photography proved useful in the optimization of change detection. We achieved single-image accuracies of over 90%, which is high compared to other studies of pixel-based classification using similar data in similar ecosystems (Siewert et al. 2015, Morozumi et al. 2019). We found that temporal smoothing had a larger influence on the accuracy of classification of individual images than spatial smoothing (fig. S3.4 – S3.9), because in reality most pixels did not show a change in land cover class. Decreasing the temporal smoothing weight led to more false positives in change detection, whereas increasing it further led to more false negatives and did not improve MCC (table S3.8 – S3.10).

The correct land cover transition was detected in 75% of cases over the 2010- 2019 period. While this is not optimal, it suggests that identified land cover changes can serve as an approximation of field-observed changes in land cover class. This is also supported by the similarity between observed transition probabilities between the two time intervals (fig. 3.6) and the similarity between transitions observed over the study area and in the validation data (fig. S3.20 & S3.21). User's and producer's accuracies of change detection (table S3.11 - S3.13) indicated that change detection accuracy varies among specific transitions. Unchanged areas achieve higher accuracies of change detection than changed areas. Overestimation of transitions among shrub, tussock and lichen in particular, likely due to poorer spectral separability (fig. S3.1 – S3.3, table S3.3 – S3.5). Transitions between open water, sedge and *Sphagnum* generally achieved higher accuracies (table S3.11 - S3.13).

3.5.4.2 Recommendations for further improvement of change detection accuracy

MRF may be a valuable technique to explore further in the context of Arctic vegetation change and may stimulate (re)use of existing image material. For instance, MRF-based approaches can be modified to explicitly penalize specific illogical class transitions (Wehmann and Liu 2015), which may prove useful in cases where a priori information is available on land cover change mechanisms. Gómez et al. (2016) provide an overview of MRF applications and post-classification amendments to enhance temporal consistency in land cover change detection. In addition, other optimization methods than ICM could be applied. ICM identifies a local optimum that may theoretically differ from the global optimum. Alternative optimization techniques such as graph cuts are demonstrated to always reach a global optimum within reasonable processing times for Potts model (Ishikawa 2003). However, we find that ICM works well in practice since classification accuracies are improved substantially and convergence was generally reached within 30 iterations (fig. S3.12).

Given the tight association between vegetation composition and microtopography (paragraph 3.5.2.5) the incorporation of multi-temporal, high resolution elevation data or other non-spectral data could substantially improve land cover change detection in Arctic ecosystems (Chasmer et al. 2014, Beamish et al. 2020). Lastly, although the different temporal development in spectral properties of plant species can complicate classification (paragraph 3.5.2.4), the use of multiple images from different moments during the growing season provides complementary information that can help distinguish different vegetation types (Westergaard-Nielsen et al. 2013).

3.5.5 Conclusions & Recommendations

To make reliable assessments of future vegetation development in the Arctic, there is an urgent need to identify underlying mechanisms of observed spatial differences in the response of Arctic vegetation to global change. During the past decade we observed a browning trend instead of greening in our Siberian lowland tundra site. This was associated with a decline of shrub and tussock dominated vegetation, which was rapidly replaced by open water, aquatic sedges and *Sphagnum* moss. These changes likely went hand in hand with surface wetting and degradation of ice-rich permafrost, with potential consequences for the greenhouse gas balance of this ecosystem. Comparison with regional dynamics of vegetation greenness and surface water presence indicates that similar to the study site, the Indigirka Lowlands have undergone substantial expansion of surface water features. The recent browning observed for the study site was evident in large parts of the Indigirka Lowlands, although specific areas (e.g. coastal tundra and drained thaw lakes) have continued greening.

Within our relatively short study period, land cover change was expressed on small spatial scales. Expansion of small water bodies and vegetation successions were only detected using very high resolution satellite data with extensive ground truthing. Although the influence of difference in sensors and seasonal timing of the images within this short timeseries cannot be ruled out completely, land cover change detection accuracy was improved after spatiotemporal regularization using Potts model and false detection of land cover change was reduced substantially. Such MRF-based techniques may be compelling tools for studies of Arctic vegetation change, which are often limited by low availability and consistency of image material.

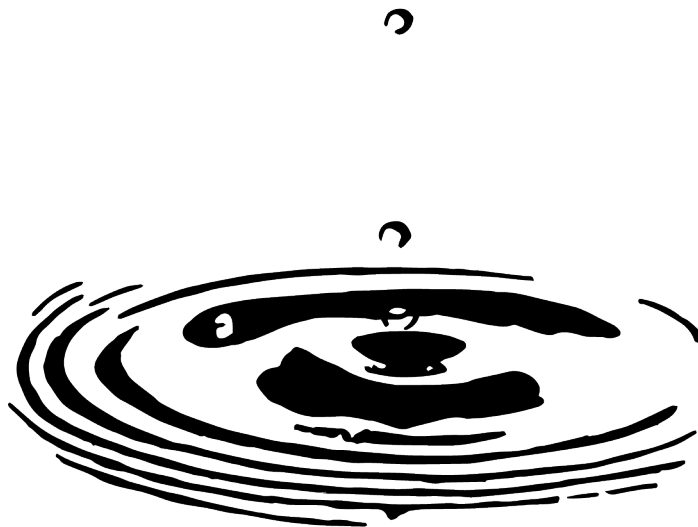
Our findings provide a contrast to earlier reports of greening and shrub expansion in the Russian Arctic and raise the question why shrubs show opposing regional trends in their expansion dynamics. Our results suggest that surface wetting and abrupt permafrost thaw could be local drivers of browning and shrub decline in this poorly drained terrain. We recommend that future research continues to relate observed large-scale trends in vegetation change to regional variability in microtopography, permafrost characteristics and hydrology. Very high resolution data proved invaluable in this context.

4.

Extremely wet summer events enhance permafrost thaw for multiple years in Siberian tundra

Rúna Í. Magnússon, Alexandra Hamm, Sergey V. Karsanaev, Juul Limpens, David Kleijn, Andrew Frampton, Trofim C. Maximov and Monique M. P. D. Heijmans

Published in *Nature Communications*, 13, 1556 (2022).



4.1 Abstract

Permafrost thaw can accelerate climate warming by releasing carbon from previously frozen soil in the form of greenhouse gases. Rainfall extremes have been proposed to increase permafrost thaw, but the magnitude and duration of this effect are poorly understood. Here we present empirical evidence showing that one extremely wet summer (+100mm; 120% increase relative to average June – August rainfall) enhanced thaw depth by up to 35% in a controlled irrigation experiment in an ice-rich Siberian tundra site. The effect persisted over two subsequent summers, demonstrating a carry-over effect of extremely wet summers. Using soil thermal hydrological modelling, we show that rainfall extremes delayed autumn freeze-up and rainfall-induced increases in thaw were most pronounced for warm summers with mid-summer precipitation rainfall extremes. Our results suggest that, with rainfall and temperature both increasing in the Arctic, permafrost will likely degrade and disappear faster than is currently anticipated based on rising air temperatures alone.

4.2 Introduction

Permafrost has been degrading rapidly and ubiquitously in response to Arctic warming (Shiklomanov et al. 2012, Liljedahl et al. 2016, Kokelj et al. 2017, Fraser et al. 2018, Biskaborn et al. 2019, Farquharson et al. 2019). Climate models suggest that 24% (RCP2.6) to 70% (RCP8.5) of near surface permafrost may disappear by 2100. This could result in the release of tens to hundreds Gt carbon into the atmosphere, further enhancing climate warming (Meredith et al. 2019). Although highly responsive to air temperature (Lawrence et al. 2015, Chadburn et al. 2017, Biskaborn et al. 2019), permafrost degradation rates also depend on other climatic, soil physical, hydrological and vegetation related factors (Romanovsky et al. 2010, Atchley et al. 2016, Loranty et al. 2018a, McGuire et al. 2018, Nitzbon et al. 2020). Rainfall is one such factor that has been associated with enhanced permafrost thaw in modelling and short-duration observational studies (Iijima et al. 2010, Neumann et al. 2019, Douglas et al. 2020, Mekonnen et al. 2021b). Arctic precipitation is anticipated to increase (Bintanja and Selten 2014, Bintanja et al. 2020) by up to 60% locally (RCP8.5) by 2100 and to increasingly shift from snow to rain due to rising air temperatures (Bintanja and Andry 2017). Increased seasonal variability of precipitation, particularly in summer, implies increased occurrence of extreme rain events (Bintanja and Selten 2014, Wang et al. 2021). However, experimental data on how this affects permafrost are currently lacking. We set out to quantify the magnitude and duration of the effect of rainfall extremes on permafrost thaw in a field experiment to contribute to improved projections of future permafrost degradation.

Observational studies of the effects of rainfall extremes on permafrost soils have shown divergent effects of rain on soil thermal regimes (Hinkel et al. 2001, Iijima et al. 2010, Zhu et al. 2017, Neumann et al. 2019, Douglas et al. 2020, Luo et al. 2020, Clayton et al. 2021). On the one hand, relatively warm infiltrating rain can enhance thaw (Iijima et al. 2010, Neumann et al. 2019, Douglas et al. 2020) through transport of heat in infiltrating rainwater into colder soils (Hinkel et al. 2001, Neumann et al. 2019, Mekonnen et al. 2021b) or by increasing soil thermal conductivity, enabling more heat to penetrate into the soil (Farouki 1981, Hinkel et al. 2001, Subin et al. 2013). On the other hand, increased soil moisture resulting from rainfall can slow down warming of cold permafrost soils (Zhu et al. 2017, Luo et al. 2020, Clayton et al. 2021) as the energy required to warm the wetter soil (heat capacity) is increased and more energy (latent heat) is required for phase changes during freezing, thawing and evaporation (Farouki 1981, Hinkel et al. 2001, Subin et al. 2013, Clayton et al. 2021). The balance between these opposing warming and cooling effects may depend, among other factors, on air temperatures and seasonal timing (Hinkel et al. 2001). Potential interactive effects between rising summer temperatures and changing precipitation patterns in the future Arctic are poorly quantified.

Lastly, it is conceivable that effects of extreme rainfall can persist over multiple years, for instance through increased soil ice contents in winters following extremely wet summers (Iijima et al. 2010) or structural alteration of the upper permafrost layer following enhanced seasonal thaw (Shur et al. 2005). The magnitude and duration of potential carry-over effects of extreme rainfall are presently unknown.

We assessed the impact of one extremely wet summer on permafrost thaw over three summers in a controlled field irrigation experiment (10 irrigated, 10 control plots) in the north-eastern Siberian lowland tundra (fig. 4.1). This region is characterized by thick, ice-rich permafrost (Olefeldt et al. 2016, Nitzbon et al. 2020) and a distinctly continental climate with warm summers (van der Kolk et al. 2016), with high potential for substantial permafrost degradation. The irrigation treatment (+100mm) was set to mimic an extremely wet summer for this ecosystem, with 191mm compared to 81mm on average in June-August (Nauta et al. 2015). To explore dependence of rainfall effects on air temperature and seasonal timing, we used a physically-based numerical model accounting for necessary thermal and hydrological processes in permafrost regions (ATS) (Coon et al. 2019). We calibrated the model using field measurements and then conducted a model-based investigation of thaw depth under various rainfall and temperature scenarios.

4.3 Methods

4.3.1 Study Site

We studied the effects of increased rainfall on permafrost thaw dynamics in a drained thaw lake basin (or “alas”) in the “Kytalyk” Nature Reserve in the Indigirka Lowlands in north-eastern Siberia (70°49'N, 147°29'E) near the town of Chokurdakh (fig. 4.1a). Such alases are representative for a major part of coastal north-eastern Siberia (Fedorov et al. 2018). The area is characterized by a shallow active layer overlying ice-rich, continuous permafrost (Van Huissteden et al. 2005). The mean annual temperature is -13.5°C, with an average July temperature of 10.0°C (1945-2019). The mean annual precipitation is 202mm, of which 81mm falls in summer (June, July and August) (1945-2019) (Trouet and Van Oldenborgh 2013, RIHMI-WDC 2020). Within the study area, elevated sites such as “Yedomas” ridges and pingos are characterized by tussock-sedge (*Eriophorum vaginatum*) and dwarf shrub vegetation. Lower elevation areas such as alases are characterized by slightly elevated shrub patches dominated by *Betula nana*, lichens and mosses, interspersed with waterlogged depressions characterized by aquatic species such as *Eriophorum angustifolium*, *Carex* spp. and *Sphagnum* spp. (Siewert et al. 2015, Magnússon et al. 2020).

4.3.2 Experimental Design

We set out 20 circular plots of 5m diameter in five clusters of four (two irrigation, two control), located in five dwarf shrub dominated tundra patches in early summer 2018. Clusters were situated next to ponds that provided water for irrigation (fig. 4.1b). Clusters were around 50 to 100 meters apart and plots within clusters were at least five meters apart. We installed a PVC well in the centre of each plot to monitor the water table. Prior to irrigation, we measured thaw depth and topsoil volumetric moisture content in nine locations per plot: eight points along the perimeter of the plot at 1m distance from the plot edge, and one in the centre. We visually assessed cover of the main plant species and variation in microtopography and assigned plots to pairs within clusters based on similarity in thaw depth, water table, soil moisture, vegetation composition and microtopography. Plots from pairs were randomly assigned to irrigation and control, although in a few cases the length of the hoses of the irrigation system dictated the subdivision. No significant differences were evident in thaw depth, water table or soil moisture prior to irrigation (table S4.5-S4.10). Over the period of July 6th to August 2nd, 2018, we supplied 100mm of irrigation to all irrigation plots and no irrigation to control plots using a motor pump (fig. 4.1c). We set the amount of irrigation to mimic the extremely wet summer of 2011 with 191mm vs. 81mm average in June-August (Nauta et al. 2015). The irrigation water supplied from ponds

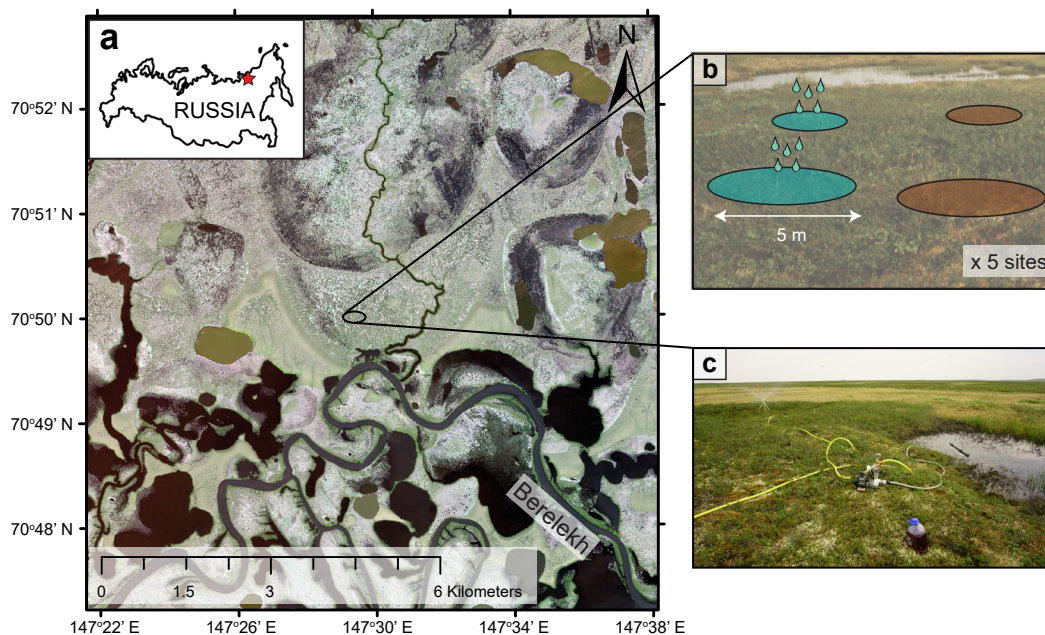


Figure 4.1) Study area and experimental setup. a) Our study area is situated in the Indigirka lowlands at the Chokurdakh Scientific Tundra Station, in a drained thaw lake basin (alas) adjoining the floodplains of the river Berelekh. Image: WorldView-2 © 2019 Maxar Technologies. b) In this alas, 5 sites were selected in shrub patches within 5 to 10m distance from a thaw pond. In each site, 4 circular plots were set out: 2 irrigated plots (blue) and 2 control plots (brown) each with 5m diameter. Plots were at least 5m apart. c) The irrigation system consisted of a filter tube and motor pump which simultaneously irrigated the 2 irrigated plots per site via hoses with a length of 10m and sprinklers.

had a chemical composition similar to that of rainwater, and the temperature of irrigation water did not exceed that of the ambient air (text S4.1). We irrigated plots on an approximately biweekly basis in amounts of 10 or 15mm with an application rate of 25mm per hour. During the summers of 2018, 2019 and 2020, we repeated measurements of thaw depth, water table and topsoil volumetric moisture content at regular intervals. In eight plots (four irrigation, four control), we installed temperature and moisture loggers at 5cm and 20cm depth. Description of all measurements and equipment is available in text S4.1.

4.3.3 Field Data Analysis

We tested treatment (factor; irrigation or control) and measurement date (factor) and their interaction for significant effects on field-measured thaw depths, water tables and topsoil volumetric moisture content using mixed effects models. To account for repeated measurement in a nested set-up, we used plot number as a random effect and tested for significance of random intercepts and slopes on a full model with interaction using likelihood ratio tests (LRTs). The significance of fixed effects was assessed using F-tests with Kenward-Rogers approximation of degrees of freedom on nested models (Halekoh and Højsgaard 2014). The optimal model structure was determined using backwards selection based on predictor p-values, Akaike's Information Criterion (AIC), normality and homoscedasticity of residuals and absence of patterns of residuals against random factors and fitted values. We allowed for transformation of dependent variables and addition of zero-inflation components to improve residual diagnostics. We performed all statistical analysis in R version 3.5.1 (R Development Core Team 2019) using the lme4 package (Bates et al. 2014). An extensive description of the procedures for statistical

analysis is available in text S4.2.

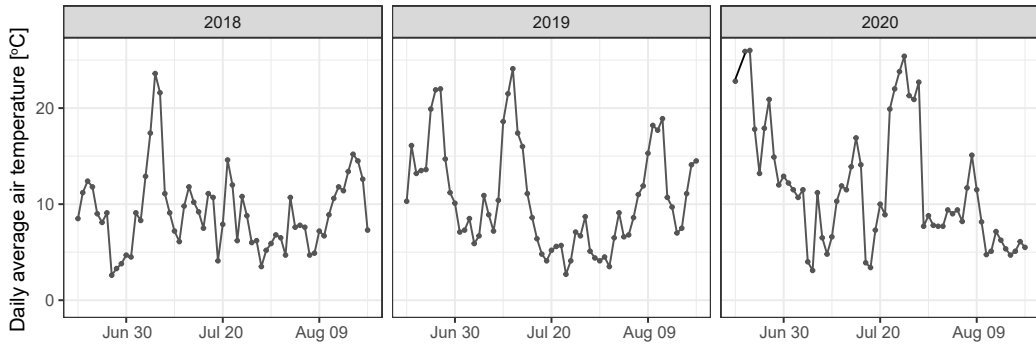
4.3.4 Modelling Study

We used the Advanced Terrestrial Simulator (ATS) (Coon et al. 2019) version 0.88 to support the field experiment with mechanistic insight and to explore the temperature sensitivity of rainfall effects using several rainfall and temperature scenarios. ATS is a fully coupled surface-subsurface thermal hydrology model, configured for permafrost applications (Painter et al. 2016). It couples the surface energy balance and snow dynamics with a subsurface thermal hydrology scheme to represent three-phase freeze- and thaw cycles accounting for moisture migration. To run the model, atmospheric data on air temperature, precipitation, incoming shortwave radiation, relative humidity and wind speed is required. Except for incoming shortwave radiation, a time series from January 1st, 1966 to July 31st, 2020 for all these values was available for Chokurdakh (WMO station code 21649, 30km northwest of the study site) from the All-Russia Research Institute of Hydrometeorological Information - World Data Centre (RIHMI-WDC 2020). Incoming shortwave radiation was retrieved from ERA5 reanalysis data (Hersbach et al. 2020). We set layer definition, parameters and boundary conditions of our one-dimensional model based on field measurements (table S4.11). We used both direct field measurements from the experimental sites and measurements from earlier studies conducted at representative locations. For a predefined set of thermal and hydrological for which no field data was available, we calibrated parameters for accurate representation of field measured thaw depths. We used literature values to define a likely range within which these parameters were calibrated (table S4.11). We used Nash-Sutcliffe Efficiency (NSE) to quantify the extent to which the modelled depth of the 0°C isotherm (the depth at which the permafrost table is situated) followed the field measured thaw depths and set parameters to maximize NSE. In addition, modelled soil moisture and soil temperature at 5cm and 20cm depth were compared visually to logger measurements after calibration. An independent check was performed by comparing model predicted thaw depths between 2007 and 2017 to field measurement series (Blok et al. 2010, Nauta et al. 2015, Li et al. 2017) at undisturbed shrub tundra plots situated at approximately 500m distance from the irrigated sites towards which the model was calibrated. An extensive description of the model calibration procedure and resulting fits with field measurement series is available in text S4.3 - S4.4.

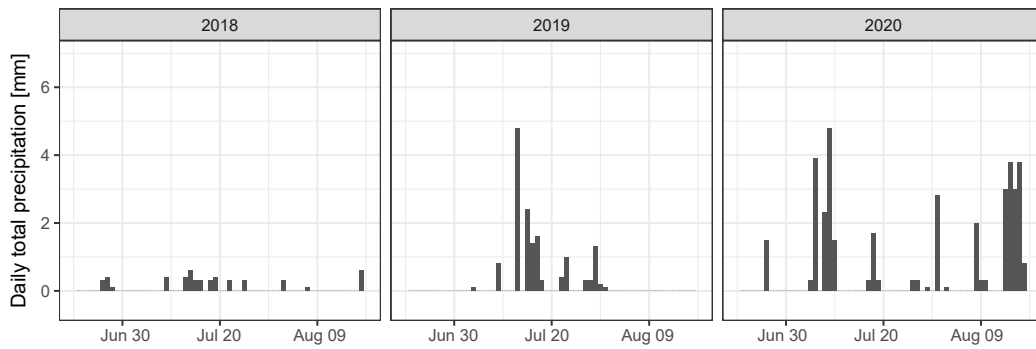
To assess sensitivity of modelled thaw dynamics and rainfall effects to selected parameters, we performed a sensitivity analysis on both active layer thickness (ALT, or maximum end-of-season depth of the 0°C isotherm) and rainfall effects on ALT (quantified as the difference in ALT between baseline runs and runs with increased rainfall) using structural increases and decreases in soil thermal-hydrological parameters. As changes in single parameters may not be representative of field-observed variability in soil properties, we modelled thaw depth dynamics across a range of soil stratigraphical (variable peat layer thickness overlying variable mineral soil textural classes) and climatic (various summer temperature and rainfall scenarios) conditions. See text S4.5 for a full description of model sensitivity analysis and analysis of rainfall effects across soil types and temperature scenarios.

We used the calibrated model parametrization to analyse various rainfall scenarios for one summer, followed by two years of baseline conditions. We established a baseline scenario with daily precipitation and temperature based on averaged forcing conditions (1979-2018) and several scenarios with varied amounts and timing of rainfall in summer based on frequency-intensity distributions of daily precipitation from the Chokurdakh record (RIHMI-WDC 2020). We simulated years with high (70th - 80th percentile of total JJA precipitation) and extreme precipitation (95th - 100th percentile of total JJA precipitation). To model the role of variability in rainfall within the summer season, high and extreme rainfall scenarios were represented both as uniform increases over the summer season and as variable increases with extreme rainfall events within the season. Furthermore, we added four scenarios with 80 additional mm of rainfall in either June, July, August or September. We complement the rainfall scenarios by adding two temperature scenarios simulating a summer of average temperature (Tavg, JJA

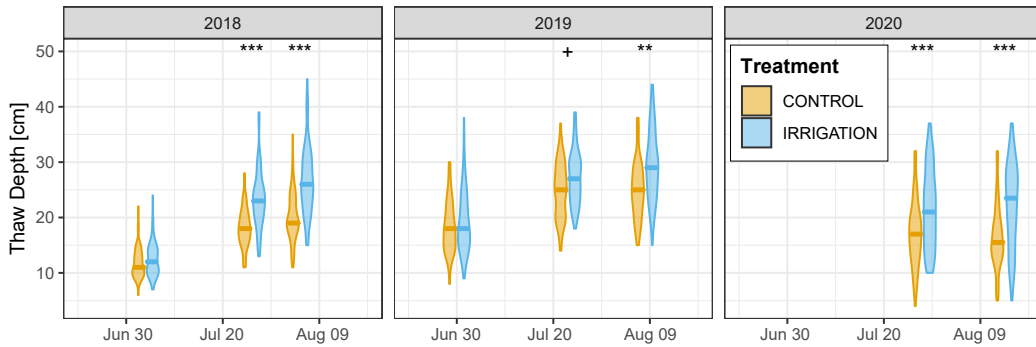
(a) Daily air temperature summer season



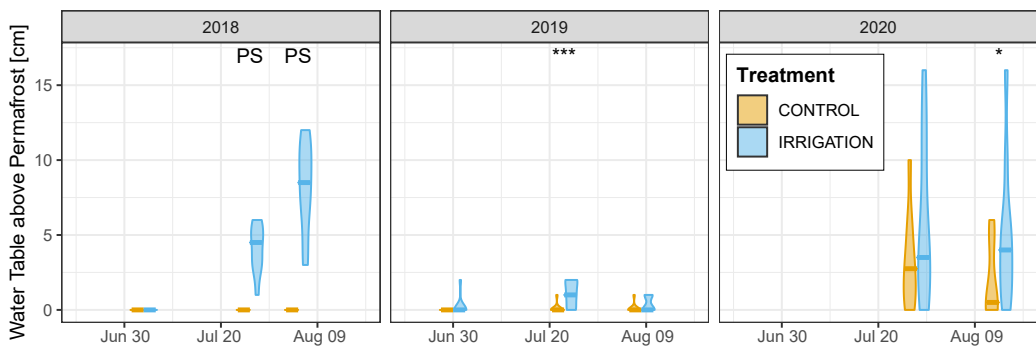
(b) Daily total precipitation summer season



(c) Development of Thaw Depth over summer season



(d) Development of Water Table above Permafrost over summer season



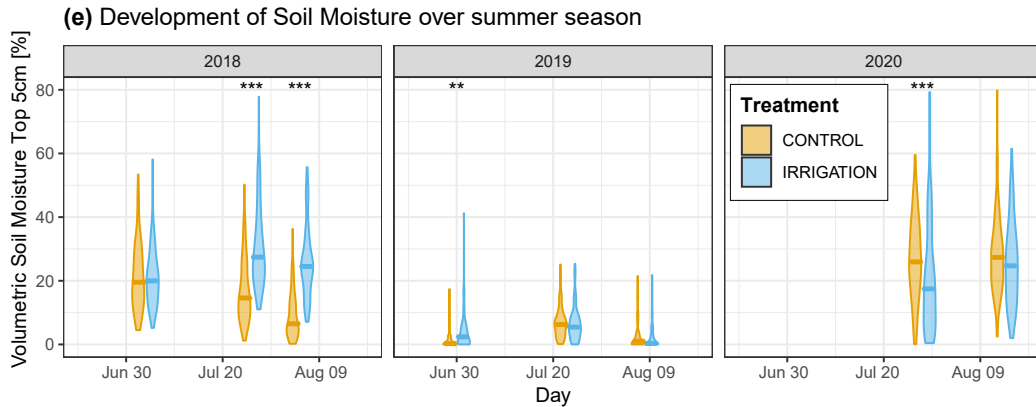


Figure 4.2) Results of the irrigation experiment. Abiotic conditions in control (orange) and irrigated (blue) plots during irrigation (2018) and subsequent summers without irrigation (2019 & 2020). The earliest 2018 measurements were taken before irrigation started. a) Average daily air temperature and b) total daily precipitation recorded in Chokurdakh (WMO station code 21649). c) Thaw depth ($n = 90$ per violin). d) Water table above permafrost in plot centres ($n = 10$ per violin). e) Volumetric soil moisture content of the topsoil (5cm depth) ($n = 90$ per violin). In c-e, violin length represents data range and violin width represents the probability density of the data distribution. Horizontal bars indicate group medians. Symbols above plots represent significant Tukey contrasts between irrigation and control per measurement date (+: $p < 0.1$, *: $p < 0.05$, **: $p < 0.01$, ***: $p < 0.001$). *PS* indicates perfect separation (see d), in which case no p-values could be derived. Model specifications and estimated marginal means are in text S4.7

$= 7.9^{\circ}\text{C}$), and a very warm summer based on the 95th - 100th percentile of mean summer temperature ($T_{\text{avg, JJA}} = 10.6^{\circ}\text{C}$). We compared the ALT and timing of complete freeze-up among the different rainfall scenarios. An elaborate description of scenario definition is available in text S4.6.

4.4 Results and Discussion

4.4.1 Field Irrigation Experiment

We found that extreme rainfall (+100mm, +120%) increased permafrost thaw depth substantially over multiple years. During the summer of irrigation, thaw depths in irrigated plots gradually increased relative to control sites up to a 32% (+6.3 cm) difference in early August (fig. 4.2c). The magnitude of this effect aligns with monitoring observations in Alaskan permafrost ecosystems, where a 10mm increase in rainfall was estimated to result in a 0.7cm increase in active layer thickness (Douglas et al. 2020). In addition, extreme rainfall increased the volumetric moisture content of the topsoil relative to control plots following irrigation (fig. 4.2e) and led to formation of a water table above the permafrost (fig. 4.2d). The following summers, thaw depths were still higher in irrigated plots than control plots in early August, with differences of 4.3cm (+18%) in 2019 and 5.6cm (+35%) in 2020. Warm temperatures during the years after irrigation (fig. 4.2a) may have contributed to the sustained increase in thaw depth. Higher topsoil moisture in early summer 2019 and a continued increase in water tables on top of the permafrost (fig. 4.2d-e) strongly suggest that added rainfall (partially) freezes up and is released in subsequent summers. Increased moisture content was observed in the topsoil as well as the subsoil (fig. S4.4) and is in line with earlier observational studies (Iwahana et al. 2005, Iijima et al. 2010). Apart from direct water input from irrigation, increased thaw depths in irrigated sites may cause lateral flow, reduced evaporation due to deeper infiltration or promoted release of water from melting of excess ground ice (Iijima et al. 2010). The roles of evaporation and ground ice melt are unknown as they were not monitored during the experiment. No significant relations were found between microtopography, thaw depths and water tables, indicating that the roles of microtopography and lateral flow were likely

limited compared to that of the irrigation treatment (fig. S4.19, table S4.12 - S4.13).

Substantial variation among observations, even within plots, suggests a high degree of spatial heterogeneity in thaw depths and soil moisture (fig. 4.2c-e). Similarly, measurements varied among individual years. In the dry summer of 2018, no water tables were observed in control plots, whereas water tables in irrigated plots varied between 3 and 12cm in early August. In 2019, soil moisture was very low in all plots and water tables were generally absent (fig. 4.2e), likely caused by hot and dry meteorological conditions in early summer 2019 (fig. 4.2a-b). In the wetter summer of 2020, higher water tables were observed, and topsoils in irrigated plots were drier than control plots, presumably related to the deeper thaw depth (fig. 4.2c). Despite this spatio-temporal variability, irrigated plots still displayed more frequent and higher water tables and deeper thaw.

4.4.2 Scenario Analysis using Numerical Modelling

A physically-based numerical model (the Advanced Terrestrial Simulator, ATS v.088) (Coon et al. 2019) driven by site meteorological data was used to provide mechanistic insight in support of the field experiment. ATS was configured for local site conditions by using field measurements to set layer properties and boundary conditions. Parameters for which no field measurements were available (water retention evaluators and soil thermal parameters) were calibrated within a predefined range based on literature values for accurate representation of thaw depth measurements from the irrigation experiment (text S4.3 – S4.4). Modelled thaw depth closely followed field measured thaw depths across both scenarios representing control and irrigated plots during the year of irrigation, except in the extremely warm summer of 2020 (fig. 4.3). Representation of site-measured soil temperature and moisture content, which were not used for model calibration, were generally accurate (fig. S4.7 - S4.8). Comparison of modelled thaw depths with historical field measurements from the same site (Blok et al. 2010, Nauta et al. 2015) indicate reasonable correspondence (NSE = 0.44, RMSE = 5.75cm, fig. S4.9) and provides an independent test of model representation of local thaw dynamics. Modelled effects of irrigation on thaw depth were smaller than those observed in the field, indicating that the model-based results are conservative estimates.

Apart from differences in instantaneous thaw depths, the model yielded a 5cm difference in maximum end-of-season thaw depth (or active layer thickness, ALT) in 2018. Such an effect roughly corresponds to that of a 1.7°C increase in mean summer temperature (fig. S4.18) (Abramov et al. 2019). Modelled ALT (control: 37cm, irrigation: 42cm) closely resembles typical ALT for this region (Abramov et al. 2019). An 8-day delay in complete freeze-up was modelled under irrigation compared to the control scenario (fig. S4.6a). Model results are in line with the experiment, showing sustained small increases in thaw depth of up to 2cm in the irrigated scenario in 2019 and 2020 and a 2-day delay in freeze-up in 2019. This suggests that the model generally reproduces site thaw dynamics satisfactorily but yields conservative estimates of the effect of extreme rainfall.

Model results suggest that increased soil moisture after irrigation remained in the soil during autumn freeze-up, resulting in increased ice content throughout the soil profile in winter in irrigated sites (fig. S4.12). Subsequent release of soil moisture in following summers (fig. S4.6b & S4.8b) likely mediated the observed carry-over effect. Irrigation increased subsoil temperatures (fig. S4.6a) and thaw depth both directly through input of heat from rainwater with a higher temperature than the subsoil (fig. S4.11) and indirectly through increased thermal conductivity of the wetter soil (fig. S4.12). In contrast, colder topsoils were observed under extreme rainfall, both in model results and field measurements (fig. S4.6a & S4.8a), as a result of evaporative cooling of the surface (fig. S4.10) (Göckede et al. 2017, Zhu et al. 2017).

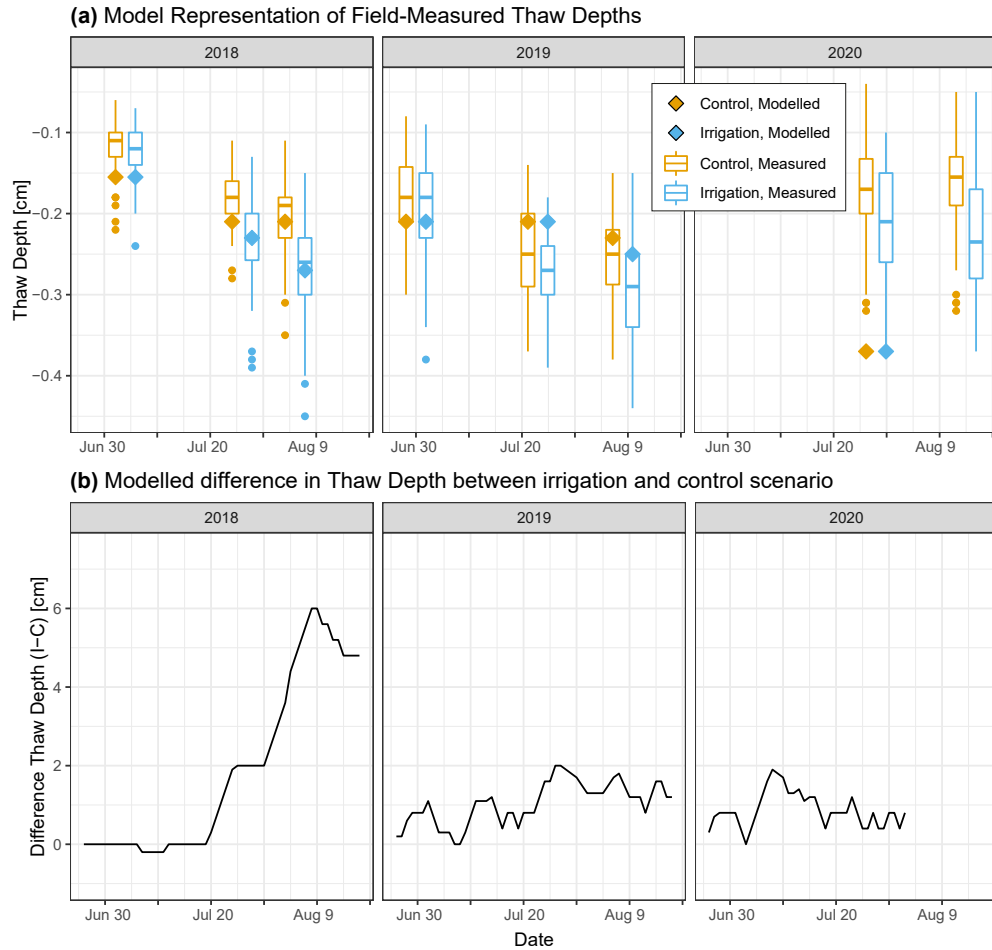


Figure 4.3) Model representation of the irrigation experiment. a) Modelled and measured thaw depth for 2018-2020 with mean field measurement values. Boxplots for measured thaw depths represent all individual measurements in irrigated (blue) and control (orange) plots ($n = 90$ per box). Centre lines represent the median, box limits represent upper and lower quartiles, whiskers represent 1.5 times the interquartile range and points represent outliers. b) Modelled difference between irrigation and control scenario, smoothed with a 5-day moving average. Modelled data is only available up until the end of the meteorological record (July 31st, 2020).

Model sensitivity analysis (text S4.10 indicates that modelled rainfall effects on permafrost thaw vary with soil hydrological and thermal parameters and layer definition (thickness of organic and mineral soil layers) (fig. S4.13). In order to explore potential implications for permafrost thaw across permafrost environments, we extended our analysis by modelling effects of rainfall across a range of soil textural classes, variable peat layer thickness and several temperature scenarios. Within this range of simulations, enhanced thaw following rainfall increases was modelled across all soil textural types. Larger rainfall effects were modelled for models with shallower peat layers, warmer summer temperatures and soil parameterizations representing coarser mineral soil texture (fig. S4.14). Although this suggests that fine-textured soils do not show above average susceptibility to rainfall effects (fig. S4.14), we did find clear effects of rainfall in our experimental sites, characterized by fine-textured soils (table S4.11). Likely, high summer temperatures during the experiment and the summers after (fig. 4.2a) contributed to the substantial field-measured effect of rainfall on thaw depth.

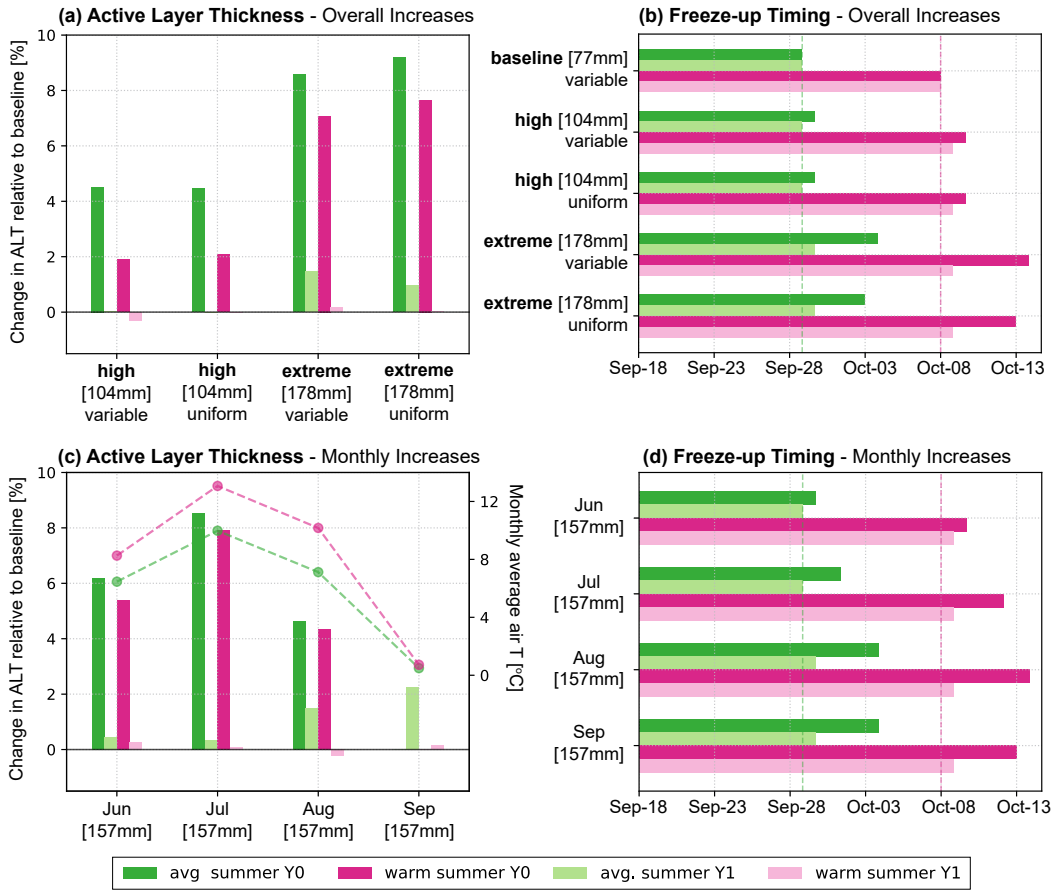


Figure 4.4) Effect of rainfall and temperature scenarios on modelled thaw dynamics. Effect of rainfall scenarios on active layer dynamics in average (green) and warm (pink) summers, for the year of altered rainfall (Y0, dark shades) and the year after (with baseline conditions) (Y1, light shades). a) Modelled percentual difference in active layer thickness (ALT) under increased June - August (JJA) rainfall, with either uniform increase of JJA rainfall or variable increase (modelled to follow observed frequency-intensity distribution). b) Modelled timing of complete freeze-up of the soil column under increased JJA rainfall. c) Modelled percentual difference in ALT under increased rainfall in particular months. Dashed lines indicate mean temperature during the month of rainfall addition in average (green) and warm (pink) summers. d) Modelled timing of complete freeze-up under increased rainfall in particular months. Changes (%) in ALT (a,c) are reported relative to baseline rainfall under the corresponding temperature scenario (average or warm summer). Positive changes percentages indicate increased ALT.

The calibrated model was used to analyse active layer thickness and freeze-up timing under rainfall and temperature scenarios based on site meteorological data (fig. S4.3). The magnitude of ALT increase under increased rainfall depended on timing of rainfall events relative to air temperature dynamics (fig. 4.4c). Under average summer temperature ($T_{avg,JJA} = 7.9^{\circ}\text{C}$), baseline ALT was 27.2cm, while extreme rainfall increased it to 29.6cm. In a warm summer ($T_{avg,JJA} = 10.6^{\circ}\text{C}$), ALT was 46.6cm under baseline conditions and 50.3cm under extreme rainfall, indicating a larger net increase in warm summers. For high and extreme rainfall scenarios, no substantial differences were evident when additional rainfall was distributed uniformly over summer (JJA), compared to scenarios where additional rainfall was added following observed frequency-intensity distribution of daily total precipitation at the site (table S4.4). July rainfall extremes had the largest effect on ALT, whereas rainfall extremes in early and late summer had a smaller effect. Generally, the largest ALT increases were observed when high temperatures and

high rainfall coincided, regardless of whether increases were uniform or variable (fig. S4.15). This suggests that the effect of rainfall strongly depends on its timing and is largest during warm conditions.

Rainfall extremes in September did not affect ALT in the same year because freeze-up had already started in September (fig. S4.16 – S4.17). However, August and September rainfall extremes have the strongest influence on freeze-up duration; the later rainfall is added to the system, the longer freeze-up is postponed. Delays of 6 to 7 days were found for the extreme rainfall scenario and August and September rainfall scenarios both in average and in warm summers (fig. 4.4b,d). This is likely explained by higher heat capacity and increased release of latent heat in wetter soils during freezing, both of which delay autumn freeze-up (Hinkel et al. 2001, Neumann et al. 2019). These results indicate that rainfall extremes not only lead to deeper thaw, but also extend the period over which soils remain (partly) unfrozen.

Model results indicate that effects of rainfall extremes vary among seasons and soil depths. Soil temperature changes were most evident in subsequent winters (fig. S4.16 - S4.17). Warming effects were visible in the topsoil in autumn and early winter due to delayed freeze-up, especially under late summer rainfall, which resulted in increases in topsoil temperature of up to 2 degrees during early winter. Modelled winter subsoil temperatures were lower than in the baseline scenario likely due to increased thermal conductivity under higher ice-content (fig. S4.12). In spring, increased ice content impedes warming of the topsoil through latent heat consumption (fig. S4.16 - S4.17). Similar changes in winter soil temperature were evident from field observations (fig. S4.8a). Soil temperatures in subsequent summers quickly returned to baseline conditions and only small differences in thaw depth persisted (fig. S4.16 – S4.17). Marginal delays in freeze-up persisted in subsequent summers, mostly under late summer and extreme rainfall and under warmer summer temperatures (fig. 4.4b,d & S4.16 - S4.17). The effects of extreme rainfall on the soil thermal regime in ice-rich Siberian lowland tundra are summarized in figure 4.5.

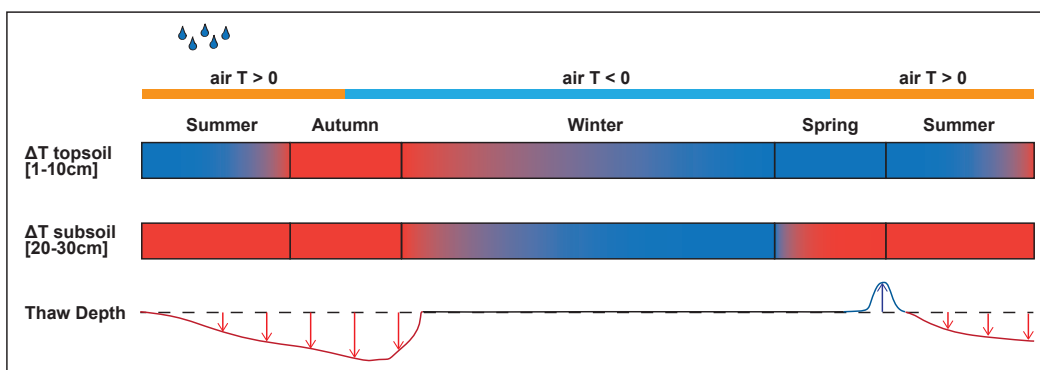


Figure 4.5) Conceptual diagram of the effect of extreme rainfall on the soil thermal regime. Schematic representation of the soil thermal regime under increased rainfall throughout the year and the following summer season, based on field observations and model results (fig. 4.1, S4.8 & S4.16-S4.17). The top two bars represent temperature differences in the organic topsoil (0-10cm depth) and mineral subsoil (20-30cm depth) relative to a situation with average rainfall. Red colours indicate warmer temperatures under extreme rainfall and blue colours represent colder temperatures under extreme rainfall. The bottom line represents differences in thaw depth compared to a situation with average rainfall, with red downward arrows representing deeper thaw, blue upward arrows indicating shallower thaw and black colours representing no thaw depth (fully frozen soil). The effects of extreme rainfall vary by depth, with topsoils exhibiting evaporative cooling and persistent warming throughout autumn and early winter, whereas subsoils show warming in summer and cooling in winter.

4.4.3 Combined dynamics of summer rainfall and air temperature determine permafrost thaw dynamics

In recent years, enhanced permafrost thaw following extreme rainfall is being increasingly reported in observational and model-based studies (Iijima et al. 2010, Neumann et al. 2019, Douglas et al. 2020, Mekonnen et al. 2021b). Our study provides the first controlled, experimental estimates of the magnitude and duration of such effects. We found a substantial increase in thaw depth (up to 35%) under a 120% increase (+100mm) in rainfall. Effects persisted for at least the two years following the rainfall treatment. Soil thermal-hydrological modelling suggests that increased rainfall likely warmed the soil through direct input of warmer rainwater into colder soils (advective heat transfer) and increased heat conduction in summer. Rather than variability in rainfall per se, modelled effects of rainfall on active layer thickness (ALT) depended strongly on timing of rainfall extremes relative to air temperature dynamics (fig. 4.4 & S4.15). Modelled increases in ALT were largest when rainfall extremes occurred during warmer mid-summer conditions (fig. 4.4c & S4.15). While the percentage increase in ALT was comparable in summers with average and high temperatures (fig. 4.4a, up to 8.5%), net increases in ALT were larger under a combined increase in rainfall extremes and air temperature (up to 2.3cm in average and 3.7cm and warm summers) (fig. S4.15). These increases may be larger in reality, since the model yielded conservative estimates of the effects of irrigation on permafrost thaw (fig. 4.3). Interactive effects with temperature may be attributed to increased heat transfer into the soil with infiltration of rainwater, since the temperature of rainwater tends to follow ambient air temperature (Neumann et al. 2019). Larger temperature gradients between soil and soil surface in warmer periods may also enhance conductive heat transport into the soil (Hinkel et al. 2001). Late summer rainfall had little to no effect on ALT in the same season, but most pronouncedly delayed freeze-up and showed the highest potential for carry-over effects (fig. 4.4c-d & S4.16 - S4.17). As the frequency of extreme rainfall events in the Arctic is anticipated to increase (Bintanja et al. 2020), it is important that rainfall effects on permafrost dynamics are accounted for in projections of future permafrost degradation. Our findings suggest that this requires high temporal resolution (ideally daily) climate data with accurate representation of rainfall extremes and concurrent air temperatures, and detailed representation of soil thermal hydrology and advective heat transfer from infiltrating rain in land surface models.

4.4.4 Implications for thermal hydrological modelling of permafrost soils

Using state-of-the-art numerical modelling of soil thermal hydrology, we were able to support field-observed effects with mechanistic insight into the effects of extreme rainfall on soil thermal dynamics. Our model parametrization represented field-measured permafrost thaw dynamics reasonably well (fig. 4.3 & S4.9). Still, modelled differences in thaw depth under increased rainfall and carry-over effects were conservative compared to those measured in the experimental treatments. This may be a result of overestimation of evaporative fluxes and resulting cooling (fig. S4.10 – S4.11). The model indicates substantial evaporative topsoil cooling (fig. S4.6a & S4.16 – S4.17), which was not as evident from field measurements (fig. S4.8a). Moreover, in its current configuration ATS only accounts for surface evaporation using a vegetation-dependent roughness length (Atchley et al. 2016), and disregards potential further effects of vegetation (e.g. transpiration, retention of moisture in moss tissue and canopy shading) (Blok et al. 2010, Atchley et al. 2016, van Huissteden 2020). This may help explain the smaller effect of rainfall in model results compared to field results (Mekonnen et al. 2021b). As future changes in Arctic vegetation are expected to alter the surface energy budget and thermal properties of permafrost soils (Loranty et al. 2018a), expansion of soil thermal hydrology models to include canopy processes and transpiration is recommended.

Lastly, fine-scale landscape heterogeneity causes a wide range of soil hydrothermal properties, which can strongly control thaw dynamics and their response to climate change (Atchley et al. 2016, Liljedahl et al. 2016, Abolt et al. 2018, Loranty et al. 2018a, Abramov et al. 2019). This was also evident from the fairly wide range of field-observed thaw depths, temperature and moisture conditions (fig. 4.2c-e & S4.4 - S4.5). Our one-dimensional numerical model only considers averaged site conditions and behaviour,

leading to potential inaccuracies and a disregard for lateral transport of moisture and heat and spatial heterogeneity of effects. Extension to 3D numerical models (Abolt et al. 2018) can be used to account for such nuances if sufficient spatially distributed field data are available.

4.4.5 Implications for permafrost ecosystems

The identified impact of rainfall on permafrost thaw dynamics suggests increased ecosystem change and feedback to climate in summers that are both warm and wet. With persistent Arctic warming and anticipated increases in rainfall extremes (Bintanja and Selten 2014, Wang et al. 2021), near-surface permafrost may degrade and disappear faster than is currently anticipated based on temperature changes alone (e.g., 40% areal loss under 2°C of warming)(Chadburn et al. 2017). This may apply especially to ice-rich permafrost, where enhanced thaw following combined warming and rainfall extremes can result in soil subsidence due to melting of abundant ground ice (thermokarst). Thermokarst triggers local feedbacks such as concentration of lateral flow, accumulation of water in the soil profile (fig. 4.2d & S4.6b) and accumulation of snow in depressions in winter, accelerating permafrost degradation over longer timescales (Jorgenson et al. 2006, Nauta et al. 2015, Atchley et al. 2016, Olefeldt et al. 2016). Extreme summer drought in contrast, may protect permafrost from high summer temperatures due to stronger thermal insulation of dry soil and reduced heat inputs from infiltration of rainwater.

Apart from deeper thaw, model results indicate delayed autumn freeze-up following rainfall extremes. Methane emissions during freeze-up are considerably higher than those during winter and spring and may constitute as much as 20% of total annual methane emissions (Mastepanov et al. 2008, Bao et al. 2020). A delayed or prolonged freeze-up period in wetter soils thereby likely enhances methane emission (Bao et al. 2020). This freeze-up delay was largest under late summer rainfall extremes (fig. 4.4d). Due to temperature increases, an increasing proportion of autumn precipitation will fall as rain rather than snow in the future (Bintanja and Selten 2014, Bintanja and Andry 2017), likely further contributing to autumn methane emissions. Additionally, warmer and wetter conditions in subsoils (fig. S4.16 - S4.17) may promote methane production (Turetsky et al. 2014, Neumann et al. 2019), while methane oxidation may be reduced in wetter and colder (fig. S4.16 – S4.17) topsoils (Göckede et al. 2017). As a result, methane emissions may increase more than would be anticipated based on temperature increases alone. Conversely, cooling of the topsoil and soil wetting can reduce CO₂ emissions through reduced ecosystem respiration (Göckede et al. 2017). However, rainfall extremes and associated cloudiness have also been observed to substantially reduce CO₂ uptake in Arctic ecosystems (Christensen et al. 2020). Effects of cloudiness were not accounted for using our methodology as irrigation was performed regardless of cloud cover and rainfall scenarios were modified without adjusting incoming shortwave radiation.

Lastly, impacts of rainfall-induced active layer deepening may vary among and within ecosystems. Although active layer deepening following extreme rainfall was modelled across a range of soil parameterizations (fig. S4.14), the magnitude of rainfall effects likely additionally depends on vegetation characteristics, topography, permafrost properties, regional climate and interactions among these. On a regional scale, climatic variability can regulate the depth of seasonally unfrozen soil and the extent to which rainwater can infiltrate, which in turn affects soil moisture dynamics and the relative importance of physical properties of the topsoil and subsoil in soil thermal-hydrological processes (fig. S4.14). This may lead to non-linear responses of permafrost thaw depth to rainfall increases under variable soil stratigraphy and physical properties (fig. S4.13 – S4.14). Topographical variability governs lateral flow and accumulation of water and heat, leading to localized effects (Neumann et al. 2019, Hamm and Frampton 2021). Lastly, vegetation can exert a strong control on the ground thermal regime (Blok et al. 2010, Loranty et al. 2018a), while vegetation itself may be subject to change under increasing rainfall. For instance, soil wetting following thermokarst can promote shifts from shrub- to graminoid dominated systems (van der Kolk et al. 2016, Magnússon et al. 2020), changing the surface energy balance (Loranty et al. 2018a). Moderate wetting however may promote shrub growth under previously

water-limited conditions (Ackerman et al. 2017, Opala-Owczarek et al. 2018). Persistent deepening of the active layer following increased rainfall can increase nutrient availability and rooting space, stimulating the growth of deeper-rooting graminoids (Wang et al. 2017). However, it may also facilitate deeper infiltration and drainage of rainwater (Liljedahl et al. 2016), resulting in a drying effect on longer timescales (see for instance reduced topsoil moisture in 2020, fig. 4.2e). Although evidence of adverse impacts of rainfall on permafrost thaw is emerging from across the Arctic, a complete perspective requires holistic monitoring of the effects of rainfall extremes across various Arctic ecosystems and climatic zones over longer time periods to better understand how environmental variability affects the sensitivity of permafrost to rainfall and temperature increases. Given the extensive need for input data and parameterization in permafrost thermal-hydrological modelling, challenges remain in upscaling to a wider Arctic context and accounting for key sources of uncertainty. Our current model representation suggests that environments with shallow organic layers, coarser soil textures and warm summers may be especially prone to increased permafrost thaw following extreme rainfall. Further extension across gradients in climate, topography, hydrology and vegetation is necessary to properly assess spatial variability in the response of permafrost thaw to rainfall.

4.4.6 Outlook

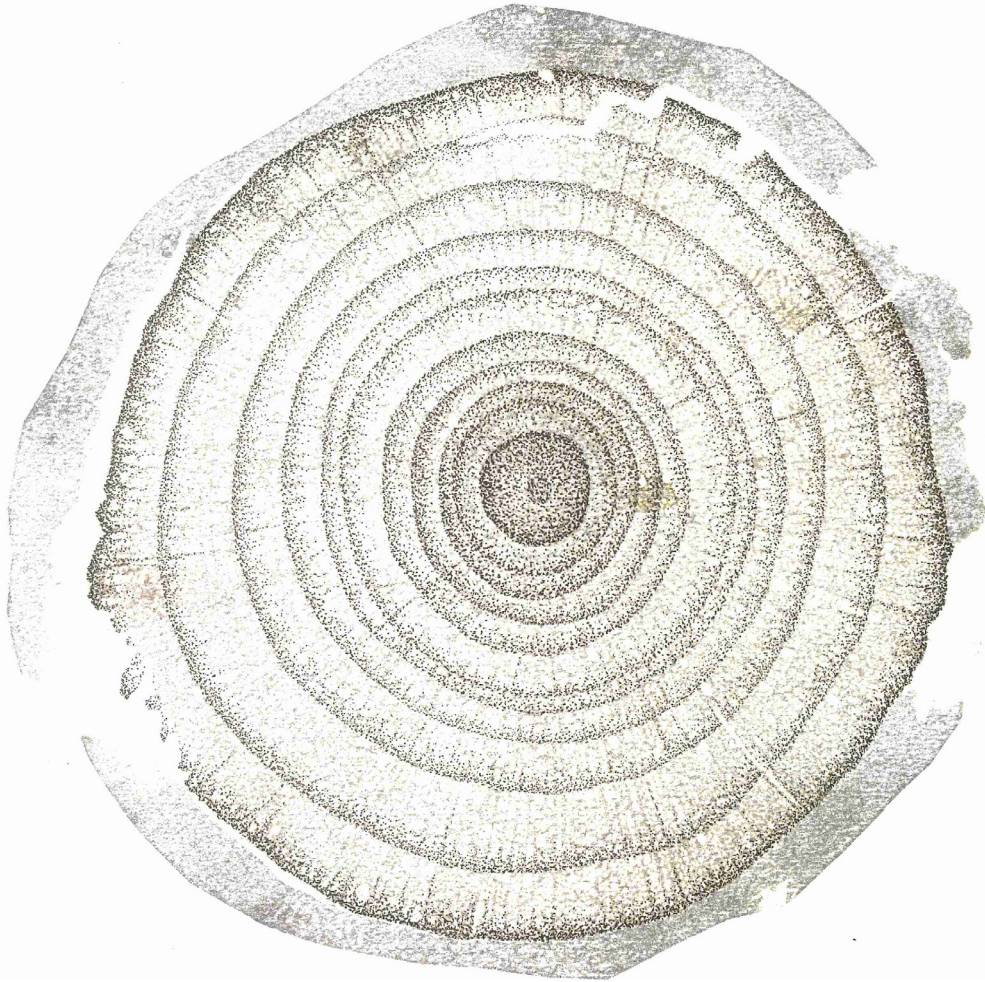
Using a controlled field experiment, we showed that extreme rainfall can enhance permafrost thaw for multiple years. Model analysis indicated that the magnitude of this effect depends on concurrent summer temperatures, with larger effects when rain falls during warm periods. Extension of our model representation to various soil textural and stratigraphical classes suggests that larger effects of rainfall on permafrost thaw may be observed in regions with shallow organic soil layers and coarse mineral soil texture. As the response of permafrost to increased rainfall likely varies across a wider range of environmental conditions with a high degree of local interaction, spatially distributed evidence is necessary to assess the sensitivity of permafrost to future rainfall increases on a panarctic scale. Our combination of field irrigation experiments, monitoring and permafrost modelling proved to be a valuable approach to do so.

Extremely wet summer events enhance permafrost thaw

5.

**Precipitation variability differentially affects growth
and temperature response of *Betula nana* across
topographical gradients in a Siberian lowland tundra site**

Rúna Í. Magnússon, Ute Sass-Klaassen, Juul Limpens, Sergey V.
Karsanaev, Susan Ras, Ko van Huissteden, Daan Blok, Monique
M.P.D. Heijmans



5.1 Abstract

Shrubs are expanding in a warming Arctic, and have the potential to influence ecosystem energy balances, permafrost processes and greenhouse gas exchange. While shrub growth generally responds positively to warming and higher moisture availability, spatial and temporal variability in climate response remains poorly understood. We constructed ring width series (1974–2018) for Arctic dwarf shrubs (*Betula nana*) for three types of subsites in the Siberian lowland tundra: (1) dry shrub-dominated patches and (2) small (< 100m²), wet thaw ponds – both in a drained thaw lake basin - and (3) a Pleistocene Yedoma ridge. To assess scalability of relations between climate and shrub growth across heterogeneous tundra environments and increasing climatic variability, we assessed decadal variability in climate-growth response across subsites. Summer temperature, summer rainfall, snow height and date of snowmelt were the main climate factors in radial stem growth across subsites. Shrubs showed increasing sensitivity to summer rainfall, especially after prolonged dry periods during 2000 to 2010. Shrubs sampled from thaw ponds showed a stronger positive response to summer rainfall, followed by high shrub mortality after an extremely wet summer. This suggests a non-linear response of *Betula nana* to summer rainfall regulated by microtopography. Shrubs sampled from an elevated (10–25m) Yedoma ridge showed a distinctly negative response to recent extreme snowfall and increasingly positive response to summer rainfall during relatively dry recent decades. Our findings suggest local landscape controls, co-limitation between temperature and moisture and nonlinearities in climate response of *Betula nana* under increasing precipitation variability and extremes. These results imply that the assessment of future shrub growth is less straightforward than assumed based on simple climate-growth correlations. Field experiments simulating (multiple) weather extremes with detailed monitoring of microsite conditions and shrub physiology would help identify relevant mechanisms for projection of future Arctic shrub growth in heterogeneous and dynamic tundra environments.

5.2 Introduction

With air temperatures in the Arctic increasing three times as fast as the global average (AMAP 2021), Arctic ecosystems are subject to drastic ecological changes (Box et al. 2019, Meredith et al. 2019, AMAP 2021). Shrubs in particular tend to respond positively to Arctic warming. This trend is evident from shrub cover and abundance data from long term monitoring sites (Elmendorf et al. 2012a, Martin et al. 2017, Bjorkman et al. 2020, Heijmans et al. 2022), warming experiments (Hobbie and Chapin III 1998, Walker et al. 2006, Elmendorf et al. 2012b, Bjorkman et al. 2020, Ercan et al. 2021), tree ring studies (Bär et al. 2008, Forbes et al. 2010, Blok et al. 2011b, Hollesen et al. 2015, Myers-Smith et al. 2015a) and satellite observations of shrub expansion (Tape et al. 2006, Forbes et al. 2010, Frost et al. 2014, Nitze and Grosse 2016). Increases in abundance, cover and height of shrub canopies affect ecosystems in multiple ways, which can result in complex and highly site-specific feedbacks (Lorantny and Goetz 2012, Heijmans et al. 2022). Increases in shrub cover and height can affect the depth, density and duration of snow cover, which generally results in increased soil temperatures in winter (Sturm et al. 2001, Myers-Smith and Hik 2013, Wilcox et al. 2019, Kropp et al. 2021). In contrast, shading of the ground surface, evapotranspiration and accumulation of organic layers generally lead to soil cooling in summer (Blok et al. 2010, Heijmans et al. 2022). Lastly, shrub growth may affect the tundra greenhouse gas balance through changes in carbon sequestration in shrub biomass (Walker et al. 2006, Forbes et al. 2010, Elmendorf et al. 2012a, Tremblay et al. 2012, McGuire et al. 2018, Mekonnen et al. 2021a). Given these substantial ecosystem impacts, it is relevant to assess to what extent future shrub expansion can be expected across a heterogeneous and rapidly warming Arctic.

Across Arctic and Alpine ecosystems, shrub growth shows strong correspondence to summer temperature (Bär et al. 2008, Forbes et al. 2010, Blok et al. 2011b, Myers-Smith et al. 2015a). Beside direct influences of warming, shrub growth may be affected by lengthening of the growing season,

advances in the timing of snow melt and deepening of the active layer in permafrost soils and resulting increases in nutrient availability (Oberbauer et al. 2013, Myers-Smith et al. 2019). The degree to which shrubs can respond to increasing summer temperatures generally depends on moisture availability. Dry conditions can limit the temperature response of tundra shrubs (Elmendorf et al. 2012a, Tape et al. 2012, Tremblay et al. 2012, Piao et al. 2014, Myers-Smith et al. 2015a, Ackerman et al. 2017, Opala-Owczarek et al. 2018, Buchwal et al. 2020) and reduce colonization (Frost et al. 2013). As a result, anticipated increases in Arctic precipitation and variability thereof (Bintanja et al. 2020) may be an important control on temperature-induced shrub growth (Myers-Smith et al. 2015a). Snow conditions and temperature during winter provide additional controls on Arctic shrub growth. Continuous snow cover protects shrubs from frost damage during the cold season (Bokhorst et al. 2009, Phoenix and Bjerke 2016, Bjerke et al. 2017, Treharne et al. 2019). Winter and spring warming can contribute positively to shrub growth (Fraser et al. 2014, Hollesen et al. 2015, Krab et al. 2018), likely as a result of earlier snowmelt and earlier drainage and warming of soils. This stimulates microbial decomposition and enhances nutrient availability in the following growing season (Sturm et al. 2005, Fraser et al. 2014, Hollesen et al. 2015). However, if extreme winter warming or early spring thaw results in removal of protective snow cover, subsequent frost events can result in shrub damage and compromised growth (Bokhorst et al. 2009, Bjerke et al. 2017, Treharne et al. 2019).

The influence of climate factors on growth of Arctic shrubs is unlikely to be spatially and temporally uniform. Contrasts in climate response across topographical and hydrological gradients are increasingly emerging from dendrochronological and monitoring studies (Opala-Owczarek et al. 2018, Black et al. 2021, Dobbert et al. 2021), both on coarser, panarctic scale with longer records (Buchwal et al. 2020), regional scale (Ropars et al. 2015, Ackerman et al. 2017) and highly local (sub-kilometer) scales (Black et al. 2021, Dobbert et al. 2021). Contrasts in moisture availability have been related to differences in shrub temperature response on panarctic (Buchwal et al. 2020) to regional scale (Ropars et al. 2015, Ackerman et al. 2017), and additional microscale variability in shrub growth has been observed under differential snow accumulation (Lawrence and Swenson 2011, Lorant and Goetz 2012, Krab et al. 2018, Wilcox et al. 2019, Dobbert et al. 2021). Additional spatial factors in climate-growth response include microclimate variability, biotic interactions, permafrost dynamics and herbivory (Martin et al. 2017). In addition, dendroclimatological studies over longer timescales often reveal non-stationary climate effects on shrub growth (Wilmking et al. 2005, D'Arrigo et al. 2008, Hollesen et al. 2015, Francon et al. 2020, Francon et al. 2021). Due to for instance non-linear growth responses, increasing climate variability or co-limitation processes, the strength or even direction of climate-growth relationships can vary over time (Jevšenak and Levanič 2016, Gamm et al. 2018, Buchwal et al. 2020). Quantitative assessment of local-scale controls on Arctic shrub climate-growth relations over longer time periods at a spatial scale relevant for tundra ecosystem heterogeneity remains a key knowledge gap that hampers projection of future shrub expansion rates (Martin et al. 2017, Myers-Smith et al. 2020, Mekonnen et al. 2021a).

Here, we study the climate response of radial stem growth in the Arctic shrub *Betula nana* in a North-Eastern Siberian tundra site across small scale (meter to kilometer) landscape heterogeneity over a time period of 45 years using a dendrochronological approach. Dendrochronology, the study of tree rings, offers a standardized way to study annual dynamics of radial stem growth of woody species across Arctic environments (Myers-Smith et al. 2015b). Radial stem growth generally corresponds to increases in above-ground shrub biomass (Le Moullec et al. 2019). We explicitly incorporate potential co-limitation by temperature and precipitation as an interactive effect, to better understand interactions between multiple climatic influences over longer timescales (Mekonnen et al. 2021a). Using this approach, we expected to capture local differences in strength and temporal development of climate-growth relations in a warming climate on ecologically relevant (meter) spatial scales. Through this study we aim to contribute to better understanding of the extent to which general relations between climate and shrub growth can be scaled across heterogeneous landscapes and future climate change.

5.3 Methods

5.3.1 Study site & species description

We conducted our dendrochronological study at the Chokurdakh Scientific Tundra station (70 °49'N, 147°29'E) in the North-Eastern Siberian lowland tundra (Indigirka Lowlands) (fig. 5.1a). On a larger scale (kilometers), the study area is characterized by thaw lakes, floodplains, overlapping drained thaw lake basins ('alases') of various ages and low ridges representing erosion remnants of late Pleistocene Yedoma deposits (van Huissteden et al. 2021) (fig. 5.1b). The area is characterized by continuous ice-rich permafrost with a shallow active layer of approximately 40-50cm (CALM 2021). Mean annual temperature and precipitation are -12.7°C and 189mm, average July temperature and precipitation are 10.6°C and 22mm (1990-2020) (RIHMI-WDC 2020). The peak growing season is July-August (Van der Molen et al. 2007). Higher elevation sites such as Yedoma ridges and pingos generally feature mixed tussock-sedge (*Eriophorum vaginatum*) and dwarf shrub vegetation. On smaller spatial scales (meters), low lying areas such as drained thaw lake basins feature slightly elevated shrub patches dominated by *Betula nana*, lichens and mosses, alternating with waterlogged depressions with standing water, aquatic sedges (e.g. *Eriophorum angustifolium*, *Carex* spp.) and peat moss (*Sphagnum* spp.) (Siewert et al. 2015, Magnússon et al. 2021). Soil properties generally vary on highly local scales, but show some correspondence with vegetation composition (table 5.1) (Bartholomeus et al. 2012).

This study focuses on the response of the Arctic dwarf birch (*Betula nana*) to a warming Arctic. *Betula nana* is one of the most widespread Arctic shrub species and may be found in Arctic tundra as well as alpine environments (GBIF 2021). Its growth form varies from low (around 5cm) and decumbent in high Arctic sites to more erect (around 30cm) under more favorable environmental conditions (De Groot et al. 1997, Myers-Smith et al. 2015b). At our sites shrubs generally reach a height of around 20cm and establish both as seedlings and ramets (vegetative clones) (Li et al. 2016). *Betula nana* is associated with moist, acidic and nutrient poor sites with thick organic layers, but does not tolerate prolonged waterlogging (De Groot et al. 1997). Its photosynthetic optimum lies around 10-13°C. Growth starts up rapidly after the thawing of the frozen topsoil and shoot growth continues until mid-summer (De Groot et al. 1997).

5.3.2 Dendrochronological data

5.3.2.1 Sampling

84 shrub ramets were sampled in thaw ponds and in shrub patches in the lakebed in the late summer of 2018 and on the Yedoma ridge in the late summer of 2020. In the lakebed, shrubs were sampled from shrub-dominated, irregular frost mounds and small (< 100m²) thaw ponds within such shrub patches in approximately equal proportions. Most shrubs sampled from thaw ponds were dead or showed signs of compromised growth (small and discoloured leaves), but the stem was generally sufficiently intact to discern tree rings. This allowed for identification of potential contrasts in shrub radial stem growth under progressive thermokarst relative to intact shrub dominated areas. On the Yedoma ridge, few thermokarst depressions occur and vegetation is relatively homogeneous (table 5.1), so no further microtopographical subdivision was made. To mitigate imbalances in sample availability among subsites, three ring width series from the ridge site were added from Blok et al. (2011), available from the ShrubHub database (Myers-Smith et al. 2015a). This resulted in three types of subsites, representing a (micro)topographic gradient from elevated ridge to lakebed shrub patches to thermokarst depressions (fig. 5.1c). Using a GPS, shrub locations were recorded with approximately 2m accuracy. Samples were taken from relatively large, undamaged shrubs where possible. Shrub roots were dug out partially to visually identify the root collar (transition between stem and root). 2cm stem segments were sampled along the main stem at the root collar, at the moss surface and just below the first above-ground branch (generally < 10cm above the moss surface) (Blok et al. 2011b, Li et al. 2016). Stem fragments were kept

Table 5.1) Differences in abiotic conditions (mean \pm standard deviation) and vegetation composition among different types of sampling locations

Variable	Date	Ridge	Drained Thaw Lake Basin		Ref.
			Ponds	Shrub Patches	
Elevation	Various	20-35 m a.m.s.l.	9-11 m a.m.s.l.		1
	July 2018	-	Ponds 30 to 50cm lower than shrub patches		2
Soil Moisture (top 5 cm)	July 2007	39.0 \pm 7.4 vol-%	30.0 \pm 6.8 vol-%		3
	July 2008	21.0 \pm 7.8 vol-%	17.5 \pm 5.4 vol-%		3
	July 2012	-	85.0 \pm 8.5 vol-% *		4
	August 2018	-	88.7 \pm 23.1 vol-%		2
Snow Height	May 2008	30.2 \pm 6.7 cm	29.5 \pm 6.9 cm		3
	April 2012	-	35.0 \pm 4.4 cm*		4
	August 2012	Turbels	Historturbels (Histrels locality)		5
Soil Type	Summer 2008	Soil stratigraphy varies on microscale (meters) based on topography and wetness			
	August 2012	12.3 \pm 8.6 cm**	20.6 \pm 5.7 cm**		5**
Organic Layer Depth	August 2019	-	24.7 \pm 5.2 cm		2
	July 2007	33.1 \pm 4.4 cm	22.4 \pm 2.9 cm		3
Thaw Depth	July 2010	28.4 \pm 5.3 cm	22.7 \pm 1.9 cm		3
	August 2012	38 \pm 11.7 cm**	43 \pm 10.3 cm**		5**
	July 2018	-	40.3 \pm 10.5 cm		2
Landscape Composition	Various	Homogeneous, with frost boils, and ice wedges several meters wide	Heterogeneous, polygons or irregular frost mounds with waterlogged depressions		5**,6
Vegetation Composition	July 2019	Tussock sedges (<i>Eriophorum vaginatum</i>), dwarf shrubs (<i>Betula nana</i> , <i>Salix pulchra</i> , <i>Salix glauca</i> , <i>Rhododendron tomentosum</i> , <i>Vaccinium vitis-idaea</i> , <i>Vaccinium uliginosum</i> , <i>Dryas octopetala</i>), mosses and lichens (a.o. <i>Polytrichum</i> and <i>Dicranum</i> spp., <i>Flavoetzeria acullata</i> , <i>Cladonia</i> spp., <i>Hylacomium splendens</i>)	Drowned shrubs, standing water, sedges (predominantly <i>Eriophorum angustifolium</i> and <i>Carex aquatilis</i>) and <i>Sphagnum</i> (mainly <i>S. subsecundum</i> and <i>S. squarrosum</i>) in older ponds.		7

Footnotes on next page

- 1) ArcticDEM (Porter et al. 2018)
- 2) Magnússon et al. 2020
- 3) Blok et al. 2010
- 4) Nauta et al. 2015
- 5) Siewert et al. 2015
- 6) Wang et al. 2016
- 7) Magnússon et al. 2021

*) Nauta et al. (2015) measured abiotic conditions in very recently formed thaw ponds whose formation was triggered by shrub removal

***) Siewert et al measured abiotic conditions in the landscape subclasses “tussock tundra”, “sedge fen” and “dwarf shrub fen”, generally equivalent to our sampling site subdivision.

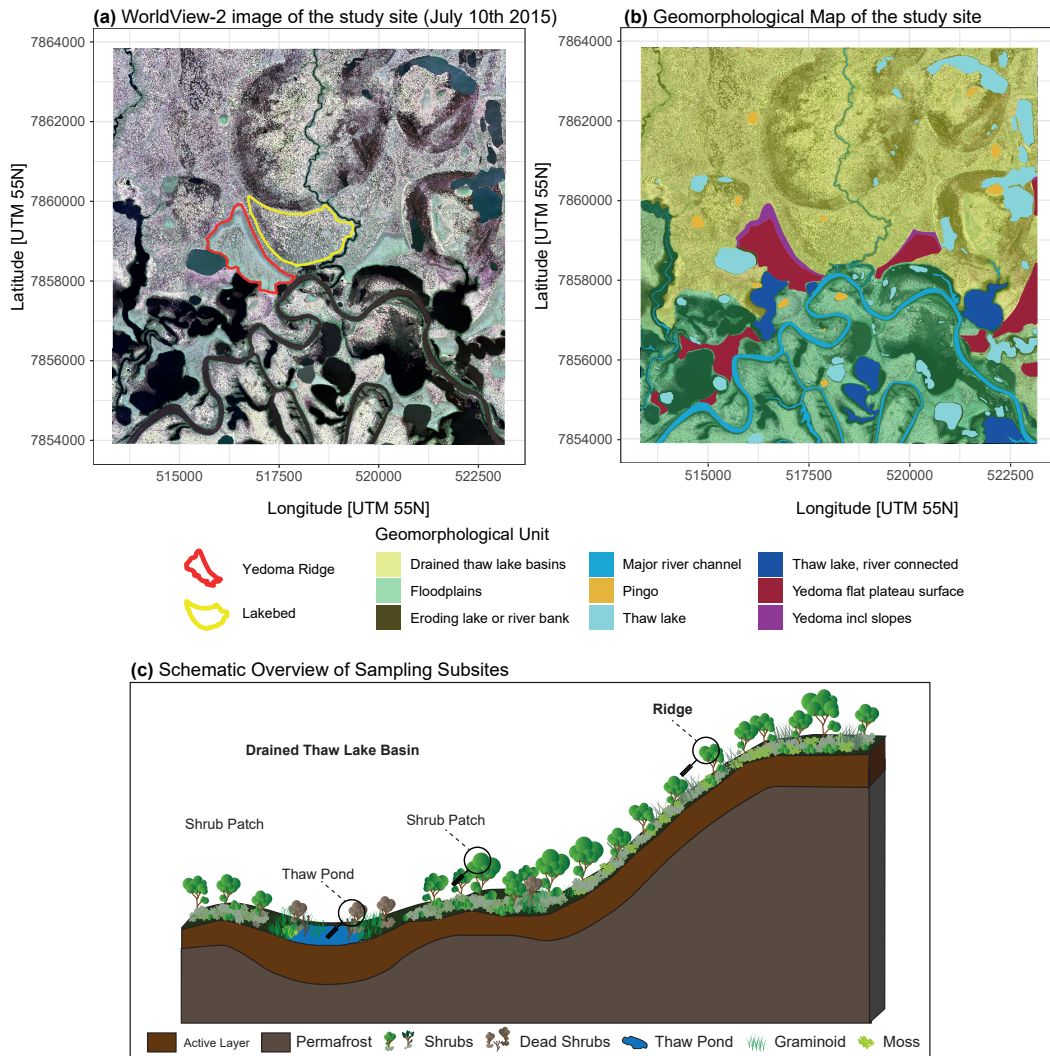


Figure 5.1) Site overview. (a) 10 x 10 km WorldView-2 image (July 2015) of the study site. WorldView 2 © MAXAR, 2019. (b) Geomorphological map of the study site by van Huissteden & Beletti Marchesini (2014), with WorldView-2 image as background. In a-b, the yellow polygon represents the drained thaw lake basin and the red polygon indicates the Yedoma ridge. (c) Schematic overview of topographical and hydrological conditions and vegetation composition in the three types of sampling subsites.

in a 1:3 solution of glycerol and alcohol (vodka). For all shrub samples from the Yedoma ridge and a subset of shrubs from the lakebed, the aboveground length of the stem was measured along the longest branch prior to cutting stem fragments.

5.3.2.2 Ring width measurement and chronology development

Sections of shrubs from thaw ponds and shrub patches were collected during the summer of 2018 and measured and crossdated earlier by Magnússon et al. (2020) for the purpose of age determination of shrubs. Samples from the Yedoma ridge were collected during summer 2020. Crossdating of ring width series of individual shrubs was carried out separately per subsite.

Due to frequently missing rings in *Betula nana* (Myers-Smith et al. 2015b), ring widths of shrub samples were measured using a hierarchical approach based on serial sectioning (Kolischuk 1990, Hallinger et al. 2010, Wilmsking et al. 2012, Myers-Smith et al. 2015a, Myers-Smith et al. 2015b). An elaborate description is available in text S5.1. Shrub ring widths were measured in CooRecorder v. 9.0 (Cybis 2019b) on high resolution microscope images of micro-thin (20 to 30 μm) radial sections of the sampled shrubs along two to four (usually three) radii per section. Sections were cut from the samples at the root collar, moss surface and below the first branch). Visual crossdating was carried out in WinTSAP v. 4.70d (Rinntech 2017). Missing rings were inserted manually by first visually crossdating radii within a section. Radii were then averaged to a section ring width series. Next, sections within a shrub were visually crossdated against other shrubs in the same subsite and checked for missing rings.

Individual sections' ring widths were detrended for age-related growth effects using C-method detrending (Biondi and Qeadan 2008) in R using the dplR package (Bunn 2008). Next, sections within a shrub were retained and averaged if they showed significant correlation among sections and otherwise omitted from analysis (see text S5.1). Then, samples with significant correlation coefficients ($p < 0.05$) compared to average detrended ring width of the rest of the dataset and a series length of at least 30 years were selected to develop a residual chronology. Exceptions were made for shrubs with shorter ring width series (25 to 30 years) but very strong visual correlation towards the rest of the dataset, or shrubs with very long ring width series ($n > 60$) but insignificant correlation ($p < 0.1$). After selection of shrubs, the first 5 years of each ring width series were removed to reduce the effect of irregular juvenile growth. Residual chronologies were developed for the overall study area (based on crossdating of samples from all three sites) and for each subsite separately, based on averaged residuals of the first-order temporal autocorrelation model fits per individual shrub, expressed as a dimensionless ring width index (RWI). We compared the different residual chronologies using lagged correlations to check for missing rings in each of the chronologies. Comparison of resulting chronologies with earlier dendrochronological work at the study site indicated strong correlations among the different chronologies of this study, and significant correlations with chronologies developed during earlier studies (Blok et al. 2011b, Li et al. 2016) (fig. S5.1). This indicates that any potential bias due to the separate measurement and initial visual crossdating process for the different sets of samples is limited.

Additionally, we exported residual RWI series for each individual shrub that was included for chronology development. Using averaged raw ring width measurements of individual shrubs, we calculated the age, final stem diameter (excluding bark tissues), average annual basal area increment and average basal area increment during the first 10 years of growth (here including the first 5 years of juvenile growth). Raw ring width measurements and ages were used to derive diameter-age curves per individual shrub. These age, diameter, length and growth relations were used to assess to what extent shrub growth strategy differs among the three subsites and among individuals.

5.3.3 Remote sensing time series

To gain a better understanding of dynamics of water, snow and vegetation seasonal phenology at the study site, and potential spatial heterogeneity therein, we extracted several coarse to very high resolution time series of remote sensing products for the study area. To approximate temporal dynamics in growing season soil moisture, we downloaded daily EUMETSAT scatterometer root zone soil moisture (RZSM) data (Datasets H141 and H142) (HSAF 2020). This coarse resolution data (10 x 10km) is available for 1992-2020 and was extracted for the topsoil layer (0-7cm). To assess potential variability in snow cover dynamics and phenology on smaller spatial scales, we selected cloud-free Sentinel-2 top-of-atmosphere reflectance (TOAR) (2016 – 2018) and surface reflectance (SR) (2019 – 2020) images from May – September from Google Earth Engine (earlier Sentinel-2 images are not available). For these images, we calculated NDVI and Pixel Snow Probability using standard Sentinel scene classification algorithms (Main-Knorn et al. 2017) (see text S5.2). We then extracted all pixel NDVI and Snow Probability values for each image in May and June for each shrub sampling site. We visualized pixel NDVI and Snow Probability values against the day of year and site type (ridge, shrub patch or pond) to assess whether snow and NDVI dynamics within the season differed among site types. Since wetness can vary on very small spatial scales in this ecosystem (Magnússon et al. 2020), we used two 2m resolution WorldView-2 satellite images to assess small scale spatial variability in surface wetness. Images were corrected to surface reflectance using MAXAR's ACOMP algorithm and were collected on July 10th 2015 and August 1st 2019. Average Normalized Difference Water Index (NDWI) values were used as an approximation of small-scale variability in terrain wetness. Since these high-resolution images were acquired at different seasonal timings, we did not derive a high resolution WorldView-2 NDVI. Lastly, we used the 2m resolution ArcticDEM (Porter et al. 2018) to extract elevation above mean sea level for each shrub sampling location, and a geomorphological map of the study area (van Huissteden and Belelli Marchesini 2014).

5.3.4 Statistical Analysis

5.3.4.1 Climate data and trends

Climate data for the site were retrieved for the Chokurdakh Meteorological Station (WMO code 29146, ± 27km Northeast from the site) from the AISORI database (<http://aisori-m.meteo.ru/waisori/>) of the All-Russia Research Institute of Hydrometeorological Information - World Data Centre (RIHMI-WDC 2020). Daily data of average, minimum and maximum temperature, total precipitation, snow height and snow extent are available for 1944-2020, but due to frequent data gaps in the first years of the record, data series for 1948-2020 were used. Based on these records we derive several annual climate variables that may potentially affect radial stem growth of *Betula nana* (expressed as annual RWI) in this ecosystem. We used a moving window correlation analysis with flexible windows size as implemented in the dendroTools package in R (Jevšenak and Levanič 2018) to explore during which periods *Betula nana* shows sensitivity to the available daily climate variables (temperature, precipitation and snow height). Sensitivity was expressed as Pearson correlation between RWI and a daily climate variable, using a 95% bootstrap (n=100) adjusted confidence interval to determine significance (Jevšenak and Levanič 2018). Moving window analysis was performed for climate variables in the current as well as previous year. We combined outcomes of the moving window analysis (fig. S5.3) with results from earlier climate-growth studies of *Betula nana* from the study site (Blok et al. 2011b, Li et al. 2016) and other Arctic environments to preselect climate variables relevant for radial stem growth of *Betula nana* in our study site (table 5.2).

The resulting climate dataset includes summer (June-July) (Blok et al. 2011b, Li et al. 2016) and winter (November-April) temperature (Hollesen et al. 2015), summer precipitation (June-July) (Blok et al. 2011b, Li et al. 2016) and snow height (rather than winter precipitation) (Bokhorst et al. 2009), for year of growth as well as previous years (fig. S5.3) (Blok et al. 2011b). Date of snowmelt and several degree day products (Wipf et al. 2006, Hallinger et al. 2010, Wipf and Rixen 2010, Francon et al. 2020, Ercan

Table 5.2) Overview of climate variables potentially relevant in climate-growth relations of *Betula nana*

Variable	Abbreviation	Description
Mean Temperature June-July	T – summer	Mean of average daily temperatures in June and July (= early summer)
Previous year's Mean Temperature June-July	T – prev.summer	T – summer of previous year
Total Precipitation June-July	P – summer	Sum of total daily precipitation in June and July
Previous year's Total Precipitation June-July	P – prev.summer	P – summer of previous year
Mean Temperature Winter	T - winter	Mean of average daily temperatures in November-April
Previous year's Mean Temperature Winter	T – prev.winter	T – winter of previous year
Max Snow Height April-May	S – spring	Maximum observed snow height in April and May
Previous year's Max Snow Height April-May	S – prev.spring	S – spring of previous year
Date of Snow melt	Melt Date	First day with no snow cover in May-June
12-month Standardized Precipitation Evapotranspiration Index (SPEI) June-July	SPEI12 - summer	Mean SPEI (calculated over 12-month period) for June - July (Vicente-Serrano et al. 2010), using Hargreaves equation for potential evapotranspiration.
Snow free growing degree days	SFGDD	Sum of temperatures > 0°C on days with no snow cover in May - July
Growing Degree days > 5°C	GDD5	Sum of temperatures > 5°C in May - July
Spring Frost Events	Spring Frost	Sum of temperatures < 0°C occurring at least 5 days after snowmelt in May-July
Winter Warming Events*	Winter Warming	Sum of temperatures > 0°C in November-April
Interaction Summer Temperature and Precipitation	int(T,P) - summer	Product of standardized T – summer and P - summer
Quadratic term for summer temperature	T ² – summer	Squared standardized T - summer

*) Winter warming events were not observed over the study period and were not considered in further statistical analysis

et al. 2021) were added to define the duration and integrated temperature of the growing season. The 12-month Standardized precipitation Evapotranspiration Index (SPEI) (Vicente-Serrano et al. 2010) over summer (June-July) was added to represent moisture availability during the growing season (Li et al. 2016, Buchwal et al. 2020). Spring frost events (total freezing degree days in June and July occurring at least 5 days after snow melt) (Wheeler et al. 2014) and winter warming events (quantified here as thawing degree days in November-April prior to snow melt) were added to represent potential frost damage prior to the growing season (Bokhorst et al. 2009, Wheeler et al. 2014, Bjerke et al. 2017, Treharne et al. 2019). As a novel aspect, we added an interaction term for summer temperature and precipitation to

represent potential co-limitation of temperature and moisture availability during the growing season (Li et al. 2016, Buchwal et al. 2020), and a quadratic term for summer temperature to represent potential effects of extremes and diminishing growth returns under increasing summer temperature (Ackerman et al. 2017) (table 5.2).

We used monthly averages of average daily temperatures, total daily precipitation and daily snow height and selected annual climate variables to visually assess changes in weather conditions over the period 1948-2020.

5.3.4.2 *Climate-Growth Relations*

As an exploratory analysis, we quantified Pearson correlation coefficients for selected (table 5.2) climate variables and RWI values for the overall chronology and three subsite chronologies, visualized as scatter matrices. Climate data was standardized prior to correlation analysis. Afterwards, regression analysis was used to study associations between climate variables and radial stem growth of *Betula nana*, including all previous year's climate variables, selected interactions and quadratic terms based on literature screening (table 5.2).

Due to the large number of potentially relevant and multicollinear climate variables, and limited number of RWI observations, we use Orthogonalized Partial Least Squares (OPLS) regression. Partial Least Squares (PLS) regression is a multivariate regression method that quantifies association between a predictor matrix X and response matrix (or variable) Y by decomposing X and Y into latent factors. Contrary to Principal Component Regression, PLS decomposes both X and Y into latent factors in such a way that the multidimensional variance in Y that is explained by multidimensional components in X is maximized (Wold 1980). Orthogonalized Partial Least Squares (OPLS) regression is an extension to PLS in which orthogonal signal correction is used to separate variation in X into variation that is non-orthogonal (correlated) to Y and variation that is not orthogonal to Y (non-correlated) (Trygg and Wold 2002, Bylesjö et al. 2006). While PLS and OPLS are identical in terms of predictive performance, OPLS allows for better characterization of predictive versus non-predictive variation in X (Bylesjö et al. 2006). (O)PLS methods are widely used in chemometrics, bioinformatics and industrial fields, but have gained popularity in other fields owing to their ability to analyse dataset with few observations relative to the number of predictors and datasets with multicollinear predictors and their lack of distributional assumptions (Wold 1980). PLS has been successfully applied to ring width indices (Kalela-Brundin 1999) and dendrometer measurements (Löffler and Pape 2020, Dobbert et al. 2021) to characterize climate-growth relations.

Here, we employ OPLS regression as implemented in the `opls()` function in the `ropls` package in R (Thévenot 2016) to quantify associations between detrended ring width indices (Y) and a large set of z-scaled annual climate statistics (X) (table 5.2). The `opls()` function performs crossvalidation to select the optimal number of latent components and uses permutation tests to provide model diagnostics. As a measure of influence of individual X variables on Y, `opls()` provides estimates of regression coefficients based on the NIPALS algorithm (Thévenot et al. 2015, Thévenot 2016). Using an OPLS model with the optimized number of components we performed bootstrapping ($n = 200$) to derive standard errors, 95% confidence intervals and p-values for each regression coefficient estimate. This resulted in estimates, significance and confidence intervals of regression coefficients for each X variable for the overall chronology and the three subsites' chronologies.

5.3.4.3 *Spatio-Temporal Variation in Climate-Growth relations*

We extended our analysis to assess spatiotemporal variability in climate-growth relations by performing OPLS climate-growth regression separately for the three subsite chronologies, and for consecutive overlapping time periods by employing a moving window analysis. The OPLS analysis was first performed

over a common time period (1974 – 2018) in which climate data was available and all chronologies had a sample depth of at least 6 individual shrubs. Patterns of climate association were compared between the subsites to assess spatial variability.

The Siberian lowland tundra landscape can be highly dynamic (Magnússon et al. 2021) and changes in weather conditions may have occurred between 1974 and 2018, which likely affects climate-growth relations over time. To assess temporal variability in climate-growth associations, we executed the OPLS analysis over 30-year time windows with a 5-year time step, both for the overall and for the subsite chronologies. To assess whether changes in climate sensitivity over time are driven by climate change, we compared strength of climate – growth associations over these 30-year time intervals with mean values and variability of climate indices in the same periods.

We further explored spatial heterogeneity in climate-growth associations by comparing sensitivity to the main climate factors identified in the OPLS regression for individual shrubs to shrub characteristics and site factors (Trouillier et al. 2018). OPLS regression coefficient estimates were obtained for climate-growth relations of individual shrubs' RWI curves over a common time period (1980-2006). This selected common period is a compromise between the number of shrubs that could be included and length of the common period. We only included those climate variables that showed significant associations with any of the site chronologies in OPLS analysis. This resulted in separate estimated coefficients for the main climate variables for each individual shrub. We then assessed Pearson correlations between these estimated coefficients, shrub age, shrub growth rates and local abiotic conditions, extracted from remote sensing products using sampling site coordinates. Extracted remote sensing products included two-summer average WorldView NDWI (July 2015, August 2019) and elevation (ArcticDEM). Shrub growth rates included average radial stem growth rate and average radial stem growth rate for the first 10 years of shrub growth. Shrub age was defined as the mean age of each shrub in the selected time period (1980-2006). Using Pearson correlations among these different datasets we assess whether individual shrubs' climate response and growth rates were related to their age or selected abiotic site conditions.

5.3.4.4 Analysis of pointer years and extreme weather conditions

Lastly, we analyzed temporal patterns of pronouncedly poor and good growth years for all three subsites using pointer years. Pointer years are years that show extremely high or low RWI in a chronology. We quantified pointer years for the three subsite chronologies over the period 1959-2018 as years in which at least 50% of individuals showed RWI scores higher or lower than 1, 1.28 or 1.645 standard deviations away from the mean as weak, strong and extreme pointer years, respectively (Neuwirth et al. 2007). We used the pointRES package in R (van der Maaten-Theunissen et al. 2015) to identify pointer years. We then compared z-scaled annual climate variables for pointer years (Bär et al. 2006), restricting the comparison to those climate variables that showed correlation with at least one of the chronologies in the OPLS analysis. We tabulated RWI scores for the three subsites in the three years that showed the highest and lowest z-scaled scores for each significant climate variable from OPLS analysis to qualitatively assess which climatic conditions are associated with distinctly strong or poor growth years across subsites.

Throughout all statistical analyses a significance criterion of $\alpha = 0.05$ was used.

5.4 Results

5.4.1 Climate Trends

Mean annual temperature at the study site shows a warming trend of 0.3°C per decade since the start of the record in 1948. Warming is particularly evident since 1980 (0.7°C per decade, fig. 5.2a,d,f) and stronger in late and early winter (April, November) than in summer (June-August) (fig. 5.2a). Growing

degree days have increased mostly in June and August, suggesting earlier onset as well as later ending of the growing season (fig. 5.2e). Precipitation shows very high year-to-year variability, but also a general trend of decreasing summer rainfall (fig. 5.2b) and decreasing SPEI12 in June-July (fig. 5.2g) since 1990 (except for some very wet years). Snow height in late winter / spring fluctuates between 25 and 75cm, but was exceptionally high (100-200cm) in 2016-2018 (fig. 5.2c). Snow melt typically occurs around early June, but shows high year-to-year variability, with a trend for later snowmelt until approximately 1980 and a weak trend for earlier snow melt since 1980 (fig. 5.2h). Scatterometer data suggest average topsoil volumetric moisture contents of 40-80% in June-August (fig. 5.2i) with higher soil moisture availability in the rainier years of 2011 and 2015 (fig. 5.2b). These data suggest a lengthening of the growing season, with generally drier conditions during the last 20 years, but high recent year-to-year variability in precipitation and snow dynamics.

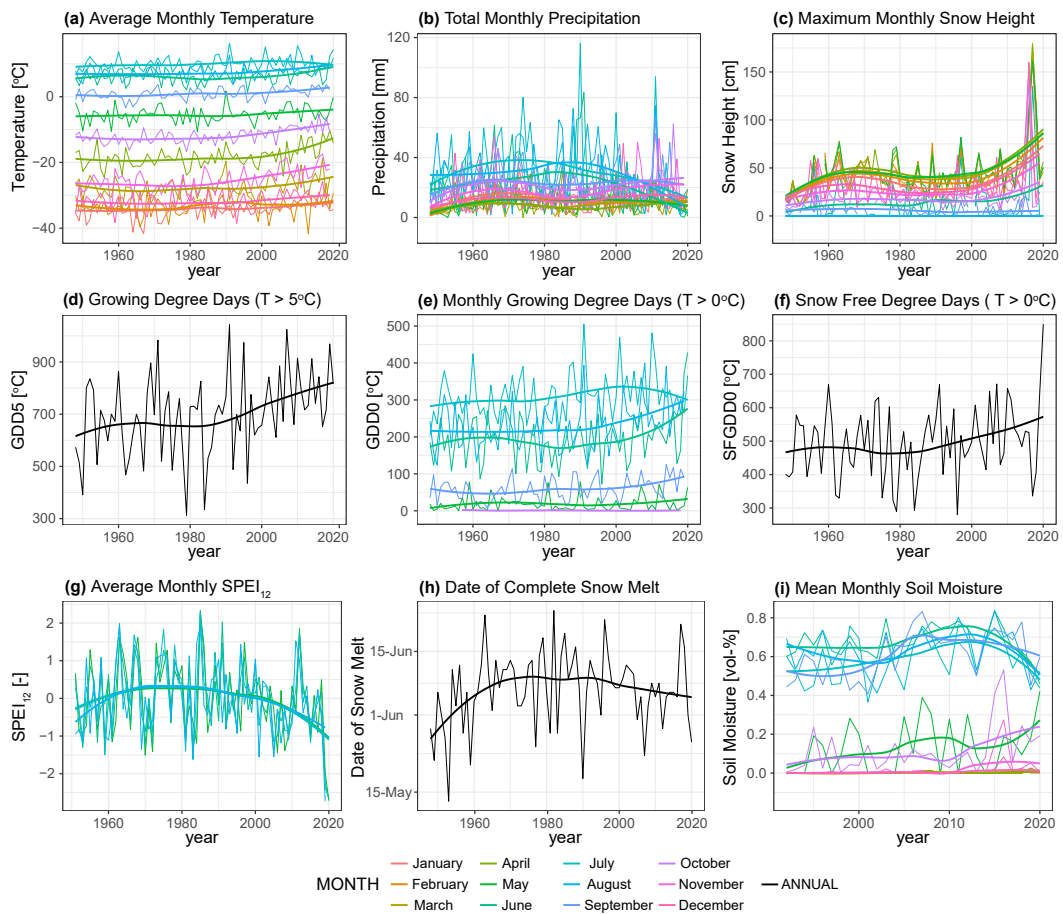


Figure 5.2) Annual and Monthly Climate Variables from 1948 to 2020, derived from the Chokurdakh Meteorological Station (WMO code 29146). Data retrieved from the AISORI database (RIHMI-WDC, 2021). EUMETSAT data (HSAF, 2020). Solid lines represent LOESS fits, thinner lines represent annual values. a) Monthly average of daily mean temperatures. b) Monthly sum of precipitation (rain and snow). c) Monthly maximum snow height. d) Total yearly GDD5 (sum of all temperatures > 5 oC). e) Total yearly GDD0 (sum of all temperatures > 0 oC), shown for May – October as other months had no temperature above 0 degrees over the observed period. f) Total annual snow free degree days (sum of all temperatures > 0 oC on days with no snow cover). g) Monthly average SPEI12 (shown for May-September only). h) Date of snow melt (first day of the year with zero snow height) i) Monthly mean soil moisture as derived from scatterometer data for a 10x10km surrounding the study site.

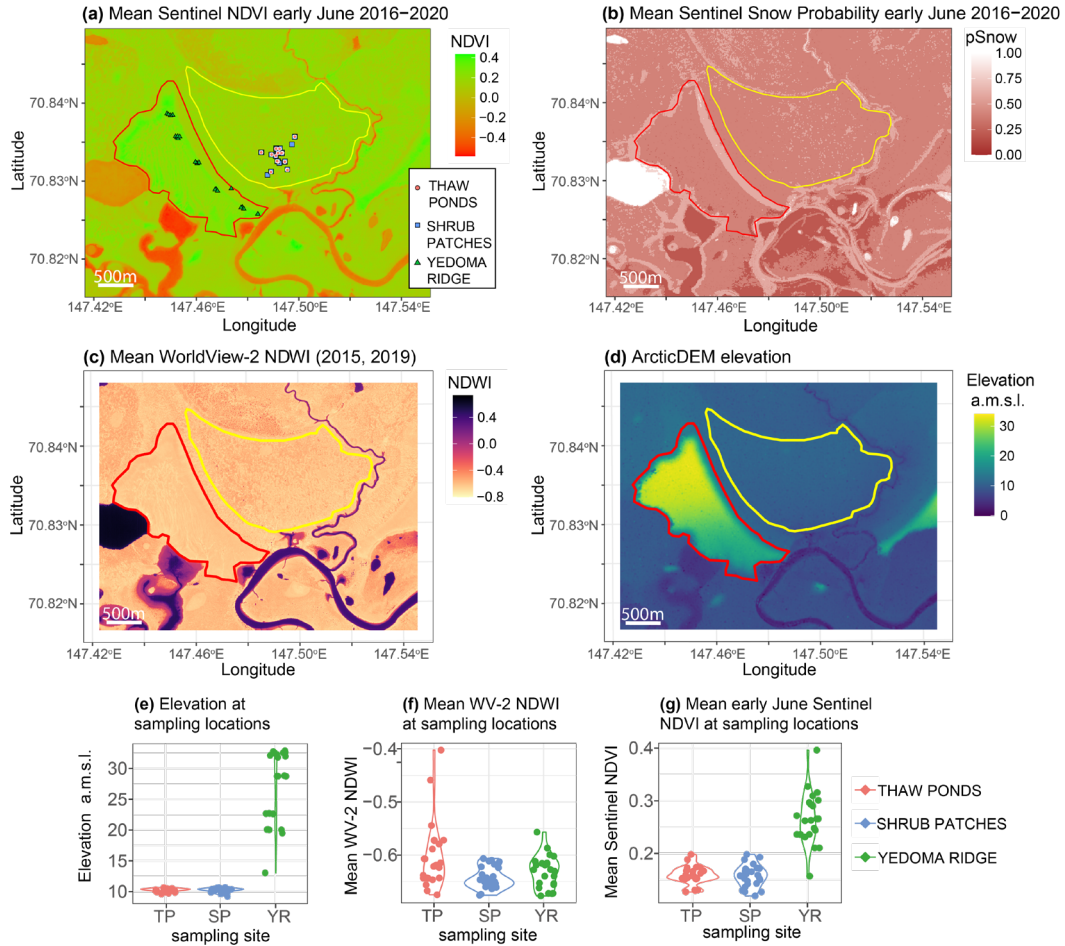


Figure 5.3) Spatial patterns of early June (June 3rd-June 12th) snow and NDVI dynamics, wetness and topography. a) Mean Sentinel-2 (2016-2020) early June NDVI. Points indicate sampling sites of shrubs selected for chronology development. Some overlap in points occurs due to proximity of sampling locations. b) Mean Sentinel-2 (2016-2020) early June pixel Snow Probability (0-1). c) Multiyear (2015, 2019) mean WorldView-2 NDWI. WorldView 2 © MAXAR, 2019. d) ArcticDEM elevation above mean sea level. In a-d, the red polygon indicates the Yedoma Ridge. The yellow polygon indicates the Drained Thaw Lake Basin. e) Elevation per sampling location of shrubs selected for chronology development. f) WorldView-2 NDWI per sampling location of shrubs selected for chronology development. g) Mean early June Sentinel-2 NDVI per sampling location of shrubs selected for chronology development.

5.4.2 Abiotic contrasts among sampling sites

Sampling locations in the lakebed ranged from approximately 9 – 11m in elevation above sea level, whereas those from the ridge ranged from only 13m on the slope of the ridge to approximately 20 – 35m on top of the ridge (fig. 5.3d,e). No substantial differences in WorldView-2 based wetness index (NDWI) were evident, except for occasionally higher wetness in ponds (fig. 5.3c,f). Sampling locations on the ridge tended to show earlier snow-free conditions (fig. 5.3b & 5.4a) and earlier greening (fig. 5.4b & 5.3a,g) during the start of the growing season, as derived from Sentinel-2 NDVI. This was especially evident on the topmost sites on the ridge (fig. 5.3a). Within the lakebed sites (thaw ponds and shrub patches), no further distinction in snow and vegetation dynamics was visible, which is

likely due to the small size of ponds (typically 2 to 7 meters in diameter) (Magnússon et al. 2020) compared to WorldView-2 and Sentinel-2 resolution. Although the difference in WorldView-2 NDWI among subsites is not very pronounced (fig. 5.3f), field observations confirm large contrasts in wetness between generally dry shrub patches and waterlogged ponds (table 5.1). Results are in line with previous observations of dry conditions in lakebed shrub patches and waterlogged to wet conditions in thaw ponds (table 5.1), but point out an additional contrast in phenology (based on NDVI) among elevated ridges and drained thaw lake basins.

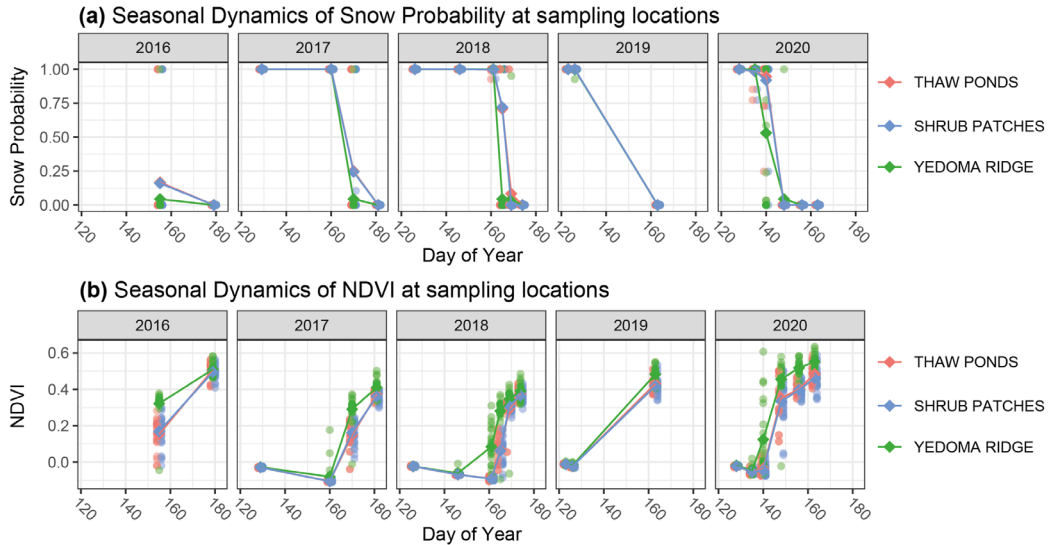


Figure 5.4) Snow and NDVI dynamics for sampling sites. a) Timeseries of Sentinel-2 TOAR / SR pixel Snow probability at sampling locations of selected shrubs for early summer (May 1st -July 1st) 2016 – 2020. b) Timeseries of Sentinel-2 TOAR / SR NDVI at sampling locations of selected shrubs for early summer (May 1st -July 1st) 2016 – 2020. Data is shown only for cloud-free images. Transparent dots indicate individual pixels, opaque dots and lines indicate subsite average. Day of year 120 corresponds to May 1st and Day of year 180 corresponds to June 30th (in non-leap years).

Table 5.3) Dendrochronological statistics of Overall and Subsite chronologies

Chronology	Mean correlation	Number of individuals	Rbar	Expressed Population Signal	Signal to Noise Ratio	AR1
Overall	0.432	57*	0.243	0.896	8.654	0.401
Ridge	0.465	16	0.288	0.740	2.844	0.441
Thaw Ponds	0.454	19	0.305	0.792	3.805	0.365
Shrub Patches	0.456	21	0.254	0.782	3.585	0.351

*) The Overall chronology included 15 ridge shrubs, 21 shrub patch shrubs and 20 ponds shrubs
 Mean correlation indicates the mean interseries correlation based on correlations of each shrub with a chronology based on all other shrub series (based on a leave one out principle).
 Rbar indicates the mean correlation between shrubs series
 Expressed population signal indicates the explanatory power of a finite sample compared to the theoretical population chronology (Wigley et al. 1984).
 Signal to noise ratio indicates the relative strength of the common variance signal present in the chronology relative to the total variance of series in the dataset (Cropper 1982).
 AR1 indicates mean first-order autoregression coefficient for shrub ring width series. Final RWI is corrected using a first-order autoregressive model.

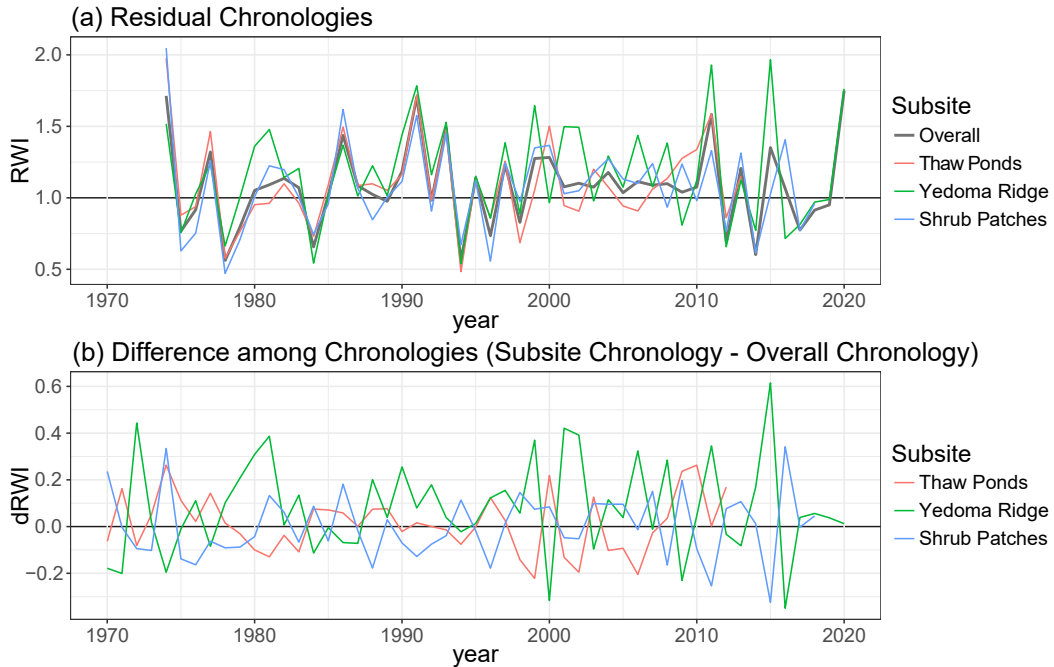


Figure 5.5) Ring Width Chronologies. a) Overall chronology and subsite residual chronologies after C-method detrending and correction for first-order temporal autocorrelation, based on a sample depth of at least 6 individuals. The chronology for Thaw Ponds shows a shorter record due to the fact that many shrubs in thaw ponds were dead and showed no more rings in recent years. b) Difference among Subsite Chronologies, visualized as the difference between each individual subsite chronology and the Overall chronology.

5.4.3 Overall site chronology and subsite chronologies

Four chronologies were developed; an Overall site chronology including shrubs from the three subsites in roughly equal proportions, a Ridge chronology for shrubs sampled on the Yedoma ridge, a Ponds chronology for shrubs sampled in thaw ponds and a Shrub Patch chronology for shrubs sampled in shrub patches in the drained thaw lake basin (table 5.3). The chronologies generally showed similar growth dynamics (fig. 5.5). Yedoma Ridge shrubs showed higher radial stem growth in particular years (1980-1981, 1999, 2001-2002) and particularly strong growth in the relatively wet summers of 2011 and 2015 (fig. 5.2 & 5.5a). Chronologies showed relatively unsynchronized and undifferentiated growth between 2000 and 2010 (fig. 5.5a). All chronologies showed significant first-order autocorrelation (table 5.3 & S5.10). Partial autocorrelation analysis indicates that Ridge shrubs showed weak but significant second order autocorrelation as well (fig. S5.10), indicating that growth was positively associated with growth up to two years earlier.

Analysis of individual shrubs' annual basal area increment and shoot length measurements reveal no substantial differences in growth patterns among the three subsites (fig. S5.4 - S5.5). Shrubs from the three subsites tended to fall in the same range of diameter-age, length-diameter and length-age ratios and showed similar ranges of average basal area increment. Shrubs from the ridge tended to show relatively low initial basal area increments in the first 10 years of growth, compared to shrubs from shrub patches and ponds in the lakebed (fig. S5.5), indicating potential differences in juvenile growth dynamics among the subsites. Although shoot lengths are comparable, field observations suggest that ridge shrubs show lower stature (Blok et al. 2010), potentially indicating a more decumbent growth form under exposed conditions and mixed vegetation composition.

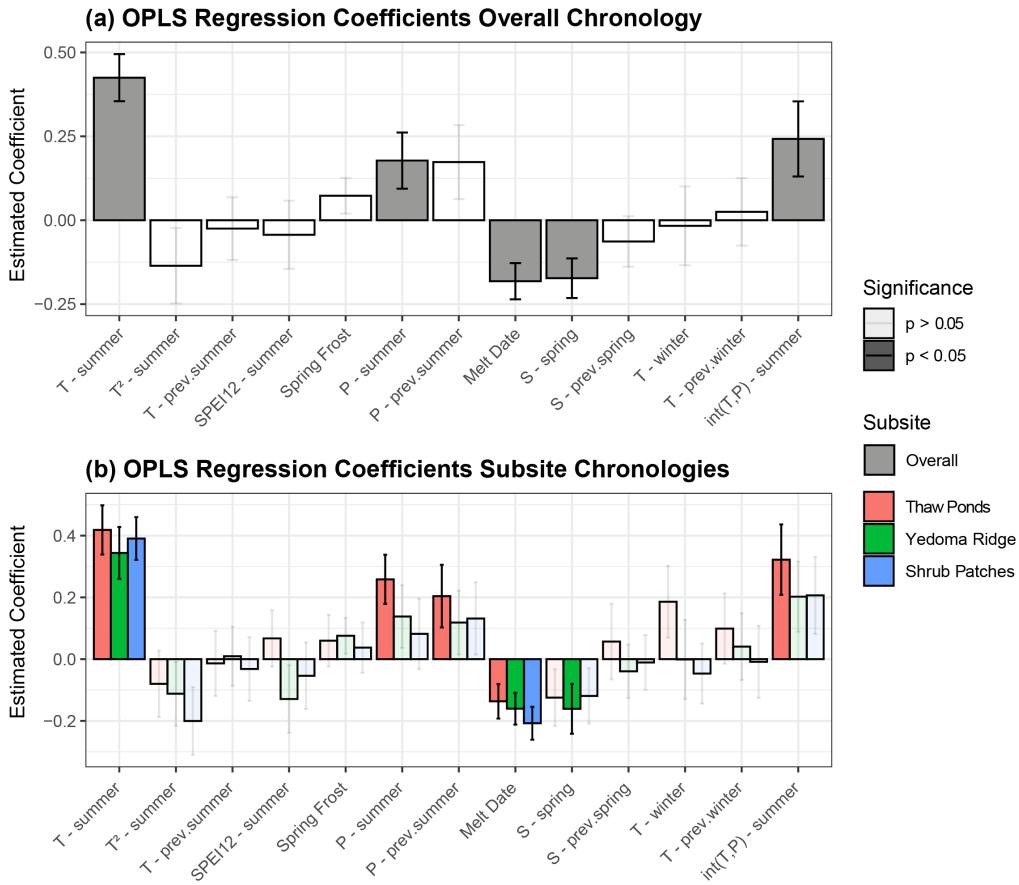


Figure 5.6) Estimated OPLS Coefficients for Climate Variables for a) Overall and b) Subsite Chronologies. T = temperature, P = precipitation, S = snow height. sum = summer (June-July), win = winter (November-April). prev = previous year. int(T,P) indicates an interactive term between summer temperature and precipitation. For explanation of selected climate variables, see table 5.2. Solid bars represent significant estimated coefficients, transparent bars represent insignificant estimated coefficients.

5.4.4 Spatiotemporal Variability in Climate Growth Relations

OPLS regression analysis suggests a relatively consistent pattern of temperature response among subsites, with site-specific contrasts mainly related to precipitation. Exploratory Pearson correlation analysis (fig. S5.6) showed similar differences in patterns of climate-growth association across subsites. Due to high correlation between summer temperature (T – summer) and the two degree day variables (GDD5 and SFGDD) (Pearson's $r > 0.96$, fig. S5.6), only summer temperature was considered in further statistical analysis. OPLS models for chronologies generally showed good fits and significant predictive performance based on permutation tests ($pQ2 < 0.05$) (table S5.1). The Overall chronology shows a positive association of radial stem growth with summer temperature, summer precipitation and their interactive term, and a negative association with date of snow melt and winter snow height (fig. 5.6a). The Yedoma Ridge chronology shows a slightly lower degree of summer temperature sensitivity, but a negative correlation with both date of snow melt and snow height in spring. Both the Shrub Patch chronology and Thaw Ponds chronology show association with summer temperatures and date of snow melt. While the Shrub Patch chronology lacks significant association with summer precipitation, the Thaw Ponds chronology shows significant association with summer and previous summer precipitation,

as well as with the interactive term for summer temperature and precipitation. This pattern indicates stronger positive response of Thaw Ponds shrubs to rainfall and some degree of co-limitation by summer temperature and rainfall, and stronger response of Yedoma Ridge shrubs to snow dynamics.

Using a moving window approach (fig. 5.7), we evaluated whether climate-growth associations differed over time in the sampling subsites. We found a generally consistent response to summer temperature over 1974 to 2018, with somewhat lower temperature sensitivity for shrubs from Thaw Ponds and the Yedoma ridge in 1979-2008. In contrast to Thaw Pond shrubs, Shrub Patch shrubs and Yedoma Ridge shrubs show no positive association with summer rainfall in the period from 1974 to 2008, but increasingly positive response afterwards (although not yet significant). This coincides with a prolonged period of low summer precipitation between 2000-2010 and 2018-2019 (fig. 5.2b). Response to interactive effects of summer rainfall and temperature are variable throughout time but seem to have increased for Yedoma Ridge shrubs in particular. Responses to summer rainfall seem to be strongly driven by positive responses to incidental rainfall extremes (fig. S5.8). All subsites show a decrease in association with the date of snow melt, indicating that with advancing snow melt date after 1980 (fig. 5.2), limitation by the onset of snow-free conditions may become increasingly lifted. The three subsites show similar dynamics indicating some sensitivity to precipitation in the previous summer season, although this association was not significant in recent decades. The association between shrub growth and spring snow height seems to be driven strongly by the negative response of Yedoma Ridge shrubs to snow height in recent decades. This increased sensitivity results entirely from low RWI following extreme snowfall in 2016-2018 (fig. 5.2c & S5.8d). These results suggest that divergence of climate-

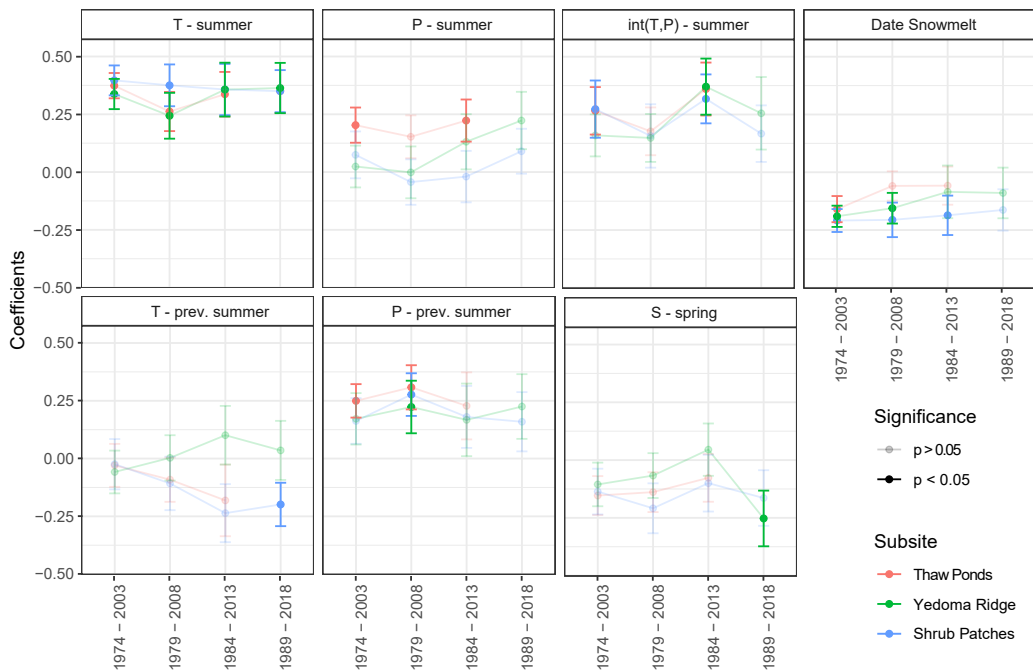


Figure 5.7) Stability of estimated OPLS regression coefficients over time for each climate variable. Only those variables that showed significant associations with any of the subsite chronologies during any of the time periods were included. Variables included in Fig. 5.6 that are not shown here (SPEI12, Spring Frost, previous spring Snow Height, Winter Temperature) showed no significant correlation with any of the chronologies in any of the 30-year periods. Note that the period 1989-2018 is omitted for the Thaw Ponds chronology, as too few observations were available to extend the chronology after 2013.

Table 5.4) Pointer Years

Year	Pointer	Subsite	Standardized score (1974-2018)*					
			T sum	T win	P sum	S spring	Snow melt date	int(T,P) sum
1974	Positive (extreme)	TP	1.29	-0.88	1.71	-0.10	-0.39	2.20
1974	Positive (strong)	SP	1.29	-0.88	1.71	-0.10	-0.39	2.20
1975	Negative (weak)	SP	-1.70	-0.34	0.68	-0.65	0.52	-1.16
1978	Negative (weak)	SP	-1.58	-0.90	-0.21	0.64	0.78	0.33
1994	Negative (strong)	TP	-0.25	-1.01	-0.43	-0.28	0.00	0.11
2010	Positive (weak)	TP	1.78	0.45	-0.58	-0.10	-0.39	-1.03
2011	Positive (extreme)	YR	1.40	2.26	1.90	-0.02	0.00	2.65

*) T = Temperature, P = Precipitation, S = Snow Height, sum = summer, win = winter

growth relations in this ecosystem is related to increased variability in summer rainfall and winter snow height, the impacts of which differ among landscape positions.

5.4.5 Response of individual shrubs to climate variables

OPLS regression of individual shrubs' RWI series against climate variables that were identified as significant for shrub growth (fig. 5.7) generally yielded poor OPLS model fits ($pQ^2 > 0.05$). Figure S5.7 shows Pearson correlation coefficients between OPLS estimated regression coefficients for climate variables at the individual shrub level, individual shrub growth characteristics (average BAI per year, average BAI during the first 10 years of growth, shrub age) and remote sensing-based terrain characteristics of the shrub's location (mean WorldView-2 NDWI, ArcticDEM elevation). This analysis indicates little association between individual shrub climate response and sampling site abiotic characteristics and shrub growth strategy, but several correlations between climate response and shrub age (fig. S5.7). Within the common time period, older shrub individuals showed a more negative response to warm winters with higher snow accumulation, while younger shrubs tended to show a moderately positive response. Older shrubs also showed a tendency ($p < 0.1$) for less positive response to summer precipitation. The restricted time period (26 years) and sample size (11 Ridge shrubs, 13 Ponds shrubs and 15 Shrub Patch shrubs) for individual shrub OPLS analysis and poor OPLS fits suggests that further differences in climatic response among individual may be confounded by substantial local and individual variation in ring width values.

5.4.6 Pointer Year Analysis

Analysis of pointer years showed that patterns of RWI extremes are fairly consistent with the outcomes of moving-window OPLS regression. We identified 1974, 1975, 1978, 1994 and 2011 as pointer years (table 5.4). Negative pointer years in the Thaw Ponds and Shrub Patches chronology were mostly associated with cold conditions, while the positive pointer year 1974 was associated with high summer temperature and precipitation. Markedly, only the Thaw Ponds chronology showed a positive pointer year in 2010, which showed high summer temperature but lower than average summer precipitation. This could hint at decreased moisture deficit in progressively wetter sites, despite the generally positive response of Thaw Pond shrubs to summer precipitation (fig. 5.6b). The Yedoma Ridge chronology showed only one positive pointer year in 2011, which showed warm summer and winter conditions and high summer precipitation.

Similarly, analysis of shrub radial stem growth in years with extreme weather conditions (identified here as the three years with highest or lowest values for a particular variable) (table S5.3), shows positive

responses to summers that are both warm and rainy. Positive responses to high temperatures or high summer precipitation alone are less common and of the three warmest years observed from 1974-2018 (1991, 2005, 2010), only the years that also showed high summer rainfall (1991) showed higher than average RWI. Negative responses to dry summers were less common, but dry summers occasionally coincided with high snowfall the winter before (2016 - 2018) (fig. S5.6). This may have mitigated moisture deficit especially in the lower elevation lakebed sites. Yedoma ridge shrubs show relatively low sensitivity to cold winter temperatures compared to shrubs from the lakebed sites. All sites showed generally lower RWI under later snow melt, but Yedoma Ridge shrubs showed a relatively consistent positive response to lower snow height, even if accompanied by cold winter temperatures (e.g. 1999). Due to shrub mortality upon waterlogging, insufficient samples from Pond shrubs were available to assess the effects of recent extreme snow accumulation on growth of shrubs from Thaw Ponds. Lastly, table 5.4 and table S5.3 suggest RWI extremes may also be driven by co-occurrence of multiple extreme weather conditions. This, and a degree of collinearity in weather data (e.g. winters with high snowfall tend to be warmer and were often followed by dry summers, fig. S5.6), makes it difficult to disentangle effects of various weather extremes.

5.5 Discussion

Beside an overall pattern of higher radial stem growth of *Betula nana* in warm and rainy summers with early snowmelt (fig. 5.6a), recent increases in precipitation variability saw differential development of precipitation response in climate-growth relations across subsites representing a topographical gradient (Thaw Ponds, Shrub Patches and Yedoma Ridge). By taking both spatial and temporal variability in climate-growth relations into account, we gained novel insight into differential impacts of a changing climate and changing occurrence of weather extremes across a heterogenous tundra landscape.

5.5.1 Climate response of *Betula nana* in the Siberian lowland tundra

Radial stem growth of *Betula nana* was best explained by summer temperature (June-July) over the studied period (1974-2018) for all subsites. Additional positive association was found with summer (June-July) precipitation and the interaction between summer temperature and precipitation. Negative associations were found with the date of snow melt and spring snow height (fig. 5.6a). These findings largely match those of earlier dendrochronological studies conducted for this site (Blok et al. 2011b, Li et al. 2016). Blok et al. (2011b), using a study period of 1948-2006, found *Betula nana* to be sensitive to summer temperatures in an approximately one-month period between mid-June and mid-July, and found a positive association between shrub radial stem growth and precipitation during the previous summer season. Li et al. (2016) found similar positive summer precipitation responses over the period 1962 to 2011 but only in relatively warm years, similar to the interactive effects identified in this study. We also identified positive associations with summer precipitation in the previous year, but only in periods before 2008, consistent with the study of Blok et al. (2011). However, contrary to earlier studies (Myers-Smith et al. 2015a, Gamm et al. 2018, Buchwal et al. 2020), we did not find poor shrub growth in any of our subsites during very dry summers, nor significant associations with SPEI. This suggests that while high precipitation enables better than average growth, low moisture availability does not necessarily lead to compromised growth in this ecosystem. This may be explained by *Betula nana*'s ability to adapt to the generally low-precipitation climate (fig. 5.2b) (De Groot et al. 1997, Fujinami et al. 2016). The generally dry period between 2000 and 2010 shows relatively undifferentiated growth dynamics and substantial variability between subsites. Afterwards, high summer rainfall in 2011 shows a distinct and sudden peak in RWI across subsites and increased common signal in the periods afterwards (fig. 5.5). This further supports a general pattern of reduced temperature response under decreases in moisture availability.

In terms of winter conditions, we found that *Betula nana* radial stem growth was negatively associated with snow melt date and spring snow height, indicating better growth under earlier snow-free conditions (fig. 5.6a). No effects of winter conditions were evident from earlier dendrochronological studies in this ecosystem (Blok et al. 2011b, Li et al. 2016), although *Betula nana* has been found to be sensitive to winter temperature and snow conditions in other ecosystems did (Hallinger et al. 2010, Hollesen et al. 2015, Dobbert et al. 2021). Yedoma Ridge shrubs in particular showed negative association with extreme winter snowfall (fig. 5.6b) and generally high RWI under low spring snow height, even if accompanied by low winter temperature (table S5.3). In contrast to other studies (Bokhorst et al. 2009, Bjerke et al. 2017, Opala-Owczarek et al. 2018, Dobbert et al. 2021), we found no negative effects of winter or spring warming on shrub growth. This is likely explained by the highly continental climate. Due to sharp transitions from extremely cold (average January temperature 1945-2019 January: -34.1°C) to fairly warm (average January temperature 1945-2019 January: 10.6°C) summer conditions, winter thaw episodes or rain on snow events were not evident from the climate record. Occasional spring frost after snow melt was generally short-lived and moderate and not significantly related to shrub growth (fig. 5.6 & S5.6). In addition, *Betula nana* is a relatively frost hardy species (De Groot et al. 1997, Hollesen et al. 2015, Dobbert et al. 2021). Our findings suggest that besides summer temperature (June-July), snow dynamics affect radial stem growth of *Betula nana* in this ecosystem, but these effects are spatially variable (fig. 5.6b & 5.7).

5.5.2 Spatiotemporal heterogeneity in climate-growth relations

5.5.2.1 Spatiotemporal contrasts in response to summer conditions

Shrubs on the elevated (± 10 -25m higher) Yedoma ridge showed slightly lower temperature sensitivity and a stronger negative response to high snow accumulation in spring compared to the two lakebed sites (fig. 5.6b). Shrubs growing on elevated sites have previously been found to show lower temperature response or productivity due to higher drainage and drier conditions (Ackerman et al. 2017, Black et al. 2021). However, drier conditions on the Yedoma Ridge are not evident from available field measurements (table 5.1) and WorldView-2 based NDWI values (fig. 5.4e). Additionally, Yedoma Ridge shrubs show no significant positive response to summer precipitation or interactive effect between summer precipitation and summer temperature (fig. 5.6b). After a series of summers with low precipitation (2000-2010) however, Yedoma Ridge shrubs responded with very high radial stem growth in the wet summers of 2011 and 2015 (fig. 5.2i). Moreover, recent decades have shown more rapid increases in summer precipitation sensitivity in the Yedoma Ridge site compared to the other subsites (fig. 5.7). This could indicate that while moisture limitation has not played a significant role in growth of *Betula nana* on elevated ridges so far, prolonged periods of low summer precipitation can induce increasing response to summer precipitation.

Counterintuitively, Thaw Pond shrubs showed a positive response to summer precipitation and a significant, positive interactive effect of summer temperature and summer precipitation (fig. 5.6b). Observations of shrub mortality upon soil subsidence and waterlogging (Nauta et al. 2015, Magnússon et al. 2020) would not suggest such a positive response to moisture. Thaw Pond shrubs were sampled from small, isolated thaw ponds surrounded by shrub dominated vegetation in which they very likely formed (Magnússon et al. 2020). Such small depressions in the landscape may become focal points for lateral flow of water and accumulation of snow, triggering a positive feedback of enhanced permafrost thaw and further soil subsidence (Nauta et al. 2015). Many thaw pond shrubs died in or shortly after the extremely wet summer of 2011 (fig. S5.9). However, the positive response to summer precipitation of shrubs sampled from such thaw ponds, prior to shrub mortality due to waterlogging, strongly suggests an initially positive response to accumulation of soil moisture in small depressions in otherwise dry soils (table 5.1). Precipitation response was least evident (fig. 5.6b & 5.7) in the shrub patch sites, which shows the lowest overall topsoil moisture levels (table 5.1). This may hint at local adaptation to generally

drier conditions or potentially rapid evapotranspiration or drainage in such sites. Enhanced response to summer precipitation followed by pond formation and shrub mortality indicates a highly localized and non-linear response of *Betula nana* to moisture; locally increased moisture availability in dry shrub dominated sites likely enhances radial stem growth and temperature sensitivity, but *Betula nana* does not tolerate permanently saturated soils (De Groot et al. 1997).

5.5.2.2 *Spatiotemporal contrasts in response to winter conditions*

Topographic gradients may affect climate-growth relations through differences in snow dynamics. A shrub's topographic position is known to influence the accumulation of snow and timing of snowmelt (Ropars et al. 2015, Opala-Owczarek et al. 2018, Francon et al. 2020), which can affect its growth (Francon et al. 2020). Deeper snow packs can provide stronger thermal insulation in winter and warmer soils and enhanced microbial turnover at the onset of the growing season (Chapin et al. 2005, Sturm et al. 2005, Hollesen et al. 2015), but may also result in delayed onset of thaw and shrub growth if snow melt is delayed (Wipf et al. 2006, Wipf and Rixen 2010, Francon et al. 2020). This effectively poses a trade-off between negative effects of delayed onset of the growing season and positive effects of warmer conditions throughout winter and spring (Hallinger et al. 2010). Shrub growth in this ecosystem seems sensitive to delayed snow melt, evident from negative association of growth with date of snow melt (fig. 5.6). However, this positive influence is decreasing over time (fig. 5.7), against a trend of earlier snow-free conditions in recent decades (fig. 5.2h). This may indicate that growth limitations related to onset of snow-free conditions become increasingly lifted. Negative effects of recent years (2016-2018) with high snow accumulation (fig. 5.2c) and late snow melt (fig. 5.2h) are most evident for the Yedoma Ridge site (fig. 5.6b & 5.7, table S5.3). Yedoma ridge shrubs were also relatively insensitive to winters with low snow cover and cold temperatures (table S5.3). Sentinel-2 images (2016 – 2020) suggest earlier snow melt and onset of vegetation growth at the Yedoma Ridge sites (fig. 5.5) and a high degree of variability in timing of snowmelt and early summer NDVI across the landscape (fig. 5.4a-b). This could imply that shrubs growing at exposed ridges are adjusted to early snow free conditions and start growth at lower temperatures. Additionally, field observations suggest that *Betula nana* individuals on exposed ridge sites show relatively low stature and more decumbent growth (Blok et al. 2010), potentially as an adaptation to low snow cover and exposure to cold winter temperatures. Earlier studies have found similar adaptations and higher tolerance of cold winter temperatures of *Betula nana* shrubs in exposed microsites (Dobbert et al. 2021). The high local variability of snow melt timing and onset of growth across the landscape (fig. 5.4), together with potential local growth adaptations to such spatial differences, suggests that the use of snow melt dates as derived from meteorological records may give a rather simplistic representation of sensitivity of growth to snow dynamics.

5.5.2.3 *Potential remaining drivers of spatiotemporal heterogeneity in climate-growth response*

Remaining mechanisms that may have influenced variability in climate sensitivity among subsites may be numerous. Due to lack of in situ measurements, the influence of potential contrasts in soil properties (table 5.1; Bartholomeus et al. 2012, Siewert et al. 2015) and potential differences in soil microbial communities could not be accounted for. Although soil properties vary considerably on spatial scales of a single meter (Bartholomeus et al. 2012), rough contrasts in thaw depth, organic layer thickness (table 5.1) and C:N ratios (Bartholomeus et al. 2012) between the Yedoma ridge and Lakebed sites may have contributed to variability in climate-growth responses. In addition, the Yedoma Ridge sites generally show more mixed vegetation composition with a higher cover of evergreen shrub species and graminoids (particularly *Eriophorum vaginatum*) compared to shrub dominated patches in the lakebed (table 5.1). Competition for resources with other tundra plant species such as tussock sedges may additionally affect climate response of *Betula nana* among sites with differences vegetation composition. Lastly, the chronology developed from Ridge shrubs shows relatively strong first order (table 5.3) and significant second order (fig. S5.10) positive temporal autocorrelation. While traditionally filtered out in dendro-climatological studies, variation in autoregressive structures can point towards intrinsic (e.g.

density-dependence, resource allocation) and trophic influences on growth (Hendrichsen et al. 2009, Forchhammer 2017). Higher autoregressive coefficients for Ridge shrubs indicate a higher degree of intrinsic controls on shrub growth, which has previously been found to affect climate sensitivity (Forchhammer 2017). Quantifying these potential localized controls would require more elaborate sampling site characterization.

Changes in climate sensitivity over time in tree ring records (non-stationarity) (Wilmking et al. 2005, D'Arrigo et al. 2008, Hollesen et al. 2015, Francon et al. 2020) may also be caused by changes in the age distribution of sampled shrub datasets over the dataset period (Voelker 2011, Gamm et al. 2018). By comparing individual shrubs' response to weather data and their mean age over a common time period (fig. S5.7), we found indications that older shrub individuals may show a more negative response to high snow accumulation in winter but less positive response to summer precipitation. This suggests that increasing shrub age over the timespan of our chronologies may have contributed to the distinctly negative response of Yedoma Ridge shrubs to recent extreme snow heights. However, the negative response of shrub growth to snow melt date is generally becoming less negative (fig. 5.7), which makes it unlikely that this is an effect of shrub age. Similarly, increasing response to summer precipitation (fig. 5.7) and recent summer rainfall extremes (table S5.3) would not be in line with generally lower summer precipitation response of older shrub individuals (fig. S5.7). We therefore do not expect changes in shrub age distribution to be an important driver of observed non-stationarity of climate-growth relations in this study.

Lastly, apart from annual growth, recruitment and mortality dynamics likely shape the temporal dynamics of shrub abundance and biomass. Li et al. (2016) found recruitment of *Betula nana* to be positively associated with summer precipitation. This may imply that with recent conditions of generally dry and few very wet summers (fig. 5.2b), shrub recruitment may also start showing stronger pulse dynamics. However, it is currently unclear how dynamics in recruitment, mortality and annual growth of *Betula nana* shrubs add up and how this affects future carbon balances, vegetation communities and surface energy balance in this ecosystem.

5.5.3 Recommendations for future dendrochronological studies of Arctic shrub climate-growth relations

Currently, our understanding of the exact mechanisms that underlie the observed spatial and temporal variability in climate-growth relations is limited. This complicates detailed interpretation of highly dynamic spatiotemporal variation in climate-growth relations in *Betula nana* in this ecosystem and complicates estimates of future growth trajectories. Continuing Arctic warming will result in an increase of extreme precipitation events as well as drought (Bintanja et al. 2020, AMAP 2021, IPCC 2021, Wang et al. 2021). We found that responses to such extremes likely depend on landscape position, preceding conditions (e.g. strong response to summer precipitation in 2011 after a series of summers with relatively little rainfall) and interactive effects between multiple weather factors (e.g. strong response to warm as well as wet summers). In addition, response to a weather extreme may not follow logically from a shrub's overall response to a weather variable; no indication of a negative response to spring snow height was evident prior to unprecedented snowfall in 2016-2018, and high local shrub mortality as a result of waterlogging in a wet summer would not follow logically from the generally positive response of *Betula nana* to summer precipitation. Under increasingly extreme conditions in Arctic ecosystems, such non-linear and local effects may become increasingly evident. This begs caution in the extrapolation of Arctic shrub climate-growth beyond current and past climatic ranges. Informed experimental manipulation of temperature, precipitation, snow and hydrological conditions across landscape gradients would be necessary to make sound projections. Particular attention should be dedicated to combined effects of multiple weather conditions and the role of moderate increases versus extreme events.

A priori knowledge of Arctic ecosystems and their dynamics in recent decades, for instance based on field measurements and satellite data, proved important for the selection of relevant spatial subunits

for climate-growth studies (table 5.1) and helped interpret results. However, field measurements suggest that microsite heterogeneity may play a role on smaller spatial scales than is evident even from relatively high-resolution data such as the ArcticDEM or WorldView and Sentinel-2 image material (table 5.1, fig. 5.3). Site conditions may also change over the studied time period due to for instance thermokarst processes. Microsite monitoring (e.g. of soil moisture and freeze-thaw cycles) at shrub sampling locations may provide better insight into links between growth and particular abiotic site conditions. In addition, detailed, plant-level physiological data of for instance sap flow (Black et al. 2021), high temporal resolution dendrometer data (Dobbert et al. 2021), carbon isotope analysis (Gamm et al. 2018) or epidermal cell analysis (Ercan et al. 2021) may help to link microsite variability to shrub radial stem growth dynamics and aid correct interpretation of often complex and non-stationary results. Such additional data could potentially be embedded into an experimental context and linked to radial stem growth dynamics to provide new insights into future Arctic shrub growth.

5.5.4 Implications for future shrub growth in the North-Eastern Siberian lowland tundra

Our results suggest increasing spatial variability and co-limitation among climate factors under increasing variability in precipitation dynamics. Combined with rapid changes to the local climate and a highly dynamic landscape (Magnússon et al. 2021), this complicates efforts to extrapolate findings over larger areas and over future climate scenarios. However, based on anticipated increases in Arctic precipitation variability and outcomes of this study, several inferences can be made about future growth of *Betula nana* in this ecosystem.

We observed a strong positive growth response of *Betula nana* shrubs during both warm and wet summers, particularly following periods of lower summer rainfall. In recent decades, warm summers were not associated with increased radial stem growth unless met by higher-than-average rainfall. This suggests that shrub growth in this ecosystem is not able to benefit from rising summer temperatures unless met by sufficient moisture availability. Strong pulse dynamics in shrub growth may be expected, based on (a)synchronicity in summer temperature and rainfall peaks. Such pulse dynamics may also shape temporal dynamics of shrub recruitment (Li et al. 2016). Differential response to summer rainfall of shrubs sampled across a gradient in (micro)-topography and soil moisture further suggests that these dynamics may vary throughout the landscape on small spatial scales, with upland sites in particular showing an increase in rainfall dependence.

Despite a distinctly positive initial response to summer precipitation, shrubs in thaw ponds eventually die abruptly as a result of waterlogging due to thermokarst, especially following an extremely wet summer. This suggests that thaw pond formation and resulting shrub mortality are likely relatively abrupt and recent processes, and that shrub growth may initially benefit from increased soil moisture in small-scale depressions. The climate response and mortality dynamics of shrubs are thereby subject to additional spatiotemporal variability resulting from the highly dynamic thermokarst landscape in drained thaw lake basins observed in this region. Locally enhanced radial stem growth and positive response to moisture availability may be an early warning sign for small-scale and abrupt loss of shrub vegetation due to thermokarst in this ecosystem.

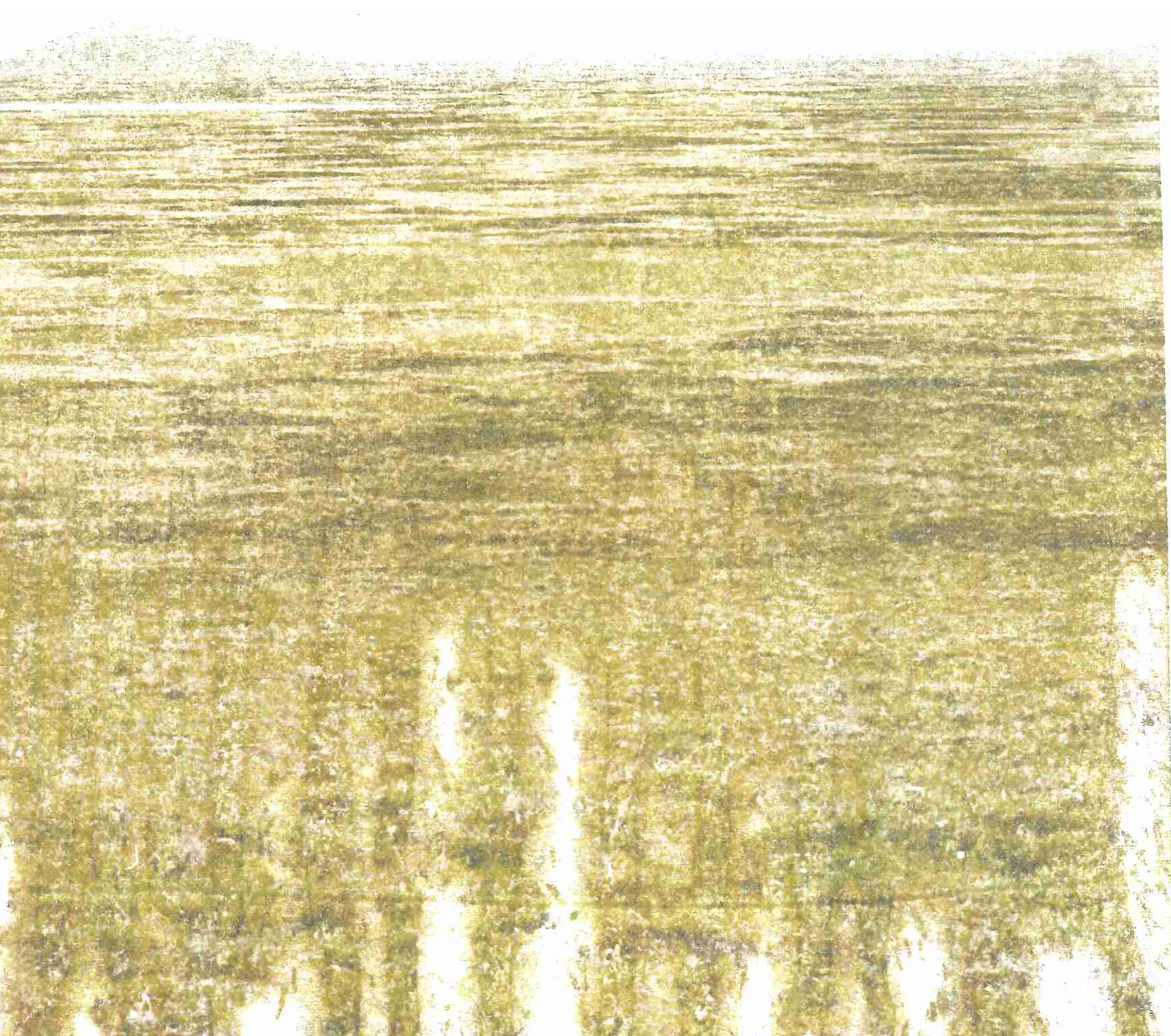
We found that responses to precipitation extremes, and especially responses to simultaneous or consecutive occurrence of multiple events did not necessarily follow logically from climate-growth relations inferred under absence of such extreme conditions and were in cases limited to specific landscape positions. This suggests decreased predictability of shrub growth under increased occurrence of weather extremes in Arctic ecosystems.



6.

**Tundra browning in the Indigirka Lowlands
(North-eastern Siberia) explained by drought, floods and
small-scale vegetation shifts**

Rúna Í. Magnússon, Finn Groten, Harm Bartholomeus, Ko van
Huissteden, Monique M. P. D. Heijmans



6.1 Abstract

In contrast to the general “greening of the Arctic”, the Siberian Indigirka Lowlands show strong “browning” (i.e., a decrease in the Normalized Difference Vegetation Index or NDVI) in various recent satellite records. Since greening and browning are generally indicative of increases and losses in photosynthetically active biomass, this browning trend may have implications for the carbon balance and vegetation of this Arctic tundra region. To assess why this area shows a reduction in greenness and assess to what extent such a reversal of Arctic greening may be expected for other Arctic regions, we studied relations between Landsat summer maximum NDVI, weather data, vegetation composition maps, topography, geomorphology and hydrology. We find that browning is associated with recent dry summer conditions, especially in upland terrain. Winters with record high snowfall and resulting floods are also associated with low NDVI, both in floodplain areas and higher elevation Yedoma plateaus. Increases in *Sphagnum* dominated area due to wetland succession processes contribute to local NDVI decrease, whereas less browning rates may be observed under expansion of mixed tussock sedge vegetation. Formation of thaw ponds and resulting shrub decline enhance browning on very local scales. However, these small-scale local vegetation shifts explain only small amounts of variance in Landsat NDVI trends compared to weather and hydrological data. Local recovery towards higher NDVI values is observed after recent floods (2016-2018), although persistently dry conditions in recent years have likely prevented recovery to higher pre-2010 NDVI values. Our results suggest that increased future precipitation variability and multi-year drought are detrimental for tundra greenness in lowland ecosystems with dry summers, but impacts vary spatially with elevation, hydrological dynamics and landscape evolution.

6.2 Introduction

One of the main manifestations of rapid climate warming in the Arctic is an increase in “greenness” of the terrestrial Arctic (Box et al. 2019, Berner et al. 2020, Myers-Smith et al. 2020, Frost et al. 2021b, Mekonnen et al. 2021a). Arctic greening is evident from a large number of studies and generally refers to increases in vegetation biomass or other productivity measures (Myers-Smith et al. 2020). Such observations may be derived from various types of studies (e.g. vegetation monitoring, warming experiments, remote sensing studies) and the term “greening” has different meanings and implications in these various fields (Myers-Smith et al. 2020). In remote sensing literature, including this study, greening and browning refer to an increase and decrease in NDVI (Normalized Difference Vegetation Index) or other vegetation index. NDVI is the most commonly used vegetation index and generally considered most suitable for monitoring of Arctic vegetation trends (Myers-Smith et al. 2020). Increases in vegetation productivity on a pan-Arctic scale are expected to result in enhanced uptake of CO₂ (McGuire et al. 2018, Meredith et al. 2019), but it is currently unclear how large this uptake may be and how large of a proportion of increasing Arctic carbon emissions (for instance from thawing permafrost) it may compensate (Abbott et al. 2016, McGuire et al. 2018, Meredith et al. 2019, Turetsky et al. 2020). In addition, despite its capability to remotely quantify general patterns of photosynthetically active vegetation, it is often unclear how NDVI changes relate to real-world changes in vegetation properties and composition and to changes in ground surface properties other than vegetation (Beamish et al. 2020, Myers-Smith et al. 2020). This complicates interpretation and forecasting of NDVI trends for the Arctic.

The Siberian Indigirka Lowlands (fig. 6.1b) are currently showing a trend break towards pronounced and increasing browning in various long term coarse to moderate resolution satellite records (fig. 6.1a) (Berner et al. 2020, Frost et al. 2021b, Magnússon et al. 2021, Mekonnen et al. 2021a). From 1985 to 2016, 4.7% of the Arctic was estimated to be browning, while 8% of the Arctic showed browning from 2000 to 2020 (Berner et al. 2020), suggesting that regional browning is increasing throughout the Arctic.

Although overall the Arctic has kept greening, it is important to improve our understanding of the drivers behind increasing regional browning (Frost et al. 2021b). Browning often manifests on smaller spatial scales and shorter timeframes than more widespread Arctic greening trends (Myers-Smith et al. 2020). This will help us to identify potential limits to Arctic greening and associated carbon uptake in a rapidly changing and heterogeneous Arctic biome.

Browning can indicate a decrease in vegetation foliage (Phoenix and Bjerke 2016, Myers-Smith et al. 2020), which may have detrimental consequences for the photosynthetic capacity and carbon sink strength of tundra regions (Treharne et al. 2019). NDVI trends are often linked with change in shrub abundance in particular (Forbes et al. 2010, Blok et al. 2011c, Boelman et al. 2011, Myers-Smith et al. 2011, Martin et al. 2017) while the role of other vegetation communities in determining NDVI is less recognized in literature (Heijmans et al. 2022). Changes in vegetation foliage may in turn be caused by extreme weather events, outbreaks of defoliating insects, permafrost thaw, flooding and other mechanisms (Phoenix and Bjerke 2016, Myers-Smith et al. 2020, Frost et al. 2021b). Apart from changes in vegetation, presence of snow or hydrological changes such as flooding or drainage may directly decrease NDVI values due to changes in infrared reflectance (Goswami et al. 2011, Reynolds and Walker 2016). Increases in surface water presence are associated with browning on a panarctic scale (Li et al. 2021). Lastly, NDVI dynamics strongly depend on the spatial scale over which they are quantified (Beamish et al. 2020, Myers-Smith et al. 2020). Coarser-resolution data are limited on their ability to detect smaller-scale patterns that may yield information on the extent and underlying mechanisms of browning (Bhatt et al. 2013), while high resolution data generally has limited temporal availability (Beamish et al. 2020, Myers-Smith et al. 2020). Strategically linking spatially limited high-resolution data to coarser regional and panarctic NDVI records is a key research priority in Arctic greening studies (Myers-Smith et al. 2020), and may explain why particular regions like the Indigirka Lowlands are browning.

NDVI dynamics in the Indigirka Lowlands may be related to various recent trends or disturbances on the ground and may thereby contain valuable information on the development of vegetation and permafrost in this remote and understudied Arctic ecosystem. In ice-rich permafrost landscapes such as the Indigirka Lowlands (Nitzbon et al. 2020), thermokarst activity can cause local waterlogging and rapid vegetation shifts from shrub dominated vegetation towards aquatic plant communities (Li et al. 2017, Magnússon et al. 2021). Such vegetation disturbance and recovery dynamics can manifest as distinct local browning events and subsequent greening (Zona et al. 2010, Reynolds and Walker 2016, Verdonen et al. 2020). It is unclear however to what extent such highly localized (sub-meter to meter scale) processes are reflected in coarser-scale regional NDVI dynamics. In addition, the Indigirka Lowlands have experienced several recent weather extremes, including record high snowfall in 2016-2018 causing widespread flooding (Tei et al. 2020) and extremely warm and dry spring and summer conditions in 2019-2020 (Overland and Wang 2021). We aim to assess to what extent these various mechanisms have contributed to strong recent browning in the Indigirka Lowlands, and whether the role of these various processes differs throughout the landscape.

To identify drivers of browning in a rapidly changing North-Eastern Siberian tundra ecosystem, we compared spatial dynamics and trends of NDVI based on very high resolution commercial WorldView-2 and Geo-Eye-1 (2m resolution), Landsat (30m resolution) and Sentinel-2 (10m resolution) satellite images vegetation cover dynamics, thematic map data, surface water dynamics and weather data to identify potential patterns and causes of browning in this region. We expected recent browning to be related to thermokarst-induced formation of small waterbodies and subsequent shifts to aquatic vegetation communities (Magnússon et al. 2021), spring and early summer flood events (Tei et al. 2020) and recent heatwaves and drought (Overland and Wang 2021). However, we expect that different types of processes that contribute to browning likely manifest on different spatial and temporal scales (Myers-

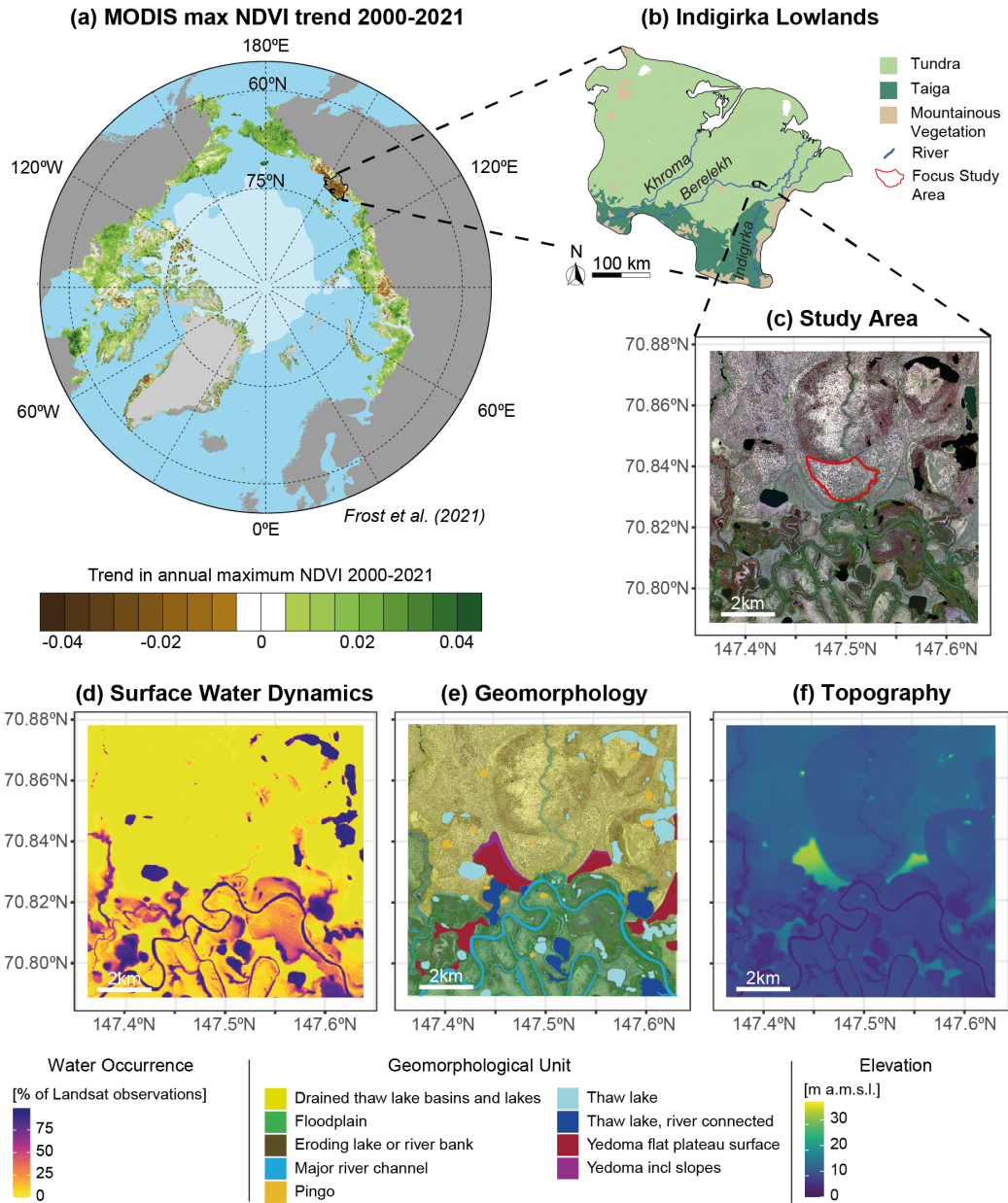


Figure 6.1) Study Site and its context within recent Arctic greening/browning dynamics. (a) Adapted from Frost et al. (2021b). MODIS NDVI trends for the entire Arctic (2000-2021) from Frost et al. (2021b)'s report on Tundra Greenness. The Indigirka Lowlands are indicated with a black outline. (b) The Indigirka Lowlands and its main vegetation zones and water bodies. White areas represent large lakes. (c) 2019 WorldView-2 satellite image of the study area. WorldView © MAXAR, 2019. The red outline indicates the extent of the vegetation maps generated by Magnússon et al. (2021) that were used for this study. (d) Surface water occurrence, expressed as the percentage of available Landsat observations in which the pixel was classified as surface water). Retrieved from the Global Surface Water Map (Pekel et al. 2016). (e) Main geomorphological units in the study area, from van Huissteden and Belelli Marchesini (2014). (f) Topography of the study area from the Arctic DEM (Porter et al. 2018).

Smith et al. 2020). By elucidating drivers of Arctic tundra greening and browning dynamics using a multi-scale approach and a wide range of spatially detailed information we contribute to assessment of Arctic greening/browning dynamics in a rapidly changing climate.

6.3 Methods

6.3.1 Study Area

NDVI trends and their relation to vegetation changes, weather trends, hydrology and terrain were studied in a 10 by 10 km area in the ‘Kytalyk’ Nature Reserve in north-eastern Siberia (70°49’N, 147°29’E) (fig. 6.1c). This lowland area consists of floodplains and drained thaw lake basins or ‘alases’, interspersed with remnants of older Yedoma deposits (fig. 6.1d). Local soils consist of a shallow 30-46 cm active layer overlaying continuous permafrost. Soils have organic layers of typically 10 to 25 cm, overlying mineral soil with silt to clay texture (Siewert et al. 2015). The upper permafrost layer contains 75% ice by volume on an average, making the region prone to thermokarst (Iwahana et al. 2014). Mean annual temperature and precipitation were -12.7°C and 189mm and average July temperature and precipitation were 10.6°C and 22mm for the period 1990-2020 (RIHMI-WDC 2020) (fig. S6.1). The growing season (with mean daily temperature above zero degrees and snow free conditions) is short and generally lasts from June to August (Van der Molen et al. 2007). Local vegetation is classified as a mixture of tussock sedge (*Eriophorum vaginatum*), dwarf shrub and moss tundra (type G4) and erect dwarf-shrub tundra (type S1) by the circumpolar Arctic vegetation map (Raynolds et al. 2019), which is typical vegetation for this region (Troeva et al. 2010). In earlier studies at this field site, six vegetation classes (shrub, tussock, lichen, sedge, *Sphagnum* and open water) have been distinguished based on the dominant plant functional type (Siewert et al. 2015, Magnússon et al. 2021). Tussock sedge is found in elevated landscape positions such as Yedoma remnants and pingos. Shrub and lichen are found on slightly elevated ice wedge polygon rims and slightly elevated (± 0.5 m) areas with high ground ice content (Wang et al. 2019). (Aquatic) sedges and *Sphagnum* are present in lower elevation sites such as low centre polygons, diffuse drainage systems and thaw ponds. Floodplains are generally dominated by sedges, willow shrubs, peat moss and grasses (Siewert et al. 2015, Magnússon et al. 2021). Apart from lakes and streams, small open water features are found in polygonal tundra, in isolated thaw ponds and in diffuse drainage systems (Magnússon et al. 2021). Detailed vegetation maps are available from Magnússon et al. (2021) for a sub-area representing a single alas (fig. 6.1c), which will be used as a focus area to study relations between vegetation compositional changes and NDVI trends.

6.3.2 Data Acquisition

6.3.2.1 Very high spatial resolution NDVI images

High resolution NDVI images (2m) were generated from three commercial very high resolution satellite images (table S6.1). A GeoEye-1 image was available for August 19th 2010, and WorldView-2 images were available for July 10th 2015 and August 1st 2019. The geometrically rectified images were atmospherically corrected by MAXAR Inc. (Denver, Colorado, USA) using AComp processing (MAXAR n.d.) to reduce possible NDVI bias due to changing illumination, viewing geometries and atmospheric conditions (Pacifiçi et al. 2014). After atmospheric correction, NDVI was calculated for all three images (2010, 2015 and 2019) from red (RED) and near-infrared (NIR) surface reflectance according to equation 6.1 (Tucker 1979).

$$\text{NDVI} = (\text{NIR} - \text{RED}) / (\text{NIR} + \text{RED}) \quad \text{eq. 6.1}$$

6.3.2.2 Functional Vegetation Maps

Three very high resolution (0.5m) functional vegetation maps were available for the study area (Magnússon et al. 2021), which were produced for a subsite within the study area (fig. 6.1c). These

maps classified the same very high resolution satellite images from 2010, 2015 and 2019 (paragraph 6.3.2.1, table S6.1) into areas dominated by shrub, tussock, lichen, sedge or *sphagnum*, or open water features. Individual images achieved high overall classification accuracy (91%-93%) when compared to field vegetation observations. These vegetation maps were produced from pan-sharpened images using a random forest classification with spatio-temporal Potts model regularization. The Potts model algorithm ensures consistent classification among images by penalizing differences in class labels among spatially and temporally adjacent pixels, so that changes in class labels over time and among neighbouring pixels are only allowed if spectral differences among pixels are sufficiently large (Potts 1952, Magnússon et al. 2021). With high overall accuracies and a consistent classification scheme among images, these maps provide a good basis for comparison of NDVI products to vegetation composition. Apart from classified vegetation maps, pixel class probabilities were derived from the initial Random Forest classification (prior to Potts model regularization).

6.3.2.3 Landsat Annual maxNDVI Time Series

An NDVI time series (1999 – 2019) was generated for the study site from LEDAPS corrected Landsat 7 & 8 surface reflectance imagery obtained from Google Earth Engine (Gorelick et al. 2017). Like most of the Arctic, this site lacks Landsat data from prior to 1999. NDVI values were calculated for each image using equation 6.1 (Tucker 1979). For each year the maximum NDVI per pixel was computed from all images between July 20th and August 5th, which corresponds with the peak of the local growing season (Van der Molen et al. 2007, Blok et al. 2011b). Images that were cloud covered (including clouds not detected by CFmask) by more than 50% were filtered out. To account for sensor discrepancies between Landsat 7 and 8, Landsat 8 images were transformed using locally parametrized linear regression (Roy et al. 2016). Such locally parameterized corrections are commonly used in order to compare NDVI values between Landsat 8 and Landsat 7 (Roy et al. 2016, Beamish et al. 2020, Chen et al. 2021). This procedure resulted in 13 maxNDVI images, of which 1999, 2000, 2003, 2007, 2009, 2010 and 2012 were available from Landsat 7 and 2014, 2015, 2016, 2017, 2018 and 2019 from Landsat 8. For comparison between very high and moderate resolution NDVI products, three additional Landsat NDVI images of the study area were selected for dates closest to the acquisition dates of the very high resolution NDVI images (August 19th 2010, July 10th 2015 and August 1st 2019), with a difference of at most three days. These images were all derived from Landsat 7 surface and underwent the same processing as described for the images used to derive annual maxNDVI series. For early August 1st 2019, a single Sentinel-2 MSI Level-2A image (10m) was obtained from Google Earth Engine (Gorelick et al. 2017). The image was atmospherically corrected using the Sen2Cor algorithm to derive surface reflectance and cloud-masked using the QA60 cloud mask band (Main-Knorn et al. 2017).

6.3.2.4 Weather Data & Thematic Map data

Daily average temperature, precipitation and snow depth data from 1999 until 2019 was retrieved for the Chokurdakh weather station 27km from the study site (WMO station code: 21946) from the AISORI database (<http://aisori-m.meteo.ru/waisori/>) of the All-Russia Research Institute of Hydrometeorological Information - World Data Centre (RIHMI-WDC 2020). All selected years (1999-2019) had at least 95% of complete daily data (346 days). For each year the average early summer temperature and total early summer precipitation (June 1st – August 5th) was calculated. Winter temperature was calculated as the average temperature between October 1st and April 31st. Maximum snow depth was calculated per winter season over the same period. We calculated the monthly Standardized Precipitation-Evapotranspiration Index (Vicente-Serrano et al. 2010) over a 12 month window (SPEI-12) as a measure of long-term moisture deficit of excess. SPEI was calculated using the spei package in R (Beguería et al. 2017) based on Hargreaves potential evapotranspiration. We used the mean SPEI-12 of June and July as a measure of summer drought. In addition, we obtained a timeseries (1999-2019) of topsoil (top 7 cm) volumetric moisture content for a 10x10km pixel containing the Chokurdakh Scientific Tundra station as derived from EUMETSAT scatterometer data (HSAF 2020).

Similar to weather variables, we calculated mean early summer (June 1st – August 5th) topsoil volumetric moisture content per year.

Existing thematic maps were used to characterize local hydrology, geomorphology and topography. We used the Global Surface Water Map (GSWM) (Pekel et al. 2016) to characterize local hydrology. From the GSWM, we extracted water occurrence data (fig. 6.1d) based on the Landsat record for the study area, indicating the percentage of years between 1999 and 2019 for which surface water was detected for a given Landsat pixel (Pekel et al. 2016). We used the 2m spatial resolution ArcticDEM digital elevation model (fig. 6.1f) (Porter et al. 2018) to characterize local topography. We used a geomorphological map of the study area (fig. 6.1e) (van Huissteden and Belelli Marchesini 2014) to represent the spatial distribution of various landforms (e.g. floodplains, drained thaw lakes basins and Yedomia plateaus).

6.3.3 Statistical Analysis

6.3.3.1 Landsat NDVI trend

We used Theil-Sen regression (Theil 1950, Sen 1968) to determine the decadal trend in annual mean maxNDVI for the study area as well as maxNDVI trends for individual pixels. Theil-Sen regression is a popular metric for NDVI trend analysis in Arctic regions (Nitze and Grosse 2016, Reynolds and Walker 2016, Lara et al. 2018, Myers-Smith et al. 2020) due to its relative insensitivity to outliers (Fernandes and Leblanc 2005). Pixels with less than 10 years' worth of data were considered inadequate for trend analysis and omitted (Forkel et al. 2013). We performed Theil-Sen regression for the mean area annual maxNDVI as well as annual maxNDVI of individual pixels. Individual pixel maxNDVI trends were visualized as maps. We used the *mblm* R package (Komsta and Komsta 2013) to perform Theil-Sen regression.

6.3.3.2 Relation of Landsat NDVI trends, weather events, hydrological dynamics and landscape

We quantified the proportion of variance in pixel maxNDVI trends explained by geomorphological unit, elevation and water occurrence (fig. 6.1d-f) using the coefficient of determination (R^2). For association between two raster datasets we use squared Pearson correlation. For association between raster values and categorical data (geomorphological unit), we report adjusted R^2 based on analysis of variance (ANOVA). To assess significance of correlation between pixel maxNDVI trends and elevation and water occurrence raster data, we used Dutilleul's modified t-test (Clifford et al. 1989, Dutilleul et al. 1993, Fortin and Payette 2002). We based Dutilleul's modified t-test on a random subsample representing 10% of the total amount of maxNDVI trend pixels (without replacement) to reduce computational demand. Dutilleul's modified t-test was implemented using the *SpatialPack* (Osorio et al. 2020) and *SpatialEco* (Evans and Ram 2021) packages in R.

To assess the degree to which maxNDVI dynamics in the study area are related to annual variation in temperature, precipitation and hydrology, we compared annual maxNDVI values per pixel with annual summer temperature, summer precipitation, winter temperature, winter snow height and scatterometer-derived topsoil moisture (paragraph 6.3.2.4) using Spearman's correlation coefficient (ρ) to account for small sample sizes. We report mean and standard deviation of individual pixel's ρ^2 for each weather variable considered. Pixels with less than 10 years of maxNDVI values were excluded. To assess spatial patterns in pixel correlation coefficients among maxNDVI values and weather variables, results were visualized as maps of correlation coefficients. We report the proportion of variance in maxNDVI – weather correlation coefficients explained by elevation, water occurrence and geomorphological unit based on R^2 as described in the paragraph above.

6.3.3.3 Relation of Landsat NDVI trends to vegetation dynamics

To assess how a change in cover of different vegetation classes may affect NDVI trends, we compared Landsat maxNDVI trends with changes in FVG composition between 2010 – 2019 as derived from the FVG maps. For this purpose, we repeated the Theil-Sen trend analysis (paragraph 6.3.3.1) within the focus study area (fig. 6.1c) for the period 2010 – 2019 to match the period and extent of the available FVG maps. We then compared net changes per FVG within each Landsat trend pixel to the magnitude of the Landsat Theil-Sen trend using Pearson correlation and report R^2 . We report significance of correlations between FVG cover change and maxNDVI trends while accounting for spatial autocorrelation using Dutilleul's modified t-test.

To support this analysis, we evaluated the extent to which differences in FVG cover were visible in various resolution NDVI products. The VHR NDVI maps (table S6.1) are the same data that were used to generate the FVG maps (Magnússon et al. 2021) and a relation between FVG type and VHR NDVI is therefore to be expected. Still, for the sake of comparison we visualized VHR NDVI per FVG class per year (2010, 2015 and 2019). For this purpose, the functional vegetation maps (0.5m resolution) were aggregated to a spatial resolution of 2 by 2 meters to match the spatial resolution of the VHR NDVI images. Only uniform vegetation pixels (i.e. all aggregated pixels belonged to the same FVG) were used for comparison. We restricted this analysis to only include 2m by 2m pixels where the FVG class maps showed an average spectral class probability of 90% or more, based on initial

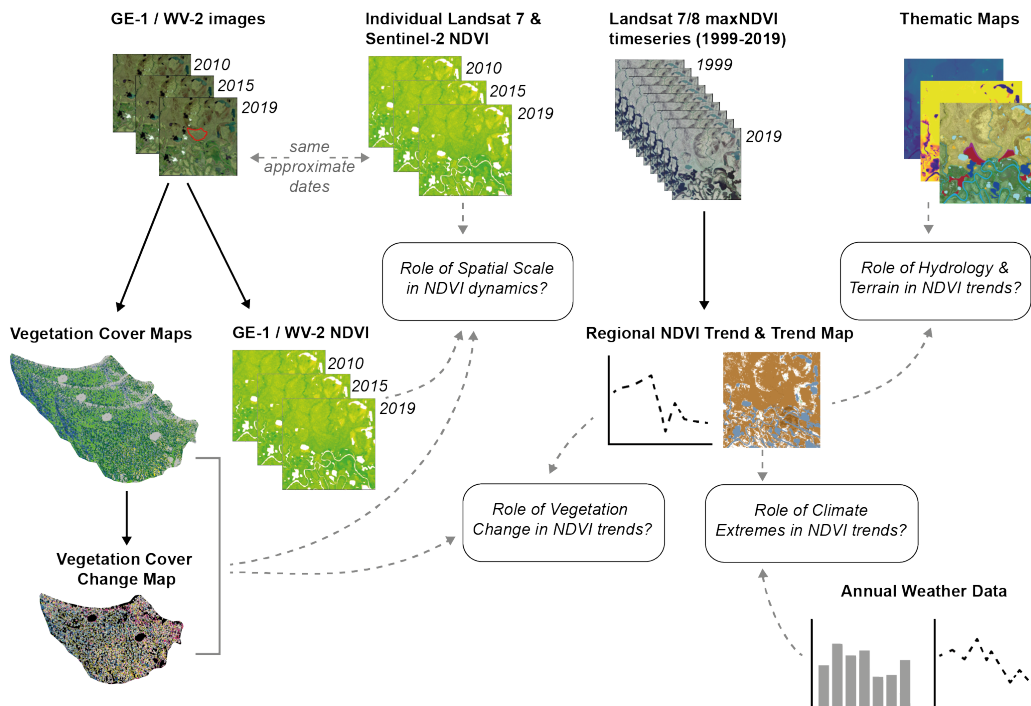


Figure 6.2) Workflow. We quantified NDVI trends in the study area using a time series of peak summer maxNDVI Landsat images. We compared pixel maxNDVI trends with annual weather data to assess relations between NDVI trends and weather extremes, and spatial patterns therein. We compared maxNDVI trends among geomorphological units, over elevation gradients and over a surface water occurrence gradient, to derive relations between NDVI dynamics, terrain and hydrology. We compared maxNDVI trends with changes in higher resolution multitemporal vegetation maps to derive relations between NDVI trends and vegetation shifts. Lastly, we compare NDVI dynamics from image material of various resolution with high resolution land cover change maps and thematic maps to assess the role of spatial resolution in NDVI dynamics.

random forest classification of the FVG maps. To assess how moderate resolution NDVI varies among pixels with different fractional cover of functional vegetation groups, we compared FVG composition within individual Landsat and Sentinel pixels to NDVI values of these Landsat and Sentinel images. We used the individual Landsat/Sentinel images that were collected at the same time as the VHR images that were used to generate the FVG maps. For each Landsat/Sentinel image, we selected pixels within the smaller subsite (fig. 6.1c) and calculated the fractional cover of the different FVGs from the corresponding FVG map within the larger Landsat/Sentinel pixels. From these pixels, we selected pixels with increasing fractional cover classes (0%, 10%, 25%, 50%, 75%, 100%) for each FVG, with a maximum deviation of 5%. To avoid confounding effects of presence of other FVGs, we selected only those pixels for which fractional cover of the remaining FVGs in the pixels was proportional to the mean FVG composition of all pixels, also with a maximum deviation of 5% from the average FVG proportion of remaining classes per pixel. For each of the resulting series, we visualized NDVI against the increasing fractional cover for each FVG.

We used FVG maps, GeoEye-1/WorldView-2 multispectral images and NDVI maps from multiple sensors to compare the scale of vegetation patches and vegetation changes and the extent to which they are visible in NDVI maps of different resolution. We calculated the mean patch size of each of the six tundra vegetation classes from the FVG maps using the Landscapemetrics R package (Hesselbarth et al. 2019). We additionally calculated the mean patch size of areas that showed a change FVG from 2010 to 2019 (i.e. adjacent pixels that show the same FVG transition). We compared these statistics to the spatial resolution of the various NDVI products used in this study. Using these statistical and visual comparisons, we assessed the extent to which vegetation shifts and thermokarst dynamics on a subdecadal timescale affect NDVI products of various resolution.

Our workflow is summarized in figure 6.2.

6.3 Results

6.3.1 Landsat NDVI trend

For the pixels with sufficient years (at least 10) of valid observations (85% of all pixels), an average maxNDVI trend of -0.0041 NDVI unit/year was found. Of these pixels, the majority (81.36%) showed significant ($p < 0.05$) browning, and 3.45% of significantly browning pixels showed browning rates stronger than -0.01 NDVI units per year. Significant greening was found only in 0.17% of pixels, with the remaining 18.47% showing no significant trend. Temporal dynamics of mean maxNDVI of the study site show a trend break, with maxNDVI decreasing rapidly between 2007 and 2010 (fig. 6.3a). After a moderate increase between 2010 and 2012, maxNDVI steadily decreases again afterwards. These dynamics were visible across the main geomorphological units in the area (Floodplains, Yedoma plateaus and Drained thaw lake basins). Floodplains however showed an especially pronounced dip in maxNDVI in 2017 (fig. S6.4), likely in response to early summer floods following extreme winter snowfall (see individual years' weather data in table S6.2, fig. S6.2). These results indicate similar browning trajectories across the landscape, with some variability likely driven by specific local hydrological events.

Although browning is ubiquitous across the landscape, some differences in magnitude are evident across elevation, geomorphological units and areas with different inundation frequency (fig. 6.4). Floodplain areas adjacent to the river Berelekh show the strongest browning trends within the study area (fig. 6.3b), although in general floodplain areas show strong variability in maxNDVI trends (fig. 6.4c). Similarly, lower elevation areas that are more prone to inundation show a larger range in maxNDVI trends than upland sites (fig. 6.4b). Lower elevation areas along the inner edges of drained thaw lake basins tend to show no trend in maxNDVI (fig. 6.3b). 99% of all Yedoma area shows significant browning, with 1% showing no significant trend. 82% of DTLB area shows significant browning, 18% shows no

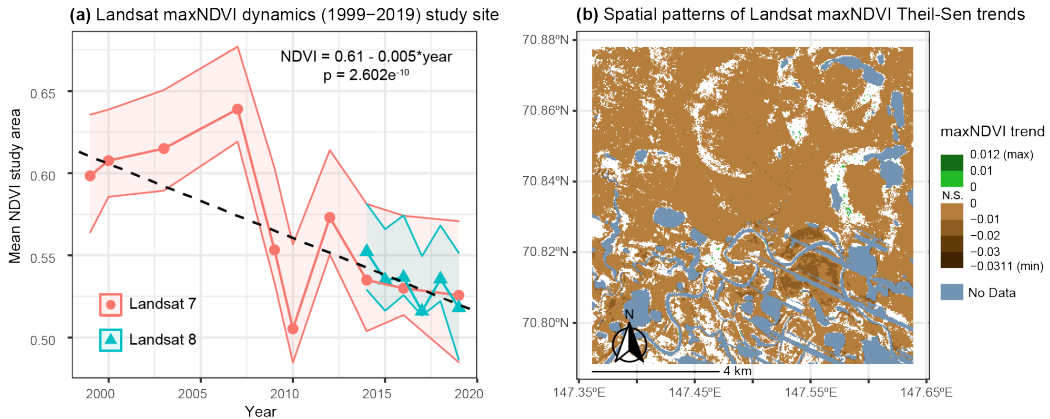


Figure 6.3 Observed Landsat maxNDVI Trends. a) Mean (point) and interquartile range (shaded area) of maxNDVI for the years during which cloud free Landsat images were available during the peak growing season (July 20th to August 5th). Landsat 8 values (blue) were corrected for discrepancies between Landsat 7 and Landsat 8 sensors based on a linear fit. Dashed line and text show Theil-Sen trend. b) Map of pixel maxNDVI Theil-Sen trends. Gray areas had less than 10 years of NDVI data and were omitted from trend analysis. Brown pixels are significantly browning, white pixels showed no significant trend ($p > 0.05$), green pixels show significant greening.

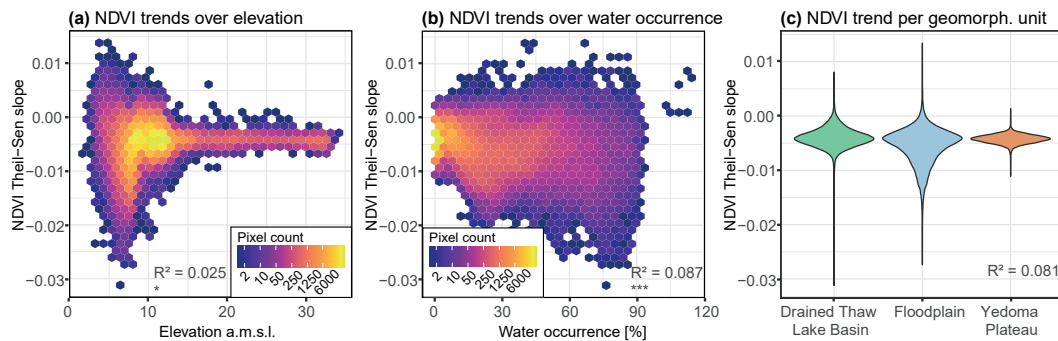


Figure 6.4 Variation in Landsat maxNDVI trends across elevation, water occurrence probability and geomorphological units. a) Hexagonal binned heatmap of the amount of pixels falling in a particular range of elevation (ArcticDEM) and maxNDVI trends. Colour scale is logarithmic. b) Hexagonal binned heatmap of the amount of pixels falling in a particular range of water occurrence probability (Global Surface Water Map) and maxNDVI trends. Colour scale is logarithmic. c) maxNDVI trends per geomorphological unit. Violin width is proportional to the probability of observing a trend of a particular magnitude within that class. p values for (a) and (b) were generated based on Dutilleul's modified t-test. N.S. = not significant, + = $p < 0.1$, * = $p < 0.05$, ** = $p < 0.01$, *** = $p < 0.001$.

significant trend and less than 0.1% shows significant greening. 68% of all Floodplain area shows significant browning, 32% shows no significant trend and less than 0.1% shows significant greening. Scarce localized greening is generally found in low elevation and occasionally inundated (fig. 6.1d) inner edges of drained thaw lake basins and floodplains. This could be an indication of terrestrialization in wetland terrain. Overall browning patterns indicate that tundra browning between 1999 and 2019 has been ubiquitous at upland sites such as Yedoma plateaus, while lower elevation areas prone to flooding show a higher variability in browning rates that are likely additionally driven by hydrological dynamics.

6.3.2 Effect vegetation compositional changes on NDVI

Our comparison of NDVI trends and changes in FVG cover per pixel between 2010 and 2019 shows that changes in cover of particular FVGs are significantly associated with Landsat maxNDVI trends, but that the proportion of variance in maxNDVI trends explained by such vegetation changes is very small (R^2 of up to 0.06) (fig. 6.5). Interestingly, changes in shrub cover within a Landsat pixel were not significantly related to maxNDVI trends (fig. 6.5a), nor were changes in sedge cover (fig. 6.5e). Pixels with increases in lichen cover showed a tendency towards stronger browning (fig. 6.5c) and pixels with increases in open water cover showed significantly stronger browning (fig. 6.5d), although the small percentual cover of these FVG within the focus study area likely also explains why variance explained by changes in these FVGs is low. Changes in *Sphagnum* and tussock vegetation show relatively stronger associations with maxNDVI trends ($R^2 = 0.060$ and $R^2 = 0.028$, respectively), with increases in tussock vegetation being associated with smaller browning rates (fig. 6.5b) and increases in *Sphagnum* being associated with stronger browning (fig. 6.4f). Tussock and *Sphagnum* are also relatively abundant FVGs that have shown a general decrease and increase (respectively) in the focus study area (Magnússon et al. 2021) which likely helps explain why these FVGs show stronger association with maxNDVI trends.

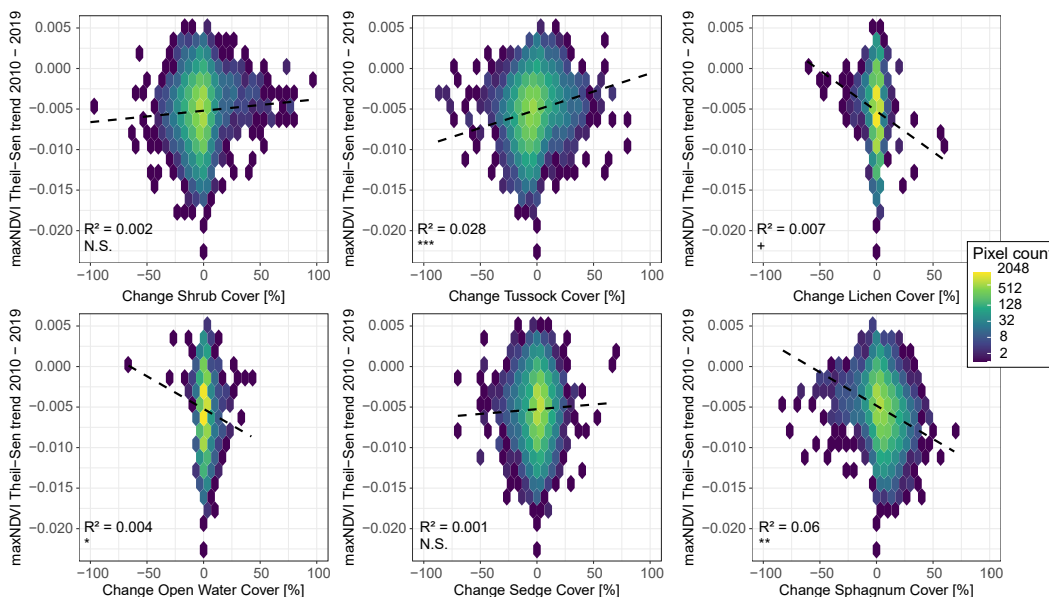


Figure 6.5) Relation between Landsat maxNDVI and vegetation cover change from high resolution classified satellite images (2010 – 2019) trends over 2010 - 2019. Scatter plots are visualized as hexagonal binned heatmaps with logarithmic colour scale, where colour indicates the number of pixels that fall within a particular range of vegetation cover change and maxNDVI trends. Text labels indicates R^2 based on Pearson's R for a linear fit. N.S. = not significant, + = $p < 0.1$, * = $p < 0.05$, ** = $p < 0.01$, *** = $p < 0.001$ (based on p values corrected for spatial autocorrelation using Dutilleul's modified t-test).

Comparison of maps of FVGs with NDVI products of variable spatial resolution indicates a similar effect of increases and decreases of particular FVGs on single-image NDVI values (fig. 6.6). Increasing cover of *Sphagnum* is most evidently associated with lower Landsat and Sentinel NDVI, while increasing tussock vegetation cover is associated with increasing NDVI (fig. 6.6a-d). The areal cover of open water features and lichen vegetation within a Landsat or Sentinel pixel is generally too low to estimate the effect of increasing lichen and open water cover within a single Landsat or Sentinel NDVI image (fig. 6.6a-d). Interestingly, increasing shrub cover is associated with higher NDVI values in Landsat and

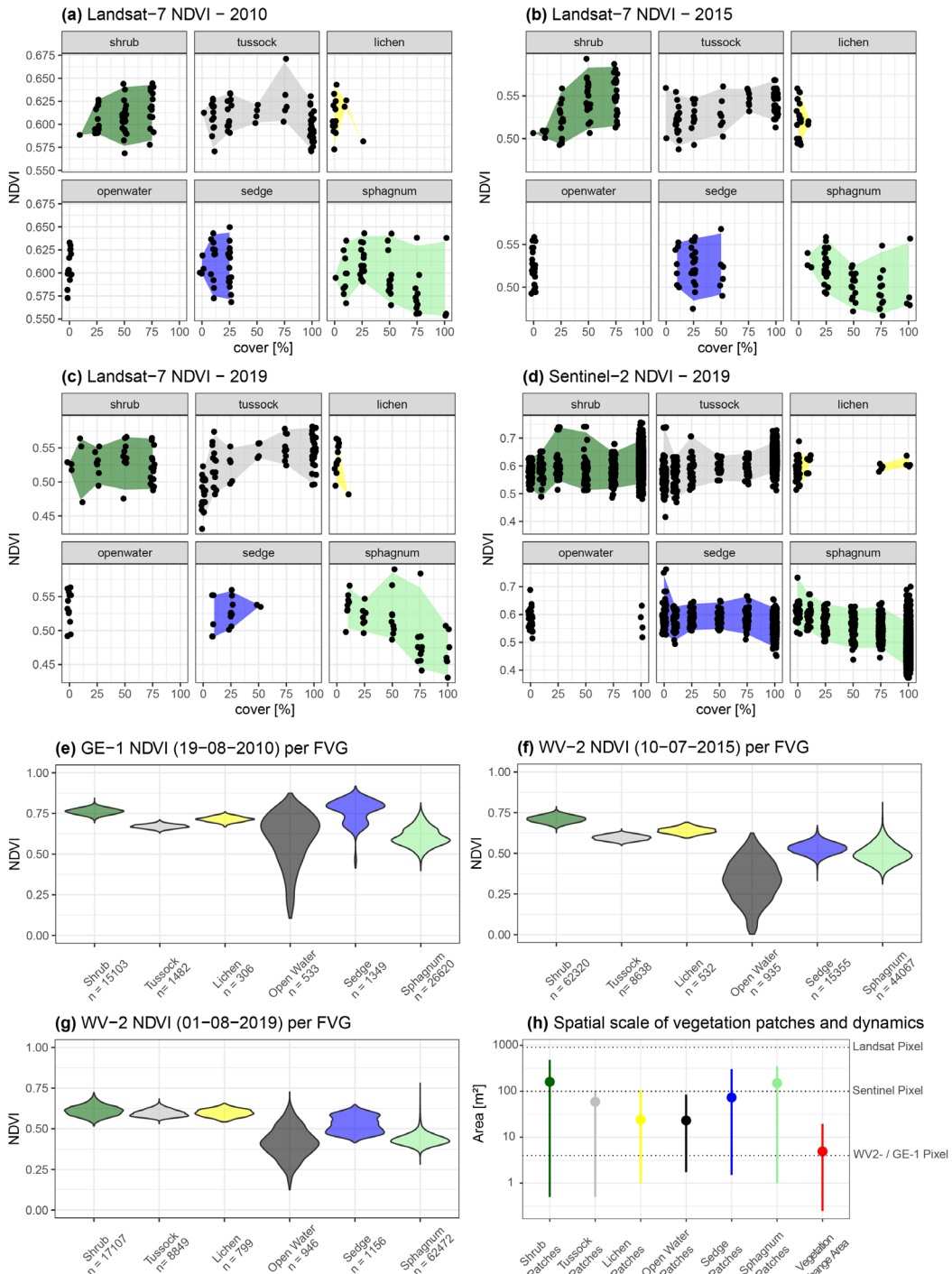


Figure 6.6) Relation of vegetation composition and NDVI across spatial scales within the focus area. a) Relation of Landsat NDVI and vegetation composition for the FVG map for 19-08-2010 and a Landsat 7 NDVI image close to the same date (22-08-2010). b) Relation of Landsat NDVI and vegetation composition for the FVG map for 10-07-2015 and a Landsat 7 NDVI image close to the same date (12-08-2015). c) Relation of Landsat NDVI and vegetation composition for the FVG map for 01-08-2019 and a Landsat 7 NDVI image on the same date

(01-08-2019). d) Relation of Sentinel NDVI and vegetation composition for the FVG map for 01-08-2019 and a Sentinel 2 NDVI image on the same date (01-08-2019). For figures a-d, pixels were selected with increasing cover of each of the FVGs and filtered for representative proportional cover of the remaining FVGs. e) GeoEye-1 NDVI per FVG, both based on the 2010 GeoEye-1 image (19-08-2010, table S6.1). f) WorldView-2 NDVI per FVG, both based on the 2015 WorldView-2 image (10-07-2015, table S6.1). g) WorldView-2 NDVI per FVG, both based on the 2019 WorldView-2 image (01-08-2019, table S6.1). For e-g, only pixels with > 90% spectral classification probability were selected. h) Median and 90%-CI of patch size per FVG (based on the 2015 FVG map) and area of FVG change from 2010 – 2019, relative to the approximate area of a GeoEye-1/WorldView-2 pixel, Sentinel-2 pixel and Landsat pixel.

WorldView-2 images from 2015 (fig. 6.6b,f), but not in images from 2019 (fig. 6.6c,d,g). The acquisition date of the 2015 WorldView-2 images is earlier in the season (early July) than those of other years (early to mid August). In addition, the summer of 2019 was very hot and dry (table S6.2). This hints at potential within-season or interannual variability in the effect of vegetation compositional changes on NDVI.

Vegetation class transitions over the 10-year time period for which detailed vegetation composition maps were available (2010 - 2019) show that vegetation compositional changes in the focus area typically occur on spatial scales of several square meters (5m², 90% CI = 0.25 – 19.5 m², fig. 6.6h). This is much smaller than the resolution of freely available Sentinel and Landsat data. The extent to which vegetation shifts are still associated with NDVI changes on coarser spatial scales likely depends on the direction and scale of specific types of vegetation change. For instance, shifts from shrub to open water due to thermokarst between 2010 and 2019 manifested on relatively large areas (\pm 15m² on average) and were associated with relatively outspoken differences in NDVI in very high resolution images (table S6.3, fig. 6.6e-g). The total fraction of the focus area affected by this transition however was very low (0.5%, table S6.3), which could potentially explain the very small but significant association between changes in open water cover and maxNDVI trends (fig. 6.5). Similarly, *Sphagnum* is associated with a relatively low NDVI in very high resolution satellite images and Sentinel NDVI (fig. 6.6a-g), likely contributing to the significant relation between *Sphagnum* cover and Landsat maxNDVI trends (fig. 6.5) at coarser scales. Frequent but generally smaller scale changes among shrub, tussock and sedge vegetation (table S6.3) are associated with smaller contrasts in very high resolution NDVI (table S6.3, fig. 6.6e-g) and not significantly associated with NDVI change (fig. 6.5). These results suggest that a substantial proportion of information on the direction and magnitude of vegetation compositional change and associated NDVI dynamics (fig. 6.6h) is averaged out in moderate (e.g. Landsat) to coarse resolution (e.g. MODIS) NDVI timeseries.

6.3.3 Association of NDVI with weather variables

NDVI dynamics from 1999 to 2019 show strong and spatially consistent patterns of association with snow dynamics, soil moisture and summer precipitation (fig. 6.7). Only 3.63% of the studied area (defined here as all pixel-based Landsat maxNDVI timeseries, excluding pixels with < 10 maxNDVI observations) showed significant correlation of annual maxNDVI with summer temperature (mean $q^2 = 0.09$, s.d. = 0.11, fig. 6.7a). This is less than might be expected due to chance with a significance criterion of $\alpha = 0.05$. Summer precipitation was significantly positively correlated with maxNDVI for 34.29% of the studied area (mean $q^2 = 0.27$, s.d. = 0.20, fig. 6.7b). 40.70% of the studied area's NDVI is significantly negatively correlated with snow height (mean $q^2 = 0.30$, s.d. = 0.20, fig. 6.7c) and 11.30% is significantly negatively correlated with winter temperature (mean $q^2 = 0.18$, s.d. = 0.14, fig. 6.7d). As warm winters and winters with a lot of snow generally coincide (table S6.2), negative correlations with snow height and winter temperatures may reflect the same dynamic. Of all annual climate variables, summer precipitation ($q = 0.580$, $p < 0.05$, $n = 13$) and snow height ($q = -0.633$, $p < 0.05$, $n = 13$) also showed the strongest association with mean annual maxNDVI over the entire region (as presented

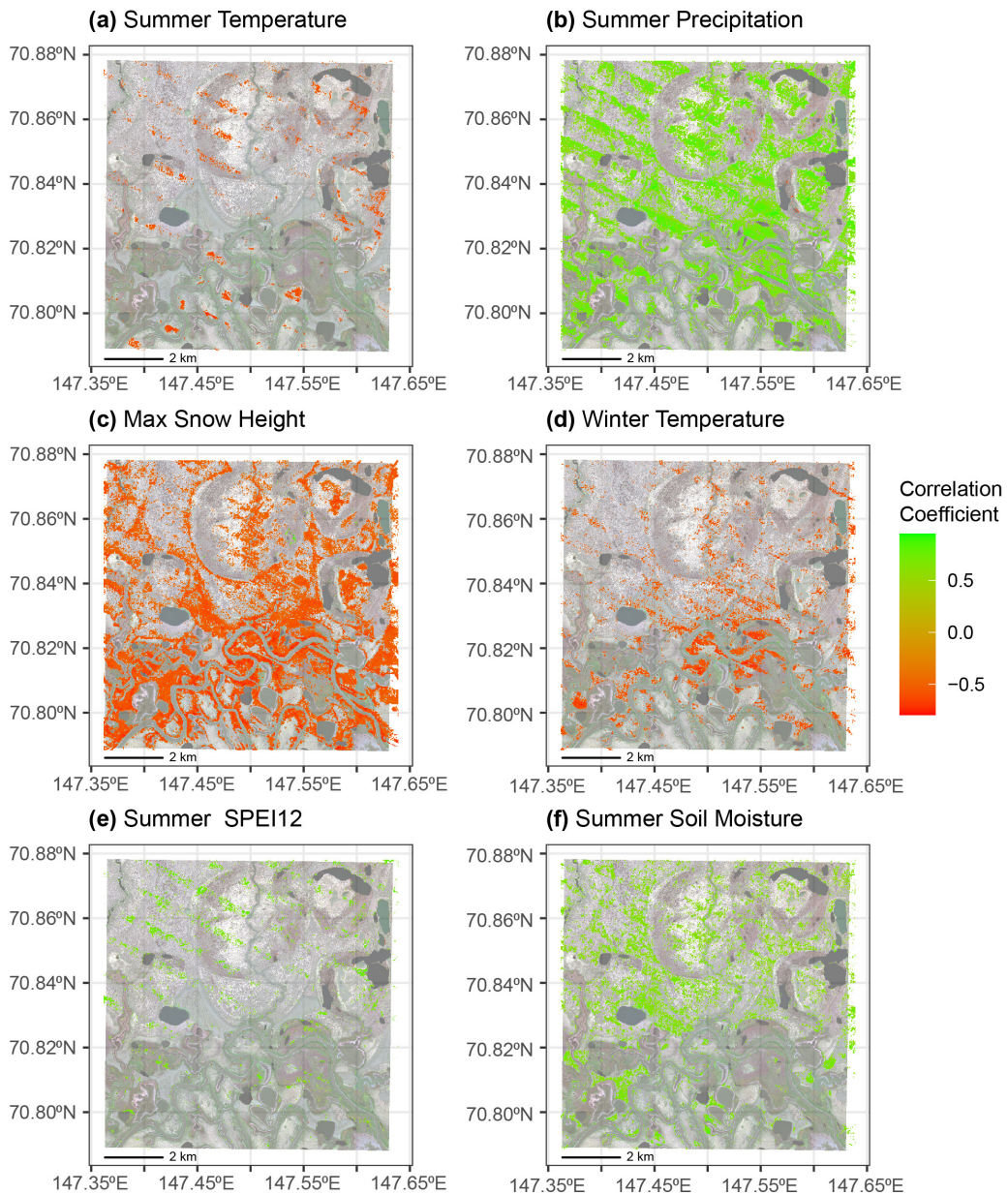


Figure 6.7) Association of annual maxNDVI values with annual weather data per Landsat maxNDVI trend pixels. Stripes are caused by scan line corrector failure in several of the Landsat 7 NDVI images. a) Association of annual Landsat maxNDVI with mean summer (June 1st – August 5th) temperature. b) Association of annual Landsat maxNDVI with total summer (June 1st – August 5th) precipitation. c) Association of annual Landsat maxNDVI with maximum winter (October 1st – April 31st) snow height. d) Association of annual Landsat maxNDVI with mean winter (October 1st – April 31st) temperature. e) Association of annual Landsat maxNDVI with mean summer (June-July) 12-month Standardized Precipitation-*evapotranspiration* Index (SPEI). e) Association of annual Landsat maxNDVI with mean summer (June 1st – August 5th) topsoil (0 – 7cm) volumetric moisture content. In all panels, insignificant associations have been filtered out and are show as transparent pixels. Basemap: 2019 WorldView-2 satellite image, © MAXAR, 2019.

in fig. 6.3a) (fig. S6.2). 4.62% of the studied area showed a significant positive correlation with the 10-month SPEI negative correlation (mean $\rho^2 = 0.11$, s.d. = 0.12, fig. 6.7e), which is roughly what may be expected based on chance at $\alpha = 0.05$. Significantly positive correlations of NDVI with topsoil moisture were found in 16.46% of the studied area (mean $\rho^2 = 0.19$, s.d. = 0.15, fig. 6.7f). This suggests that the influence of summer temperature and 10-month SPEI on local NDVI dynamics is limited, and that low NDVI in recent years is strongly associated with low summer precipitation, low soil moisture and warm winters with high snow accumulation.

Several spatial patterns are present in NDVI – weather data associations (fig. 6.7). Positive association of annual maxNDVI with summer precipitation and topsoil moisture are mostly evident in upland terrain (fig. 6.7b,f). Responses to summer precipitation and soil moisture are significantly higher in pixels with higher elevation and lower water occurrence frequency (fig. S6.3). Negative association of annual maxNDVI with snow height and winter temperature are stronger both in lower elevation floodplains and in higher elevation Yedomá plateaus (fig. 6.7c-d & S6.3). Interestingly, the slightly elevated margins and centres of drained thaw lake basins already show stronger response to snow height and topsoil moisture (fig. 6.7d,f), while these sites are generally only several meters higher than surrounding drained thaw lake basins. These trends indicate that sensitivity of tundra NDVI to precipitation varies throughout the landscape on sub-kilometer scale, with small topographic contrasts (range of meters to approximately 25 meters, fig. 6.1f) already affecting NDVI response to extreme snowfall and drought.

6.4. Discussion

With this study, we set out to assess whether recent browning of the Indigirka Lowlands could be explained by weather dynamics (particularly recent heatwaves and drought), floods and small scale vegetation shifts related to thermokarst. Our results suggest that recent browning is indeed related to summer drought, excessive winter snowfall and resulting flooding and to a smaller extent local vegetation shifts towards *Sphagnum*-dominated vegetation. Small-scale topographical contrasts and hydrological dynamics strongly regulate the role of these different mechanisms in NDVI dynamics across the landscape. Below, we will first discuss how browning dynamics identified in this study relate to previous findings of tundra browning. Then we will discuss the influence, spatial scale and dynamics associated with different drivers of browning (recent summer drought, flood events and thermokarst-induced vegetation shifts). Finally, we discuss implications for the Indigirka Lowlands region and for future Arctic greening in general. We conclude with a general summary of our main results and recommendations for future remote sensing studies of underlying mechanisms of tundra browning.

6.4.1 The Indigirka Lowlands in the context of panarctic NDVI dynamics

With an areal mean maxNDVI trend of -0.0041 NDVI units per year and 81% of available pixels showing significant browning, we find strong and widespread browning for our study area compared to previously reported NDVI trends for the Indigirka Lowlands region or for the Arctic in general (National Academies of Sciences and Medicine 2019, Berner et al. 2020, Myers-Smith et al. 2020, Frost et al. 2021b, Magnússon et al. 2021, Mekonnen et al. 2021a). Although the Arctic has generally continued to show increases in NDVI (Frost et al. 2021b), Landsat records indicate increasing occurrence of local browning across the Arctic, with 4.5% browning from 1985-2016, 6.0% browning from 2000-2016 (Berner et al. 2020) and 8% browning from 2000-2020, much of which is concentrated in the Indigirka Lowlands region (Mekonnen et al. 2021a). Apart from our study site being one of the most pronouncedly browning Arctic sites, these findings suggest that browning in the Indigirka Lowlands has been intensifying during the past decade (Magnússon et al. 2021, Mekonnen et al. 2021a). Understanding the mechanisms underlying this trend break from panarctic NDVI is important to assess future occurrence of Arctic browning.

On a panarctic scale, Landsat NDVI generally shows positive associations with summer warming in recent decades (Berner et al. 2020), which is in contrast with our results (fig. 6.7a). We find browning to be mostly explained by decreasing summer precipitation and soil moisture and extreme snowfall (fig. 7b,f & S6.2). Our work adds to increasing evidence that the influence of changes in Arctic temperature and precipitation on tundra NDVI differs among landforms and regions (Lara et al. 2018, Berner et al. 2020, Frost et al. 2021a). On a panarctic level, greening is more evident in upland regions with temperatures increase as long as moisture availability is not limited, while browning is more evident in lowland regions that show a drying trend (Berner et al. 2020). In the relatively warm and strongly maritime Yukon-Kuskokwim delta, Frost et al. (2021a) found positive associations of various NDVI products with summer temperature, whereas relations with summer precipitation were absent or even negative for lowland sites. However, in relatively arid Northern Alaskan regions, Chen et al. (2021) found strong dependence of NDVI on soil moisture and precipitation variables. Lara et al. (2018) found that the response of Landsat NDVI to year-round temperatures and precipitation varies among geomorphological subunits, with particularly negative responses to precipitation increases and positive responses to temperature increases in wet sites such as tundra ponds. Consistent with these earlier findings, we find stronger positive responses to summer precipitation and soil moisture in elevated Yedoma plateaus (fig. 6.7b,f). Lack of positive response to summer temperatures (fig. 6.7a), positive response to rainfall and soil moisture (fig. 6.7b,f) and low NDVI during the warm and dry summers of 2010 and 2018-2019 (fig. 6.3a) indicate that in this continental region with relatively dry summers (fig. S6.1) (Fujinami et al. 2016), recent NDVI dynamics are driven by moisture-limitation. This is also consistent with recent dendrochronological studies that report increasingly negative responses of shrub growth to summer temperature increases in moisture-limited ecosystems (Gamm et al. 2018, Buchwal et al. 2020). This suggests that both the regional water balance and topography influence the response of panarctic tundra NDVI to changes in temperature and precipitation.

6.4.2 Association of NDVI with weather patterns and hydrology

Despite the low amount of available Landsat scenes for peak summer periods between 1999-2019 and occasional missing pixel data due to scan line corrector failure (Storey et al. 2005), associations of annual maxNDVI and weather data show spatially consistent patterns (fig. 6.7) and annual dynamics (fig. 6.3a) that correspond with annual variability in temperatures and precipitation (table S6.2, fig. S6.1). This suggests that identified associations between weather data and NDVI dynamics are representative of climatic influences on vegetation growth in this area. Over the studied period (1999-2019), the study area shows a general decrease in summer precipitation and SPEI-12, with the exception of high rainfall in 2011 causing SPEI-12 to temporarily increase (2011-2012) (fig. S6.1). Snow height shows strong positive anomalies from 2016-2018, while 2019-2020 show anomalously high summer temperatures and record-low SPEI-12 (fig. S6.1). Browning of the study area may be a response to persistent decreases in summer rainfall and water balance (as evident from SPEI-12) from 1990 to 2010. While summer rainfall and SPEI-12 are already substantially lower than the long-term (1990-2020) average in the period 2004-2020 (table S6.2, fig. S6.1), maxNDVI decreases particularly between 2007 and 2010 (fig. 6.3a). This implies that especially multi-year drought may be detrimental for vegetation productivity and maxNDVI. While the wetter period in 2011 (table S6.2, fig. S6.1) is reflected by a degree of recovery in maxNDVI between 2010 and 2012 (fig. 6.3a), continuing decreases in summer rainfall and SPEI-12 from 2011-2020 (table S6.2, fig. S6.1) may have prevented recovery to pre-2010 maxNDVI values. Consistent with these dynamics, we found NDVI dynamics to be positively associated with summer rainfall and soil moisture (fig. 6.7). We found stronger moisture dependence in upland sites such as Yedoma plateaus and elevated margins of alases (fig. 6.7). This is in line with earlier ecological and remote sensing studies, that have found reduced temperature response of shrub growth in moisture limited upland sites (Ackerman et al. 2017) and larger NDVI increases in upland tundra with higher moisture availability (Berner et al. 2020). Sites with permanently wet conditions (e.g. low elevation areas on alases) did not show soil moisture or rainfall dependency (fig. 6.7b,f) and occasionally showed greening (fig. 6.3b), which is consistent with

findings that sites with higher soil moisture or water flow accumulation show stronger response of NDVI to temperature increases (Naito and Cairns 2011, Tape et al. 2012, Campbell et al. 2021). These findings all point towards an important role of local water availability in NDVI dynamics.

Comparison of annual weather variables and maxNDVI across the landscape additionally revealed a negative response of maxNDVI to extreme snow accumulation during the warm winters of 2016 – 2018 (fig. 6.7c-d). This negative response was evident both in low-elevation floodplains and upland Yedoma plateaus (fig. 6.7c-d & S6.3). High snow accumulation led to extensive floods throughout the Indigirka Lowlands in 2017, which led to severe growth declines in larch forests surrounding the Indigirka river (Tei et al. 2020) and strong browning surrounding the Khroma and Indigirka rivers (Magnússon et al. 2021). This is consistent with record low NDVI in floodplain areas in 2017 (fig. S6.4), which were indeed entirely flooded for much of the summer season during that year (Heijmans, pers. obs.). This makes waterlogging in the early summer season due to high snow accumulation a likely cause of the particularly strong browning observed around the river Berelekh (fig. 6.3b). Interestingly, the dry and warm year 2019 (fig. S6.1) showed a pronounced increase in NDVI particularly in floodplain areas while Yedoma plateaus and drained thaw lake basins continued browning (fig. S6.4). In addition, the few areas that showed greening or no significant change in maxNDVI were generally situated around lakes and in wet areas along the inner circumference of drained thaw lake basins (fig. 6.3b). This could be indicative of vegetation succession where aquatic species colonize lake margins (Troeva et al. 2010, Roach et al. 2011) and recently drained parts of thaw lakes (Morgenstern et al. 2013). This suggests that while floodplains and connected lowland areas are particularly sensitive to NDVI decreases due to flooding following extreme snowfall, periodically inundated sites also show rapid recovery of vegetation and NDVI in warm years.

The negative response of maxNDVI to warm winters with high snow accumulation on Yedoma plateaus and other elevated sites (fig. 6.7c-d) likely reflects a mechanism other than flooding, as spring and early summer floods do not reach these elevated sites (fig. 6.1d, Heijmans, pers. obs.). Alpine and Arctic tundra species growing on exposed ridges are generally well adapted to lower snow cover and cold exposure (Löffler and Pape 2020, Dobbert et al. 2021) and show rapid growth following snowmelt (Francon et al. 2020, Dobbert et al. 2021). Hence, prolonged snow cover may compromise growth especially at higher elevation sites (Francon et al. 2020). Additionally, the summers of 2016 and 2017 following high snowfall were relatively cold (fig. S6.1), although summer temperature responses were not evident in the study area (fig. 6.7a). Elevated sites feature mixed tundra vegetation communities with different species composition compared to lower elevation sites (Siewert et al. 2015), of which particular species may show pronouncedly negative responses to high and prolonged snow cover. Lastly, high amounts of snowmelt may induce erosion or waterlogging in small drainage features. Pronouncedly negative correlation of maxNDVI with snow height at margins of drained thaw lake basins and edges of Yedoma plateaus (fig. 6.7d) is in line with such a mechanism. Additional spatial patterns in browning rates that could indicate a role of erosion may require higher resolution maxNDVI time series to become evident. Detailed field data and experimentation would help identify mechanisms that explain this local negative response to warm winters with high snow accumulation.

6.4.3 Association of NDVI with vegetation dynamics

Only a relatively small degree of browning in this region is explained by small-scale thermokarst and associated succession dynamics towards wetland vegetation (fig. 6.5). In a focus study area representing a single drained thaw lake basin, we found NDVI declines to be somewhat stronger in locations with increasing cover of open water and *Sphagnum* vegetation and decreasing cover of mixed tussock sedge vegetation. Relatively high NDVI of tussock sedge vegetation (Loranty et al. 2011, Reynolds et al. 2019) and low NDVI for open water features and *Sphagnum* vegetation (Schubert et al. 2010, Lin et al. 2012, Reynolds and Walker 2016) are consistent with earlier studies of associations between vegetation

composition and NDVI. However, in contrast with earlier research into relations of vegetation cover and NDVI (Forbes et al. 2010, Blok et al. 2011c, Boelman et al. 2011, Loranty et al. 2011), we find relatively little association between shrub cover and NDVI (fig. 6.5-6.6). WorldView-2 and Landsat 7 images from 2015 provide an interesting exception; here, higher shrub cover shows stronger association with NDVI (fig. 6.6b,f). Since these are earlier season images (July 10th and 12th), this hints at potential differences in NDVI contrasts among tundra vegetation functional groups throughout the season. The very late summer GeoEye-1 image from 2010 (August 2019) (fig. 6.6e) in contrast shows relatively high NDVI values associated with sedge vegetation compared to other years. Indeed, accounting for differences in phenological phases has been found to improve classification of tundra vegetation types based on Landsat data in Greenland (Karami et al. 2018). Additionally, 2015 was a relatively wet summer compared to 2010 and 2019 (fig. S6.1). Shrub vegetation NDVI was particularly low in 2019 (fig. 6.6g), and field observations in this dry year (fig. S6.1) confirm a relatively high amount of standing dead shrubs (Magnússon & Heijmans, pers. obs.). These findings indicate that contrasts in NDVI among tundra vegetation functional groups, and hence the effects of vegetation shifts on NDVI values, likely depend on seasonal timing and moisture availability.

An increasing degree of association between vegetation cover and NDVI (fig. 6.6a-g) in smaller spatial resolution data suggests that highly localized (fig. 6.6h) and frequent vegetation shifts (Magnússon et al. 2021) with variable impacts on NDVI (table S6.3) may be increasingly averaged out in coarser resolution NDVI products. This may also explain why larger-scale phenomena such as weather dynamics and floods explain more variance in coarser-scale Landsat NDVI trends compared to highly localized and variable processes such as vegetation changes. Contrary to our expectation, the effect of local shrub decline due to formation of thaw ponds explained only very little variance in Landsat NDVI trends (fig. 6.5) (< 1%). Formation of thermokarst ponds in shrub vegetation affected only 0.5% of the focus study area (table S6.3) and is followed by colonization of sedge vegetation on subdecadal timescales (Magnússon et al. 2021). In addition, not all thaw ponds show low NDVI values in the very high resolution images (fig. 6.6e-g), which may also result from sparse vegetation cover or their shallow depth (Grosse et al. 2008). This likely explains why thaw pond formation only marginally affects NDVI trends and that if the effects of thermokarst and rapid vegetation dynamics on NDVI are to be captured at subdecadal timescales, image material with a spatial resolution at least comparable to that of the WorldView-2 and GeoEye-1 dataset used here (2m) or even smaller resolution data (e.g. drone data) with high temporal availability is necessary. While small-scale thermokarst does not seem to currently contribute to coarser-scale browning, increased cover of *Sphagnum* vegetation (Magnússon et al. 2021) seems to have contributed to enhanced browning (fig. 6.5). Despite high classification accuracy (91-93%), the use of classified maps of vegetation functional groups may be a source of uncertainty and direct comparison of NDVI trends with ground-measured changes in vegetation composition remain necessary to accurately constrain effects of vegetation changes on NDVI trends.

6.4.4 Implications for the Indigirka Lowlands ecosystem

Based on current IPCC scenarios of 1.5 – 4.0°C global warming, temperature increases of 3.7 – 9.6°C (1.9 – 6.0°C in June-August) and precipitation increases of 15 – 38% (7.2 – 14% in June-August) are predicted for the Russian Arctic (IPCC 2021). Increased occurrence of heatwaves and increased interannual variability in precipitation is expected, with both dry periods and precipitation extremes increasing (IPCC 2021, Wang et al. 2021). Warming air temperatures and increased occurrence of extreme precipitation may further promote permafrost degradation, thermokarst and vegetation disturbance in this ice-rich ecosystem (Biskaborn et al. 2019, Douglas et al. 2020, Nitzbon et al. 2020, Magnússon et al. 2022). Our findings suggest that NDVI dynamics are not significantly associated with warming, and especially prolonged periods of hot and dry summers may be detrimental to vegetation growth. This would suggest that increases in temperature and precipitation for this region will only be beneficial for tundra greenness and vegetation productivity if increased variability in precipitation doesn't result in

increased occurrence of multi-year drought. While increases in heatwaves and precipitation are evident, there is still considerable uncertainty whether drought events will increase or decrease in the Russian Arctic and much of the polar regions (IPCC 2021). Recent heatwaves and drought events have been attributed to complex interactions of anthropogenic warming, atmospheric teleconnection patterns and snow albedo feedbacks (Overland and Wang 2021, Collow et al. 2022), which complicates prediction of such events in the future (Overland and Wang 2021). Better quantification of future drought spells is essential to assess risk of future tundra browning and potentially other events such as wildfires.

Particularly in lowland ecosystems adjacent to major river systems, increased occurrence of tundra browning events may be expected as a result of waterlogging. Flooding frequency for Siberian rivers is expected to increase by 2 - 5%, with local increases of up to 10% for the Indigirka river (Shkolnik et al. 2018). This will likely result in further negative impacts on tundra NDVI, but also boreal forest growth, infrastructure (Tei et al. 2020) and nesting site availability for birds (Haverkamp et al. 2022). However, our results suggest that in river-adjacent tundra floodplains with graminoid, peat moss and willow vegetation, effects on NDVI may be short-lived if followed by drier, warm summers. The effects of thermokarst and associated highly localized vegetation shifts towards aquatic species such as *Sphagnum* at the expense of higher NDVI vegetation types may contribute to future local browning, but on a small and local scale compared to climatological and hydrological drivers. Apart from impacts on NDVI, such processes have been observed to result in increased methane emissions and carbon source dynamics in Siberian tundra ecosystems (Nauta et al. 2015, Beckebanze et al. 2022). Hence, ignoring their presence and impact may lead to overestimation of carbon uptake by tundra vegetation (Beckebanze et al. 2022). Our analysis of vegetation compositional change and its relation to NDVI dynamics was limited to a smaller subsite representing a drained thaw lake basin. Although such features occupy a large proportion of the North-Eastern Siberian tundra (Fedorov et al. 2018), vegetation dynamics and thermokarst activity differ among landforms and stages of development of drained thaw lake basins (Jorgenson and Shur 2007, Zona et al. 2010, Morgenstern et al. 2013, Jones et al. 2022). In general, our findings suggest that browning in this region is both trend- and event based (sensu (Myers-Smith et al. 2020)) and that the relative role of browning events (floods) and trends (increased drought and to a minor extent vegetation successional processes) also differs with landscape position and landscape evolution.

6.4.5 Future Research

Our remote sensing based study has provided valuable insights into the mechanisms that underlie strong recent browning in the Indigirka Lowlands, despite a continued trend of overall Arctic greening. In this ice-rich, strongly continental lowland tundra ecosystem, browning was associated with persistent drought, recent snowfall extremes and resulting floods and, to a very minor extent, thermokarst and related changes in vegetation composition. To better understand whether such processes may induce tundra browning in the future in other Arctic regions, future studies should address the following remaining knowledge gaps.

To better assess the extent to which drought may induce future tundra browning in the future, several knowledge gaps remain. While persistent drought is clearly associated with browning, we cannot yet draw robust conclusions about the duration and intensity of drought or critical biophysical thresholds required to trigger tundra browning, nor can we accurately assess recovery dynamics following drought or flood events of variable intensity and duration. This requires further and longer term studies of NDVI following climatic extremes, as well as better forecasting of future Arctic climatic extremes. Experimental studies could potentially contribute greatly to our understanding of NDVI impacts and recovery following climatic extremes and drought episodes of variable duration. The fact that the recent climate record for our site has shown both periods of dry heatwaves, extreme snowfall and floods and extreme rainfall within a period of only ten years suggests that simulation of multiple consecutive extremes may be a valuable addition to simulate a rapidly changing Arctic.

To assess the degree to which NDVI dynamics are indicative of highly localized and spatially variable processes such as thermokarst and changes in vegetation composition and properties, a multi-scale approach is necessary (Myers-Smith et al. 2020). For our ecosystem, NDVI products with spatial resolutions of at most 2m but preferably less seem to be appropriate given the spatial dimensions on which vegetation changes manifest on timescales of approximately 10 years. This likely differs among ecosystems. Comparison of localized NDVI-impacts with coarser resolution NDVI timeseries that are typically used for monitoring (e.g. Landsat and, with increasing temporal availability, Sentinel data) may indicate how and on what timescales such small scale changes on the ground propagate to larger spatial scales. Increasing availability of very high resolution image products and drone technology opens up the possibility of strategically repeated acquisition of high resolution NDVI data for comparison with field-measured changes and longer-term, coarser resolution NDVI timeseries. Although naturally occurring vegetation shifts remain a key process to monitor, a potentially strategic way to quickly gain insight into the effect of tundra vegetation changes on NDVI may be monitoring of multi-resolution NDVI under targeted removal of particular plant functional groups on various spatial scales. Lastly, with respect to impacts of vegetation composition and properties on NDVI, collection of multiple NDVI data points per season would likely also allow better assessment of the contribution of different vegetation groups to changes in NDVI.



7.

General Discussion



Since 1971, the Arctic regions have warmed three times faster than the global average warming rate (AMAP 2021). Changes in Arctic ecosystems as a result of warming affect global sea level, large-scale climate patterns and atmospheric concentrations of greenhouse gases across the globe. Understanding rates, drivers and triggers of changes in Arctic ecosystems is essential to assess to what extent feedbacks in Arctic ecosystems will affect future life on Earth. To contribute to this substantial challenge, I focussed on rates of permafrost degradation and vegetation changes under a changing climate in the North-Eastern Siberian lowland tundra region. These lowland tundra ecosystems cover large parts of the Russian Arctic and contain permafrost that is rich in ice and carbon, giving them high potential for permafrost degradation and carbon emissions in a warming climate (paragraph 1.6). I set out to (1) determine whether this region showed a net expansion or decline of shrub vegetation, and how this relates to permafrost degradation, (2) assess the impact of future extreme rainfall events of permafrost and vegetation in this ecosystem and (3) to quantify the long-term development of permafrost and vegetation following local abrupt thaw of permafrost. I have addressed these knowledge gaps using experimental data and monitoring data from a study site in the Siberian lowland tundra, climate time series, remote sensing data and tree ring records. In the general discussion below I will reflect on the implications of these results for the North-Eastern Siberian Lowland Tundra ecosystem. I will focus particularly on shrub dynamics, the role of climate changes and extremes in permafrost degradation and the degradation-recovery dynamics of small tundra ponds. I conclude with a summary of my main findings and recommendations for future studies.

7.1 Shrub decline and browning in the Siberian lowland tundra

7.1.1 Shrub dynamics at the Kytalyk site

Thermokarst turned out to be a key driver of shrub decline that manifested on small spatial scales (sub-meter to meter) over subdecadal to decadal timescales (Chapter 2 & 3). Studying a chronosequence of thaw ponds of various age classes, I found that these small-scale thermokarst features expand at the expense of shrub dominated vegetation at mean rates of around 30 to 50cm per year (fig. 2.2). These findings were confirmed by a land cover change analysis (Chapter 3) using the same very high resolution satellite images over a larger area (a drained thaw lake basin of 2.33 km²). This area showed a net shift towards a sedge- and peat moss dominated state. The area of thaw ponds and other open water features increased by around 50% from 2010 to 2019, mostly at the expense of shrub vegetation (fig. 3.4). Similar increases in surface area of small-scale thermokarst water bodies were observed in the North-Eastern Siberian Alazeya basin (Grigoriev et al. 2009) and this is a likely future trajectory in a warming climate in this ice-rich region (Grigoriev et al. 2009, Nitzbon et al. 2020). Local shrub decline due to thermokarst outpaces potential shrub recovery (Chapter 2) and the studied drained thaw lake basin shows a net trend of shrub decline and expansion of aquatic vegetation in the past decade (2010 - 2019) (fig. 3.5). Hence, my results show that in highly dynamic, ice-rich and warming drained thaw lake basins, shrub decline rather than shrub expansion may occur as a result of thermokarst activity.

Dynamics of shrub decline or expansion may vary across landscape gradients. Observations on slightly elevated terrain (thaw lake margins, pingos) reveal that the locally dominant mixed vegetation type (tussock sedges, dwarf shrubs, mosses and graminoids, see table 3.1) hardly shows any transition or indication of thermokarst (fig. 3.7). This suggests that thermokarst-induced shrub decline predominantly occurs in lower elevation terrain such as drained thaw lake basins and that, apart from climate patterns, landscape evolution, topography and ground ice conditions are important factors that determine tundra landscapes' sensitivity to thermokarst induced local vegetation shifts (Jorgenson et al. 2015, Heijmans et al. 2022). This is consistent with observations of preferential secondary thermokarst activity in previously affected terrain such as drained thaw lake basins (Morgenstern et al. 2013) and illustrates

the importance of drained thaw lake basins in the context of thermokarst and shrub expansion (Chen et al. 2021, Jones et al. 2022). An interesting novel aspect is that such contrasts in vegetation dynamics are already visible within the highly limited elevation range found in the Kytalyk area (fig. 6.1) within a timespan of only 10 years. Differences in species composition, thermokarst occurrence, vegetation dynamics (fig. 3.7) and NDVI dynamics (fig. 6.7) were already evident in landscape features that are elevated only several meters above the drained thaw lake basin's level, such as pingos and lake margins. This showcases how meter to kilometer scale topography and landscape history affect spatio-temporal dynamics of shrub vegetation.

7.1.2 Shrub growth and tundra greenness in a changing climate

While temperatures during the summer season remain an important driver of shrub growth, NDVI dynamics and, in recent decades, shrub growth records hint at an increasing and spatially variable influence of precipitation on tundra vegetation growth (Chapter 5 & 6). In support of quantification of recent changes in shrub cover across the landscape (Chapter 3), I created and analysed several 45-year long tree ring records for Arctic dwarf birch (*Betula nana subs. exilis*), sampled across a topographic gradient (Chapter 5). *Betula nana* is a common Arctic tundra species and the most abundant shrub species at the study site. In addition, I quantified Landsat-based NDVI trends for a 10 by 10km area around the study site as a measure of overall tundra greenness and photosynthetic activity, which I compared to terrain and changes in cover of functional vegetation groups (Chapter 6). Radial growth of *Betula nana*, as evident from tree rings, is generally higher in warm summers with early snowmelt and sufficient moisture availability (fig 5.6). This is consistent with earlier findings in the same study area (Blok et al. 2011b, Li et al. 2016) and across the Arctic (Myers-Smith et al. 2015a, Buchwal et al. 2020). Although a consistently positive response to summer temperature dominated the climate-growth response of *Betula nana*, the response of growth to precipitation, and particularly to precipitation extremes, showed increasing variability among higher (Yedomo ridge) and lower (small-scale thermokarst depressions) landscape positions (fig. 5.6 - 5.7). Association between local Landsat annual peak summer maximum NDVI with precipitation and soil moisture also varied over contrasts in geomorphology, topography and flooding frequency (fig. 6.7). This shows how on the one hand both tundra greenness and shrub growth are generally promoted by warm summers with relatively high rainfall. On the other hand, topographical differences and redistribution of water and snow throughout the landscape induce differential responses to precipitation dynamics on spatial scales of kilometers to meters (fig. 7.1). This suggests that relations between precipitation, shrub growth and tundra greenness may only be spatially scalable to a limited extent, even within ecosystems.

Both radial growth of *Betula nana* and Landsat maxNDVI appeared limited by recent dry conditions in the study site. NDVI appeared more sensitive to low summer rainfall and soil moisture than radial growth of *Betula nana* (Chapter 5 & 6), which could indicate some degree of adaptation of *Betula nana* to dry conditions (De Groot et al. 1997) compared to other local tundra species. The response of *Betula nana* radial growth to summer rainfall seemed to differ among landforms and time periods, and mainly manifested as a co-limitation of summer temperature and rainfall rather than a direct effect. The response of *Betula nana* radial growth to rainfall (or to simultaneous peaks in summer temperature and rainfall) shows nuanced divergences among landforms over time (fig. 5.6 - 5.7). Plausible mechanisms that likely drive this spatio-temporal heterogeneity include different baseline moisture conditions and redistribution of water across (micro)topographical gradients, changes in longer term climatic conditions (drought, particularly), changes in occurrence of rainfall extremes over time and, lastly, changes in the landscape itself (in this case increased wetness and ponding due to thermokarst) (Chapter 5, fig. 7.1b). It is striking that under the dry conditions of the last two decades, *Betula nana* only showed positive growth anomalies in summers with both warm and wet conditions (fig. 5.7, fig. 7.1a) while NDVI showed no positive response to summer temperature at all (fig. 6.7). The initially positive response of shrubs in thaw ponds to summer rainfall, followed by waterlogging and high shrub mortality after an exceptionally

rainy summer (Chapter 5) likely indicate that the response of tundra vegetation to moisture is in itself non-linear. In general my results fit an emerging perspective that tundra NDVI and shrub growth are strongly driven by co-limitation of temperature and moisture. This is evident from regional contrasts in temperature and moisture response of shrub growth and NDVI among wetter and drier tundra regions (Chen et al. 2021, Buchwal et al., 2020, Frost et al. 2021a) as well as the role of topography and site climatology in determining the response of NDVI to warming (Berner et al. 2018, Mekonnen et al. 2021a). My research (Chapter 5 & 6) confirms that apart from large-scale to regional contrasts in climate, modest local elevation differences across geomorphological units and as a result of thermokarst drive redistribution of water and snow throughout the landscape and result in heterogeneity in climate response of vegetation. Anticipated increases in Arctic rainfall will likely have a generally positive effect on shrub growth (fig. 5.6) and NDVI (fig. 6.7) in this relatively dry Arctic region. However, increased variability and extremes in precipitation (Bintanja et al. 2020, IPCC 2021, Wang et al. 2021) could induce stronger pulse dynamics in tundra greenness, shrub dynamics and thermokarst. Exact dynamics will likely differ over topographical gradients, with shrubs and NDVI responding positively to alleviation of moisture limitation in warm summers, but negatively to local waterlogging.

The response of shrub growth and NDVI to precipitation in winter also varied across the landscape and over time (Chapter 5 & 6). A period of record-high snowfall during the past decade (fig. 5.2, fig. 7.1c) triggered record-high water levels in the Indigirka river which persisted over a substantial period into the summer season, causing widespread inundation of floodplains (Tei et al. 2020). This is reflected in a pronounced local decrease of Landsat NDVI (Chapter 6) and regional MODIS EVI (Chapter 3) particular to floodplain areas. However, Landsat maxNDVI dynamics suggest a rapid recovery of NDVI during the dry, warm years following this extreme flood event (Chapter 6). With anticipated increases in winter precipitation (Bintanja and Selten 2014, IPCC 2021) and flood events (Shkolnik et al. 2018), such periodic browning events will likely occur more frequently. Apart from floodplains, severe floods may reach low lying areas in surrounding drained thaw lake basins, which may be less adapted to periodic waterlogging and may potentially show more lasting impacts on permafrost (van Huissteden et al. 2021), shrub growth and NDVI. Interestingly, negative impacts of extreme snowfall were not limited to flooded areas, as Landsat maxNDVI and shrub radial growth on high elevation landscape positions both showed negative responses to recent extreme snow accumulation (fig. 5.6 & 6.7). This similar response suggests that either Landsat maxNDVI is strongly determined by growth of *Betula nana*, contrary to findings of Blok et al. (2011b), or that these negative impacts of extreme snowfall are evident for a broader range of species at higher elevation sites. A negative response to high snow accumulation may be explained by shortening of the growing season (Hallinger et al. 2010, Francon et al. 2020) under otherwise earlier snow-free conditions and NDVI increases (fig. 5.4 - 5.5), or erosion during runoff of snowmelt (Chapter 6). Identification of underlying mechanisms would require further study (Chapter 5). These findings demonstrate how snowfall extremes are associated with differential impact on shrub growth, greening and browning depending on topographical and hydrological context (fig. 7.1c). Additionally, unstable relations between snow height and shrub growth over space and time (fig. 5.7) show that responses to extreme conditions do not necessarily follow logically from climate-growth relations under baseline conditions. This suggests that climate-growth relations (or climate - NDVI relations) under moderate climatic variability may only hold limited information for shrub growth under future climatic extremes.

7.1.3 Towards improved projection of future tundra greening and shrubification

Analysis of NDVI dynamics (Chapter 6) in recent decades in the most pronouncedly browning region in the Arctic indicated summer drought and extreme flooding as the most likely underlying factors of reduced tundra vegetation productivity. Comparison with coarse resolution MODIS EVI time series (fig. 3.2) suggests that the identified dynamic (fig. 6.3) of increasing NDVI prior to 2010 and browning between 2010 and 2019 is representative for the majority of the Indigirka lowlands region.

However, panarctic NDVI dynamics are currently monitored at spatial resolutions of several kilometers to at best several hundreds or tens of meters (Berner et al. 2020, Myers-Smith et al. 2020, Frost et al. 2021b, Mekonnen et al. 2021a). Local feedbacks such as thermokarst, vegetation shifts and dynamics of methane hotspots occur on smaller spatial scales and are at risk of being overlooked in coarser scale remote monitoring of the Arctic (fig. 6.6) (Muster et al. 2013, Nauta et al. 2015, Beckebanze et al. 2022). Secondary thermokarst in drained thaw lake basins and associated shrub decline and increases in wetland vegetation were shown to contribute to recent Landsat browning only to a small extent (fig. 6.5), but a degree of differentiation in Landsat and Sentinel NDVI with vegetation composition was evident (fig. 6.6). Substantial challenges remained in relating this localised impact to larger-scale NDVI dynamics in a highly dynamic ecosystem (Chapter 6). An obvious course for future research would be to monitor relations between vegetation compositional changes and NDVI over longer timescales, as very small contrasts in vegetation composition over time may not be reflected on spatial scales of current longer term NDVI time series. However, subpixel heterogeneity in vegetation development (e.g. with highly localised greening and highly localised browning both taking place) could average out any relation between NDVI time series and vegetation change on the ground (fig. 7.1d) (Myers-Smith et al. 2020). Time series of very high resolution NDVI products from commercial sources or drones would likely help to link changes on the ground to panarctic NDVI time series. Standardisation of acquisition protocols for in-situ remote sensing and field data are key for upscaling to a panarctic context (Myers-Smith et al. 2020). However, Chapter 6 and earlier studies point out several potential challenges to such an approach; namely the short time frame for acquisition of suitable images and the major role of within-season phenological development of various plant functional groups in determining NDVI (fig. 6.6) (Beamish et al. 2020, Myers-Smith et al. 2020). Image regularisation techniques can resolve part of the spectral variability among images acquired at different seasonal timing for purposes of land cover change characterization (Chapter 3) and may assist multitemporal high resolution vegetation change analysis. But perhaps more importantly, within-season variability of spectral properties of various vegetation classes could be seen as an asset that can help link NDVI dynamics to the phenology of particular plant groups (Karami et al. 2018, Heijmans et al. 2022). The availability of multiple scenes per summer season in high resolution would likely support characterization of the degree to which various plant functional groups contribute to tundra productivity throughout the season.

To improve our understanding of the role of future climate regimes on tundra productivity and shrub growth, informed experimentation combined with monitoring of key variables (e.g. shrub radial growth, plant physiological aspects, permafrost thaw depth, soil moisture) remains crucial. Results from Chapter 5 & 6 indicate that the result of future climate change and weather extremes in particular may be less predictable than extrapolation of current climate-growth relations would suggest. Response to extreme summer rainfall for instance may result in contrasting shrub growth and NDVI dynamics across topographical gradients and among wet or moisture-limited sites or regions, which would require future experiments to incorporate a range of spatial variability and contrasting climatic conditions. Further differentiation may result from moderate increases in a particular weather variable compared to extremes (as was likely the case for recent extreme snow height) and combinations of particular conditions or extremes (as evident from interactive effects between summer temperature and rainfall). Such considerations could help inform (combinations of) experimental treatments for future field research. However, to better inform treatment levels for field manipulation studies, more detailed forecasting of year-to-year variability and recurrence of extremes would be helpful. Lastly, due to its important role in determining highly local as well as regional variability in climate-growth relations, higher resolution spatial data of soil moisture would help to upscale results of experimental findings.

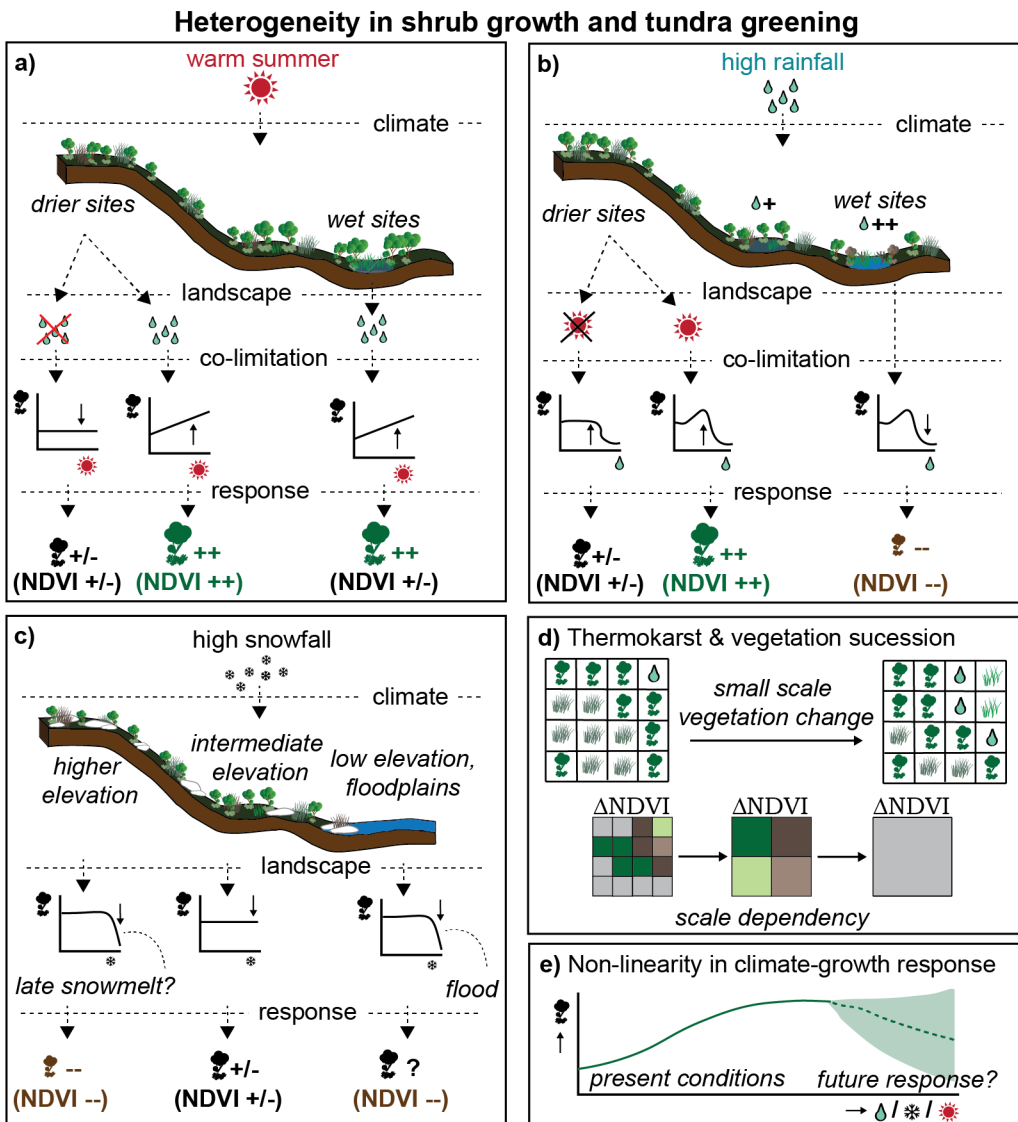


Figure 7.1) Graphical synthesis of observed sources of heterogeneity in relations between climate, shrub growth and NDVI in the North-Eastern Siberian lowland tundra. In general, the local response of shrub growth and NDVI to climate is mediated by terrain variability, co-limitation and non-linearity in response. a) No significant response of NDVI to summer temperatures was observed, although temporary increases in NDVI seemed to occur following warm summers with high rainfall. Shrub growth showed a generally positive response to summer temperatures, but this response became increasingly co-limited by moisture availability under dry conditions. b) NDVI showed a generally positive response to summer rainfall that was particularly evident in higher elevation sites. If met by high summer temperatures, shrub growth responds positively to high summer rainfall. This response seemed to be enhanced initially by moisture concentration in small-scale depressions, although ultimately waterlogging results in shrub mortality and low NDVI on a local scale. c) Extreme snow accumulation in winter led to low NDVI in floodplains due to flooding, but NDVI and shrub growth also showed decreases in high elevation terrain. This may be explained by relations between topography, snow accumulation and onset of snow-free conditions during the growing season, although exact mechanisms were not identified. d) Lastly, highly localised thermokarst and vegetation succession processes may affect NDVI trends, although this influence becomes increasingly averaged out with coarser spatial resolution of NDVI time series (Myers-Smith et al. 2020). Here,

green colours indicate increasing NDVI, brown colours indicate decreasing NDVI and grey colours indicate no significant change. e) Tree ring analysis on *Betula nana* indicated non-stationary response to precipitation over time. Climate responses appeared to be non-linear (i.e. response to extreme conditions may be different from response to intermediate variability) and were regulated by co-limitation by temperature and moisture. As a result, responses to extreme rainfall or snowfall in the future may not always result logically from climate-growth relationships under present conditions.

7.2 Effect of summer rainfall extremes on permafrost thaw

7.2.1 Accelerated permafrost thaw in a rainier Arctic?

I found a pronounced increase in permafrost thaw rates following simulated extreme rainfall. Using a controlled experimental set-up showed that this increase results from increased rainwater inputs and that it can last multiple years (fig. 4.1). Simulations with a site-calibrated thermal-hydrological model suggest that rainfall effects may be most pronounced when accompanied by high summer temperatures (fig. 4.3). Such an effect may be explained by higher conductivity of wetter soils under a large temperature gradient (Hinkel et al. 2001), and higher temperature of rainwater during warm periods (Byers et al. 1949, Neumann et al. 2019). Plots in which rainfall was experimentally increased showed an increase in internal water tables in the two summers following the treatment, which indicates persistent subsoil wetting due to freezing and thawing of water deeper in the soil, even if topsoil moisture showed no more increase (fig. 4.1). Warm temperatures in the years after irrigation (2019 and 2020) may have contributed to enhanced thaw in later years by establishing a strong gradient in surface - subsoil temperatures. My findings are in line with observational studies from subarctic and Arctic Alaska and Central Siberia, where pronounced soil warming and active layer deepening was observed in summers with extreme rainfall (Iijima et al. 2010, Neumann et al. 2019, Douglas et al. 2020). Ecosystem models have predicted enhanced thaw due to increased heat advection and thermal conductivity following increased rainfall across Alaska (Grant et al. 2017, Mekonnen et al. 2021b). From a geomorphological perspective, extreme rainfall may additionally increase erosion on slopes and thereby accelerate hillslope thermokarst processes such as thaw slumping (Kokelj et al. 2015, Christensen et al. 2020). These findings suggest that accelerated warming and degradation of permafrost under extreme summer rainfall may be observed more generally.

However, contrasting evidence from different Arctic and Alpine regions indicates that the effect of summer rainfall extremes on permafrost may vary across sites based on baseline climatic conditions, topography and potentially other factors. In the Tibetan Plateau, researchers have found soil cooling following heavy rain events. These effects were mainly observed in topsoils and generally attributed to loss of latent heat due to enhanced evaporation (fig. 4.4) (Zhu et al. 2017, Luo et al. 2020). Where measured, deeper soil layers in this region also show warming under extreme rainfall (Luo et al., 2020). In another Siberian lowland tundra site, wetter sites also showed colder topsoil and warmer subsoil relative to drier, artificially drained sites (Göckede et al. 2019). This suggests that the effects of rainfall and soil moisture on the soil thermal regime may vary with depth (cooling in topsoil and warming in subsoil) and thereby likely also with the depth at which permafrost is located. In wetter soils near saturation, (Clayton et al. 2021) found higher bulk volumetric water to be associated with shallower thaw depth due to the dominance of latent heat requirements and heat capacity over thermal conductivity. The only other permafrost irrigation study that I am aware of that also reports thaw depths is Zhirkov et al. (2021), who interestingly report lower overall ground temperatures but deeper thaw depth in experimentally irrigated plots in Central Yakutia. Upon continuation of irrigation for three years, irrigated pots started to show shallower thaw depths relative to control plots, which was attributed to increases in soil moisture and latent heat requirements (Zhirkov et al. 2021). This would be in line with observations of Clayton et al. (2021). Lastly, (Karjalainen et al. 2019) found a positive association of active mean annual ground temperature and rainfall up to a threshold of 250mm per year, after which more rainfall was associated

with colder soils. This suggests that the effects of summer rainfall on permafrost thaw may additionally depend on baseline moisture content, with increases in soil moisture beyond a particular threshold reducing thaw depths due to increases in heat capacity and latent heat requirements during soil warming in spring and summer. As a final consideration, topographical variability and subsurface connectivity may regulate rainfall effects on permafrost through redistribution of water and energy throughout the landscape (Walvoord and Kurylyk 2016, Neumann et al. 2019, Hamm and Frampton 2021). Progressive degradation of ice-rich permafrost introduces additional microtopographic variability which can result in local positive feedbacks on permafrost degradation (Nauta et al. 2015), which can either enhance or reduce regional sensitivity to thaw on a very local scale. Such intricacies make it difficult to assess what percentage of permafrost terrain is sensitive to rainfall-induced thaw. However, comparison of my results with the existing knowledge base suggests that warm, ice-rich and otherwise relatively dry permafrost ecosystems may be especially sensitive to rainfall-induced permafrost degradation.

7.2.2 Implications of increased rainfall extremes for permafrost

My findings imply that anticipated increases in Arctic rainfall, both due to overall increases in precipitation and an increase in the rain to snow ratio, can accelerate permafrost thaw for multiple years, especially when they coincide with periods of warm temperatures (Chapter 4). As the majority of the Arctic is experiencing both warming and increases in rainfall extremes (AMAP 2021), this may lead to faster permafrost degradation than would be expected based on effects of warming alone. This could also suggest that lower-latitude Arctic regions or strongly continental sites with higher summer temperatures (such as the Kytalyk site) are particularly sensitive to rainfall-induced thaw. Observations of soil cooling following rainfall extremes are generally confined to upper soil layers (Zhu et al. 2017, Luo et al. 2020), which may occur alongside deeper soil warming and increases in thaw depth (Chapter 4) (Göckede et al. 2019). This suggests that the depth at which permafrost is located and how this relates to the depth to which heat advection and conduction can penetrate into the soil may provide additional, important controls on rainfall-induced permafrost thaw. Reduced active layer thaw depth and ground temperatures under increases in soil moisture content beyond a particular threshold (Karjalainen et al. 2019, Clayton et al. 2021, Zhirkov et al. 2021) suggest that extreme rainfall in otherwise drier areas would increase thaw depths, while sustained increases in rainfall in soils near saturation may lead to cooling. At the Kytalyk site, the generally dry conditions in recent decades (fig. 5.2) may have contributed to the large observed effect. This additionally suggests that anticipated increased variability of rainfall may have a more detrimental effect on permafrost thaw depths than sustained increases in precipitation and surface wetting alone. The present generation of climate models used for large-scale assessment of future areal loss of permafrost and permafrost carbon emissions have limited spatial and temporal resolution and soil depth representation (Burke et al. 2020). In addition, considerable uncertainty remains in predictions of future frequency and intensity of extreme rainfall events (Bintanja et al. 2020). This makes it unlikely that the impact of future increases in rainfall extremes on permafrost stability and carbon emissions is currently properly constrained, and calls for further research on multiple fronts (see paragraph 7.2.3 below).

7.2.3 Towards panarctic assessment of rainfall effects on permafrost thaw

To assess the degree to which increased rainfall and variability thereof may enhance future permafrost thaw across permafrost ecosystems, spatially distributed evidence is necessary (fig. 7.2). While recent years have seen emerging evidence of the importance of rain in permafrost dynamics (Karjalainen et al. 2019, Douglas et al. 2020, Mekonnen et al. 2021b) the current evidence base still yields insufficient insight into the mechanisms that determine rainfall sensitivity across different permafrost environments. An intuitive first step would be to repeat irrigation studies across Arctic ecosystems with diverse climates across gradients in topography, ground ice content, soils and vegetation. Panarctic monitoring initiatives such as the International Tundra Experiment (ITEX) already exist for the effect of warming on tundra

vegetation (Henry and Molau 1997, Elmendorf et al. 2012b). A similar setup for rainfall impacts (Grysko et al. 2021) would enable simultaneous monitoring of geophysical and ecological changes following extreme rainfall. To upscale findings across the permafrost region, physically based models that incorporate thermal and hydrological processes relevant for permafrost such as the Advanced Terrestrial Simulator (used in Chapter 4) may be valuable. Lastly, existing databases such as the Circumpolar Active Layer Monitoring network (CALM) may be used to relate time series of active layer depth to precipitation records. However, low temporal resolution (CALM reports only end-of-season thaw depth) and limited length of time series (at the time of writing 32 years at most but often less than 20) currently limit such studies. Closer integration between geophysical and ecological disciplines (Heijmans et al. 2022) and combinations of experimental work, modelling and analysis of observational records across heterogeneous permafrost ecosystems would likely prove most insightful.

In a broader sense, my finding that extreme rainfall affected permafrost for multiple years fits an emerging perspective of the importance of legacy effects of climatic extremes on permafrost, ecosystem functioning and the carbon balance of the Arctic (Bokhorst et al. 2022). This clearly demonstrates a need for monitoring periods longer than a single year or a few years post-disturbance (as is currently the case for Chapter 4 and in many other studies) (Bokhorst et al. 2022) (fig. 7.2). Longer-term monitoring should also shed light on recovery times following such disturbances, which would likely help implement the effects of extreme events such as rainfall extremes and thermokarst disturbances in global climate models (Heijmans et al. 2022). Due to the tight coupling between permafrost dynamics, hydrology and vegetation (Box 1.1), long term monitoring should ideally also encompass secondary effects such as changes in vegetation composition and changes in microtopography in case of ice-rich permafrost. With extended and broader monitoring, impacts of extreme rainfall on permafrost ecosystems could be assessed more holistically.

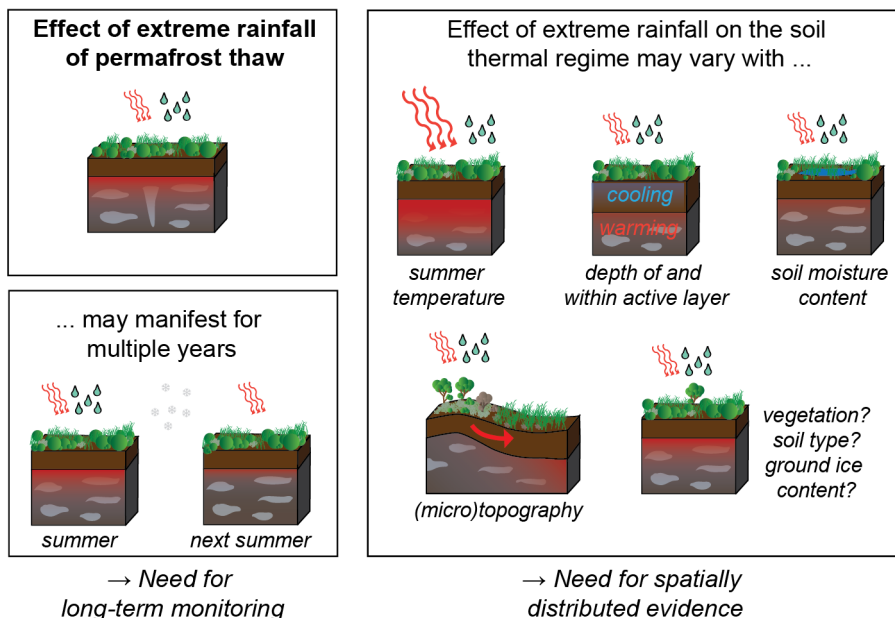


Figure 7.2) Graphical synthesis of observed effects of rainfall extremes on permafrost degradation and suggestions for future research. Red shades indicate permafrost thaw under extreme rainfall. Due to the multiyear legacy effect that was observed in the experiment of Chapter 4, and potential environmental heterogeneity in rainfall effects on permafrost, I recommend gathering spatially distributed evidence of effects of extreme rainfall on permafrost over multi-year periods (at least 3 years).

7.3 Permafrost degradation - recovery dynamics in the Siberian Lowland Tundra

7.3.1 Thaw ponds in the North-Eastern Siberian Lowland tundra: dynamics and implications

Chapters 2 & 3 revealed a highly dynamic and heterogeneous system in a drained thaw lake basin. The area of thaw ponds and other open water bodies resulting from small scale thermokarst is increasing (fig. 3.4), but these shallow (fig. 2.5) water bodies fill in with aquatic vegetation and terrestrialize on decadal timescales. Based on ponds' dimensions and expansion and terrestrialization dynamics, evident from repeated very high resolution satellite images (fig. 2.2), I estimated that ponds expand over mean timescales of 20 years and terrestrialize over similar timescales into sedge and *Sphagnum* dominated sites. Rather than spatially uniform expansion and contraction, ponds may "crawl" across the landscape, expanding on one side and terrestrializing on the other (Chapter 2). It is conceivable that during their development ponds encounter other small scale depressions or diffuse drainage systems and drain, although such processes were not observed in the field. Presence of recruiting shrubs in terrestrialized thaw ponds, particularly once peat moss has established, indicates a potential return to a shrub dominated state. However, ages of recruiting shrubs (fig. 2.3) and vegetation succession rates (fig. 3.5) indicate that this requires longer timescales than those associated with pond formation and expansion and terrestrialization in sedge and peat moss dominated sites (fig. 2.6). As a result, shrub patches affected by thermokarst currently show a net transition towards *Sphagnum* dominated vegetation, despite the rapid initial colonisation and terrestrialisation by aquatic species.

These observed landscape dynamics have implications for the local permafrost thermal regime and, to a marginal extent, tundra greenness. Local thermokarst and vegetation succession towards *Sphagnum* communities were associated with decreases in NDVI in high-resolution satellite data (fig. 6.6), but the extent to which this could be observed in time series of Landsat NDVI was limited (fig. 6.5). Different plant species or functional groups are associated with different surface energy balances, snow dynamics and insulative properties of the ground surface (Beringer et al. 2005, Wilcox et al. 2019, Grunberg et al. 2020, Heijmans et al. 2022). Hence, permafrost thaw depths and greenhouse gas dynamics vary among vegetation successional stadia (Chapter 2) (Jorgenson et al. 2015, Heijmans et al. 2022). Thaw pond formation and aquatic vegetation succession were associated with clear increases and decreases in surface elevation and permafrost thaw depth, which suggests that vegetation succession assists permafrost recovery (fig. 2.5). *Sphagnum* dominated vegetation communities still show deeper thaw than the shrub dominated, slightly elevated frost mounds in which thaw ponds originally formed (fig. 2.5), which indicates that, likely, longer timescales are necessary for complete permafrost recovery and shrub establishment following pond terrestrialization. These dynamics are to some extent contrary to panarctic observations of warmer soils under shrubs, relative to graminoid or lower stature vegetation (Kropp et al. 2021). In such cases, taller shrub canopies trap more snow in winter, thereby insulating the soil during the cold season and raising annual mean soil temperatures (Sturm et al. 2001, Kropp et al. 2021). An important divergence in this effect is evident among seasons, with predominantly warming insulative effects during winter, but cooling insulative effects of shrub canopies in summer (Heijmans et al. 2022). This would explain why low stature shrub canopies and associated understories of dry moss and lichens are associated with shallow thaw depths compared to other vegetation groups. Additionally, in this ice-rich ecosystem disturbance of the shrub canopy and thermokarst result in formation of depressions (of approximately 75cm depth, fig. 2.5) that trap more snow in winter than shrub canopies (Blok et al. 2010, Nauta et al. 2015). This likely explains the lack of soil warming effects of shrub canopies in this ecosystem and contributes to the very strong coupling of permafrost thaw depth, terrain height, wetness and vegetation communities.

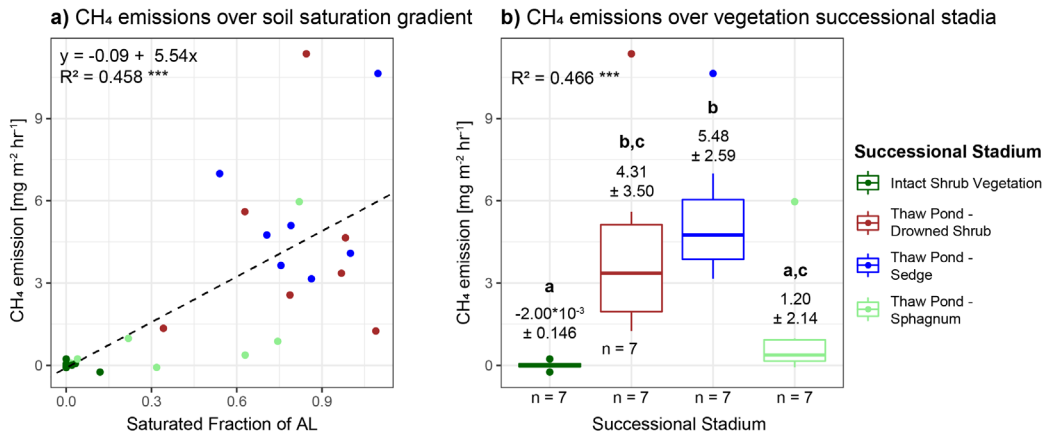


Figure 7.3) Methane fluxes over a gradient of soil saturation and thaw pond successional stadia. In a), the saturated fraction of the active layer (AL) was calculated as the height of standing water above the permafrost table divided by the thaw depth. b) indicates contrasts in methane flux among intact shrub vegetation and several thaw pond successional stadia (following classification from Chapter 2). Methane fluxes were calculated from linear increases in methane concentration measured in 4 samples taken at 15 minute intervals from a transparent gas flux chamber installed on collars in 7 thaw ponds and adjacent intact shrub area. Methane concentrations were measured using a gas chromatograph with flame ionisation detector. Relations with the saturated fraction of the active layer and with successional stadia were calculated using a mixed effects model with unique ponds as a random intercept. Significance of predictors was assessed using F-tests with Kenward-Rogers approximation of degrees of freedom (following the statistical methods of Chapter 2). R^2 indicates pseudo-R squared for mixed effects models (Nakagawa et al. 2017). In b), numbers represent group means and standard deviations. Bold letters a, b and c indicate significance of pairwise contrasts (after Bonferroni correction) based on Tukey contrasts, where classes that share a letter do not significantly differ from each other.

Lastly, this gradient in abiotic and biotic conditions over permafrost degradation and recovery stadia likely impacts the greenhouse gas balance of this ecosystem, as small tundra ponds are known hotspots of methane emissions (Nauta et al. 2015, Beckebanze et al. 2022). Measurements from Van Huissteden et al. (2005) and unpublished chamber flux measurements of methane from the site (fig. 7.3) show a general pattern of neutral methane source/sink dynamics in shrub dominated vegetation, with steep increases in methane emissions in wet, subsided sites dominated by drowned shrub vegetation and colonising sedges. Methane emissions are strongly reduced after colonisation by *Sphagnum* and associated lowering of the water table, consistent with hypothesised methane oxidation in aerated peat discussed in Chapter 2. This confirms that these small scale thermokarst ponds are methane sources, but terrestrialization and colonisation by *Sphagnum* reduce their methane source strength (fig. 7.3b). Still, *Sphagnum* dominated sites remain a methane source compared to intact shrub dominated vegetation, especially if a fraction of the active layer remains water-saturated (fig. 7.3a). This suggests that thaw ponds may continue to contribute to methane emissions also after terrestrialization and initial permafrost recovery. To estimate the resulting net contribution of these thaw ponds to greenhouse gas emissions over their lifetime, monitoring of longer term successional dynamics and additional greenhouse gases is necessary (see paragraph 7.3.2 below).

7.3.2 Thermokarst dynamics and landscape evolution in the future Arctic

Thaw lakes and drained thaw lake basins cover approximately 20% of the Arctic permafrost region, and the area of drained thaw lake basins is increasing across the Arctic (Jones et al. 2022). This highlights the importance of understanding vegetation succession, permafrost aggradation and carbon cycle dynamics

in the context of drained thaw lake development (Jones et al. 2022). Drained thaw lakes generally progress through rapid establishment of graminoid vegetation and increases in productivity following drainage (Zona et al. 2010, Chen et al. 2021, Jones et al. 2022). Older drained thaw lake basins progress towards lower productivity species and increased differentiation in vegetation communities due to differential frost heave and secondary thermokarst (Zona et al. 2010, Morgenstern et al. 2013, Jones et al. 2022). Recent Holocene (5.7 ka BP to present) landscape dynamics in the Siberian Arctic have shown episodes of higher and lower thermokarst activity that preferentially take place in existing drained thaw lake basins (Morgenstern et al. 2013). In this context, observed increases in pond formation and other thermokarst activity and aquatic vegetation expansion (Chapters 2 & 3) may represent the onset of such a periodical increase in secondary thermokarst activity. Under ongoing climate warming however, developmental trajectories of drained thaw lake basins become increasingly uncertain (Jones et al. 2022). Continued monitoring of thermokarst, vegetation succession, greenhouse gas fluxes and permafrost aggradation across developmental stadia of these highly dynamic North-Eastern Siberian drained thaw lakes remains key to assess potential impacts of climate change and triggers or thresholds in ecosystem response.

Degradation and recovery dynamics of thermokarst features may be altered under progressive climate change. Estimates of degradation and recovery rates in various types of permafrost ecosystems are based on climatological conditions of the present or recent past. Permafrost aggradation or re-establishment of previously dominant vegetation types following thermokarst disturbance may be limited by changes in future climate, increased disturbance frequencies of large-scale changes in hydrological connectivity (Jorgenson et al. 2010, Baltzer et al. 2014, Turetsky et al. 2020, Heijmans et al. 2022, Jones et al. 2022). Emerging evidence points towards an important role for rainfall within this perspective. Rainfall extremes affect the permafrost thermal regime (Chapter 4) (Neumann et al. 2019, Douglas et al. 2020), and annual total rainfall is strongly associated with the permafrost thermal regime on a panarctic scale (Karjalainen et al. 2019). Vegetation dynamics (paragraph 7.1) and shrub recruitment rates (Li et al. 2016) also show sensitivity to summer rainfall, which may have implications for shrub recolonization of terrestrializing thermokarst features. Hence, future research should ideally address both the temperature and precipitation sensitivity of degradation and recovery rates of Arctic vegetation and permafrost and of key processes therein.

As of yet, it remains unclear whether the identified vegetation successional processes and permafrost degradation and aggradation would result in a full cyclical development towards the previously dominant shrub communities and permafrost status. With a limited timespan, my research has likely mostly identified relatively rapid successional processes and extended monitoring is necessary to better quantify slower successional processes related to potential recovery of shrub vegetation and aggradation of permafrost. Beside continued monitoring, high resolution historical imagery, ground ice stratigraphy and paleorecords (e.g. from peat cores) would aid characterization of timescales associated with full developmental trajectories of small scale thermokarst ponds. Studies of degradation-aggradation dynamics in ice wedge permafrost for instance has indicated that degradation-aggradation development may result in “quasi-cyclic” succession, due to structural alterations of ground ice relative to pre-thermokarst conditions (Jorgenson et al. 2015, Kanevskiy et al. 2017). Interestingly such developments may also affect the susceptibility of permafrost terrain to future thermokarst (Jorgenson et al. 2015, Kanevskiy et al. 2017). Future research in North-eastern Siberian lowland tundra ecosystems will be necessary to determine whether and on what timescales small-scale thaw ponds show quasi- or fully cyclical development, how this shapes their net contribution to the tundra carbon balance and how they will affect the landscape’s future susceptibility to thermokarst.

Based on similarity of observed degradation and recovery dynamics with processes reported in other (sub)Arctic ecosystems (Chapter 2) (Robinson and Moore 2000, Myers-Smith et al. 2008, Jorgenson et

al. 2015, Kanevskiy et al. 2017, Turetsky et al. 2020, Heijmans et al. 2022), it is plausible that observed small-scale dynamics of thermokarst degradation and vegetation-mediated recovery are representative for other rapidly warming ice-rich lowland tundra ecosystems (Turetsky et al. 2020, Heijmans et al. 2022). However, future research would have to indicate typical ranges of thermokarst activity across diverse landforms in the North-Eastern Siberian Lowland tundra and other Arctic regions in a warming climate. This thesis and several other studies have found that large scale detection of thermokarst from remotely sensed data requires images with a spatial resolution of at most several meters, but ideally sub-meter resolution (Chapter 6) (Grosse et al. 2008, Muster et al. 2013). Coarser resolution datasets (e.g. Landsat, 30m resolution) may only detect 1 to 13% of the total amount of water bodies in tundra wetland environments (Muster et al. 2013) and hence lead to substantial underestimation of small-scale hotspots of change and greenhouse gas emissions. Underdetection of these point disturbances is a key source of uncertainty and underestimation in the assessment of Arctic greenhouse gas emissions (Turetsky et al. 2019, Natali et al. 2021, Miner et al. 2022). Coordinated very high resolution change detection of cover of small scale water features across diverse Arctic ecosystems would help to establish a baseline of thermokarst activity and spatiotemporal dynamics of methane hotspots across the Arctic.

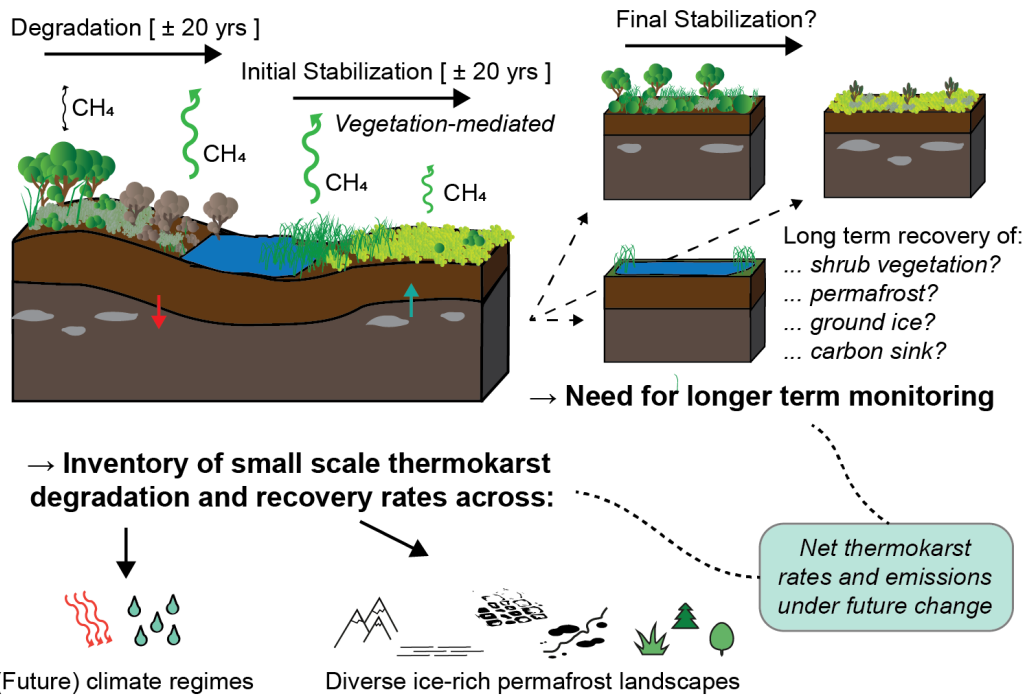


Figure 7.4) Graphical synthesis of the identified coupled dynamics of vegetation and permafrost in small thaw ponds and future research needs. Degradation, expansion and terrestrialization of small-scale thaw ponds was observed on decadal timescales, with a degree of recovery of permafrost and reduction of methane emissions upon transition to a peat moss dominated system. It is unclear however whether long-term recovery of shrub vegetation and permafrost may occur or whether alternative, non-cyclical trajectories may exist (e.g. renewed thaw lake formation, succession towards alternative vegetation). Additionally, reconfiguration of permafrost and ground ice may result in altered ecosystem properties and climate sensitivity. To inform assessments of the contribution of small-scale thermokarst phenomena to GHG emissions of permafrost ecosystems and panarctic permafrost degradation, it is crucial that future research quantifies the climate sensitivity of degradation and recovery processes in thermokarst development within various landscape contexts. Turetsky et al. (2020) provide a first benchmark for a model-based implementation of such an upscaling approach based on field data, but also stress the need to evaluate the sensitivity of thermokarst and recovery rates to future climate change.

7.4 Final Conclusions: Greening, browning, drying and drowning in the North-Eastern Siberian lowland tundra

Contrary to numerous reports of shrub expansion across Arctic tundra ecosystems, I found substantial decreases in shrub cover in a North-Eastern Siberian tundra site resulting from small-scale thermokarst and waterlogging and shifts to aquatic vegetation types. In a drained thaw lake basin, the area of small open water bodies doubled within a decade. Although vegetation succession enables rapid terrestrialization of ponds and initial decreases in methane emission and permafrost thaw depth, degradation rates outpace the long term recovery of shrub vegetation communities and permafrost, if this occurs at all. Future research will need to indicate how rates associated with degradation and recovery of thermokarst features may change in a rapidly warming Arctic, and whether particular landforms, vegetation types and regions may be more or less sensitive to potential increases in thermokarst.

I found that the response of permafrost and tundra vegetation to summer precipitation is sensitive to extremes and their timing. Extreme rainfall can enhance thaw depths of permafrost for multiple consecutive years and is likely further enhanced by simultaneous temperature peaks. Vegetation indices based on satellite images showed a pronouncedly positive association with rainfall during the relatively dry recent decades. The response of shrub growth to rainfall extremes mainly manifested as co-limitation of temperature responses by rainfall. Positive responses to high summer rainfall seemed to become more evident under increasing longer term moisture limitation. This indicates the need for better forecasting of precipitation extremes and dry periods to inform projections of future tundra productivity and permafrost thaw. Increased precipitation variability may additionally result in divergent responses across topographic gradients and increase spatio-temporal heterogeneity in future tundra greening.

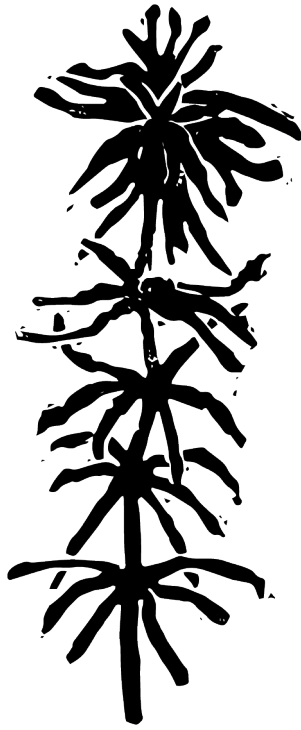
Hence, the next generation of experimental studies of effects of climate change on permafrost ecosystems should ideally go beyond gradual changes in single climatic or abiotic parameters, but address the role of extremes, combinations of multiple extremes and the role of recurrence dynamics. Tight coupling of vegetation and permafrost processes and the role of legacy effects indicates the need for long-term, holistic monitoring. Lastly, processes of permafrost degradation and vegetation shifts under climatic change should be understood within their landscape context to enable upscaling to a panarctic context.

A final recommendation stems from the detrimental impact of a global pandemic and a war on opportunities for field monitoring for this thesis and research in the Siberian Arctic in general. Due to restrictions on travel and collaboration after 2019, slower successional processes and duration of legacy effects of climatic extremes could not be quantified. This thesis is thereby likely biased towards rapid processes and direct impacts of climate extremes. Lack of knowledge of Russian ecosystems and their role in our climate will likely persist, and panarctic monitoring databases start showing gaps. The risks of such discontinuities should force researchers to improve local collaboration and contingency plans to safeguard long-term monitoring and encourage policymakers to think twice before imposing barriers to international scientific collaboration.



8.

Supplementary Material



Supplementary Data for

**Rapid Vegetation Succession and Coupled Permafrost Dynamics in Arctic Thaw
Ponds in the Siberian Lowland Tundra**

Rúna Í. Magnússon, Juul Limpens, Ko van Huissteden, David Kleijn, Trofim C. Maximov,
Ronny Rotbarth, Ute Sass-Klaassen, Monique M. P. D. Heijmans

Published in Journal of Geophysical Research: Biogeosciences, 125, e2019JG005618 (2020).

All Supplementary Materials belonging to this chapter can be found in the published version:

DOI: <https://doi.org/10.1029/2019JG005618>



Supplementary Data for

Shrub decline and expansion of wetland vegetation revealed by very high resolution land cover change detection in the Siberian lowland tundra

Rúna Í. Magnússon, Juul Limpens, David Kleijn, Ko van Huissteden, Trofim C. Maximov, Sylvain Lobry, Monique M. P. D. Heijmans

Published in Science of the Total Environment, 782, 146877 (2022).

All Supplementary Materials belonging to this chapter can be found in the published version:

DOI: <https://doi.org/10.1016/j.scitotenv.2021.146877>



Video S3.1 can be found on Youtube

Link: https://youtu.be/O_8u6lMx5B0



Supplementary Data for

**Extremely wet summer events enhance permafrost thaw for multiple years
in Siberian tundra**

Rúna Í. Magnússon, Alexandra Hamm, Sergey V. Karsanaev, Juul Limpens, David Kleijn,
Andrew Frampton, Trofim C. Maximov and Monique M. P. D. Heijmans

Published in Nature Communications, 13, 1556 (2022).

All Supplementary Materials belonging to this chapter can be found in the published version:

DOI: <https://doi.org/10.1038/s41467-022-29248-x>



Supplementary Data for

**Precipitation variability differentially affects growth and temperature response of
Betula nana across topographical gradients in a Siberian lowland tundra site**

Rúna Í. Magnússon, Ute Sass-Klaassen, Juul Limpens, Sergey V. Karsanaev, Susan Ras, Ko
van Huissteden, Daan Blok, Monique M.P.D. Heijmans

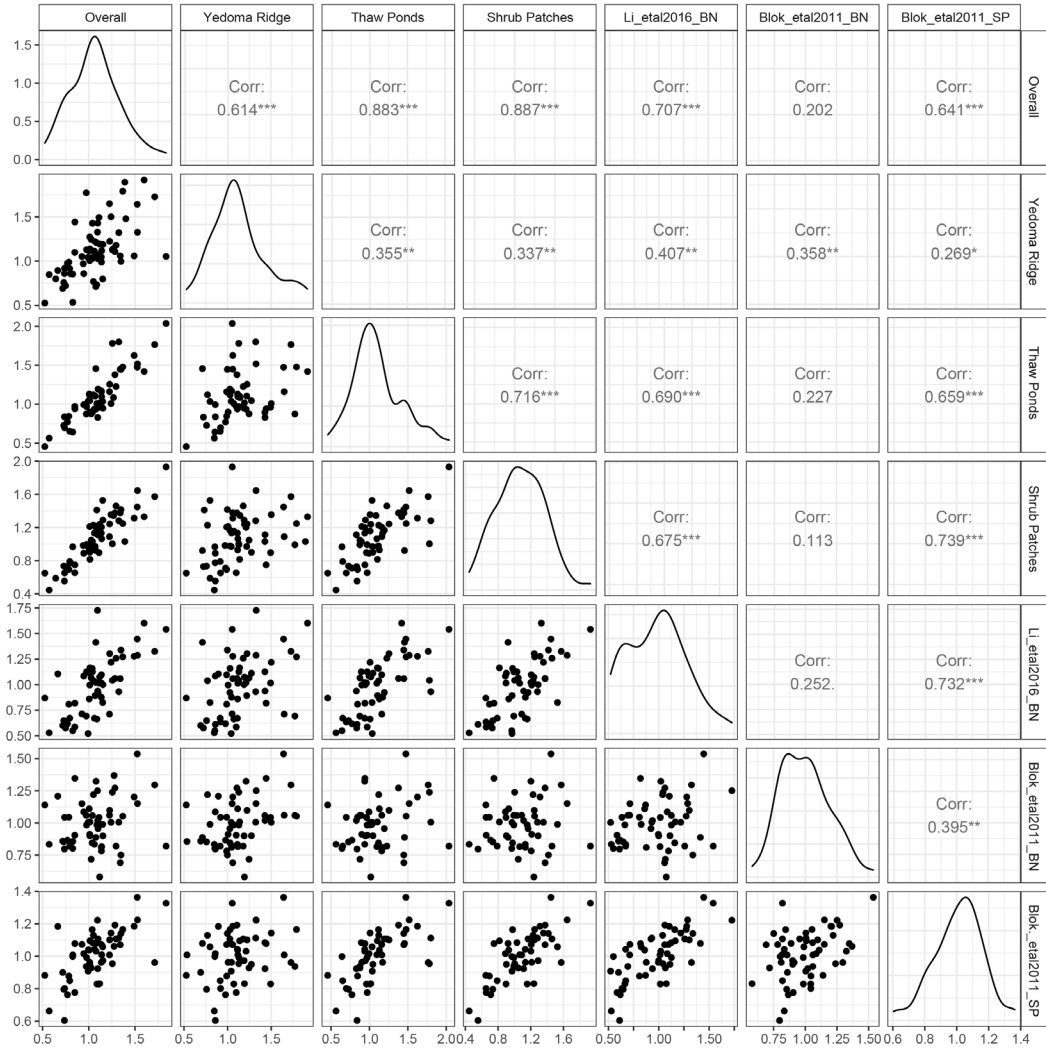


Figure S5.1) Comparison of chronologies of this study (Overall chronology and subsites) with earlier chronologies developed for *Betula nana* (BN) in this study site (Blok et al. 2011b, Li et al. 2016) and a *Salix pulchra* (SP) chronology (Blok et al. 2011b). Li et al. (2016) only sampled from shrub patches and shallow thermokarst depressions within shrub patches. Blok et al. (2011b) sampled from shrub patches, Yedoma ridge and other geomorphological units. This study used a residual chronology after C-method detrending and correction for first-order autocorrelation. Li et al. (2016) and Blok et al. (2011b) used a residual chronology after detrending with a negative exponential and correcting for first-order autocorrelation. The chronologies used for this study were crossdated independently from the chronologies by Li et al. (2016) and Blok et al. (2011b), but the Ridge chronology included two samples from Blok et al. (2011b).

*** = $p < 0.001$, ** = $p < 0.01$, * = $p < 0.05$, . = $p < 0.1$

Text S5.1. Ring width measurement

Text S5.1.1 Serial sectioning

Since dwarf shrubs display (partially) missing rings, crossdating ring width measurements can be challenging (Kolischuk 1990, Myers-Smith et al. 2015b). We therefore adopted a serial sectioning approach, in which multiple stem sections of the same shrub are sampled, and ring widths are measured across multiple radii per section. Ring width curves are first compared among radii and then among sections, to ensure that no (partially) missing rings have been overlooked (Gärtner et al. 2014). Serial sectioning thereby reduces loss of samples or confounding effects due to missing rings (Hallinger et al. 2010, Wilmking et al. 2012, Myers-Smith et al. 2015a, Myers-Smith et al. 2015b). Serial sectioning also ensures that as many rings as possible are included in each individual, especially if the root collar can be identified and sampled (Myers-Smith et al. 2015b).

Text S5.1.2 Sample preparation

From each section, a cross-section of 20 to 30 μm thickness was cut in radial direction on a GSL1 sledge microtome (WSL, Birmensdorf, Switzerland). These cross-sections were stained using a safranin/astra blue mixture (Gärtner and Schweingruber 2013) for 15 minutes and then rinsed using demi water and ethanol solutions of increasing purity (50, 70, 96 and 100%). Samples were washed with Roti®-Clear liquid and finally embedded in Roti®-Mount resin on a glass slide. We made overlapping images of 300 dpi of each section using a Leica DFC320 camera mounted on a Leica DM2500 microscope set at varying magnification (usually 50x, sometimes smaller or larger depending on the sample's average ring width (all Leica Microsystems, Wetzlar, Germany). Images were stitched together to create high resolution images per section in PTGui v. 2.9.1 (New House Internet Services, Rotterdam, The Netherlands).

Text S5.1.3 Crossdating and Chronology Development

Ring width measurements were crossdated hierarchically following Hallinger et al. (2010). Ring widths were measured manually on each section image along two to four (usually three) radii in Coorecorder v. 9.0 (Cybis 2019b). All ring width measurements of radii within a section (in .pos format) were inspected visually, corrected for missing rings, averaged in CDendro v. 9. (Cybis 2019a) and saved in Heidelberg format (.fh). We then visually crossdated section ring width curves in WinTSAP v. 4.70d (Rinntech 2017), starting with sections within a shrub, and then visually crossdating measurements among different shrubs. Missing rings were inserted manually in skeleton plots, only if this hugely improved visual fit and if the stitched images showed indications that a missing ring might be present (e.g. a sequence of very unclear and small rings).

Ring widths were exported to .rwl format, read into R using the dplR package (Bunn 2008) and detrended using C-method detrending (Biondi and Qeadan 2008). We first selected all detrended sections within a shrub and averaged measurements to single shrub averages if the sections within a shrub showed significant correlation ($p < 0.05$). Sections with insignificant correlation among sections that could not be resolved during crossdating were omitted. Shrub averages were then subjected to statistical crossdating evaluation based on correlation of shrub-averaged detrended ring widths with average detrended ring widths of all other shrubs. If this resulted in a significant correlation ($p < 0.05$), the shrub ring width series was kept. If not, it was omitted from chronology development and climate-growth analysis. Finally, a chronology for the dataset was developed by averaging the residuals of first-order autocorrelation model fit per shrub (residual chronology), resulting in a dimensionless ring width index (RWI). We excluded the first 5 years of shrub growth per section since juvenile growth tends to be highly irregular. Chronology values of years with a sample depth of less than 4 were omitted from further analysis. In addition to chronologies, we calculated individual shrubs' ring width indices (RWI's) as the residuals of a first-order temporal autocorrelation model applied to individual shrubs' detrended ring width values. Our workflow is summarized in figure S5.2.

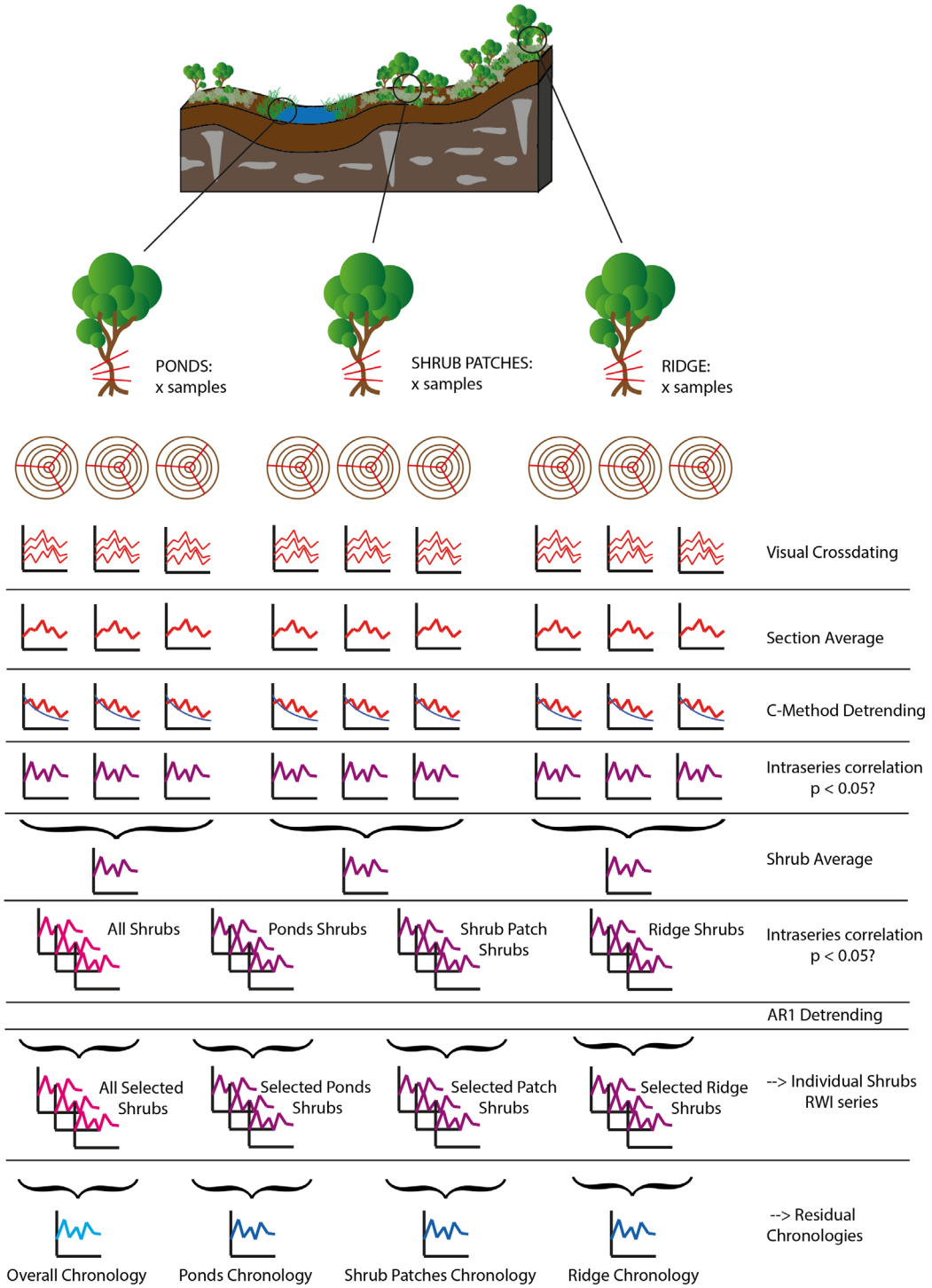


Figure S5.2) Visual summary of dendrochronological data analysis.

Text S5.2. Sentinel Data Processing

For selected, cloud-free Sentinel-2 surface reflectance (2019-2020) and top-of-atmosphere reflectance (2016-2018) scenes, we calculated NDVI and pixel snow probability using the snow detection and NDVI algorithm used for Sentinel-2 Level-2A processing (Main-Knorn et al. 2017) (see also <https://sentinel.esa.int/web/sentinel/home>). The following algorithms were applied to each pixel:

Text S5.2.1. NDVI

Normalized Difference Vegetation Index (NDVI) = (Band 8 - Band 4) / (Band 8 + Band 4)

Text S5.2.2. Pixel Snow Probability

Normalized Difference Vegetation Index (NDVI) = (Band 3 - Band 11) / (Band 3 + Band 11)

1. NDSI < 0.20 → snow probability = 0
 NDSI > 0.42 → snow probability = 1
 0.20 < NDSI < 0.42 → 0 < snow probability < 1 (linear interpolation)
 → Pass to step 2
2. Band 8 < 0.15 → snow probability = 0
 Band 8 > 0.35 → snow probability = 1
 0.15 < Band 8 < 0.35 → 0 < snow probability < 1 (linear interpolation)
 → Multiply outcome step 1 with outcome step 2, pass to step 3
3. Band 2 < 0.18 → snow probability = 0
 Band 2 > 0.22 → snow probability = 1
 0.18 < Band 2 < 0.22 → 0 < snow probability < 1 (linear interpolation)
 → Multiply outcome step 2 with outcome step 3, pass to step 4
4. Band 2/Band 4 < 0.85 → snow probability = 0
 Band 2/Band 4 > 0.95 → snow probability = 1
 0.85 < Band 2/Band 4 < 0.95 → 0 < snow probability < 1 (linear interpolation)
 → Multiply outcome step 3 with outcome step 4

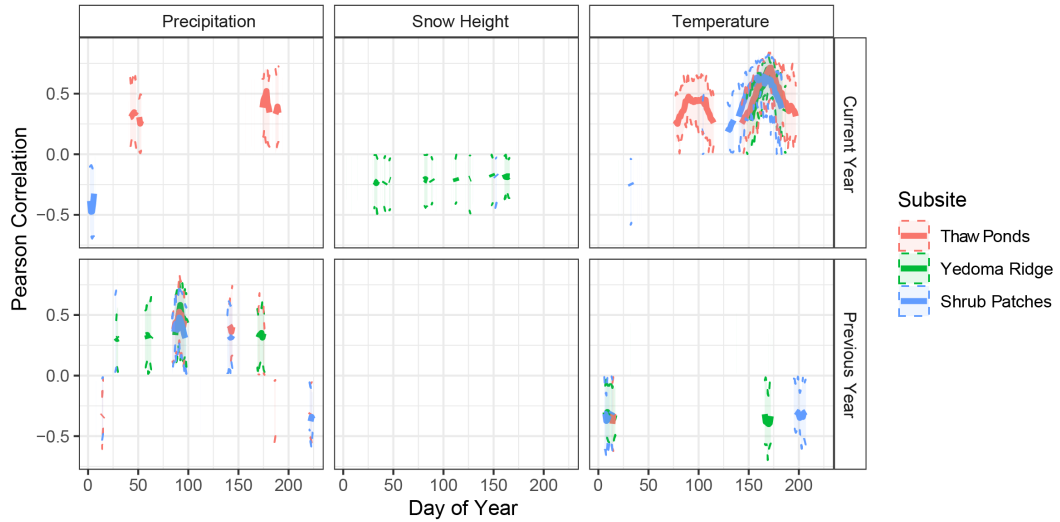


Figure S5.3) Results of moving window analysis of climate sensitive periods for growth of *Betula nana*. Growth correlated most strongly with temperatures in June and July. Shrubs in ponds showed positive correlation for earlier season temperatures (March, April), and all chronologies showed sensitivity for temperatures of the preceding year. For precipitation, growth correlated with summer precipitation for shrubs from Thaw Ponds only. Correlation with previous year's precipitation was found, with variable timing for the different subsite chronologies. For snow height, growth showed correlation throughout the year for Yedoma Ridge sites.



Figure S5.4) Diameter – age plots for individual shrub's rings across the three types of subsites.

Supplementary Material

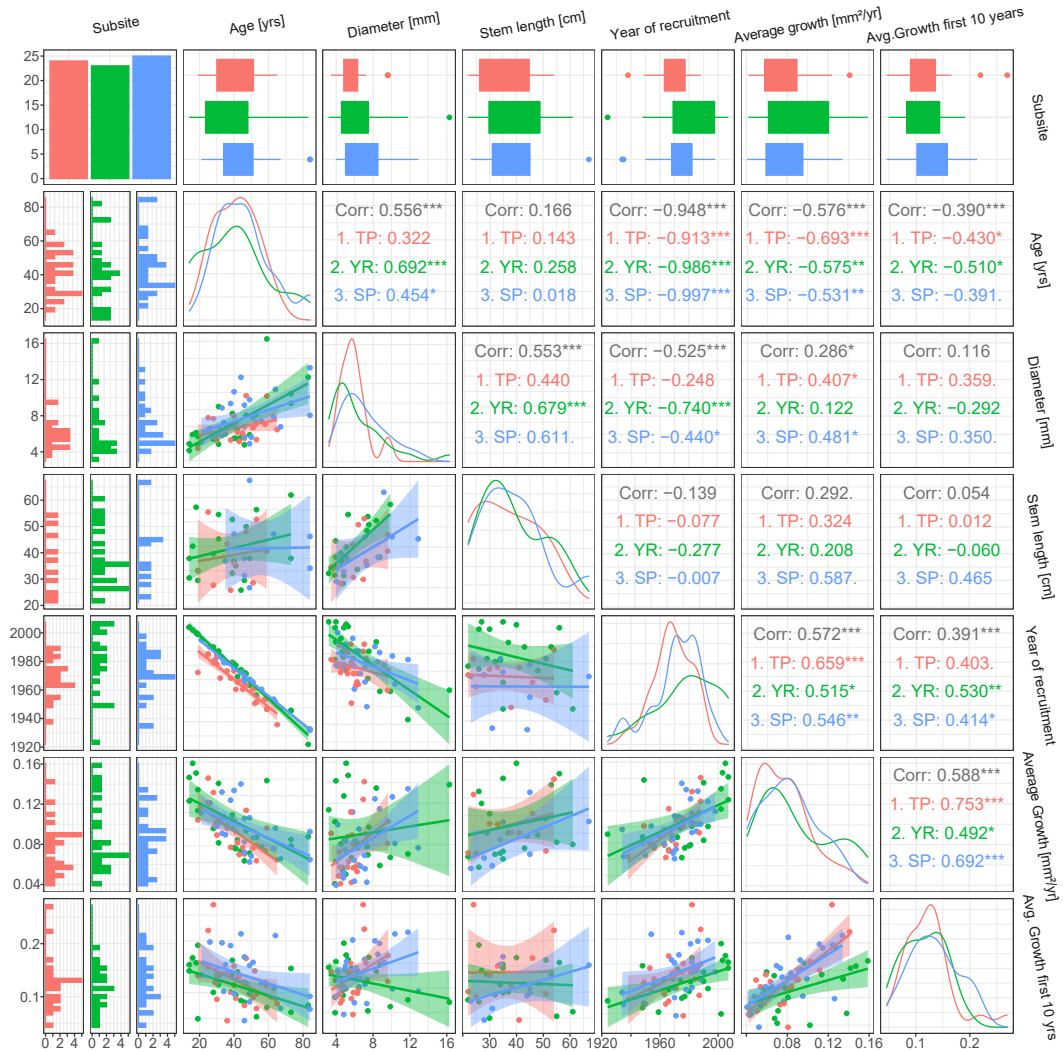
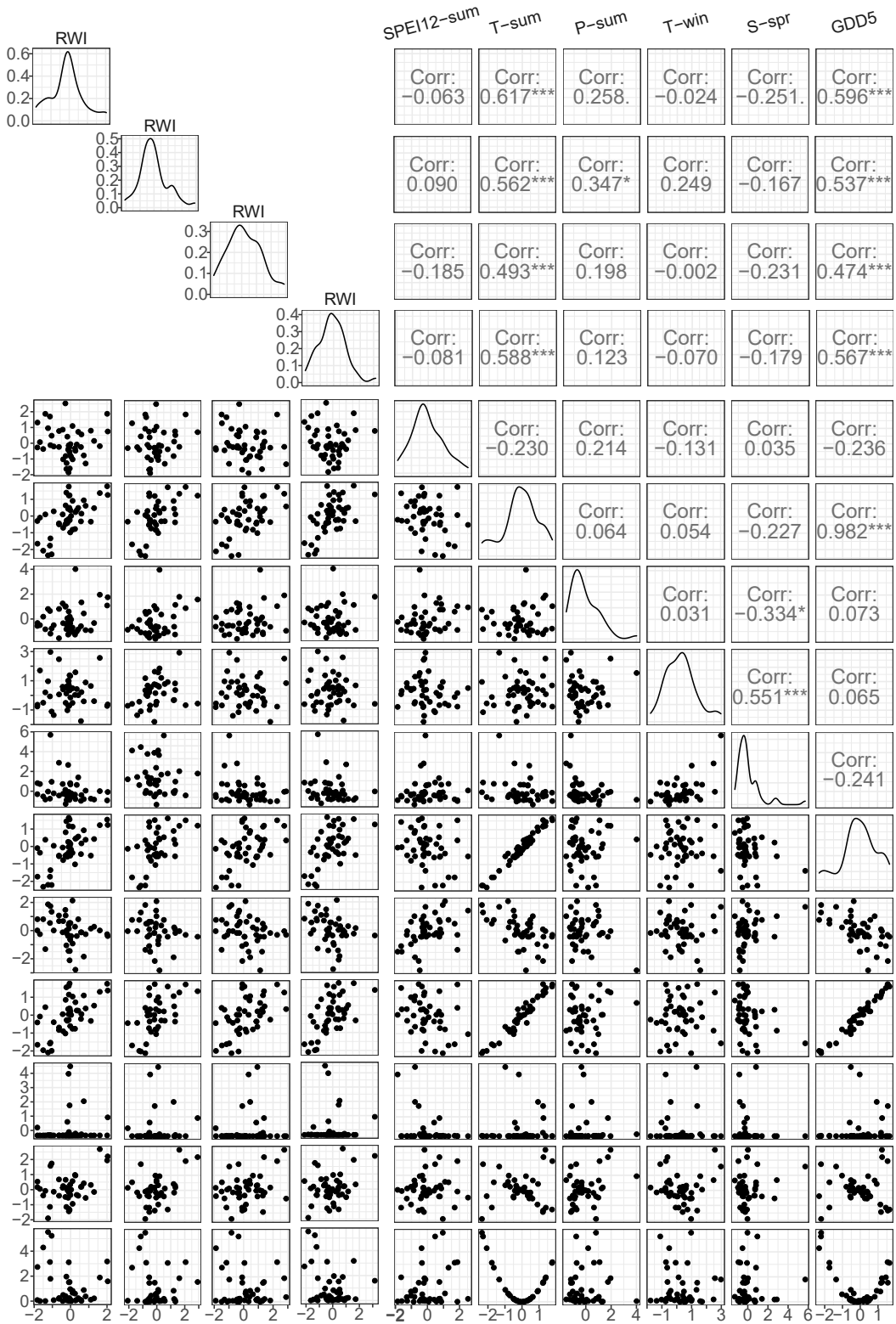


Figure S5.5) Growth properties of individual shrubs, coloured by subsite type (TP = Thaw Ponds, YR = Yedoma Ridga, SP = Shrub Patches). Age = age of a shrubs (number of rings). Diameter = diameter of wood tissue of the shrub (excl. the pith, which is of negligible size). Stem length is the length of the longest branch to the moss surface for the sampled individual. Year of recruitment is the year to which the first ring was crossdated. Average growth is mean basal area increment (mm² yr⁻¹). Avg. Growth First 10 yrs mean basal area increment (mm² yr⁻¹) during the first 10 years of growth. Shrubs show similar ranges and dynamics across subsites, although ridge shrubs seem to have lower start growth (Average Growth first 10 years) compared to the same eventual size and mean BAI over their lifetime. Reported correlations are Pearson's R.

*** = $p < 0.001$, ** = $p < 0.01$, * = $p < 0.05$, . = $p < 0.1$



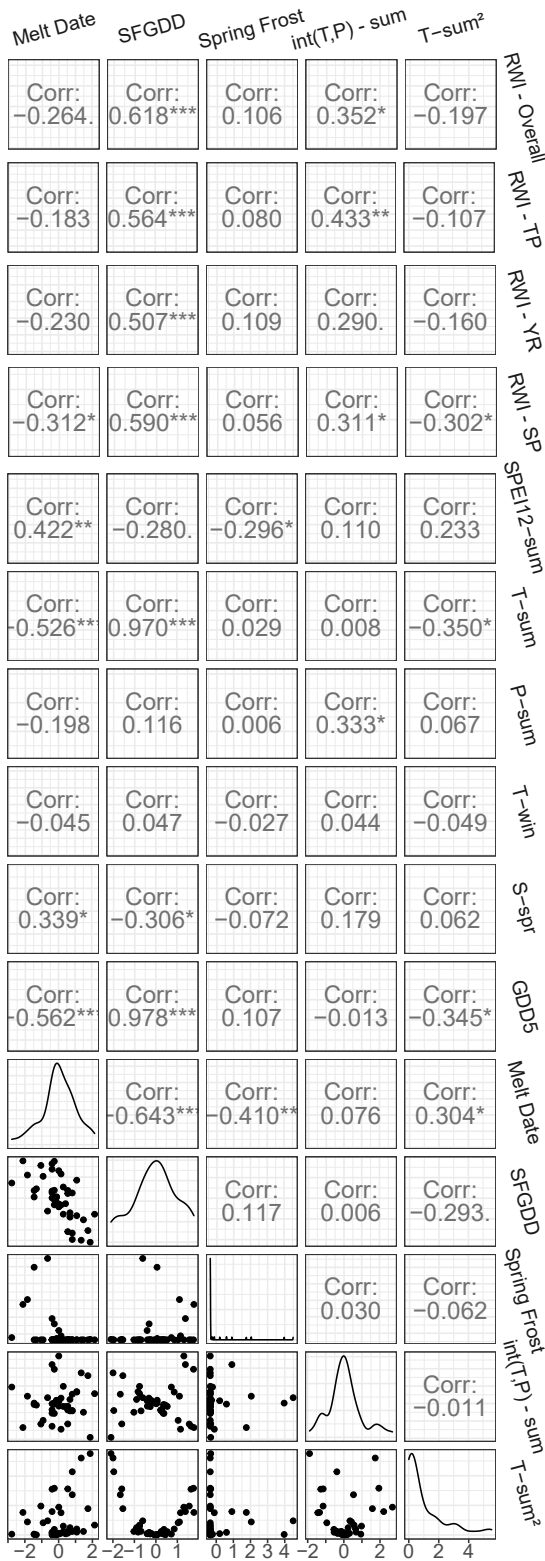


Figure S5.6 (both pages). Correlation matrices of RWI chronologies (Overall, Ridge, Ponds and Shrub patches) and standardized, preselected (table 5.2 in main text) climate variables. Reported correlations are Pearson correlation coefficients. *** = $p < 0.001$, ** = $p < 0.01$, * = $p < 0.05$, . = $p < 0.1$

Table S5.1. OPLS model fits

Chronology	Obs	Vars	Pred	Orth	R ² X	R ² Y	Q ²	pR ² Y	pQ ²	RMSEE
Full Chronology OPLS models										
Overall	45	14	1	3	0.520	0.986	0.972	0.01	0.01	0.034
Yedomia Ridge	45	14	1	3	0.513	0.992	0.982	0.01	0.01	0.031
Thaw Ponds	40	14	1	3	0.460	0.989	0.968	0.01	0.01	0.033
Shrub Patches	45	14	1	3	0.514	0.991	0.977	0.01	0.01	0.030
Moving Window OPLS models										
1974-2003 YR	30	14	1	3	0.517	0.993	0.951	0.01	0.01	0.028
1974-2003 TP	30	14	1	2	0.430	0.981	0.838	0.01	0.01	0.047
1974-2003 SP	30	14	1	3	0.516	0.990	0.948	0.01	0.01	0.036
1979-2008 YR	30	14	1	2	0.363	0.991	0.931	0.01	0.01	0.030
1979-2008 TP	30	14	1	2	0.325	0.987	0.900	0.01	0.01	0.031
1979-2008 SP	30	14	1	3	0.492	0.990	0.938	0.01	0.01	0.027
1984-2013 YR	30	14	1	2	0.316	0.988	0.921	0.01	0.01	0.039
1984-2013 TP	30	14	1	3	0.447	0.988	0.941	0.01	0.01	0.032
1984-2013 SP	30	14	1	2	0.356	0.983	0.917	0.01	0.01	0.035
1989-2018 YR	30	14	1	3	0.505	0.992	0.962	0.01	0.01	0.035
1989-2018 SP	30	14	1	3	0.475	0.993	0.973	0.01	0.01	0.023

Obs: number of observations (in this case, years), Vars: number of X variables, Pred: number of predictive components (always 1 for OPLS), Orth: number of orthogonal components, R²X: sum of squares for variation in the X matrix (cumulative), R²Y: sum of squares for variation in Y (cumulative), Q²: fraction of total variation in Y that can be explained by X (cumulative), pR²Y: significance of R²Y based on permutation testing, pQ²: significance of Q² based on permutation testing, RMSEE: square root of the mean error between the actual and the predicted responses (internal 7-fold cross-validation)

Supplementary Material

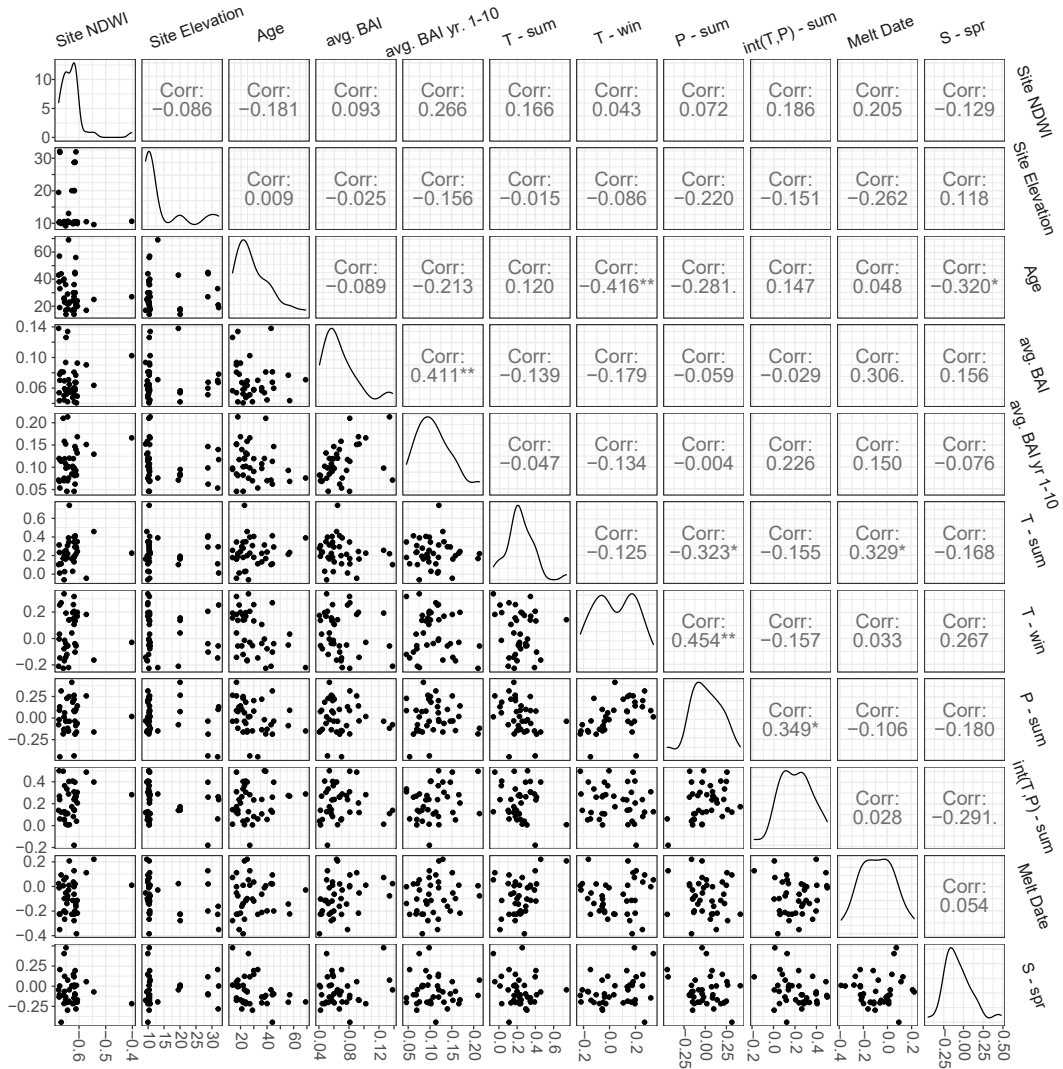


Figure S5.7) Correlation of individual shrub's estimated OPLS regression coefficients for summer temperature (T - sum), summer precipitation (P - sum), interaction between summer temperature and precipitation (int(T,P) - sum), winter temperature (T - win) and snow height in spring (S - spr), shrub characteristics (mean age during the common time interval, mean BAI and mean BAI for the first 10 years of growth) and abiotic site conditions (Mean WorldView-2 NDWI, ArcticDEM elevation). OPLS estimated coefficients were computed over a common time period (1980-2005) for all shrubs.

*** = $p < 0.001$, ** = $p < 0.01$, * = $p < 0.05$, . = $p < 0.1$

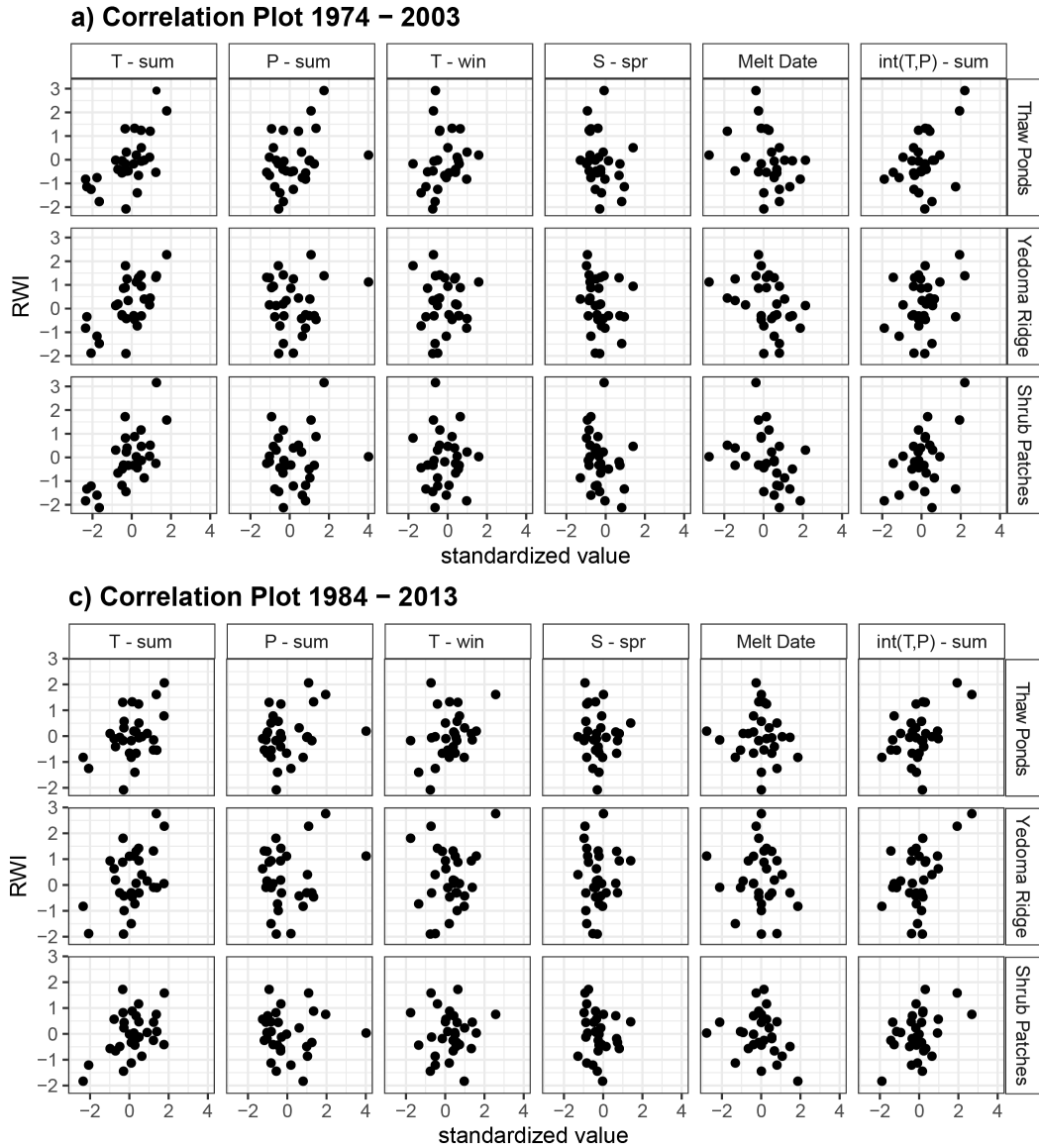
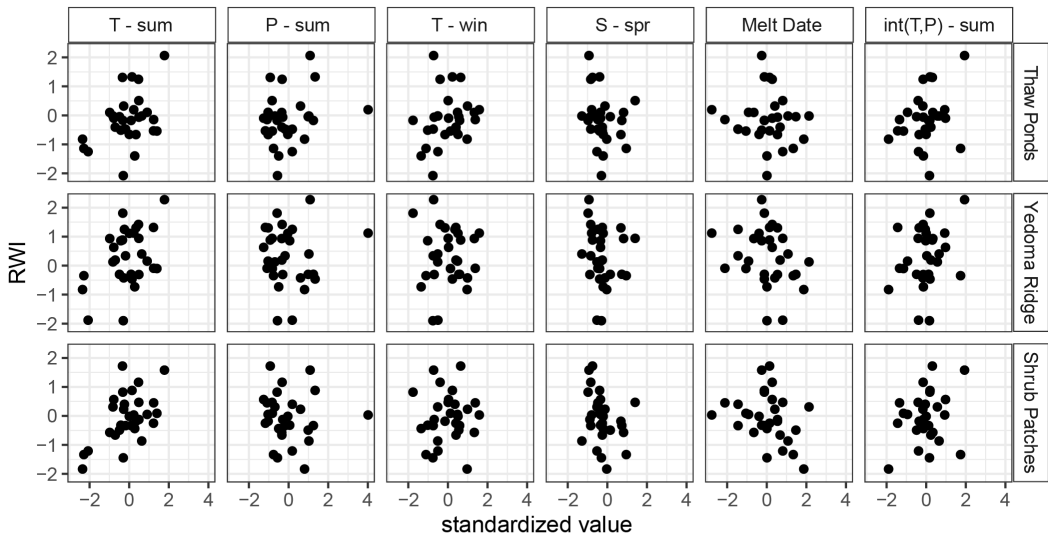


Figure S5.8 (both pages). Moving window scatter plots for the three subsite chronologies and main climate factors. X-axis contain standardized values for climate variables (over the whole time period 1974–2018), Y-axis shows C-method detrended RWI values with first-order temporal autocorrelation removed. a) Period 1974 – 2003, b) period 1979–2008, c) period 1984 – 2013, d) period 1989–2018. Note that due to absence of chronology values for shrubs from Thaw Ponds, the correlations for Thaw Ponds RWI in panel d is based on fewer years and largely the same as in c.

b) Correlation Plot 1979 – 2008



d) Correlation Plot 1989 – 2018

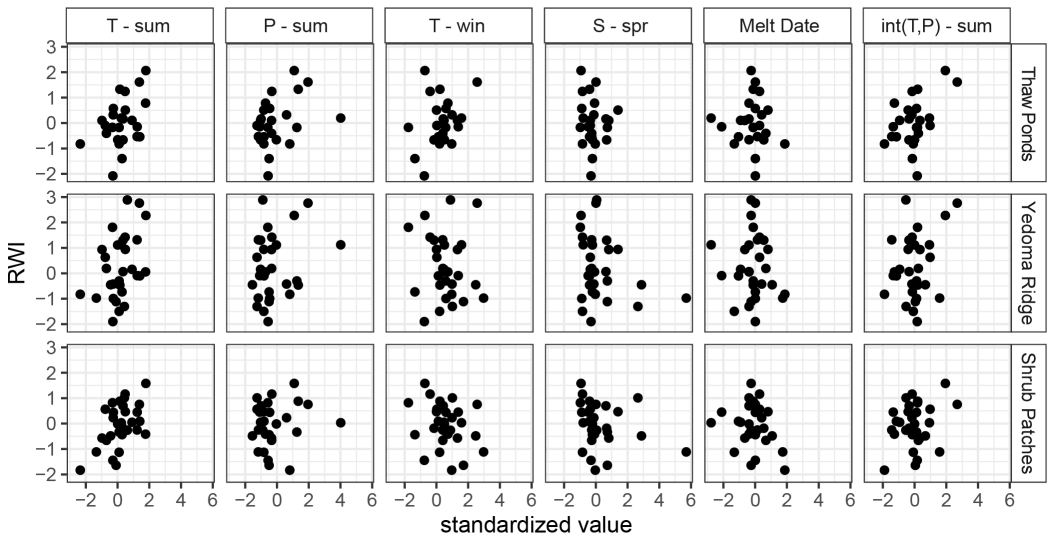


Table S5.3. Climate Extremes Analysis

Extreme	Year	z-score ¹	RWI ²			Remark
			TP ³	SP	YR	
Low Summer Temperature	1996	-2.27	0.86	0.56*	0.86	also late snowmelt
	1979	-2.21	0.76*	0.71*	1	also low winter temperature
	1984	-2	0.73*	0.74*	0.54*	
High Summer Temperature	1991	1.8	1.72**	1.58*	1.78**	also low snow cover and high int(T,P)
	2010	1.78	1.34	0.98	1.12	
	2005	1.42	0.94	1.13	1.07	
High Summer Precipitation	1990	3.81	1.16	1.11	1.44*	also early snowmelt
	2011	1.9	1.59*	1.33	1.93**	also warm winter and high int(T,P)
	1974	1.71	1.98**	2.05**	1.52*	also high int(T,P)
Low Summer Precipitation	2018	-1.34		0.96	0.97	also high snow height and high winter temperature
	2004	-1.08	1.08	1.27	1.29	
	2016	-1.07		1.41*	0.72*	also high snow height
High Winter Temperature	2017	2.66		0.77*	0.81	also high snow height, late snowmelt
	2011	2.26	1.59*	1.33	1.93**	also high summer precipitation and high int(T,P)
	2018	2.17		0.96	0.97	also low summer precipitation and high snow height
Low Winter Temperature	1999	-2	1.05	1.35	1.64*	also low snow height
	1998	-1.6	0.69*	0.97	0.89	
	1979	-1.36	0.76*	0.71*	1	also low summer temperature
Late Snowmelt	1982	2.07	1.1	1.2	1.14	
	1996	1.81	0.86	0.56*	0.86	also low summer temperature
	2017	1.68		0.77*	0.81	also high snow height and high winter temperature
Early Snowmelt	1990	-2.72	1.16	1.11	1.44*	also high summer precipitation
	2007	-2.07	1.06	1.24	1.08	
	1977	-1.81	1.46*	1.26	1.24	
High Spring Snow	2017	4.63		0.77*	0.81	also late snowmelt and high winter temperature
	2018	2.32		0.96	0.97	also low summer precipitation and high winter temperature
	2016	2.14		1.41*	0.72*	also low summer precipitation
Low Spring Snow	1988	-1.09	1.1	0.85	1.22	
	1999	-0.83	1.05	1.35	1.64*	also low winter temperature
	1991	-0.79	1.72**	1.58*	1.78**	also high summer temperature and high int(T,P)

High Interaction Summer Temp.& Precipitation ⁴	2011	2.65	1.59*	1.33	1.93**	also high summer precipitation and high winter temperature
	1974	2.2	1.98**	2.05**	1.52*	also high summer precipitation
	1991	1.97	1.72**	1.58*	1.78**	also high summer temperature and low snow height

- 1) Standardized value of the climate variable considered for this extreme year
- 2) RWI for the three subsites (TP = thaw ponds, YR = yedoma ridge and SP = shrub patches). Colours and stars indicate significantly positive or negative RWI based standard deviations following Neuwirth et al. (2007), where * indicates RWI's at least one to two standard deviations higher (light green) or lower (light red) than the mean RWI over the study period (1959-2018), and ** indicates RWI's at least two standard deviations higher (green) or lower (red).
- 3) Due to the fact that most shrubs in ponds were dead and did not show rings in recent years (fig. 5.5 in main text), RWI values for ponds in most recent years are not reported.
- 4) Only those years in which both summer temperature and precipitation were high were included here (years during which both are very low also result in a high interaction but were not considered here)

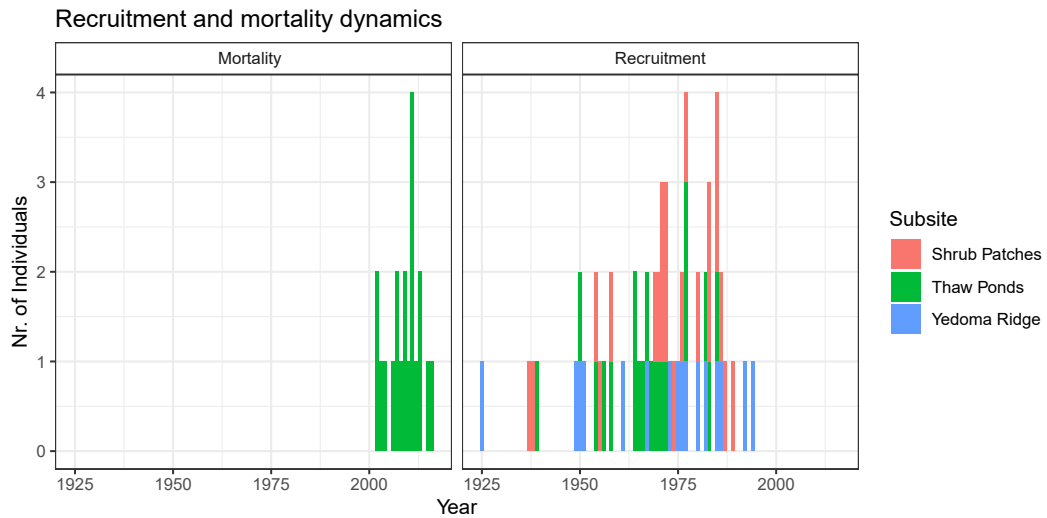


Figure S5.9) Stacked bar graph of recruitment and mortality dynamics of selected shrubs. a) shows the year of the first identified ring (in either of the three sections) for shrubs from the three subsites. b) Shows the final year of growth for shrubs sampled from thaw ponds.

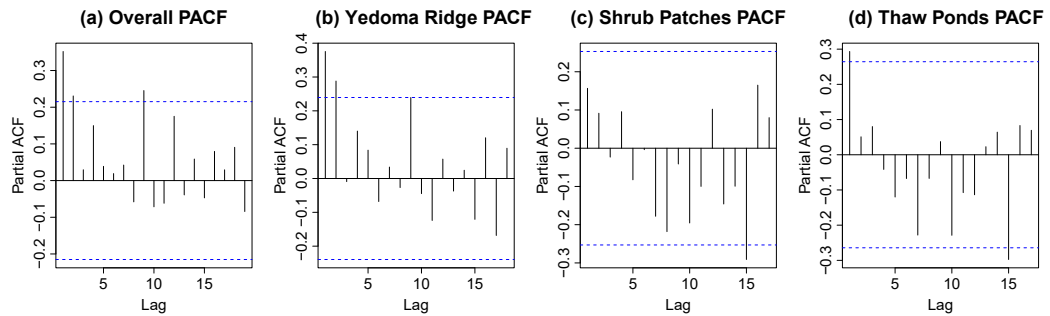


Figure S5.10) Autoregressive dynamics of overall and subsite chronologies. Blue dotted line indicates a 95% confidence interval. a) Partial Autocorrelation plot for Overall chronology. b) Partial Autocorrelation plot for Yedoma Ridge chronology. c) Partial Autocorrelation plot for Shrub Patches chronology. d) Partial Autocorrelation plot for Thaw Ponds chronology.

Supplementary Data for

**Tundra browning in the Indigirka Lowlands (North-eastern Siberia) explained by
drought, floods and small-scale vegetation shifts**

Rúna Í. Magnússon, Finn Groten, Harm Bartholomeus, Ko van Huissteden, Monique M. P.
D. Heijmans

Table S6.1. Satellite data specifications

	2010 Image	2015 Image	2019 Image
Satellite	GeoEye-1	WorldView-2	WorldView-2
Year	2010	2015	2019
Bands MSI	Blue 450-510nm Green 510-580nm Red 655-690nm NIR 780-920nm	Blue 442-515nm Green 506-586nm Red 624-694nm NIR 765-920nm	Blue 442-515nm Green 506-586nm Red 624-694nm NIR 765-920nm
Pixel Size	MSI 2.0m PAN 0.5m	MSI 2.0m PAN 0.5m	MSI 2.0m PAN 0.5m
Acquisition Date & Time (GMT)	2010-08-19 02:45	2015-07-10 2:47	2019-08-01 02:22
Local time (GMT + 11)	13:45	13:47	13:22
Dynamic range	11 bits	11 bits	11 bits
Sun Elevation	31.8°	41.3°	37.4°
Scan Direction	Reverse	Forward	Forward
Collection Elevation	61.4°	72.9°	86.6°
Collection Azimuth	340.2°	322.5°	185.9°
Sun Azimuth	189.1°	198.9°	181.9°
Bounding box (WGS84)	Northwest corner: 70.8806N, 147.3625E Southeast corner: 70.7875N, 147.6350E		

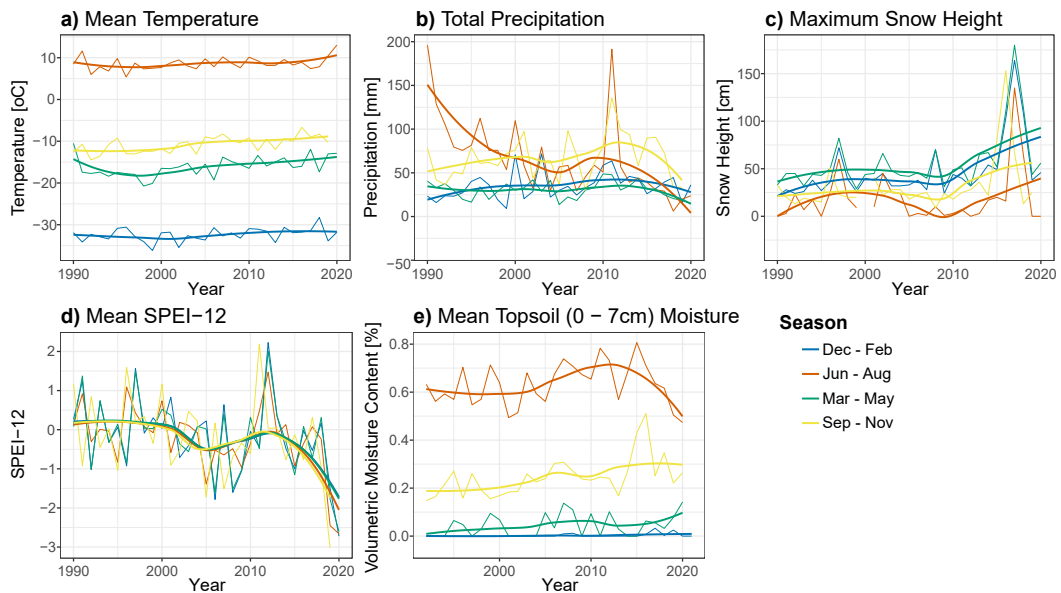


Figure S6.1) Annual weather data for the study site for 1990 – 2020 for the winter (December – February), spring (March – May), summer (June – August) and autumn (September – November) months with LOESS fits. Data for December-February uses data from December of the previous year. (a) Mean Temperature. (b) Total Precipitation. (c) Maximum Snow Height. (d) Mean SPEI-12 (12-moth Standardized Precipitation Evapotranspiration Index). (e) Mean Volumetric Topsoil Moisture. (a-c) are derived from meteorological data from the Chokurdakh Meteorological Station, WMO station code: 21946. (d) is calculated from precipitation and Hargreaves potential evapotranspiration after Vicente-Serrano et al. (2010). (e) is retrieved from EUMETSAT scatterometer data (HSAF 2020).

Table S6.2. Climate data for the studied period

Year	Summer Temp.* [oC]	Winter Temp.** [oC]	Summer Prec.* [mm]	Max. Winter Snow Height** [cm]	12-month*** SPEI [-]	Soil Moisture* [%]
1999	7.64	-28.70	36	29	-0.11	0.72
2000	8.15	-25.48	97	44	0.58	0.66
2001	10.26	-25.16	16.5	-	-0.09	0.48
2002	9.31	-26.30	21	66	0.05	0.56
2003	8.30	-24.42	73.4	34	-0.02	0.74
2004	6.64	-25.77	16.5	42	-0.18	0.56
2005	10.40	-26.12	36.5	42	-1.31	0.52
2006	8.19	-24.88	52.8	46	-0.64	0.68
2007	10.10	-23.92	20.9	40	-0.37	0.73
2008	6.79	-23.92	43	70	-0.56	0.75
2009	7.78	-24.56	41.8	31	-0.99	0.67
2010	10.56	-24.57	35.4	49	-0.19	0.64
2011	10.43	-22.08	144.5	47	-0.06	0.78
2012	8.37	-25.52	46.4	32	1.71	0.76
2013	8.64	-24.85	22.2	65	0.03	0.59
2014	9.01	-23.52	38.1	67	0.16	0.68
2015	8.90	-24.14	28.1	52	-1.01	0.80
2016	9.16	-24.62	15.1	110	-0.25	0.71
2017	6.33	-20.91	18.8	180	-0.01	0.60
2018	7.48	-22.51	4.7	115	-0.10	0.63
2019	10.24	-23.53	15.1	44	-2.31	0.54

*) Over the period of June 1st – August 5th

**) Over the period of October 1st to April 31st

***) Over the period June-July

Supplementary Material

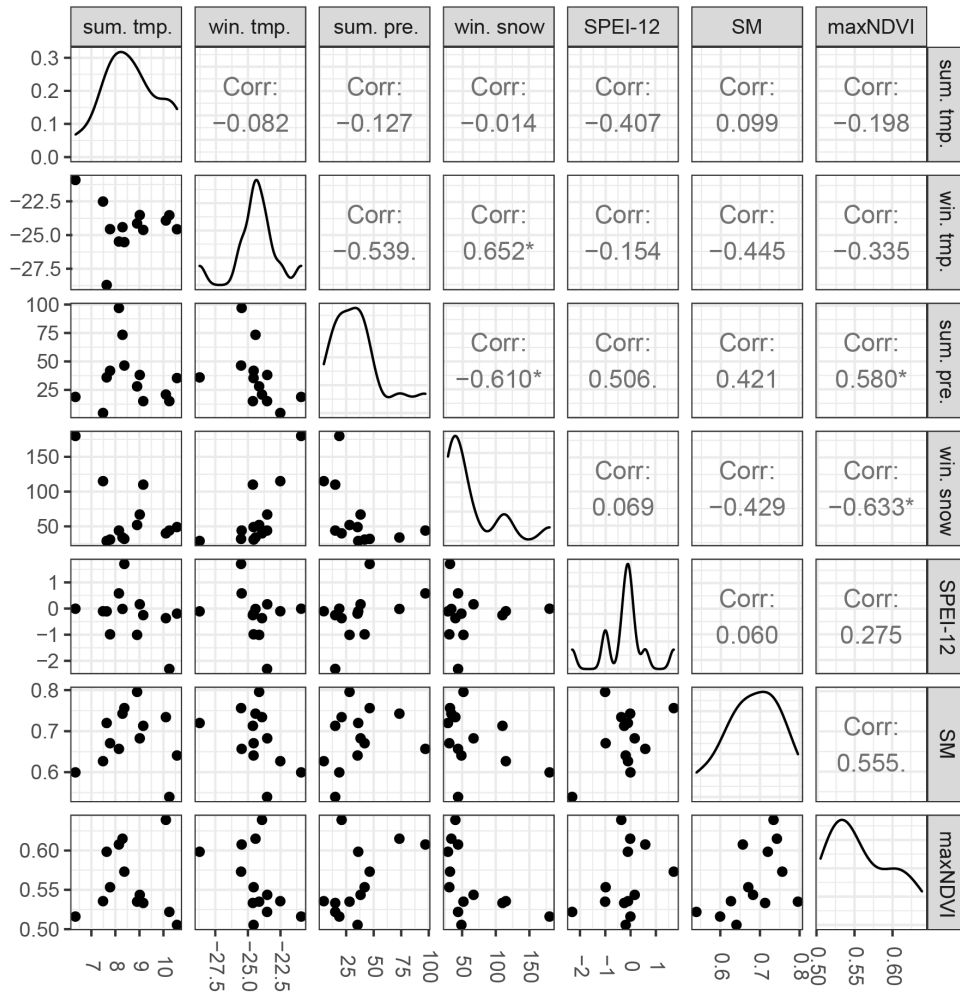
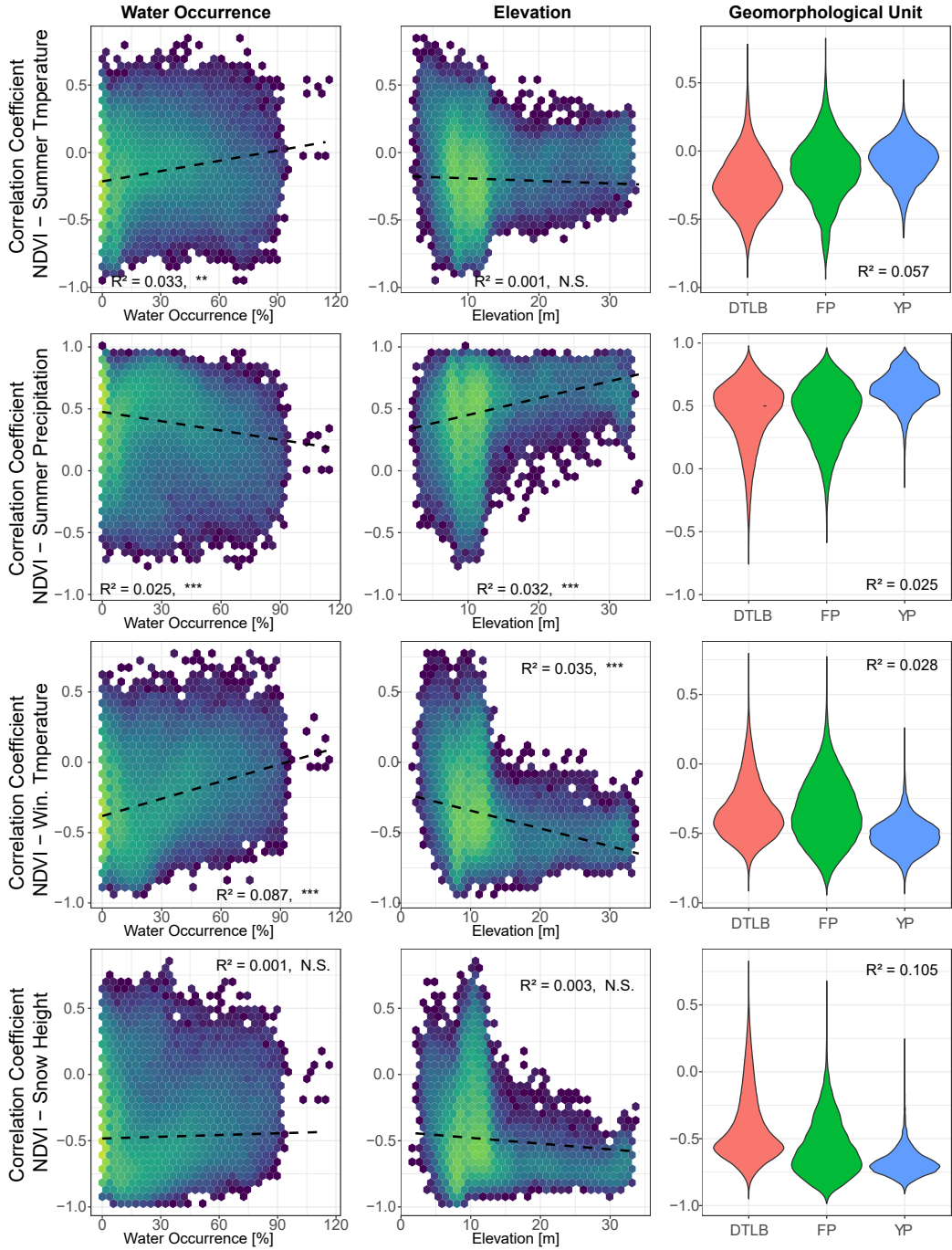


Figure S6.2) Spearman correlation coefficients (“Corr.”) and p-values between mean area annual maxNDVI and annual weather variables (n = 13). sum. tmp = summer temperature, sum. pre = summer precipitation, win. tmp = winter temperature, win. snow = maximum winter snow height, SPEI-12 is mean June-July 12 month SPEI. SM = summer topsoil (0- 7cm) volumetric moisture content.

*** = $p < 0.001$, ** = $p < 0.01$, * = $p < 0.05$, , = $p < 0.1$



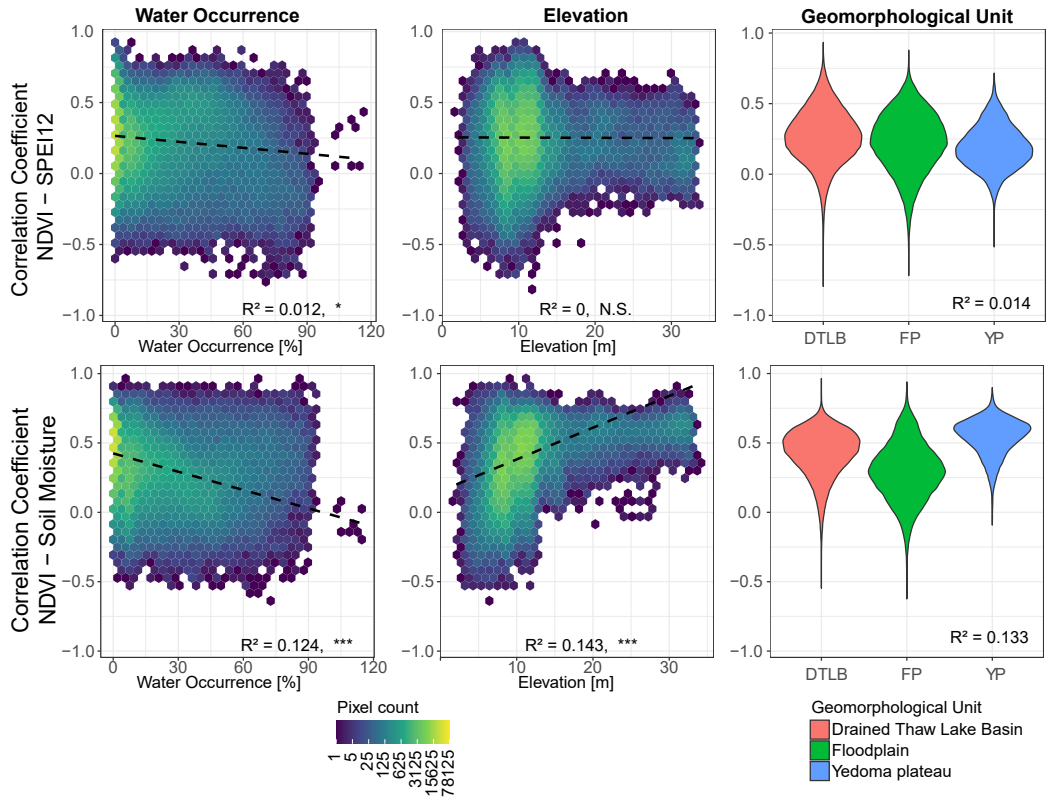


Figure S6.3) (both pages). Variation in correlation coefficients of annual maxNDVI and weather variables across elevation, water occurrence probability and geomorphological units. p values for associations with elevation and water occurrence were generated based on Dutilleul's modified t-test. No p-values are reported for association with geomorphological class based on ANOVAs.

*** = $p < 0.001$, ** = $p < 0.01$, * = $p < 0.05$, + = $p < 0.1$, N.S. = not significant.

Table S6.3. Vegetation composition change dimensions, areal cover and effect on VHR NDVI

Vegetation Change	Mean area of change [m ²]*	Standard deviation area of change [m ²]*	%- of focus study area affected	Mean VHR NDVI change relative to mean NDVI change area**	Standard deviation of mean NDVI change**	Number of pixels used for mean NDVI change**
shrub to tussock	7.00	18.46	3.13	0.02	0.04	3011
shrub to lichen	2.59	6.58	0.37	0.01	0.03	182
shrub to open water	14.69	21.58	0.46	-0.13	0.09	753
shrub to sedge	5.93	9.33	2.23	-0.04	0.06	1398
shrub to <i>sphagnum</i>	2.83	4.27	0.89	-0.09	0.05	265
tussock to shrub	5.41	19.29	2.68	0.04	0.05	2123
tussock to lichen	2.39	3.30	0.19	0.03	0.04	30
tussock to open water	4.11	5.90	0.05	-0.10	0.10	26
tussock to sedge	5.14	7.76	2.53	0.01	0.05	1312
tussock to <i>sphagnum</i>	6.19	12.55	4.17	-0.03	0.04	2838
lichen to shrub	2.75	16.99	0.17	0.07	0.03	210
lichen to tussock	3.64	7.92	0.47	0.05	0.03	258
lichen to open water	4.68	6.56	0.02	-0.18	0.08	17
lichen to sedge	2.70	3.62	0.05	0.01	0.06	18
lichen to <i>sphagnum</i>	2.06	2.80	0.05	-0.02	0.02	12
open water to shrub	1.81	2.34	0.02			
open water to tussock	1.64	2.47	0.01			
open water to lichen	0.56	0.37	0.00			
open water to sedge	6.03	8.15	0.28	0.00	0.09	131
open water to <i>sphagnum</i>	1.20	1.50	0.01			
sedge to shrub	3.44	6.40	0.50	0.01	0.05	253
sedge to tussock	4.12	10.91	0.77			
sedge to lichen	1.69	1.73	0.02	-0.02	0.05	589
sedge to open water	4.21	8.08	0.08	-0.07	0.05	58
sedge to <i>sphagnum</i>	5.20	15.73	2.87	-0.10	0.06	2346
<i>sphagnum</i> to shrub	2.62	9.15	0.33	0.07	0.05	241
<i>sphagnum</i> to tussock	4.78	11.24	1.26	0.05	0.07	926
<i>sphagnum</i> to lichen	1.57	1.67	0.02			
<i>sphagnum</i> to open water	15.78	42.40	0.02	0.08	0.03	27
<i>sphagnum</i> to sedge	2.46	4.98	0.65	0.08	0.07	233

*) Mean area and standard deviation of a distinct patch showing each vegetation class transition were calculated using the landscapemetrics R package (Hesselbarth et al. 2019).

**) Mean NDVI change relative to mean NDVI change was calculated as the mean difference between 2019 and

Supplementary Material

2010 very high resolution NDVI (GeoEye-1 and WorldView-2) relative to the mean NDVI change between 2010 and 2019 for the entire focus study area. We only report mean and standard deviation for class transitions for which at least 10 pixels were present. We only used NDVI pixels (2m x 2m) that showed one single class transition based on FVG maps (0.5m x 0.5m) and neglected NDVI pixels with mixed class changes.

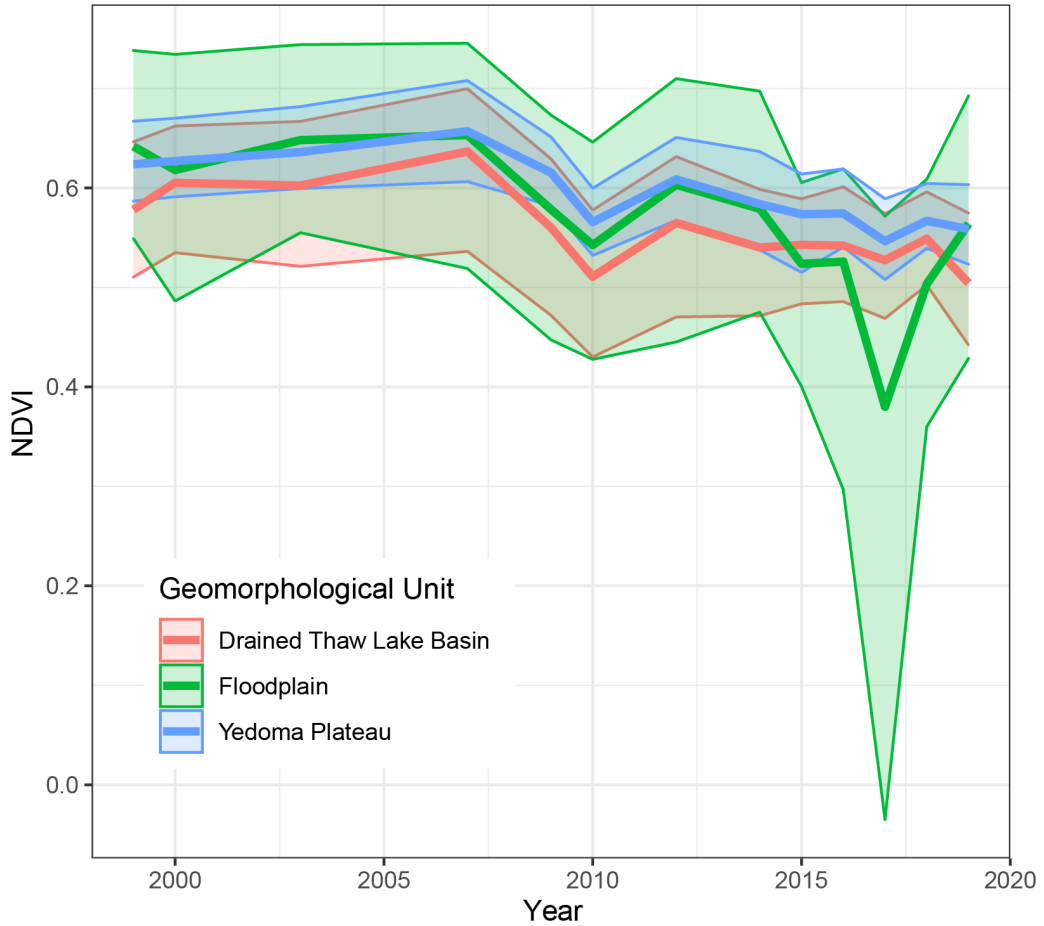
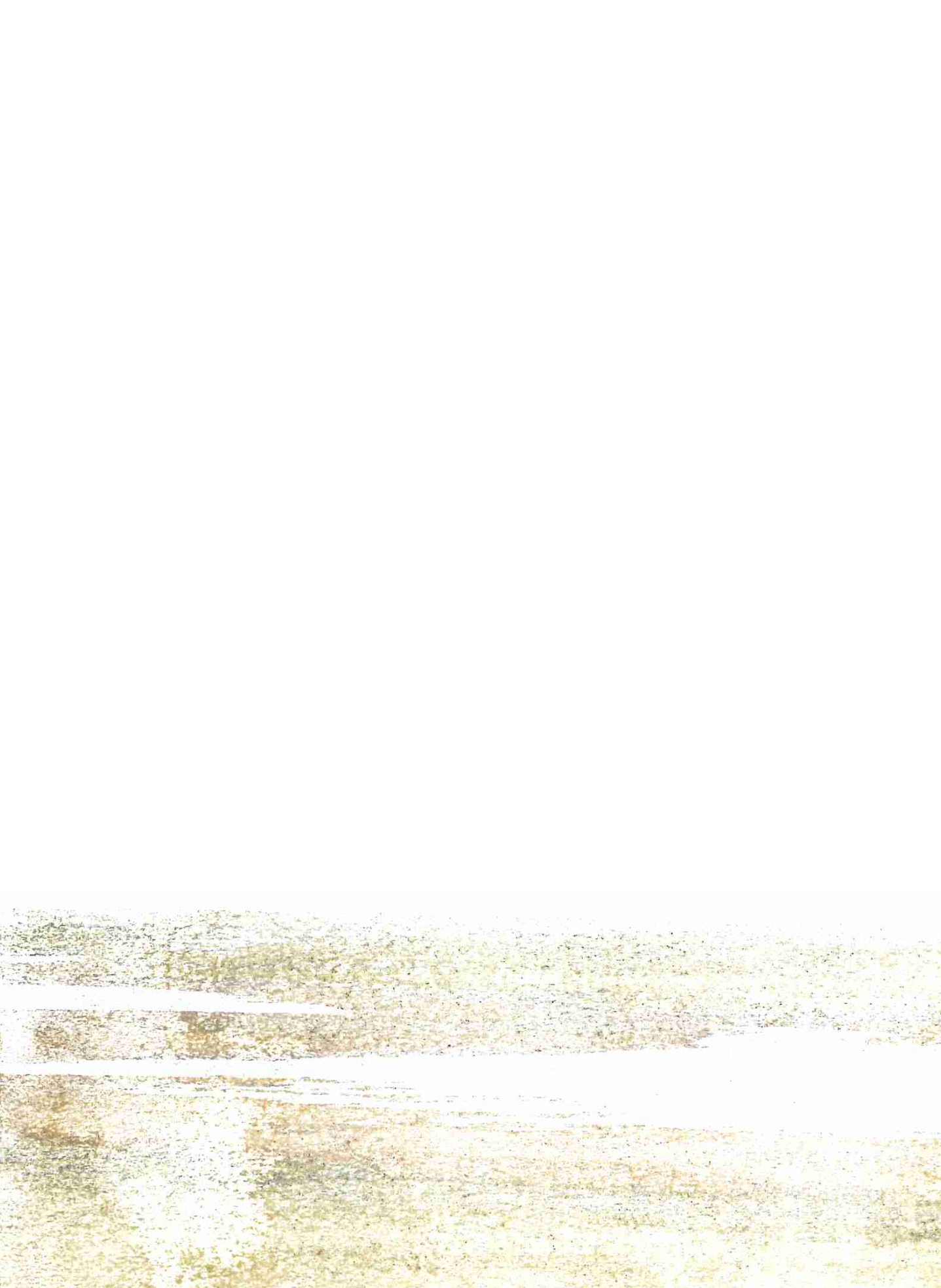


Figure S6.4) NDVI trajectory of main geomorphological units in the study area. Lines indicate mean NDVI per unit per year, shaded area represents a 90% confidence interval.



9.

References



A

- Abbott, B. W., J. B. Jones, E. A. Schuur, F. S. Chapin III, W. B. Bowden, M. S. Bret-Harte, H. E. Epstein, M. D. Flannigan, T. K. Harms, and T. N. Hollingsworth. 2016. Biomass offsets little or none of permafrost carbon release from soils, streams, and wildfire: an expert assessment. *Environmental Research Letters* 11:034014.
- Abolt, C. J., M. H. Young, A. L. Atchley, and D. R. Harp. 2018. Microtopographic control on the ground thermal regime in ice wedge polygons. *The Cryosphere* 12:1957–1968.
- Abramov, A., S. Davydov, A. Ivashchenko, D. Karelin, A. Kholodov, G. Kraev, A. Lupachev, A. Maslakov, V. Ostroumov, E. Rivkina, D. Shmelev, V. Sorokovikov, O. Tregubov, A. Veremeeva, D. Zamolodchikov, and S. Zimov. 2019. Two decades of active layer thickness monitoring in northeastern Asia. *Polar Geography* 44:186–202.
- Ackerman, D., D. Griffin, S. E. Hobbie, and J. C. Finlay. 2017. Arctic shrub growth trajectories differ across soil moisture levels. *Global Change Biology* 23:4294–4302.
- AMAP. 2017. Snow, water, ice and permafrost in the Arctic (SWIPA) 2017. Arctic Monitoring and Assessment Programme (AMAP). Oslo, Norway.
- AMAP. 2021. Arctic Climate Change Update 2021: Key Trends and Impacts. Summary for Policymakers. Tromsø, Norway.
- Anderson, J. E., T. A. Douglas, R. A. Barbato, S. Saari, J. D. Edwards, and R. M. Jones. 2019. Linking vegetation cover and seasonal thaw depths in interior Alaska permafrost terrains using remote sensing. *Remote sensing of Environment* 233:111363.
- Anderson, M. J. 2001. A new method for non-parametric multivariate analysis of variance. *Austral ecology* 26:32–46.
- Anderson, M. J. 2006. Distance-based tests for homogeneity of multivariate dispersions. *Biometrics* 62:245–253.
- Andresen, C. G., and V. L. Loughheed. 2015. Disappearing Arctic tundra ponds: Fine-scale analysis of surface hydrology in drained thaw lake basins over a 65 year period (1948–2013). *Journal of Geophysical Research: Biogeosciences* 120:466–479.
- Aspinall, R. J., and M. Hill. 1997. Land cover change: a method for assessing the reliability of land cover changes measured from remotely-sensed data. Pages 269–271 in *IGARSS'97. 1997 IEEE International Geoscience and Remote Sensing Symposium Proceedings. Remote Sensing-A Scientific Vision for Sustainable Development*. IEEE.
- Assmann, J. J., I. H. Myers-Smith, J. T. Kerby, A. M. Cunliffe, and G. N. Daskalova. 2020. Drone data reveal heterogeneity in tundra greenness and phenology not captured by satellites. *Environmental Research Letters* 15:125002.
- Atchley, A. L., E. T. Coon, S. L. Painter, D. R. Harp, and C. J. Wilson. 2016. Influences and interactions of inundation, peat, and snow on active layer thickness. *Geophysical Research Letters* 43:5116–5123.

B

- Baltzer, J. L., T. Veness, L. E. Chasmer, A. E. Sniderhan, and W. L. Quinton. 2014. Forests on thawing permafrost: fragmentation, edge effects, and net forest loss. *Global Change Biology* 20:824–834.
- Bao, T., X. Xu, G. Jia, D. P. Billesbach, and R. C. Sullivan. 2020. Much stronger tundra methane emissions during autumn-freeze than spring-thaw. *Global Change Biology* 27:376–387.
- Bär, A., A. Bräuning, and J. Löffler. 2006. Dendroecology of dwarf shrubs in the high mountains of Norway—A methodological approach. *Dendrochronologia* 24:17–27.
- Bär, A., R. Pape, A. Bräuning, and J. Löffler. 2008. Growth-ring variations of dwarf shrubs reflect regional climate signals in alpine environments rather than topoclimatic differences. *Journal of Biogeography* 35:625–636.
- Bartholomeus, H., G. Schaeppman-Strub, D. Blok, R. Sofronov, and S. Udaltsov. 2012. Spectral estimation of soil properties in siberian tundra soils and relations with plant species composition. *Applied and Environmental Soil Science* 2012:241535.
- Bates, D., M. Mächler, B. Bolker, and S. Walker. 2014. Fitting linear mixed-effects models using lme4.

References

- arXiv preprint arXiv:1406.5823.
- Beamish, A., M. K. Reynolds, H. Epstein, G. V. Frost, M. J. Macander, H. Bergstedt, A. Bartsch, S. Kruse, V. Miles, C. M. Tanis, B. Heim, M. Fuchs, S. Chabrilat, I. Shevtsova, M. Verdonen, and J. Wagner. 2020. Recent trends and remaining challenges for optical remote sensing of Arctic tundra vegetation: A review and outlook. *Remote sensing of Environment* 246:111872.
- Beckebanze, L., Z. Rehder, D. Holl, C. Wille, C. Mirbach, and L. Kutzbach. 2022. Ignoring carbon emissions from thermokarst ponds results in overestimation of tundra net carbon uptake. *Biogeosciences* 19:1225-1244.
- Beguéría, S., S. M. Vicente-Serrano, and M. S. Beguéría. 2017. Package 'spei': Calculation of the Standardised Precipitation-Evapotranspiration Index. R CRAN Project.
- Bell, K. L., and L. Bliss. 1980. Plant reproduction in a high arctic environment. *Arctic and Alpine Research* 12:1-10.
- Benham, E., R. Ahrens, and W. Nettleton. 2009. Clarification of Soil Texture Class Boundaries. National Soil Survey Centre. USDA-NRCS, Lincoln, Nebraska.
https://www.nrcs.usda.gov/Internet/FSE_DOCUMENTS/nrcs142p2_031477.pdf
- Beringer, J., F. S. Chapin, C. C. Thompson, and A. D. McGuire. 2005. Surface energy exchanges along a tundra-forest transition and feedbacks to climate. *Agricultural and Forest Meteorology* 131:143-161.
- Berner, L. T., P. Jantz, K. D. Tape, and S. J. Goetz. 2018. Tundra plant above-ground biomass and shrub dominance mapped across the North Slope of Alaska. *Environmental Research Letters* 13:035002.
- Berner, L. T., R. Massey, P. Jantz, B. C. Forbes, M. Macias-Fauria, I. Myers-Smith, T. Kumpula, G. Gauthier, L. Andreu-Hayles, B. V. Gaglioti, P. Burns, P. Zetterberg, R. D'Arrigo, and S. J. Goetz. 2020. Summer warming explains widespread but not uniform greening in the Arctic tundra biome. *Nature communications* 11:4621.
- Besag, J. 1986. On the statistical analysis of dirty pictures. *Journal of the Royal Statistical Society: Series B (Methodological)* 48:259-279.
- Bhatt, U., D. Walker, M. Reynolds, P. Bieniek, H. Epstein, J. Comiso, J. Pinzon, C. Tucker, and I. Polyakov. 2013. Recent declines in warming and vegetation greening trends over pan-Arctic tundra. *Remote Sensing* 5:4229-4254.
- Bhatt, U. S., D. A. Walker, M. K. Reynolds, P. A. Bieniek, H. E. Epstein, J. C. Comiso, J. E. Pinzon, C. J. Tucker, M. Steele, and W. Ermold. 2017. Changing seasonality of panarctic tundra vegetation in relationship to climatic variables. *Environmental Research Letters* 12:055003.
- Bhattacharyya, A. 1946. On a Measure of Divergence between Two Multinomial Populations. *Sankhyā: The Indian Journal of Statistics (1933-1960)* 7:401-406.
- Bieniek, P. A., U. S. Bhatt, D. A. Walker, M. K. Reynolds, J. C. Comiso, H. E. Epstein, J. E. Pinzon, C. J. Tucker, R. L. Thoman, and H. Tran. 2015. Climate drivers linked to changing seasonality of Alaska coastal tundra vegetation productivity. *Earth Interactions* 19:1-29.
- Billings, W. D., and H. A. Mooney. 1968. The ecology of arctic and alpine plants. *Biological reviews* 43:481-529.
- Bintanja, R., and O. Andry. 2017. Towards a rain-dominated Arctic. *Nature Climate Change* 7:263-267.
- Bintanja, R., and F. Selten. 2014. Future increases in Arctic precipitation linked to local evaporation and sea-ice retreat. *Nature* 509:479-482.
- Bintanja, R., K. van der Wiel, E. Van der Linden, J. Reusen, L. Bogerd, F. Krikken, and F. Selten. 2020. Strong future increases in Arctic precipitation variability linked to poleward moisture transport. *Science advances* 6:eaax6869.
- Biondi, F., and F. Qeadan. 2008. A theory-driven approach to tree-ring standardization: defining the biological trend from expected basal area increment. *Tree-ring research* 64:81-96.
- Biskaborn, B. K., S. L. Smith, J. Noetzli, H. Matthes, G. Vieira, D. A. Streletskiy, P. Schoeneich, V. E. Romanovsky, A. G. Lewkowicz, and A. Abramov. 2019. Permafrost is warming at a global scale. *Nature communications* 10:1-11.
- Bjerke, J. W., S. Rune Karlsen, K. Arild Høgda, E. Malnes, J. U. Jepsen, S. Lovibond, D. VikhamarSchuler, and H. Tømmervik. 2014. Record-low primary productivity and high plant damage in the Nordic Arctic Region in 2012 caused by multiple weather events and pest outbreaks.

- Environmental Research Letters 9:084006.
- Bjerke, J. W., R. Treharne, D. Vikhamar-Schuler, S. R. Karlsen, V. Ravolainen, S. Bokhorst, G. K. Phoenix, Z. Bochenek, and H. Tømmervik. 2017. Understanding the drivers of extensive plant damage in boreal and Arctic ecosystems: Insights from field surveys in the aftermath of damage. *Science of the Total Environment* 599:1965-1976.
- Bjorkman, A. D., M. G. Criado, I. H. Myers-Smith, V. Ravolainen, I. S. Jónsdóttir, K. B. Westergaard, J. P. Lawler, M. Aronsson, B. Bennett, and H. Gardfjell. 2020. Status and trends in Arctic vegetation: Evidence from experimental warming and long-term monitoring. *Ambio* 49:678-692.
- Bjorkman, A. D., I. H. Myers-Smith, S. C. Elmendorf, S. Normand, N. Ruger, P. S. A. Beck, A. BlachOvergaard, D. Blok, J. H. C. Cornelissen, B. C. Forbes, D. Georges, S. J. Goetz, K. C. Guay, G. H. R. Henry, J. HilleRisLambers, R. D. Hollister, D. N. Karger, J. Kattge, P. Manning, J. S. Prevey, C. Rixen, G. Schaepman-Strub, H. J. D. Thomas, M. Vellend, M. Wilms, S. Wipf, M. Carbognani, L. Hermanutz, E. Levesque, U. Molau, A. Petraglia, N. A. Soudzilovskaia, M. J. Spasojevic, M. Tomaselli, T. Vowles, J. M. Alatalo, H. D. Alexander, A. Anadon-Rosell, S. Angers-Blondin, M. te Beest, L. Berner, R. G. Bjork, A. Buchwal, A. Buras, K. Christie, E. J. Cooper, S. Dullinger, B. Elberling, A. Eskelinen, E. R. Frei, O. Grau, P. Grogan, M. Hallinger, K. A. Harper, M. Heijmans, J. Hudson, K. Hulber, M. Iturrate-Garcia, C. M. Iversen, F. Jaroszynska, J. F. Johnstone, R. H. Jorgensen, E. Kaarlejarvi, R. Klady, S. Kuleza, A. Kulonen, L. J. Lamarque, T. Lantz, C. J. Little, J. D. M. Speed, A. Michelsen, A. Milbau, J. Nabe-Nielsen, S. S. Nielsen, J. M. Ninot, S. F. Oberbauer, J. Olofsson, V. G. Onipchenko, S. B. Rumpf, P. Semenchuk, R. Shetti, L. S. Collier, L. E. Street, K. N. Suding, K. D. Tape, A. Trant, U. A. Treier, J. P. Tremblay, M. Tremblay, S. Venn, S. Weijers, T. Zamin, N. Boulanger-Lapointe, W. A. Gould, D. S. Hik, A. Hofgaard, I. S. Jonsdottir, J. Jorgenson, J. Klein, B. Magnusson, C. Tweedie, P. A. Wookey, M. Bahn, B. Blonder, P. M. van Bodegom, B. Bond-Lamberty, G. Campetella, B. E. L. Cerabolini, F. S. Chapin, W. K. Cornwell, J. Craine, M. Dainese, F. T. de Vries, S. Diaz, B. J. Enquist, W. Green, R. Milla, U. Niinemets, Y. Onoda, J. C. Ordóñez, W. A. Ozinga, J. Penuelas, H. Poorter, P. Poschlod, P. B. Reich, B. Sande, B. Schamp, S. Sheremetev, and E. Weiher. 2018. Plant functional trait change across a warming tundra biome. *Nature* 562:57-+.
- Black, K. L., C. A. Wallace, and J. L. Baltzer. 2021. Seasonal thaw and landscape position determine foliar functional traits and whole-plant water use in tall shrubs on the low arctic tundra. *New Phytologist* 231:94-107.
- Blok, D., M. Heijmans, G. Schaepman-Strub, J. van Ruijven, F. Parmentier, T. Maximov, and F. Berendse. 2011a. The cooling capacity of mosses: controls on water and energy fluxes in a Siberian tundra site. *Ecosystems* 14:1055-1065.
- Blok, D., M. M. Heijmans, G. Schaepman-Strub, A. Kononov, T. Maximov, and F. Berendse. 2010. Shrub expansion may reduce summer permafrost thaw in Siberian tundra. *Global Change Biology* 16:1296-1305.
- Blok, D., U. Sass-Klaassen, G. Schaepman-Strub, M. Heijmans, P. Sauren, and F. Berendse. 2011b. What are the main climate drivers for shrub growth in Northeastern Siberian tundra? *Biogeosciences* 8:1169-1179.
- Blok, D., G. Schaepman-Strub, H. Bartholomeus, M. Heijmans, T. C. Maximov, and F. Berendse. 2011c. The response of Arctic vegetation to the summer climate: relation between shrub cover, NDVI, surface albedo and temperature. *Environmental Research Letters* 6:035502.
- Boelman, N. T., L. Gough, J. R. McLaren, and H. Greaves. 2011. Does NDVI reflect variation in the structural attributes associated with increasing shrub dominance in arctic tundra? *Environmental Research Letters* 6:035501.
- Bokhorst, S., J. H. C. Cornelissen, and S. Veraverbeke. 2022. Long-term legacies of seasonal extremes in Arctic ecosystem functioning. *Global Change Biology* 28:3161-3162
- Bokhorst, S. F., J. W. Bjerke, H. Tømmervik, T. V. Callaghan, and G. K. Phoenix. 2009. Winter warming events damage sub-Arctic vegetation: consistent evidence from an experimental manipulation and a natural event. *Journal of Ecology* 97:1408-1415.
- Bonan, G. 2015. *Ecological climatology: concepts and applications*. Cambridge University Press, Cambridge, United Kingdom.

References

- Bonfils, C., T. Phillips, D. Lawrence, P. Cameron-Smith, W. Riley, and Z. Subin. 2012. On the influence of shrub height and expansion on northern high latitude climate. *Environmental Research Letters* 7:015503.
- Box, J. E., W. T. Colgan, T. R. Christensen, N. M. Schmidt, M. Lund, F.-J. W. Parmentier, R. Brown, U. S. Bhatt, E. S. Euskirchen, and V. E. Romanovsky. 2019. Key indicators of Arctic climate change: 1971–2017. *Environmental Research Letters* 14:045010.
- Brooks, M. E., K. Kristensen, K. J. van Benthem, A. Magnusson, C. W. Berg, A. Nielsen, H. J. Skaug, M. Machler, and B. M. Bolker. 2017. glmmTMB balances speed and flexibility among packages for zero-inflated generalized linear mixed modeling. *The R journal* 9:378-400.
- Brown, J., O. Ferrians Jr, J. A. Heginbottom, and E. Melnikov. 1997. Circum-Arctic map of permafrost and ground-ice conditions. US Geological Survey Reston, VA.
- Buchwal, A., P. F. Sullivan, M. Macias-Fauria, E. Post, I. H. Myers-Smith, J. C. Stroeve, D. Blok, K. D. Tape, B. C. Forbes, and P. Ropars. 2020. Divergence of Arctic shrub growth associated with sea ice decline. *Proceedings of the National Academy of Sciences* 117:33334-33344.
- Bunn, A. G. 2008. A dendrochronology program library in R (dplR). *Dendrochronologia* 26:115-124.
- Büntgen, U., L. Hellmann, W. Tegel, S. Normand, I. Myers-Smith, A. V. Kirilyanov, D. Nievergelt, and F. H. Schweingruber. 2015. Temperature-induced recruitment pulses of Arctic dwarf shrub communities. *Journal of Ecology* 103:489-501.
- Burke, E. J., Y. Zhang, and G. Krinner. 2020. Evaluating permafrost physics in the Coupled Model Intercomparison Project 6 (CMIP6) models and their sensitivity to climate change. *The Cryosphere* 14:3155-3174.
- Byers, H. R., H. Moses, and P. J. Harney. 1949. Measurement of rain temperature. *Journal of Atmospheric Sciences* 6:51-55.
- Bylesjö, M., M. Rantalainen, O. Cloarec, J. K. Nicholson, E. Holmes, and J. Trygg. 2006. OPLS discriminant analysis: combining the strengths of PLS-DA and SIMCA classification. *Journal of Chemometrics* 20:341-351.

C

- Cai, S., D. Liu, D. Sulla-Menashe, and M. A. Friedl. 2014. Enhancing MODIS land cover product with a spatial-temporal modeling algorithm. *Remote sensing of Environment* 147:243-255.
- Callaghan, T. V., R. Cazzolla Gatti, and G. Phoenix. 2021. The need to understand the stability of Arctic vegetation during rapid climate change: An assessment of imbalance in the literature. *Ambio* 51:1034-1044.
- Callaghan, T. V., M. Johansson, R. D. Brown, P. Y. Groisman, N. Labba, V. Radionov, R. S. Bradley, S. Blangy, O. N. Bulygina, and T. R. Christensen. 2011. Multiple effects of changes in Arctic snow cover. *Ambio* 40:32-45.
- CALM. 2021. Circumpolar Active Layer Monitoring Network. <https://www2.gwu.edu/~calm/> accessed 12-05-2022.
- Camill, P., A. Barry, E. Williams, C. Andreassi, J. Limmer, and D. Solick. 2009. Climate-vegetation-fire interactions and their impact on long-term carbon dynamics in a boreal peatland landscape in northern Manitoba, Canada. *Journal of Geophysical Research: Biogeosciences* 114.:G04017.
- Campbell, T. K. F., T. C. Lantz, and R. H. Fraser. 2018. Impacts of climate change and intensive lesser snow goose (*Chen caerulescens caerulescens*) activity on surface water in high Arctic pond complexes. *Remote Sensing* 10:1892.
- Campbell, T. K. F., T. C. Lantz, R. H. Fraser, and D. Hogan. 2021. High Arctic vegetation change mediated by hydrological conditions. *Ecosystems* 24:106-121.
- Canty, A., and B. Ripley. 2021. Package 'boot': Bootstrap R (S-Plus) Functions. R CRAN Project.
- Caswell, H., and T. Takada. 2004. Elasticity analysis of density-dependent matrix population models: the invasion exponent and its substitutes. *Theoretical Population Biology* 65:401-411.
- CAVMTeam. 2003. Circumpolar Arctic Vegetation. US Fish and Wildlife Service.
- Chadburn, S. E., E. J. Burke, P. M. Cox, P. Friedlingstein, G. Hugelius, and S. Westermann. 2017. An observation-based constraint on permafrost loss as a function of global warming. *Nature Climate Change* 7:340-344.

- Chapin, F. S., M. Sturm, M. C. Serreze, J. P. McFadden, J. R. Key, A. H. Lloyd, A. D. McGuire, T. S. Rupp, A. H. Lynch, J. P. Schimel, J. Beringer, W. L. Chapman, H. E. Epstein, E. S. Euskirchen, L. D. Hinzman, G. Jia, C. L. Ping, K. D. Tape, C. D. C. Thompson, D. A. Walker, and J. M. Welker. 2005. Role of land-surface changes in Arctic summer warming. *science* 310:657-660.
- Chasmer, L., C. Hopkinson, T. Veness, W. Quinton, and J. Baltzer. 2014. A decision-tree classification for low-lying complex land cover types within the zone of discontinuous permafrost. *Remote sensing of Environment* 143:73-84.
- Chen, Y., A. Liu, and X. Cheng. 2021. Vegetation grows more luxuriantly in Arctic permafrost drained lake basins. *Glob. Chang. Biol* 27:5865-5876.
- Chicco, D., and G. Jurman. 2020. The advantages of the Matthews correlation coefficient (MCC) over F1 score and accuracy in binary classification evaluation. *BMC genomics* 21:6.
- Christensen, T., M. Lund, K. Skov, J. Abermann, E. Lopez-Blanco, J. Scheller, M. Scheel, M. Jackowicz-Korczynski, K. Langley, and M. Murphy. 2020. Multiple Ecosystem Effects of Extreme Weather Events in the Arctic. *Ecosystems* 24:122–136.
- Christensen, T. R., T. Johansson, H. J. Åkerman, M. Mastepanov, N. Malmer, T. Friborg, P. Crill, and B. H. Svensson. 2004. Thawing sub-arctic permafrost: Effects on vegetation and methane emissions. *Geophysical Research Letters* 31:L04501.
- Clarke, K. R. 1993. Non-parametric multivariate analyses of changes in community structure. *Australian journal of ecology* 18:117-143.
- Clayton, L. K., S. Kevin, J. B. Michael, B.-C. Laura, C. Jingyi, H. C. Richard, C. C. Albert, B.-D. Kazem, G. Sarah, J. Elchin, L. Lin, M. Roger John, M. Mahta, P. Andrew, V. R. Adrian, R. S. Sean, S. Taylor, T. Alireza, W. Kang, J. W. Cathy, A. Z. Howard, Z. Tingjun, and Z. Yuhuan. 2021. Active layer thickness as a function of soil water content. *Environmental Research Letters* 16:055028.
- Clifford, P., S. Richardson, and D. Hemon. 1989. Assessing the significance of the correlation between two spatial processes. *Biometrics* 45:123-134.
- Collow, A. B. M., N. P. Thomas, M. G. Bosilovich, Y.-K. Lim, S. D. Schubert, and R. D. Koster. 2022. Seasonal Variability in the Mechanisms Behind the 2020 Siberian Heatwaves. *Journal of Climate* 35:3075-3090.
- Comyn-Platt, E., G. Hayman, C. Huntingford, S. E. Chadburn, E. J. Burke, A. B. Harper, W. J. Collins, C. P. Webber, T. Powell, and P. M. Cox. 2018. Carbon budgets for 1.5 and 2 C targets lowered by natural wetland and permafrost feedbacks. *Nature Geoscience* 11:568-573.
- Congalton, R. G. 1991. A review of assessing the accuracy of classifications of remotely sensed data. *Remote sensing of Environment* 37:35-46.
- Coon, E., M. Berndt, A. Jan, D. Svyatsky, A. Atchley, E. Kikinon, D. Harp, G. Manzini, E. Shelef, and K. Lipnikov. 2019. Advanced Terrestrial Simulator. <https://github.com/amanzi/ats>
- Crate, S., M. Ulrich, J. O. Habeck, A. R. Desyatkin, R. V. Desyatkin, A. N. Fedorov, T. Hiyama, Y. Iijima, S. Ksenofontov, C. Meszaros, and H. Takakura. 2017. Permafrost livelihoods: A transdisciplinary review and analysis of thermokarst-based systems of indigenous land use. *Anthropocene* 18:89-104.
- Cropper, J. P. 1982. Climate Reconstructions (1801 to 1938) Inferred from Tree-Ring Width Chronologies of the North American Arctic. *Arctic and Alpine Research* 14:223-241.
- Cybis. 2019a. CDendro. Cybis Elektronik & Data AB, Saltsjöbaden, Sweden.
- Cybis. 2019b. CooRecorder. Cybis Elektronik & Data AB, Saltsjöbaden, Sweden.

D

- D'Arrigo, R., R. Wilson, B. Liepert, and P. Cherubini. 2008. On the 'divergence problem' in northern forests: a review of the tree-ring evidence and possible causes. *Global and Planetary Change* 60:289-305.
- Dalla Santa, G., A. Galgaro, R. Sassi, M. Cultrera, P. Scotton, J. Mueller, D. Bertermann, D. Mendrinós, R. Pasquali, R. Perego, S. Pera, E. Di Sipio, G. Cassiani, M. De Carli, and A. Bernardi. 2020. An updated ground thermal properties database for GSHP applications. *Geothermics* 85:101758.
- Daniels, R. E., and A. Eddy. 1990. *Handbook of European sphagna*. HMSO, London.

References

- Davison, A. C., and D. V. Hinkley. 1997. *Bootstrap Methods and their Application*. Cambridge University Press, Cambridge.
- De Groot, W., P. Thomas, and R. W. Wein. 1997. *Betula nana* L. and *Betula glandulosa* Michx. *Journal of Ecology* 85:241-264.
- Desyatkin, A. R., F. Takakai, and R. Hatano. 2014. Flood effect on CH₄ emission from the almas in Central Yakutia, East Siberia. *Soil science and plant nutrition* 60:242-253.
- Didan, K. 2015a. MOD13Q1 MODIS/Terra vegetation indices 16-day L3 global 250m SIN grid V006. NASA EOSDIS Land Processes DAAC.
- Didan, K. 2015b. MYD13Q1 MODIS/Aqua vegetation indices 16-day L3 global 250m SIN grid V006. NASA EOSDIS Land Processes DAAC.
- Dobbert, S., R. Pape, and J. Löffler. 2021. How does spatial heterogeneity affect inter- and intraspecific growth patterns in tundra shrubs? *Journal of Ecology* 109:4115-4131.
- Domine, F., M. Barrere, and S. Morin. 2016. The growth of shrubs on high Arctic tundra at Bylot Island: impact on snow physical properties and permafrost thermal regime. *Biogeosciences* 13:6471-6486.
- Donner, N., N. S. Karpov, P. de Klerk, and H. Joosten. 2007. Distribution, diversity, development and dynamics of polygon mires: examples from Northeast Yakutia (Siberia). *Peatlands International* 1/2007:36-40
- Douglas, T. A., M. R. Turetsky, and C. D. Koven. 2020. Increased rainfall stimulates permafrost thaw across a variety of Interior Alaskan boreal ecosystems. *npj Climate and Atmospheric Science* 3:1-7.
- Dutilleul, P., P. Clifford, S. Richardson, and D. Hemon. 1993. Modifying the t test for assessing the correlation between two spatial processes. *Biometrics* 49:305-314.

E

- Elmendorf, S. C., G. H. Henry, R. D. Hollister, R. G. Björk, N. Boulanger-Lapointe, E. J. Cooper, J. H. Cornelissen, T. A. Day, E. Dorrepaal, and T. G. Elumeeva. 2012a. Plot-scale evidence of tundra vegetation change and links to recent summer warming. *Nature Climate Change* 2:453.
- Elmendorf, S. C., G. H. R. Henry, R. D. Hollister, R. G. Bjork, A. D. Bjorkman, T. V. Callaghan, L. S. Collier, E. J. Cooper, J. H. C. Cornelissen, T. A. Day, A. M. Fosaa, W. A. Gould, J. Gretarsdottir, J. Harte, L. Hermanutz, D. S. Hik, A. Hofgaard, F. Jarrad, I. S. Jonsdottir, F. Keuper, K. Klanderud, J. A. Klein, S. Koh, G. Kudo, S. I. Lang, V. Loewen, J. L. May, J. Mercado, A. Michelsen, U. Molau, I. H. Myers-Smith, S. F. Oberbauer, S. Pieper, E. Post, C. Rixen, C. H. Robinson, N. M. Schmidt, G. R. Shaver, A. Stenstrom, A. Tolvanen, O. Totland, T. Troxler, C. H. Wahren, P. J. Webber, J. M. Welker, and P. A. Wookey. 2012b. Global assessment of experimental climate warming on tundra vegetation: heterogeneity over space and time. *Ecology Letters* 15:164-175.
- Epstein, H., U. Bhatt, M. Reynolds, D. Walker, B. Forbes, G. Phoenix, J. W. Bjerke, H. Tømmervik, S. R. Karlsen, and R. Myneni. 2018. Tundra greenness. [in Arctic Report Card 2018], <https://www.arctic.noaa.gov/Report-Card>.
- Epstein, H. E., I. Myers-Smith, and D. A. Walker. 2013. Recent dynamics of arctic and sub-arctic vegetation. *Environmental Research Letters* 8:015040.
- Epstein, H. E., M. K. Reynolds, D. A. Walker, U. S. Bhatt, C. J. Tucker, and J. E. Pinzon. 2012. Dynamics of aboveground phytomass of the circumpolar Arctic tundra during the past three decades. *Environmental Research Letters* 7:015506.
- Ercan, F. E., J. Mikola, T. Silver, K. Myller, E. Vainio, S. Slowińska, M. Slowiński, M. Lamentowicz, D. Blok, and F. Wagner-Cremer. 2021. Effects of experimental warming on *Betula nana* epidermal cell growth tested over its maximum climatological growth range. *Plos One* 16:e0251625.
- ESRI. 2019. ArcGIS Desktop. Environmental Systems Research Institute, Redlands, CA.
- Eugster, W., W. R. Rouse, R. A. Pielke Sr, J. P. Mcfadden, D. D. Baldocchi, T. G. F. Kittel, F. S. Chapin III, G. E. Liston, P. L. Vidale, and E. Vaganov. 2000. Land-atmosphere energy exchange in Arctic tundra and boreal forest: available data and feedbacks to climate. *Global Change*

Biology 6:84-115.

- Euskirchen, E., A. McGuire, T. Rupp, F. Chapin, and J. Walsh. 2009. Projected changes in atmospheric heating due to changes in fire disturbance and the snow season in the western Arctic, 2003–2100. *Journal of Geophysical Research: Biogeosciences* 114:G04022.
- Evans, J. S., and K. Ram. 2021. Package ‘spatialEco’. R CRAN Project.

F

- Farouki, O. T. 1981. Thermal properties of soils. COLD REGIONS RESEARCH AND ENGINEERING LAB HANOVER NH.
- Farquharson, L. M., V. E. Romanovsky, W. L. Cable, D. A. Walker, S. V. Kokelj, and D. Nicolsky. 2019. Climate change drives widespread and rapid thermokarst development in very cold permafrost in the Canadian High Arctic. *Geophysical Research Letters* 46:6681-6689.
- Fedorov, A., R. Ivanova, H. Park, T. Hiyama, and Y. Iijima. 2014. Recent air temperature changes in the permafrost landscapes of northeastern Eurasia. *Polar Science* 8:114-128.
- Fedorov, A. N., N. F. Vasilyev, Y. I. Torgovkin, A. A. Shestakova, S. P. Varlamov, M. N. Zheleznyak, V. Shepelev, P. Y. Konstantinov, S. S. Kalinicheva, and N. I. Basharin. 2018. PermafrostLandscape Map of the Republic of Sakha (Yakutia) on a Scale 1: 1,500,000. *Geosciences* 8:465.
- Fernandes, R., and S. G. Leblanc. 2005. Parametric (modified least squares) and non-parametric (Theil–Sen) linear regressions for predicting biophysical parameters in the presence of measurement errors. *Remote sensing of Environment* 95:303-316.
- Fischer, E. M., and R. Knutti. 2015. Anthropogenic contribution to global occurrence of heavy precipitation and high-temperature extremes. *Nature Climate Change* 5:560-564.
- Forbes, B. C., M. M. Fauria, and P. Zetterberg. 2010. Russian Arctic warming and ‘greening’ are closely tracked by tundra shrub willows. *Global Change Biology* 16:1542-1554.
- Forchhammer, M. 2017. Sea-ice induced growth decline in Arctic shrubs. *Biology Letters* 13:20170122.
- Forkel, M., N. Carvalhais, J. Verbesselt, M. D. Mahecha, C. S. Neigh, and M. Reichstein. 2013. Trend change detection in NDVI time series: Effects of inter-annual variability and methodology. *Remote Sensing* 5:2113-2144.
- Fortin, M.-J., and S. Payette. 2002. How to test the significance of the relation between spatially autocorrelated data at the landscape scale: a case study using fire and forest maps. *Ecoscience* 9:213-218.
- Francon, L., C. Corona, I. Till-Bottraud, P. Choler, B. Carlson, G. Charrier, T. Améglio, S. Morin, N. Eckert, and E. Roussel. 2020. Assessing the effects of earlier snow melt-out on Alpine shrub growth: the sooner the better? *Ecological Indicators* 115:106455.
- Francon, L., C. Corona, I. Till-Bottraud, P. Choler, E. Roussel, B. Z. Carlson, S. Morin, B. Girard, and M. Stoffel. 2021. Shrub growth in the Alps diverges from air temperature since the 1990s. *Environmental Research Letters* 16:074026.
- Fraser, R. H., S. V. Kokelj, T. C. Lantz, M. McFarlane-Winchester, I. Olthof, and D. Lacelle. 2018. Climate sensitivity of high Arctic permafrost terrain demonstrated by widespread ice-wedge thermokarst on Banks Island. *Remote Sensing* 10:954.
- Fraser, R. H., T. C. Lantz, I. Olthof, S. V. Kokelj, and R. A. Sims. 2014. Warming-induced shrub expansion and lichen decline in the Western Canadian Arctic. *Ecosystems* 17:1151-1168.
- Frost, G., U. Bhatt, M. Macander, A. Hendricks, and M. Jorgenson. 2021a. Is Alaska’s Yukon–Kuskokwim Delta Greening or Browning? Resolving Mixed Signals of Tundra Vegetation Dynamics and Drivers in the Maritime Arctic. *Earth Interactions* 25:76-93.
- Frost, G., T. Christopherson, M. Jorgenson, A. Liljedahl, M. Macander, D. Walker, and A. Wells. 2018a. Regional Patterns and Asynchronous Onset of Ice-Wedge Degradation since the Mid20th Century in Arctic Alaska. *Remote Sensing* 10:1312.
- Frost, G., M. Macander, U. Bhatt, L. Berner, J. Bjerke, H. Epstein, B. Forbes, S. Goetz, M. Lara, T. Park, G. Phoenix, S. Serbin, H. Tommervik, D. Walker, and Y. D. 2021b. Tundra Greenness. [in Arctic Report Card 2021], <https://www.arctic.noaa.gov/Report-Card>.
- Frost, G. V., U. S. Bhatt, H. E. Epstein, I. Myers-Smith, G. K. Phoenix, L. T. Berner, J. W. Bjerke, B. C.

References

- Forbes, S. J. Goetz, J. T. Kerby, M. J. Macander, T. Park, M. K. Reynolds, H. Tømmervik, and D. A. Walker. 2020. Tundra Greenness. [in Arctic Report Card 2021], <https://www.arctic.noaa.gov/Report-Card>.
- Frost, G. V., H. E. Epstein, and D. A. Walker. 2014. Regional and landscape-scale variability of Landsat-observed vegetation dynamics in northwest Siberian tundra. *Environmental Research Letters* 9:025004.
- Frost, G. V., H. E. Epstein, D. A. Walker, G. Matyshak, and K. Ermokhina. 2013. Patterned-ground facilitates shrub expansion in Low Arctic tundra. *Environmental Research Letters* 8:015035.
- Frost, G. V., H. E. Epstein, D. A. Walker, G. Matyshak, and K. Ermokhina. 2018b. Seasonal and longterm changes to active-layer temperatures after tall shrubland expansion and succession in Arctic tundra. *Ecosystems* 21:507-520.
- Fujinami, H., T. Yasunari, and T. Watanabe. 2016. Trend and interannual variation in summer precipitation in eastern Siberia in recent decades. *International Journal of Climatology* 36:355-368.
- ### G
- Gamm, C. M., P. F. Sullivan, A. Buchwal, R. J. Dial, A. B. Young, D. A. Watts, S. M. P. Cahoon, J. M. Welker, and E. Post. 2018. Declining growth of deciduous shrubs in the warming climate of continental western Greenland. *Journal of Ecology* 106:640-654.
- Gamon, J. A., K. F. Huemmrich, R. S. Stone, and C. E. Tweedie. 2013. Spatial and temporal variation in primary productivity (NDVI) of coastal Alaskan tundra: Decreased vegetation growth following earlier snowmelt. *Remote sensing of Environment* 129:144-153.
- Gao, Y., and J. Couwenberg. 2015. Carbon accumulation in a permafrost polygon peatland: steady long-term rates in spite of shifts between dry and wet conditions. *Global Change Biology* 21:803-815.
- Gärtner, H., S. Lucchinetti, and F. H. Schweingruber. 2014. New perspectives for wood anatomical analysis in dendrosciences: the GSL1-microtome. *Dendrochronologia* 32:47-51.
- Gärtner, H., and F. Schweingruber. 2013. Microscopic preparation techniques for plant stem analysis. Verlag Dr. Kessel, Remagen-Oberwinter.
- GBIF. 2021. *Betula nana* L. in GBIF Secretariat. GBIF Backbone Taxonomy. Checklist dataset <https://doi.org/10.15468/39omei> accessed via GBIF.org on 2022-04-04.
- GCOS. n.d. Permafrost ESSENTIAL CLIMATE VARIABLE (ECV) FACTSHEET. <https://gcos.wmo.int/en/essential-climate-variables/permafrost> accessed 02-06-2022.
- Geman, S., and D. Geman. 1984. Stochastic relaxation, Gibbs distributions, and the Bayesian restoration of images. *IEEE Transactions on pattern analysis and machine intelligence*. PAMI6:721-741.
- Göckede, M., F. Kittler, M. J. Kwon, I. Burjack, M. Heimann, O. Kolle, N. Zimov, and S. Zimov. 2017. Shifted energy fluxes, increased Bowen ratios, and reduced thaw depths linked with drainage-induced changes in permafrost ecosystem structure. *The Cryosphere* 11:2975-2996.
- Göckede, M., M. J. Kwon, F. Kittler, M. Heimann, N. Zimov, and S. Zimov. 2019. Negative feedback processes following drainage slow down permafrost degradation. *Global Change Biology* 25:3254-3266.
- Gómez, C., J. C. White, and M. A. Wulder. 2016. Optical remotely sensed time series data for land cover classification: A review. *ISPRS Journal of Photogrammetry and Remote Sensing* 116:55-72.
- Gorelick, N., M. Hancher, M. Dixon, S. Ilyushchenko, D. Thau, and R. Moore. 2017. Google Earth Engine: Planetary-scale geospatial analysis for everyone. *Remote sensing of Environment* 202:18-27.
- Gorham, E. 1991. Northern peatlands: role in the carbon cycle and probable responses to climatic warming. *Ecological applications* 1:182-195.
- Goswami, S., J. A. Gamon, and C. E. Tweedie. 2011. Surface hydrology of an arctic ecosystem: Multiscale analysis of a flooding and draining experiment using spectral reflectance. *Journal of Geophysical Research: Biogeosciences* 116:G00I07.
- Grant, R., Z. Mekonnen, W. Riley, H. Wainwright, D. Graham, and M. Torn. 2017. Mathematical

- modelling of arctic polygonal tundra with ecosys: 1. Microtopography determines how active layer depths respond to changes in temperature and precipitation. *Journal of Geophysical Research: Biogeosciences* 122:3161-3173.
- Grigoriev, M., V. Kunitsky, R. Chzhan, and V. Shepelev. 2009. On the variation in geocryological, landscape and hydrological conditions in the Arctic zone of East Siberia in connection with climate warming. *Geography and Natural Resources* 30:101-106.
- Grosse, G., J. Harden, M. Turetsky, A. D. McGuire, P. Camill, C. Tarnocai, S. Frolking, E. A. Schuur, T. Jorgenson, and S. Marchenko. 2011. Vulnerability of high-latitude soil organic carbon in North America to disturbance. *Journal of Geophysical Research: Biogeosciences* 116:G00K06.
- Grosse, G., V. Romanovsky, K. Walter, A. Morgenstern, H. Lantuit, and S. Zimov. 2008. Distribution of thermokarst lakes and ponds at three yedoma sites in Siberia. Ninth International Conference on Permafrost.
- Grunberg, I., E. J. Wilcox, S. Zwieback, P. Marsh, and J. Boike. 2020. Linking tundra vegetation, snow, soil temperature, and permafrost. *Biogeosciences* 17:4261-4279.
- Grysko, R., E. Plekhanova, J. Oehri, S. V. Karsanaev, T. C. Maximov, and G. Schaepman-Strub. 2021. Design of the tundra rainfall experiment (TRainEx) to simulate future summer precipitation scenarios. *MethodsX* 8:101331.
- GTN-P. 2016. Global Terrestrial Network for Permafrost Database: Permafrost Temperature Data (TSP - Thermal State of Permafrost). Akureyri, Iceland. <https://gtnp.arcticportal.org/>.

H

- Halekoh, U., and S. Højsgaard. 2014. A kenward-roger approximation and parametric bootstrap methods for tests in linear mixed models—the R package pbrtest. *Journal of Statistical Software* 59:1-30.
- Hallinger, M., M. Manthey, and M. Wilmking. 2010. Establishing a missing link: warm summers and winter snow cover promote shrub expansion into alpine tundra in Scandinavia. *New Phytologist* 186:890-899.
- Hamm, A., and A. Frampton. 2021. Impact of lateral groundwater flow on hydrothermal conditions of the active layer in a high-Arctic hillslope setting. *The Cryosphere* 15:4853-4871.
- Hartig, F. 2017. Package ‘DHARMA’: residual diagnostics for hierarchical (multi-level/mixed) regression models. R CRAN Project.
- Haverkamp, P. J., I. Byskatova-Harmey, N. Germogenov, and G. Schaepman-Strub. 2022. Increasing Arctic Tundra Flooding Threatens Wildlife Habitat and Survival: Impacts on the Critically Endangered Siberian Crane (*Grus leucogeranus*). *Frontiers in Conservation Science* 3:799998.
- Heijmans, M. M., R. Í. Magnússon, M. J. Lara, G. V. Frost, I. H. Myers-Smith, J. van Huissteden, M. T. Jorgenson, A. N. Fedorov, H. E. Epstein, and D. M. Lawrence. 2022. Tundra vegetation change and impacts on permafrost. *Nature Reviews Earth & Environment* 3:68-84.
- Hendrichsen, D. K., C. J. Topping, and M. C. Forchhammer. 2009. Predation and fragmentation portrayed in the statistical structure of prey time series. *BMC Ecology* 9:10.
- Henry, G., and U. Molau. 1997. Tundra plants and climate change: the International Tundra Experiment (ITEX). *Global Change Biology* 3:1-9.
- Hersbach, H., B. Bell, P. Berrisford, S. Hirahara, A. Horányi, J. Muñoz-Sabater, J. Nicolas, C. Peubey, R. Radu, and D. Schepers. 2020. The ERA5 global reanalysis. *Quarterly Journal of the Royal Meteorological Society* 146:1999-2049.
- Hesselbarth, M. H., M. Sciaini, K. A. With, K. Wiegand, and J. Nowosad. 2019. landscapemetrics: An open-source R tool to calculate landscape metrics. *Ecography* 42:1648-1657.
- Hijmans, R. J., J. v. Etten, M. Sumner, J. Cheng, A. Bevan, R. Bivand, L. Busetto, M. Canty, D. Forrest, A. Ghosh, D. Golicher, J. Gray, J. A. Greenberg, P. Hiemstra, K. Hingee, C. Karney, M. Mattiuzzi, S. Mosher, J. Nowosad, E. Pebesma, O. P. Lamigueiro, E. B. Racine, B. Rowlingson, A. Shortridge, B. Venables, and R. Wueest. 2020. Package “raster”: Geographic Data Analysis and Modeling. R CRAN Project.
- Hinkel, K., F. Paetzold, F. Nelson, and J. Bockheim. 2001. Patterns of soil temperature and moisture in the active layer and upper permafrost at Barrow, Alaska: 1993–1999. *Global and Planetary Change* 29:293-309.

References

- Hjort, J., D. Streletskiy, G. Doré, Q. Wu, K. Bjella, and M. Luoto. 2022. Impacts of permafrost degradation on infrastructure. *Nature Reviews Earth & Environment* 3:24-38.
- Hobbie, J. E., G. R. Shaver, E. B. Rastetter, J. E. Cherry, S. J. Goetz, K. C. Guay, W. A. Gould, and G. W. Kling. 2017. Ecosystem responses to climate change at a Low Arctic and a High Arctic longterm research site. *Ambio* 46:160-173.
- Hobbie, S. E., and F. S. Chapin III. 1998. The response of tundra plant biomass, aboveground production, nitrogen, and CO₂ flux to experimental warming. *Ecology* 79:1526-1544.
- Hollesen, J., A. Buchwal, G. Rachlewicz, B. U. Hansen, M. O. Hansen, O. Stecher, and B. Elberling. 2015. Winter warming as an important co-driver for *Betula nana* growth in western Greenland during the past century. *Global Change Biology* 21:2410-2423.
- Holmes, R. L. 1983. Computer-assisted quality control in tree-ring dating and measurement. *Tree Ring Bulletin*, 43:69-78.
- HSAF. 2020. Scatterometer Root Zone Soil Moisture (RZSM) Data Record 10km resolution - Multimission. EUMETSAT SAF on Support to Operational Hydrology and Water Management. <https://navigator.eumetsat.int/product/EO:EUM:DAT:0231>
- Hudson, J. M., and G. Henry. 2009. Increased plant biomass in a High Arctic heath community from 1981 to 2008. *Ecology* 90:2657-2663.
- Huebner, D. C., and M. S. Bret-Harte. 2019. Microsite conditions in retrogressive thaw slumps may facilitate increased seedling recruitment in the Alaskan Low Arctic. *Ecology and Evolution* 9:1880-1897.
- Hugelius, G., J. Strauss, S. Zubrzycki, J. W. Harden, E. A. G. Schuur, C. L. Ping, L. Schirrmeister, G. Grosse, G. J. Michaelson, C. D. Koven, J. A. O'Donnell, B. Elberling, U. Mishra, P. Camill, Z. Yu, J. Palmtag, and P. Kuhry. 2014. Estimated stocks of circumpolar permafrost carbon with quantified uncertainty ranges and identified data gaps. *Biogeosciences* 11:6573-6593.

I

- Iijima, Y., A. N. Fedorov, H. Park, K. Suzuki, H. Yabuki, T. C. Maximov, and T. Ohata. 2010. Abrupt increases in soil temperatures following increased precipitation in a permafrost region, central Lena River basin, Russia. *Permafrost and Periglacial Processes* 21:30-41.
- Iijima, Y., H. Park, P. Y. Konstantinov, G. G. Pudov, and A. N. Fedorov. 2017. Active-Layer Thickness Measurements Using a Handheld Penetrometer at Boreal and Tundra Sites in Eastern Siberia. *Permafrost and Periglacial Processes* 28:306-313.
- IPCC. 2021. Climate Change 2021: The Physical Science Basis. Contribution of Working Group I to the Sixth Assessment Report of the Intergovernmental Panel on Climate Change.
- Ishikawa, H. 2003. Exact optimization for Markov random fields with convex priors. *IEEE Transactions on pattern analysis and machine intelligence* 25:1333-1336.
- Iturrate-García, M., M. J. O'Brien, O. Khitun, S. Abiven, P. A. Niklaus, and G. Schaeppman-Strub. 2016. Interactive effects between plant functional types and soil factors on tundra species diversity and community composition. *Ecology and Evolution* 6:8126-8137.
- Iwahana, G., T. Machimura, Y. Kobayashi, A. N. Fedorov, P. Y. Konstantinov, and M. Fukuda. 2005. Influence of forest clear-cutting on the thermal and hydrological regime of the active layer near Yakutsk, eastern Siberia. *Journal of Geophysical Research: Biogeosciences* 110:G02004.
- Iwahana, G., S. Takano, R. E. Petrov, S. Tei, R. Shingubara, T. C. Maximov, A. N. Fedorov, A. R. Desyatkin, A. N. Nikolaev, and R. V. Desyatkin. 2014. Geocryological characteristics of the upper permafrost in a tundra-forest transition of the Indigirka River Valley, Russia. *Polar Science* 8:96-113.

J

- Jafarov, E. E., D. R. Harp, E. T. Coon, B. Dafflon, A. P. Tran, A. L. Atchley, Y. Lin, and C. J. Wilson. 2020. Estimation of subsurface porosities and thermal conductivities of polygonal tundra by coupled inversion of electrical resistivity, temperature, and moisture content data. *The Cryosphere* 14:77-91.
- Jan, A., E. T. Coon, and S. L. Painter. 2020. Evaluating integrated surface/subsurface permafrost

- thermal hydrology models in ATS (v0. 88) against observations from a polygonal tundra site. *Geoscientific Model Development* 13:2259-2276.
- Jevšenak, J., and T. Levanič. 2016. Should artificial neural networks replace linear models in tree ring based climate reconstructions? *Dendrochronologia* 40:102-109.
- Jevšenak, J., and T. Levanič. 2018. dendroTools: R package for studying linear and nonlinear responses between tree-rings and daily environmental data. *Dendrochronologia* 48:32-39.
- Jones, B. M., C. D. Arp, K. M. Hinkel, R. A. Beck, J. A. Schmutz, and B. Winston. 2009. Arctic Lake Physical Processes and Regimes with Implications for Winter Water Availability and Management in the National Petroleum Reserve Alaska. *Environmental Management* 43:1071-1084.
- Jones, B. M., G. Grosse, L. M. Farquharson, P. Roy-Léveillé, A. Veremeeva, M. Z. Kanevskiy, B. V. Gaglioti, A. L. Breen, A. D. Parsekian, and M. Ulrich. 2022. Lake and drained lake basin systems in lowland permafrost regions. *Nature Reviews Earth & Environment* 3:85-98.
- Jones, M. C., J. Harden, J. O'Donnell, K. Manies, T. Jorgenson, C. Treat, and S. Ewing. 2017. Rapid carbon loss and slow recovery following permafrost thaw in boreal peatlands. *Global Change Biology* 23:1109-1127.
- Jorgenson, M., and G. Grosse. 2016. Remote sensing of landscape change in permafrost regions. *Permafrost and Periglacial Processes* 27:324-338.
- Jorgenson, M., M. Kanevskiy, Y. Shur, N. Moskalenko, D. Brown, K. Wickland, R. Striegl, and J. Koch. 2015. Role of ground ice dynamics and ecological feedbacks in recent ice wedge degradation and stabilization. *Journal of Geophysical Research: Earth Surface* 120:2280-2297.
- Jorgenson, M., V. Romanovsky, J. Harden, Y. Shur, J. O'Donnell, E. A. Schuur, M. Kanevskiy, and S. Marchenko. 2010. Resilience and vulnerability of permafrost to climate change. *Canadian Journal of Forest Research* 40:1219-1236.
- Jorgenson, M., Y. L. Shur, and E. R. Pullman. 2006. Abrupt increase in permafrost degradation in Arctic Alaska. *Geophysical Research Letters* 33:L02503.
- Jorgenson, M. T., and Y. Shur. 2007. Evolution of lakes and basins in northern Alaska and discussion of the thaw lake cycle. *Journal of Geophysical Research: Earth Surface* 112:F02S17.
- Juzsak, I., W. Eugster, M. Heijmans, and G. Schaepman-Strub. 2016. Contrasting radiation and soil heat fluxes in Arctic shrub and wet sedge tundra. *Biogeosciences* 13:4049-4064.
- Juzsak, I., M. Iturrate-Garcia, J.-P. Gastellu-Etchegorry, M. E. Schaepman, T. C. Maximov, and G. Schaepman-Strub. 2017. Drivers of shortwave radiation fluxes in Arctic tundra across scales. *Remote sensing of Environment* 193:86-102.

K

- Kalela-Brundin, M. 1999. Climatic information from tree-rings of *Pinus sylvestris* L. and a reconstruction of summer temperatures back to AD 1500 in Femundsmarka, eastern Norway, using partial least squares regression (PLS) analysis. *The Holocene* 9:59-77.
- Kanevskiy, M., Y. Shur, T. Jorgenson, D. R. Brown, N. Moskalenko, J. Brown, D. A. Walker, M. K. Reynolds, and M. Buchhorn. 2017. Degradation and stabilization of ice wedges: Implications for assessing risk of thermokarst in northern Alaska. *Geomorphology* 297:20-42.
- Karami, M., A. Westergaard-Nielsen, S. Normand, U. A. Treier, B. Elberling, and B. U. Hansen. 2018. A phenology-based approach to the classification of Arctic tundra ecosystems in Greenland. *ISPRS Journal of Photogrammetry and Remote Sensing* 146:518-529.
- Karjalainen, O., M. Luoto, J. Aalto, and J. Hjort. 2019. New insights into the environmental factors controlling the ground thermal regime across the Northern Hemisphere: a comparison between permafrost and non-permafrost areas. *The Cryosphere* 13:693-707.
- Keuper, F., E. Dorrepaal, P. M. van Bodegom, R. van Logtestijn, G. Venhuizen, J. van Hal, and R. Aerts. 2017. Experimentally increased nutrient availability at the permafrost thaw front selectively enhances biomass production of deep-rooting subarctic peatland species. *Global Change Biology* 23:4257-4266.
- Keuper, F., P. M. van Bodegom, E. Dorrepaal, J. T. Weedon, J. van Hal, R. S. van Logtestijn, and R. Aerts. 2012. A frozen feast: Thawing permafrost increases plant-available nitrogen in subarctic peatlands. *Global Change Biology* 18:1998-2007.
- Kirpotin, S. N., T. V. Callaghan, A. M. Peregon, A. S. Babenko, D. I. Berman, N. A. Bulakhova, A. A.

References

- Byzaakay, T. M. Chernykh, V. Chursin, and E. A. Interesova. 2021. Impacts of environmental change on biodiversity and vegetation dynamics in Siberia. *Ambio* 50:1926-1952.
- Kokelj, S., J. Tunnicliffe, D. Lacelle, T. Lantz, K. Chin, and R. Fraser. 2015. Increased precipitation drives mega slump development and destabilization of ice-rich permafrost terrain, northwestern Canada. *Global and Planetary Change* 129:56-68.
- Kokelj, S. V., and M. Jorgenson. 2013. Advances in thermokarst research. *Permafrost and Periglacial Processes* 24:108-119.
- Kokelj, S. V., T. C. Lantz, J. Tunnicliffe, R. Segal, and D. Lacelle. 2017. Climate-driven thaw of permafrost preserved glacial landscapes, northwestern Canada. *Geology* 45:371-374.
- Kolischuk, V. G. 1990. Dendroclimatological Study of Prostrate Woody Plants. In E. Cook, Kairiukstis, L., editor. *Methods of Dendrochronology: Applications in the Environmental Sciences*. Kluwer Academic Publishers, Dordrecht.
- Komsta, L., and M. L. Komsta. 2013. Package 'mblm'. R CRAN Project.
- Koven, C. D., W. J. Riley, and A. Stern. 2013. Analysis of permafrost thermal dynamics and response to climate change in the CMIP5 Earth System Models. *Journal of Climate* 26:1877-1900.
- Koven, C. D., B. Ringeval, P. Friedlingstein, P. Ciais, P. Cadule, D. Khvorostyanov, G. Krinner, and C. Tarnocai. 2011. Permafrost carbon-climate feedbacks accelerate global warming. *Proceedings of the National Academy of Sciences of the United States of America* 108:14769-14774.
- Krab, E. J., J. Roennefarth, M. Becher, G. Blume-Werry, F. Keuper, J. Klaminder, J. Kreyling, K. Makoto, A. Milbau, and E. Dorrepaal. 2018. Winter warming effects on tundra shrub performance are species-specific and dependent on spring conditions. *Journal of Ecology* 106:599-612.
- Kreplin, H. N., C. S. Santos Ferreira, G. Destouni, S. D. Keesstra, L. Salvati, and Z. Kalantari. 2021. Arctic wetland system dynamics under climate warming. *Wiley Interdisciplinary Reviews: Water* 8:e1526.
- Kropp, H., M. M. Loranty, S. M. Natali, A. L. Kholodov, A. V. Rocha, I. Myers-Smith, B. W. Abbot, J. Abermann, E. Blanc-Betes, D. Blok, G. Blume-Werry, J. Boike, A. L. Breen, S. M. P. Cahoon, C. T. Christiansen, T. A. Douglas, H. E. Epstein, G. V. Frost, M. Goeckede, T. T. Hoye, S. D. Mamet, J. A. O'Donnell, D. Olefeldt, G. K. Phoenix, V. G. Salmon, A. B. K. Sannel, S. L. Smith, O. Sonnentag, L. S. Vaughn, M. Williams, B. Elberling, L. Gough, J. Hjort, P. M. Lafleur, E. S. Euskirchen, M. P. D. Heijmans, E. R. Humphreys, H. Iwata, B. M. Jones, M. T. Jorgenson, I. Grunberg, Y. Kim, J. Laundre, M. Mauritz, A. Michelsen, G. Schaepman-Strub, K. D. Tape, M. Ueyama, B. Y. Lee, K. Langley, and M. Lund. 2021. Shallow soils are warmer under trees and tall shrubs across Arctic and Boreal ecosystems. *Environmental Research Letters* 16:015001.
- Ksenofontov, S., N. Backhaus, and G. Schaepman-Strub. 2019. 'There are new species': indigenous knowledge of biodiversity change in Arctic Yakutia. *Polar Geography* 42:34-57.
- Kuhn, M., J. Wing, S. Weston, A. Williams, C. Keefer, A. Engelhardt, T. Cooper, Z. Mayer, B. Kenkel, R. C. Team, M. Benesty, R. Lescarbeau, A. Ziem, L. Scrucca, Y. Tang, C. Candan, and T. Hunt. 2020. Package "caret": Classification and Regression Training. R CRAN Project.
- Kuhry, P., B. J. Nicholson, L. D. Gignac, D. H. Vitt, and S. E. Bayley. 1993. Development of Sphagnum dominated peatlands in boreal continental Canada. *Canadian Journal of Botany* 71:10-22.
- Kwon, M. J., F. Beulig, I. Ilie, M. Wildner, K. Kysel, L. Merbold, M. D. Mahecha, N. Zimov, S. A. Zimov, and M. Heimann. 2017. Plants, microorganisms, and soil temperatures contribute to a decrease in methane fluxes on a drained Arctic floodplain. *Global Change Biology* 23:2396-2412.

L

- Lara, M. J., I. Nitzke, G. Grosse, P. Martin, and A. D. McGuire. 2018. Reduced arctic tundra productivity linked with landform and climate change interactions. *Scientific reports* 8:2345.
- Lawrence, D. M., C. D. Koven, S. C. Swenson, W. J. Riley, and A. Slater. 2015. Permafrost thaw and resulting soil moisture changes regulate projected high-latitude CO₂ and CH₄ emissions. *Environmental Research Letters* 10:094011.
- Lawrence, D. M., and S. C. Swenson. 2011. Permafrost response to increasing Arctic shrub

- abundance depends on the relative influence of shrubs on local soil cooling versus largescale climate warming. *Environmental Research Letters* 6:045504.
- Le Moullec, M., A. Buchwal, R. van der Wal, L. Sandal, and B. B. Hansen. 2019. Annual ring growth of a widespread high arctic shrub reflects past fluctuations in community-level plant biomass. *Journal of Ecology* 107:436-451.
- Lenth, R. 2018. Package ‘emmeans’: Estimated marginal means, aka least-squares means. R CRAN Project.
- Li, B. 2017. A clash of plants: Vegetation succession and its interaction with permafrost dynamics in the Arctic lowland tundra. [PhD Thesis. Wageningen University].
- Li, B., M. M. Heijmans, F. Berendse, D. Blok, T. Maximov, and U. Sass-Klaassen. 2016. The role of summer precipitation and summer temperature in establishment and growth of dwarf shrub *Betula nana* in northeast Siberian tundra. *Polar Biology* 39:1245-1255.
- Li, B., M. M. Heijmans, D. Blok, P. Wang, S. V. Karsanaev, T. C. Maximov, J. van Huissteden, and F. Berendse. 2017. Thaw pond development and initial vegetation succession in experimental plots at a Siberian lowland tundra site. *Plant and Soil* 420:147-162.
- Li, J., M. Holmgren, and C. Xu. 2021. Greening vs browning? Surface water cover mediates how tundra and boreal ecosystems respond to climate warming. *Environmental Research Letters* 16:104004.
- Liaw, A. 2018. package “randomForest”: Classification and regression based on a forest of trees using random inputs, based on Breiman (2001). R CRAN Project.
- Liljedahl, A. K., J. Boike, R. P. Daanen, A. N. Fedorov, G. V. Frost, G. Grosse, L. D. Hinzman, Y. Iijma, J. C. Jorgenson, and N. Matveyeva. 2016. Pan-Arctic ice-wedge degradation in warming permafrost and its influence on tundra hydrology. *Nature Geoscience* 9:312.
- Lin, D., D. Johnson, C. Andresen, and C. Tweedie. 2012. High spatial resolution decade-time scale land cover change at multiple locations in the Beringian Arctic (1948–2000s). *Environmental Research Letters* 7:025502.
- Löffler, J., and R. Pape. 2020. Thermal niche predictors of alpine plant species. *Ecology* 101:e02891.
- Loranty, M. M., B. W. Abbott, D. Blok, T. A. Douglas, H. E. Epstein, B. C. Forbes, B. M. Jones, A. L. Kholodov, H. Kropp, and A. Malhotra. 2018a. Reviews and syntheses: Changing ecosystem influences on soil thermal regimes in northern high-latitude permafrost regions. *Biogeosciences* 15:5287-5313.
- Loranty, M. M., S. P. Davydov, H. Kropp, H. D. Alexander, M. C. Mack, S. M. Natali, and N. S. Zimov. 2018b. Vegetation Indices Do Not Capture Forest Cover Variation in Upland Siberian Larch Forests. *Remote Sensing* 10:1686.
- Loranty, M. M., and S. J. Goetz. 2012. Shrub expansion and climate feedbacks in Arctic tundra. *Environmental Research Letters* 7:011005.
- Loranty, M. M., S. J. Goetz, and P. S. Beck. 2011. Tundra vegetation effects on pan-Arctic albedo. *Environmental Research Letters* 6:024014.
- Luo, D., H. Jin, V. F. Bense, X. Jin, and X. Li. 2020. Hydrothermal processes of near-surface warm permafrost in response to strong precipitation events in the Headwater Area of the Yellow River, Tibetan Plateau. *Geoderma* 376:114531.

M

- Macias-Fauria, M., B. C. Forbes, P. Zetterberg, and T. Kumpula. 2012. Eurasian Arctic greening reveals teleconnections and the potential for structurally novel ecosystems. *Nature Climate Change* 2:613-618.
- Macleod, R. D., and R. G. Congalton. 1998. A quantitative comparison of change-detection algorithms for monitoring eelgrass from remotely sensed data. *Photogrammetric engineering and remote sensing* 64:207-216.
- Magnússon, R. Í., A. Hamm, S. V. Karsanaev, J. Limpens, D. Kleijn, A. Frampton, T. C. Maximov, and M. M. Heijmans. 2022. Extremely wet summer events enhance permafrost thaw for multiple years in Siberian tundra. *Nature communications* 13:1-10.
- Magnússon, R. Í., J. Limpens, D. Kleijn, K. van Huissteden, T. C. Maximov, S. Lobry, and M. M. P. D. Heijmans. 2021. Shrub decline and expansion of wetland vegetation revealed by very high

References

- resolution land cover change detection in the Siberian lowland tundra. *Science of the Total Environment* 782:146877.
- Magnússon, R. Í., J. Limpens, J. van Huissteden, D. Kleijn, T. C. Maximov, R. Rotbarth, U. SassKlaassen, and M. M. P. D. Heijmans. 2020. Rapid vegetation succession and coupled permafrost dynamics in Arctic thaw ponds in the Siberian lowland tundra. *Journal of Geophysical Research: Biogeosciences* 125:e2019JG005618.
- Main-Knorn, M., B. Pflug, J. Louis, V. Debaecker, U. Müller-Wilm, and F. Gascon. 2017. Sen2Cor for sentinel-2. Page 1042704 in *Image and Signal Processing for Remote Sensing XXIII*. International Society for Optics and Photonics.
- Martin, A. C., E. S. Jeffers, G. Petrokofsky, I. Myers-Smith, and M. Macias-Fauria. 2017. Shrub growth and expansion in the Arctic tundra: an assessment of controlling factors using an evidencebased approach. *Environmental Research Letters* 12:085007.
- Mastepanov, M., C. Sigsgaard, E. J. Dlugokencky, S. Houweling, L. Ström, M. P. Tamstorf, and T. R. Christensen. 2008. Large tundra methane burst during onset of freezing. *Nature* 456:628-630.
- Matthews, B. W. 1975. Comparison of the predicted and observed secondary structure of T4 phage lysozyme. *Biochimica et Biophysica Acta (BBA)-Protein Structure* 405:442-451.
- MAXAR. n.d. Atmospheric Compensation - MAXAR AComp Pre-Processing.
- McGraw, J. B., and F. S. Chapin III. 1989. Competitive ability and adaptation to fertile and infertile soils in two *Eriophorum* species. *Ecology* 70:736-749.
- McGuire, A. D., D. M. Lawrence, C. Koven, J. S. Clein, E. Burke, G. Chen, E. Jafarov, A. H. MacDougall, S. Marchenko, and D. Nicolsky. 2018. Dependence of the evolution of carbon dynamics in the northern permafrost region on the trajectory of climate change. *Proceedings of the National Academy of Sciences* 115:3882-3887.
- Mekonnen, Z. A., W. J. Riley, L. T. Berner, N. J. Bouskill, M. S. Torn, G. Iwahana, A. L. Breen, I. H. Myers-Smith, M. G. Criado, and Y. Liu. 2021a. Arctic tundra shrubification: a review of mechanisms and impacts on ecosystem carbon balance. *Environmental Research Letters* 16:053001.
- Mekonnen, Z. A., W. J. Riley, R. F. Grant, and V. E. Romanovsky. 2021b. Changes in precipitation and air temperature contribute comparably to permafrost degradation in a warmer climate. *Environmental Research Letters* 16:024008.
- Meredith, M., M. Sommerkorn, S. Cassotta, C. Derksen, A. Ekaykin, A. Hollowed, G. Kofinas, A. Mackintosh, J. Melbourne-Thomas, M. M. C. Muelbert, G. Ottersen, H. Pritchard, and E. A. G. Schuur. 2019. Polar Regions. In: *IPCC Special Report on the Ocean and Cryosphere in a Changing Climate* in D. C. R. [H.-O. Pörtner, V. Masson-Delmotte, P. Zhai, M. Tignor, E. Poloczanska, K. Mintenbeck, A. Alegría, M. Nicolai, A. Okem, J. Petzold, B. Rama, N.M. Weyer (eds)].
- Miner, K. R., M. R. Turetsky, E. Malina, A. Bartsch, J. Tamminen, A. D. McGuire, A. Fix, C. Sweeney, C. D. Elder, and C. E. Miller. 2022. Permafrost carbon emissions in a changing Arctic. *Nature Reviews Earth & Environment* 3:55-67.
- Minke, M., N. Donner, N. Karpov, P. de Klerk, and H. Joosten. 2009. Patterns in vegetation composition, surface height and thaw depth in polygon mires in the Yakutian Arctic (NE Siberia): a microtopographical characterisation of the active layer. *Permafrost and Periglacial Processes* 20:357-368.
- Morgenstern, A., G. Grosse, F. Günther, I. Fedorova, and L. Schirrmeister. 2011. Spatial analyses of thermokarst lakes and basins in Yedoma landscapes of the Lena Delta. *The Cryosphere* 5:849-867.
- Morgenstern, A., M. Ulrich, F. Günther, S. Roessler, I. V. Fedorova, N. A. Rudaya, S. Wetterich, J. Boike, and L. Schirrmeister. 2013. Evolution of thermokarst in East Siberian ice-rich permafrost: A case study. *Geomorphology* 201:363-379.
- Morozumi, T., R. Shingubara, R. Suzuki, H. Kobayashi, S. Tei, S. Takano, R. Fan, M. Liang, T. Maximov, and A. Sugimoto. 2019. Estimating methane emissions using vegetation mapping in the taiga-tundra boundary of a north-eastern Siberian lowland. *Tellus B: Chemical and Physical Meteorology* 71:1581004.
- Muller, M. R., and J. Middleton. 1994. A Markov model of land-use change dynamics in the Niagara

Chapter 9

- Region, Ontario, Canada. *Landscape ecology* 9:151-157.
- Muller, S. 1947. Permafrost or permanently frozen ground and related engineering problems. JW Edwards. Ann Arbor.
- Muster, S., B. Heim, A. Abnizova, and J. Boike. 2013. Water body distributions across scales: A remote sensing based comparison of three arctic tundra wetlands. *Remote Sensing* 5:1498-1523.
- Myers-Smith, I., J. Harden, M. Wilmsking, C. Fuller, A. McGuire, and F. Chapin Iii. 2008. Wetland succession in a permafrost collapse: interactions between fire and thermokarst. *Biogeosciences* 5:1273-1286.
- Myers-Smith, I. H., S. C. Elmendorf, P. S. Beck, M. Wilmsking, M. Hallinger, D. Blok, K. D. Tape, S. A. Rayback, M. Macias-Fauria, and B. C. Forbes. 2015a. Climate sensitivity of shrub growth across the tundra biome. *Nature Climate Change* 5:887.
- Myers-Smith, I. H., B. C. Forbes, M. Wilmsking, M. Hallinger, T. Lantz, D. Blok, K. D. Tape, M. MaciasFauria, U. Sass-Klaassen, E. Levesque, S. Boudreau, P. Ropars, L. Hermanutz, A. Trant, L. S. Collier, S. Weijers, J. Rozema, S. A. Rayback, N. M. Schmidt, G. Schaepman-Strub, S. Wipf, C. Rixen, C. B. Menard, S. Venn, S. Goetz, L. Andreu-Hayles, S. Elmendorf, V. Ravolainen, J. Welker, P. Grogan, H. E. Epstein, and D. S. Hik. 2011. Shrub expansion in tundra ecosystems: dynamics, impacts and research priorities. *Environmental Research Letters* 6:045509.
- Myers-Smith, I. H., M. M. Grabowski, H. J. D. Thomas, S. Angers-Blondin, G. N. Daskalova, A. D. Bjorkman, A. M. Cunliffe, J. J. Assmann, J. S. Boyle, E. McLeod, S. McLeod, R. Joe, P. Lennie, D. Arey, R. R. Gordon, and C. D. Eckert. 2019. Eighteen years of ecological monitoring reveals multiple lines of evidence for tundra vegetation change. *Ecological Monographs* 89:e01351.
- Myers-Smith, I. H., M. Hallinger, D. Blok, U. Sass-Klaassen, S. A. Rayback, S. Weijers, A. J. Trant, K. D. Tape, A. T. Naito, and S. Wipf. 2015b. Methods for measuring arctic and alpine shrub growth: a review. *Earth-Science Reviews* 140:1-13.
- Myers-Smith, I. H., J. T. Kerby, G. K. Phoenix, J. W. Bjerke, H. E. Epstein, J. J. Assmann, C. John, L. Andreu-Hayles, S. Angers-Blondin, P. S. A. Beck, L. T. Berner, U. S. Bhatt, A. D. Bjorkman, D. Blok, A. Bryn, C. T. Christiansen, J. H. C. Cornelissen, A. M. Cunliffe, S. C. Elmendorf, B. C. Forbes, S. J. Goetz, R. D. Hollister, R. de Jong, M. M. Loranty, M. Macias-Fauria, K. Maseyk, S. Normand, J. Olofsson, T. C. Parker, F.-J. W. Parmentier, E. Post, G. Schaepman-Strub, F. Stordal, P. F. Sullivan, H. J. D. Thomas, H. Tømmervik, R. Treharne, C. E. Tweedie, D. A. Walker, M. Wilmsking, and S. Wipf. 2020. Complexity revealed in the greening of the Arctic. *Nature Climate Change* 10:106-117.
- Myers-Smith, I. H., and D. S. Hik. 2013. Shrub canopies influence soil temperatures but not nutrient dynamics: an experimental test of tundra snow–shrub interactions. *Ecology and Evolution* 3:3683-3700.

N

- Naito, A. T., and D. M. Cairns. 2011. Relationships between Arctic shrub dynamics and topographically derived hydrologic characteristics. *Environmental Research Letters* 6:045506.
- Nakagawa, S., P. C. Johnson, and H. Schielzeth. 2017. The coefficient of determination R^2 and intraclass correlation coefficient from generalized linear mixed-effects models revisited and expanded. *Journal of the Royal Society Interface* 14:20170213.
- Natali, S. M., J. P. Holdren, B. M. Rogers, R. Treharne, P. B. Duffy, R. Pomerance, and E. MacDonald. 2021. Permafrost carbon feedbacks threaten global climate goals. *Proceedings of the National Academy of Sciences* 118:e2100163118.
- National Academies of Sciences, E., and Medicine. 2019. *Understanding Northern Latitude Vegetation Greening and Browning: Proceedings of a Workshop*. The National Academies Press, Washington, DC.
- Nauta, A. L., M. M. Heijmans, D. Blok, J. Limpens, B. Elberling, A. Gallagher, B. Li, R. E. Petrov, T. C. Maximov, and J. Van Huissteden. 2015. Permafrost collapse after shrub removal shifts tundra ecosystem to a methane source. *Nature Climate Change* 5:67.
- Neumann, R. B., C. J. Moorberg, J. D. Lundquist, J. C. Turner, M. P. Waldrop, J. W. McFarland, E. S.

References

- Euskirchen, C. W. Edgar, and M. R. Turetsky. 2019. Warming effects of spring rainfall increase methane emissions from thawing permafrost. *Geophysical Research Letters* 46:1393-1401.
- Neuwirth, B., F. H. Schweingruber, and M. Winiger. 2007. Spatial patterns of central European pointer years from 1901 to 1971. *Dendrochronologia* 24:79-89.
- Nitzbon, J., S. Westermann, M. Langer, L. C. P. Martin, J. Strauss, S. Laboor, and J. Boike. 2020. Fast response of cold ice-rich permafrost in northeast Siberia to a warming climate. *Nature communications* 11:2201.
- Nitze, I., and G. Grosse. 2016. Detection of landscape dynamics in the Arctic Lena Delta with temporally dense Landsat time-series stacks. *Remote sensing of Environment* 181:27-41.
- Notz, D., and J. Stroeve. 2016. Observed Arctic sea-ice loss directly follows anthropogenic CO₂ emission. *science* 354:747-750.
- O**
- O'Donnell, J., J. W. Harden, A. D. McGuire, and V. Romanovsky. 2011. Exploring the sensitivity of soil carbon dynamics to climate change, fire disturbance and permafrost thaw in a black spruce ecosystem. *Biogeosciences* 8:1367-1382.
- Oberbauer, S., S. Elmendorf, T. Troxler, R. Hollister, A. Rocha, M. Bret-Harte, M. Dawes, A. Fosaa, G. Henry, and T. Høye. 2013. Phenological response of tundra plants to background climate variation tested using the International Tundra Experiment. *Philosophical Transactions of the Royal Society B: Biological Sciences* 368:20120481.
- Oksanen, J., F. G. Blanchet, R. Kindt, P. Legendre, P. R. Minchin, R. O'hara, G. L. Simpson, P. Solymos, M. H. H. Stevens, and H. Wagner. 2015. Package 'vegan': Community ecology package. R CRAN Project.
- Olefeldt, D., S. Goswami, G. Grosse, D. Hayes, G. Hugelius, P. Kuhry, A. D. McGuire, V. Romanovsky, A. B. K. Sannel, and E. Schuur. 2016. Circumpolar distribution and carbon storage of thermokarst landscapes. *Nature communications* 7:13043.
- Opala-Owczarek, M., E. Pirożnikow, P. Owczarek, W. Szymański, B. Luks, D. Kępski, M. Szymanowski, B. Wojtuń, and K. Migala. 2018. The influence of abiotic factors on the growth of two vascular plant species (*Saxifraga oppositifolia* and *Salix polaris*) in the High Arctic. *Catena* 163:219-232.
- Osorio, F., R. Vallejos, F. Cuevas, D. Mancilla, and M. F. Osorio. 2020. Package 'SpatialPack'. R CRAN Project.
- Osterkamp, T., M. Jorgenson, E. Schuur, Y. Shur, M. Kanevskiy, J. Vogel, and V. Tumskoy. 2009. Physical and ecological changes associated with warming permafrost and thermokarst in interior Alaska. *Permafrost and Periglacial Processes* 20:235-256.
- Overland, J. E. 2020. Less climatic resilience in the Arctic. *Weather and Climate Extremes* 30:100275.
- Overland, J. E., and M. Wang. 2021. The 2020 Siberian heat wave. *International Journal of Climatology* 41:E2341-E2346.
- P**
- Pacifici, F., N. Longbotham, and W. J. Emery. 2014. The importance of physical quantities for the analysis of multitemporal and multiangular optical very high spatial resolution images. *IEEE transactions on geoscience and remote sensing* 52:6241-6256.
- Painter, S. L., E. T. Coon, A. L. Atchley, M. Berndt, R. Garimella, J. D. Moulton, D. Svyatskiy, and C. J. Wilson. 2016. Integrated surface/subsurface permafrost thermal hydrology: Model formulation and proof-of-concept simulations. *Water Resources Research* 52:6062-6077.
- Parmentier, F.-J. W., J. v. Huissteden, N. Kip, H. Op den Camp, M. Jetten, T. Maximov, and A. Dolman. 2011a. The role of endophytic methane oxidizing bacteria in submerged Sphagnum in determining methane emissions of Northeastern Siberian tundra. *Biogeosciences* 8:1267-1278.
- Parmentier, F., M. Van Der Molen, J. Van Huissteden, S. Karsanaev, A. Kononov, D. Suzdalov, T. Maximov, and A. Dolman. 2011b. Longer growing seasons do not increase net carbon uptake

- in the northeastern Siberian tundra. *Journal of Geophysical Research: Biogeosciences* 116:G04013.
- Payette, S., A. Delwaide, M. Caccianiga, and M. Beauchemin. 2004. Accelerated thawing of subarctic peatland permafrost over the last 50 years. *Geophysical Research Letters* 31:L18208.
- Pearson, R. G., S. J. Phillips, M. M. Lorant, P. S. Beck, T. Damoulas, S. J. Knight, and S. J. Goetz. 2013. Shifts in Arctic vegetation and associated feedbacks under climate change. *Nature Climate Change* 3:673-677.
- Pekel, J.-F., A. Cottam, N. Gorelick, and A. S. Belward. 2016. High-resolution mapping of global surface water and its long-term changes. *Nature* 540:418-422.
- Peterson, K., and W. Billings. 1980. Tundra vegetational patterns and succession in relation to microtopography near Atkasook, Alaska. *Arctic and Alpine Research* 12:473-482.
- Phillips, M. E. 1954. *Eriophorum Angustifolium* Roth. *Journal of Ecology* 42:612-622.
- Phoenix, G. K., and J. W. Bjerke. 2016. Arctic browning: extreme events and trends reversing arctic greening. *Global Change Biology* 22:2960-2962.
- Piao, S., H. Nan, C. Huntingford, P. Ciais, P. Friedlingstein, S. Sitch, S. Peng, A. Ahlström, J. G. Canadell, and N. Cong. 2014. Evidence for a weakening relationship between interannual temperature variability and northern vegetation activity. *Nature communications* 5:1-7.
- Plug, L. J., C. Walls, and B. Scott. 2008. Tundra lake changes from 1978 to 2001 on the Tuktoyaktuk Peninsula, western Canadian Arctic. *Geophysical Research Letters* 35:L03502.
- Podger, N. E., W. Colwell, and M. Taylor. 2011. GeoEye-1 radiance at aperture and planetary reflectance. *GeoEye*.
- Porter, C., P. Morin, I. Howat, M.-J. Noh, B. Bates, K. Peterman, S. Keese, M. Schlenk, J. Gardiner, and K. Tomko. 2018. ArcticDEM. *Harvard Dataverse* 1:2018-2030.2008.
- Potts, R. 1952. Some generalized order-disorder transformations. Pages 106-109 in *Mathematical proceedings of the Cambridge philosophical society*. Cambridge University Press.

R

- R Development Core Team. 2019. R: A language and environment for statistical computing. R Foundation for Statistical Computing, Vienna, Austria.
- Raynolds, M. K., and D. A. Walker. 2016. Increased wetness confounds Landsat-derived NDVI trends in the central Alaska North Slope region, 1985–2011. *Environmental Research Letters* 11:085004.
- Raynolds, M. K., D. A. Walker, K. J. Ambrosius, J. Brown, K. R. Everett, M. Kanevskiy, G. P. Kofinas, V. E. Romanovsky, Y. Shur, and P. J. Webber. 2014. Cumulative geocological effects of 62 years of infrastructure and climate change in ice-rich permafrost landscapes, Prudhoe Bay Oilfield, Alaska. *Global Change Biology* 20:1211-1224.
- Raynolds, M. K., D. A. Walker, A. Balsler, C. Bay, M. Campbell, M. M. Cherosov, F. J. Daniëls, P. B. Eidesen, K. A. Ermokhina, and G. V. Frost. 2019. A raster version of the Circumpolar Arctic Vegetation Map (CAVM). *Remote sensing of Environment* 232:111297.
- Regmi, P., G. Grosse, M. Jones, B. Jones, and K. Anthony. 2012. Characterizing post-drainage succession in thermokarst lake basins on the Seward Peninsula, Alaska with TerraSAR-X backscatter and Landsat-based NDVI data. *Remote Sensing* 4:3741-3765.
- Richter-Menge, J., M. L. Druckenmiller, J. Andersen, L. M. Andreassen, E. H. Baker, T. J. Ballinger, L. T. Berner, G. H. Bernhard, U. S. Bhatt, and J. W. Bjerke. 2020. The Arctic. *Bulletin of the American Meteorological Society* 101:S239-S286.
- RIHMI-WDC. 2020. All-Russian Research Institute of Hydrometeorological Information - World Data Centre. <http://aisori-m.meteo.ru/waisori/>.
- Rinntech. 2017. TSAP-Win. RINNTECH, Heidelberg, Germany.
- Roach, J., B. Griffith, D. Verbyla, and J. Jones. 2011. Mechanisms influencing changes in lake area in Alaskan boreal forest. *Global Change Biology* 17:2567-2583.
- Robinson, S. D., and T. Moore. 2000. The influence of permafrost and fire upon carbon accumulation in high boreal peatlands, Northwest Territories, Canada. *Arctic, Antarctic, and Alpine Research* 32:155-166.
- Rodenhizer, H., J. Ledman, M. Mauritz, S. M. Natali, E. Pegoraro, C. Plaza, E. Romano, C. Schädel, M.

References

- Taylor, and E. Schuur. 2020. Carbon Thaw Rate Doubles When Accounting for Subsidence in a Permafrost Warming Experiment. *Journal of Geophysical Research: Biogeosciences* 125:e2019JG005528.
- Romanovsky, V. E., S. L. Smith, and H. H. Christiansen. 2010. Permafrost thermal state in the polar Northern Hemisphere during the international polar year 2007–2009: a synthesis. *Permafrost and Periglacial Processes* 21:106-116.
- Ropars, P., E. Lévesque, and S. Boudreau. 2015. How do climate and topography influence the greening of the forest-tundra ecotone in northern Québec? A dendrochronological analysis of *Betula glandulosa*. *Journal of Ecology* 103:679-690.
- Routh, J., G. Hugelius, P. Kuhry, T. Filley, P. K. Tillman, M. Becher, and P. Crill. 2014. Multi-proxy study of soil organic matter dynamics in permafrost peat deposits reveal vulnerability to climate change in the European Russian Arctic. *Chemical geology* 368:104-117.
- Roy, D. P., V. Kovalsky, H. Zhang, E. F. Vermote, L. Yan, S. Kumar, and A. Egorov. 2016. Characterization of Landsat-7 to Landsat-8 reflective wavelength and normalized difference vegetation index continuity. *Remote sensing of Environment* 185:57-70.

S

- Schirrneister, L., D. Froese, V. Tumskoy, G. Grosse, and S. Wetterich. 2013. Yedoma: Late Pleistocene ice-rich syngenetic permafrost of Beringia. *Encyclopedia of Quaternary Science*. 2nd edition:542-552.
- Schubert, P., L. Eklundh, M. Lund, and M. Nilsson. 2010. Estimating northern peatland CO₂ exchange from MODIS time series data. *Remote sensing of Environment* 114:1178-1189.
- Schuh, C., A. Frampton, and H. H. Christiansen. 2017. Soil moisture redistribution and its effect on inter-annual active layer temperature and thickness variations in a dry loess terrace in Adventdalen, Svalbard. *The Cryosphere* 11:635-651.
- Schuur, E. A., J. Bockheim, J. G. Canadell, E. Euskirchen, C. B. Field, S. V. Goryachkin, S. Hagemann, P. Kuhry, P. M. Laflour, and H. Lee. 2008. Vulnerability of permafrost carbon to climate change: Implications for the global carbon cycle. *Bioscience* 58:701-714.
- Schuur, E. A., and M. C. Mack. 2018. Ecological response to permafrost thaw and consequences for local and global ecosystem services. *Annual Review of Ecology, Evolution, and Systematics* 49:279-301.
- Schuur, E. A., A. D. McGuire, C. Schädel, G. Grosse, J. Harden, D. J. Hayes, G. Hugelius, C. Koven, P. Kuhry, and D. M. Lawrence. 2015. Climate change and the permafrost carbon feedback. *Nature* 520:171.
- Screen, J. A., and I. Simmonds. 2010. The central role of diminishing sea ice in recent Arctic temperature amplification. *Nature* 464:1334-1337.
- Sen, P. K. 1968. Estimates of the regression coefficient based on Kendall's tau. *Journal of the American statistical association* 63:1379-1389.
- Seppala, M. 1988. Palsas and related forms. *Advances in Periglacial Geomorphology*: 247-277.
- Serra, P., X. Pons, and D. Saurí. 2003. Post-classification change detection with data from different sensors: Some accuracy considerations. *International Journal of Remote Sensing* 24:3311-3340.
- Shiklomanov, N. I., D. A. Streletskiy, and F. E. Nelson. 2012. Northern hemisphere component of the global circumpolar active layer monitoring (CALM) program. Pages 377-382 in *Proc. 10th Int. Conf. on Permafrost*.
- Shkolnik, I., T. Pavlova, S. Efimov, and S. Zhuravlev. 2018. Future changes in peak river flows across northern Eurasia as inferred from an ensemble of regional climate projections under the IPCC RCP8.5 scenario. *Climate dynamics* 50:215-230.
- Shur, Y., K. M. Hinkel, and F. E. Nelson. 2005. The transient layer: implications for geocryology and climate-change science. *Permafrost and Periglacial Processes* 16:5-17.
- Shur, Y., M. T. Jorgenson, and M. Z. Kanevskiy. 2011. Permafrost. Pages 841-848 in V. P. Singh, P. Singh, and U. K. Haritashya, editors. *Encyclopedia of Snow, Ice and Glaciers*. Springer Netherlands, Dordrecht.
- Siewert, M. B., J. Hanisch, N. Weiss, P. Kuhry, T. C. Maximov, and G. Hugelius. 2015. Comparing

- carbon storage of Siberian tundra and taiga permafrost ecosystems at very high spatial resolution. *Journal of Geophysical Research: Biogeosciences* 120:1973-1994.
- Singh, A. 1989. Review article digital change detection techniques using remotely-sensed data. *International Journal of Remote Sensing* 10:989-1003.
- Slater, A. G., and D. M. Lawrence. 2013. Diagnosing present and future permafrost from climate models. *Journal of Climate* 26:5608-5623.
- Smith, S. L., H. B. O'Neill, K. Isaksen, J. Noetzli, and V. E. Romanovsky. 2022. The changing thermal state of permafrost. *Nature Reviews Earth & Environment* 3:10-23.
- Solberg, A. H. S., T. Taxt, and A. K. Jain. 1996. A Markov random field model for classification of multisource satellite imagery. *IEEE transactions on geoscience and remote sensing* 34:100-113.
- Song, C., C. E. Woodcock, K. C. Seto, M. P. Lenney, and S. A. Macomber. 2001. Classification and change detection using Landsat TM data: when and how to correct atmospheric effects? *Remote sensing of Environment* 75:230-244.
- Soudzilovskaia, N. A., P. M. Bodegom, and J. H. Cornelissen. 2013. Dominant bryophyte control over high-latitude soil temperature fluctuations predicted by heat transfer traits, field moisture regime and laws of thermal insulation. *Functional Ecology* 27:1442-1454.
- Stieglitz, M., S. Déry, V. Romanovsky, and T. Osterkamp. 2003. The role of snow cover in the warming of arctic permafrost. *Geophysical Research Letters* 30:1721.
- Stier, A. C., S. W. Geange, K. M. Hanson, and B. M. Bolker. 2013. Predator density and timing of arrival affect reef fish community assembly. *Ecology* 94:1057-1068.
- Stocker, T. F., D. Qin, G.-K. Plattner, M. Tignor, S. K. Allen, J. Boschung, A. Nauels, Y. Xia, B. Bex, and B. Midgley. 2013. IPCC, 2013: climate change 2013: the physical science basis. Contribution of working group I to the fifth assessment report of the intergovernmental panel on climate change. Cambridge University Press.
- Storey, J., J. Lacasse, R. Smilek, T. Zeiler, P. Scaramuzza, R. Rengarajan, and M. Choate. 2005. Image Impact of the Landsat 7 ETM+ Scan Line Corrector Failure.
- Ström, L., M. Mastepanov, and T. R. Christensen. 2005. Species-specific effects of vascular plants on carbon turnover and methane emissions from wetlands. *Biogeochemistry* 75:65-82.
- Ström, L., T. Tagesson, M. Mastepanov, and T. R. Christensen. 2012. Presence of *Eriophorum scheuchzeri* enhances substrate availability and methane emission in an Arctic wetland. *Soil Biology and Biochemistry* 45:61-70.
- Sturm, M., J. P. McFadden, G. E. Liston, F. S. Chapin, C. H. Racine, and J. Holmgren. 2001. Snow-shrub interactions in Arctic tundra: A hypothesis with climatic implications. *Journal of Climate* 14:336-344.
- Sturm, M., J. Schimel, G. Michaelson, J. M. Welker, S. F. Oberbauer, G. E. Liston, J. Fahnestock, and V. E. Romanovsky. 2005. Winter biological processes could help convert arctic tundra to shrubland. *Bioscience* 55:17-26.
- Subin, Z. M., C. D. Koven, W. J. Riley, M. S. Torn, D. M. Lawrence, and S. C. Swenson. 2013. Effects of soil moisture on the responses of soil temperatures to climate change in cold regions. *Journal of Climate* 26:3139-3158.
- Sundh, I., C. Mikkelä, M. Nilsson, and B. H. Svensson. 1995. Potential aerobic methane oxidation in a Sphagnum-dominated peatland—Controlling factors and relation to methane emission. *Soil Biology and Biochemistry* 27:829-837.

T

- Tape, K., M. Sturm, and C. Racine. 2006. The evidence for shrub expansion in Northern Alaska and the Pan-Arctic. *Global Change Biology* 12:686-702.
- Tape, K. D., M. Hallinger, J. M. Welker, and R. W. Ruess. 2012. Landscape heterogeneity of shrub expansion in Arctic Alaska. *Ecosystems* 15:711-724.
- Tarnocai, C., J. Canadell, E. A. Schuur, P. Kuhry, G. Mazhitova, and S. Zimov. 2009. Soil organic carbon pools in the northern circumpolar permafrost region. *Global biogeochemical cycles* 23.
- Tei, S., T. Morozumi, S. Nagai, S. Takano, A. Sugimoto, R. Shingubara, R. Fan, A. Fedorov, T. Gavril'yeva, and N. Tananaev. 2020. An extreme flood caused by a heavy snowfall over the

References

- Indigirka River basin in Northeastern Siberia. *Hydrological Processes* 34:522-537.
- Teltewskoi, A., F. Beermann, I. Beil, A. Bobrov, P. De Klerk, S. Lorenz, A. Lüder, D. Michaelis, and H. Joosten. 2016. 4000 years of changing wetness in a permafrost polygon peatland (Kytalyk, NE Siberia): A comparative high-resolution multi-proxy study. *Permafrost and Periglacial Processes* 27:76-95.
- Theil, H. 1950. A rank-invariant method of linear and polynomial regression analysis. *Indagationes Mathematicae* 12:173.
- Thévenot, E. A. 2016. Package 'ropls': PCA, PLS (-DA) and OPLS (-DA) for multivariate analysis and feature selection of omics data. R CRAN Project.
- Thévenot, E. A., A. Roux, Y. Xu, E. Ezan, and C. Junot. 2015. Analysis of the Human Adult Urinary Metabolome Variations with Age, Body Mass Index, and Gender by Implementing a Comprehensive Workflow for Univariate and OPLS Statistical Analyses. *Journal of Proteome Research* 14:3322-3335.
- Treat, C. C., M. C. Jones, P. Camill, A. Gallego-Sala, M. Garneau, J. W. Harden, G. Hugelius, E. Klein, U. Kokfelt, and P. Kuhry. 2016. Effects of permafrost aggradation on peat properties as determined from a pan-Arctic synthesis of plant macrofossils. *Journal of Geophysical Research: Biogeosciences* 121:78-94.
- Treharne, R., J. W. Bjerke, H. Tømmervik, L. Stendardi, and G. K. Phoenix. 2019. Arctic browning: Impacts of extreme climatic events on heathland ecosystem CO₂ fluxes. *Global Change Biology* 25:489-503.
- Tremblay, B., E. Lévesque, and S. Boudreau. 2012. Recent expansion of erect shrubs in the Low Arctic: evidence from Eastern Nunavik. *Environmental Research Letters* 7:035501.
- Troeva, E. I., A. P. Isaev, M. M. Cherosov, and N. Karpov. 2010. *The Far North: Plant Biodiversity and Ecology of Yakutia*. Springer Science & Business Media.
- Trouet, V., and G. J. Van Oldenborgh. 2013. KNMI Climate Explorer: a web-based research tool for high-resolution paleoclimatology. *Tree-ring research* 69:3-14.
- Trouillier, M., V. der Maaten-Theunissen, J. E. Harvey, D. Würth, M. Schnittler, and M. Wilmking. 2018. Visualizing individual tree differences in tree-ring studies. *Forests* 9:216.
- Trygg, J., and S. Wold. 2002. Orthogonal projections to latent structures (O-PLS). *Journal of Chemometrics* 16:119-128.
- Tucker, C. J. 1979. Red and photographic infrared linear combinations for monitoring vegetation. *Remote sensing of Environment* 8:127-150.
- Turetsky, M., R. Wieder, D. Vitt, R. Evans, and K. Scott. 2007. The disappearance of relict permafrost in boreal north America: Effects on peatland carbon storage and fluxes. *Global Change Biology* 13:1922-1934.
- Turetsky, M. R., B. W. Abbott, M. C. Jones, K. W. Anthony, D. Olefeldt, E. A. Schuur, C. Koven, A. D. McGuire, G. Grosse, and P. Kuhry. 2019. Permafrost collapse is accelerating carbon release. *Nature* 569:32-34.
- Turetsky, M. R., B. W. Abbott, M. C. Jones, K. W. Anthony, D. Olefeldt, E. A. G. Schuur, G. Grosse, P. Kuhry, G. Hugelius, C. Koven, D. M. Lawrence, C. Gibson, A. B. K. Sannel, and A. D. McGuire. 2020. Carbon release through abrupt permafrost thaw. *Nature Geoscience* 13:138-143.
- Turetsky, M. R., A. Kotowska, J. Bubier, N. B. Dise, P. Crill, E. R. Hornibrook, K. Minkinen, T. R. Moore, I. H. Myers-Smith, and H. Nykänen. 2014. A synthesis of methane emissions from 71 northern, temperate, and subtropical wetlands. *Global Change Biology* 20:2183-2197.

U

- Updike, T., and C. Comp. 2010. Radiometric use of WorldView-2 imagery. Technical Note. DigitalGlobe.
- USDA-ARS, U. S. S. L. 2019. ROSETTA Class Average Hydraulic Parameters. in A. W. E. a. S. R. Unit, editor. U.S. DEPARTMENT OF AGRICULTURE Agricultural Research Service, Riverside, California.

V

- van Breemen, N. 1995. How Sphagnum bogs down other plants. *Trends in ecology & evolution* 10:270-275.
- van der Kolk, H.-J., M. M. Heijmans, J. van Huissteden, J. W. Pullens, and F. Berendse. 2016. Potential Arctic tundra vegetation shifts in response to changing temperature, precipitation and permafrost thaw. *Biogeosciences* 13:6229-6245.
- van der Maaten-Theunissen, M., E. van der Maaten, and O. Bouriaud. 2015. pointRes: An R package to analyze pointer years and components of resilience. *Dendrochronologia* 35:34-38.
- van der Molen, M., J. Van Huissteden, F. Parmentier, A. Petrescu, A. Dolman, T. Maximov, A. Kononov, S. Karsanaev, and D. Suzdalov. 2007. The growing season greenhouse gas balance of a continental tundra site in the Indigirka lowlands, NE Siberia. *Biogeosciences* 4:985-1003
- van Everdingen, R. O. 2005. Multi-language glossary of permafrost and related ground-ice terms. National Snow and Ice Data Center/World Data Center for Glaciology, Boulder, Boulder, USA.
- van Huissteden, J. 2020. Thawing Permafrost: Permafrost Carbon in a Warming Arctic. Springer Nature.
- van Huissteden, J., and L. Belleli Marchesini. 2014. Geomorphological and cryological map of Kytalyk, Russia, links to shapefiles. PANGAEA.
- van Huissteden, J., and A. Dolman. 2012. Soil carbon in the Arctic and the permafrost carbon feedback. *Current Opinion in Environmental Sustainability* 4:545-551.
- van Huissteden, J., T. Maximov, and A. Dolman. 2005. High methane flux from an arctic floodplain (Indigirka lowlands, eastern Siberia). *Journal of Geophysical Research: Biogeosciences* 110:G02002.
- van Huissteden, J., T. Maximov, and A. Dolman. 2009. Correction to “High methane flux from an arctic floodplain (Indigirka lowlands, eastern Siberia)”. *Journal of Geophysical Research: Biogeosciences* 114: G02002.
- van Huissteden, J., K. Teshebaeva, Y. Cheung, R. Í. Magnússon, H. Noorbergen, S. V. Karsanaev, T. C. Maximov, and A. J. Dolman. 2021. Geomorphology and InSAR-Tracked Surface Displacements in an Ice-Rich Yedoma Landscape. *Frontiers in Earth Science* 9:680565.
- van Huissteden, J. H., MMPD, J. Dean, O. Meisel, A. Goovaerts, F. Parmentier, G. Schaepman-Strub, L. Belleli Marchesini, A. Kononov, T. Maximov, A. Borges, and S. Bouillon. 2017. Thaw pond dynamics and carbon emissions in a Siberian lowland tundra landscape. Page 5661 in EGU General Assembly. European Geophysics Union, Vienna.
- Verdonen, M., L. T. Berner, B. C. Forbes, and T. Kumpula. 2020. Periglacial vegetation dynamics in Arctic Russia: decadal analysis of tundra regeneration on landslides with time series satellite imagery. *Environmental Research Letters* 15:105020.
- Vicente-Serrano, S. M., S. Beguería, and J. I. López-Moreno. 2010. A Multiscalar Drought Index Sensitive to Global Warming: The Standardized Precipitation Evapotranspiration Index. *Journal of Climate* 23:1696-1718.
- Virkkala, A.-M., A. M. Abdi, M. Luoto, and D. B. Metcalfe. 2019. Identifying multidisciplinary research gaps across Arctic terrestrial gradients. *Environmental Research Letters* 14:124061.
- Voelker, S. L. 2011. Age-Dependent Changes in Environmental Influences on Tree Growth and Their Implications for Forest Responses to Climate Change. Pages 455-479 in F. C. Meinzer, B. Lachenbruch, and T. E. Dawson, editors. *Size- and Age-Related Changes in Tree Structure and Function*. Springer Netherlands, Dordrecht.
- Voigt, C., R. E. Lamprecht, M. E. Marushchak, S. E. Lind, A. Novakovskiy, M. Aurela, P. J. Martikainen, and C. Biasi. 2017. Warming of subarctic tundra increases emissions of all three important greenhouse gases - carbon dioxide, methane, and nitrous oxide. *Global Change Biology* 23:3121-3138.
- Vonk, J. E., S. Tank, and M. A. Walvoord. 2019. Integrating hydrology and biogeochemistry across frozen landscapes. *Nature communications* 10:1-4.

References

W

- Walker, D. A., M. K. Raynolds, F. J. Daniëls, E. Einarsson, A. Elvebakk, W. A. Gould, A. E. Katenin, S. S. Kholod, C. J. Markon, and E. S. Melnikov. 2005. The circumpolar Arctic vegetation map. *Journal of Vegetation Science* 16:267-282.
- Walker, M., D. A. Walker, and K. R. Everett. 1989. Wetland soils and vegetation, arctic foothills, Alaska. US Department of the Interior, Fish and Wildlife Service, Research and Development Washington, DC. Biological Report 89(7)
- Walker, M. D., C. H. Wahren, R. D. Hollister, G. H. Henry, L. E. Ahlquist, J. M. Alatalo, M. S. Bret-Harte, M. P. Calef, T. V. Callaghan, and A. B. Carroll. 2006. Plant community responses to experimental warming across the tundra biome. *Proceedings of the National Academy of Sciences* 103:1342-1346.
- Walker, M. D., D. A. Walker, and N. A. Auerbach. 1994. Plant communities of a tussock tundra landscape in the Brooks Range Foothills, Alaska. *Journal of Vegetation Science* 5:843-866.
- Walsh, J. E., T. J. Ballinger, E. S. Euskirchen, E. Hanna, J. Mård, J. E. Overland, H. Tangen, and T. Vihma. 2020. Extreme weather and climate events in northern areas: A review. *EarthScience Reviews* 209:103324.
- Walter, K. M., S. Zimov, J. P. Chanton, D. Verbyla, and F. S. Chapin III. 2006. Methane bubbling from Siberian thaw lakes as a positive feedback to climate warming. *Nature* 443:71.
- Walvoord, M. A., and B. L. Kurylyk. 2016. Hydrologic impacts of thawing permafrost—A review. *Vadose Zone Journal* 15:1-20.
- Wang, J., Y. Zhao, C. Li, L. Yu, D. Liu, and P. Gong. 2015. Mapping global land cover in 2001 and 2010 with spatial-temporal consistency at 250m resolution. *ISPRS Journal of Photogrammetry and Remote Sensing* 103:38-47.
- Wang, P., J. de Jager, A. Nauta, J. van Huissteden, M. C. Trofim, and J. Limpens. 2019. Exploring nearsurface ground ice distribution in patterned-ground tundra: correlations with topography, soil and vegetation. *Plant and Soil* 444:251-265.
- Wang, P., Q. Huang, Q. Tang, X. Chen, J. Yu, S. P. Pozdnyakov, and T. Wang. 2021. Increasing annual and extreme precipitation in permafrost-dominated Siberia during 1959–2018. *Journal of Hydrology* 603:126865.
- Wang, P., J. Limpens, L. Mommer, J. van Ruijven, A. L. Nauta, F. Berendse, G. Schaeppman-Strub, D. Blok, T. C. Maximov, and M. M. Heijmans. 2017. Above-and below-ground responses of four tundra plant functional types to deep soil heating and surface soil fertilization. *Journal of Ecology* 105:947-957.
- Wang, P., J. Limpens, A. Nauta, C. van Huissteden, S. Quirina van Rijssel, L. Mommer, H. de Kroon, T. C. Maximov, and M. M. Heijmans. 2018. Depth-based differentiation in nitrogen uptake between graminoids and shrubs in an Arctic tundra plant community. *Journal of Vegetation Science* 29:34-41.
- Wang, P., L. Mommer, J. van Ruijven, F. Berendse, T. C. Maximov, and M. M. Heijmans. 2016. Seasonal changes and vertical distribution of root standing biomass of graminoids and shrubs at a Siberian tundra site. *Plant and Soil* 407:55-65.
- Wehmann, A., and D. Liu. 2015. A spatial-temporal contextual Markovian kernel method for multitemporal land cover mapping. *ISPRS Journal of Photogrammetry and Remote Sensing* 107:77-89.
- Wein, R. W. 1973. *Eriophorum Vaginatum* L. *Journal of Ecology* 61:601-615.
- Westergaard-Nielsen, A., M. Lund, B. U. Hansen, and M. P. Tamstorf. 2013. Camera derived vegetation greenness index as proxy for gross primary production in a low Arctic wetland area. *ISPRS Journal of Photogrammetry and Remote Sensing* 86:89-99.
- Wheeler, J. A., G. Hoch, A. J. Cortés, J. Sedlacek, S. Wipf, and C. Rixen. 2014. Increased spring freezing vulnerability for alpine shrubs under early snowmelt. *Oecologia* 175:219-229.
- Wigley, T. M. L., K. R. Briffa, and P. D. Jones. 1984. On the Average Value of Correlated Time Series, with Applications in Dendroclimatology and Hydrometeorology. *Journal of Applied Meteorology and Climatology* 23:201-213.
- Wilcox, E. J., D. Keim, T. de Jong, B. Walker, O. Sonnentag, A. E. Sniderhan, P. Mann, and P. Marsh. 2019. Tundra shrub expansion may amplify permafrost thaw by advancing snowmelt timing. *Arctic Science* 5:202-217.

Chapter 9

- Wilmking, M., R. D'arrigo, G. Jacoby, and G. Juday. 2005. Increased temperature sensitivity and divergent growth trends in circumpolar boreal forests. *Geophysical Research Letters* 32:L15715.
- Wilmking, M., M. Hallinger, R. Van Bogaert, T. Kyncl, F. Babst, W. Hahne, G. Juday, M. De Luis, K. Novak, and C. Völm. 2012. Continuously missing outer rings in woody plants at their distributional margins. *Dendrochronologia* 30:213-222.
- Wipf, S., and C. Rixen. 2010. A review of snow manipulation experiments in Arctic and alpine tundra ecosystems. *Polar Research* 29:95-109.
- Wipf, S., C. Rixen, and C. P. H. Mulder. 2006. Advanced snowmelt causes shift towards positive neighbour interactions in a subarctic tundra community. *Global Change Biology* 12:1496-1506.
- Wold, H. 1980. Model Construction and Evaluation When Theoretical Knowledge Is Scarce: Theory and Application of Partial Least Squares. Pages 47-74 in J. A. N. Kmenta and J. B. Ramsey, editors. *Evaluation of Econometric Models*. Academic Press.
- Wolfe, B. B., E. M. Light, M. L. Macrae, R. I. Hall, K. Eichel, S. Jasechko, J. White, L. Fishback, and T. W. Edwards. 2011. Divergent hydrological responses to 20th century climate change in shallow tundra ponds, western Hudson Bay Lowlands. *Geophysical Research Letters* 38:L23402.
- Woo, M.-k., and K. L. Young. 2006. High Arctic wetlands: their occurrence, hydrological characteristics and sustainability. *Journal of Hydrology* 320:432-450.

Y

- Yang, D., D. Kane, Z. Zhang, D. Legates, and B. Goodison. 2005. Bias corrections of long-term (1973–2004) daily precipitation data over the northern regions. *Geophysical Research Letters* 32:L19501.
- Yershov, E. D. 2004. *General geocryology*. Cambridge university press.
- Yoo, A. B., M. A. Jette, and M. Grondona. 2003. Slurm: Simple linux utility for resource management. Pages 44-60 in *Workshop on Job Scheduling Strategies for Parallel Processing*.

Z

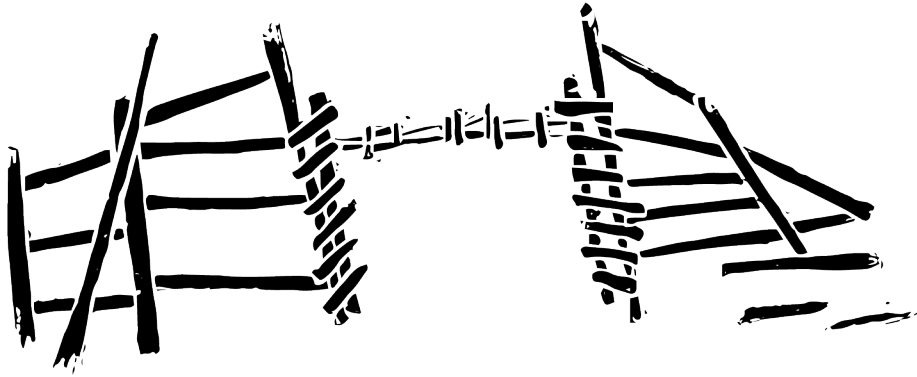
- Zhang, T. 2005. Influence of the seasonal snow cover on the ground thermal regime: An overview. *Reviews of Geophysics* 43:RG4002.
- Zhirkov, A., P. Permyakov, Z. Wen, and A. Kirillin. 2021. Influence of Rainfall Changes on the Temperature Regime of Permafrost in Central Yakutia. *Land* 10:1230.
- Zhu, X., T. Wu, R. Li, C. Xie, G. Hu, Y. Qin, W. Wang, J. Hao, S. Yang, and J. Ni. 2017. Impacts of summer extreme precipitation events on the hydrothermal dynamics of the active layer in the Tanggula permafrost region on the Qinghai-Tibetan plateau. *Journal of Geophysical Research: Atmospheres* 122:11,549-511,567.
- Zoltai, S. 1993. Cyclic development of permafrost in the peatlands of northwestern Alberta, Canada. *Arctic and Alpine Research* 25:240-246.
- Zoltai, S., and C. Tarnocai. 1975. Perennially frozen peatlands in the western Arctic and Subarctic of Canada. *Canadian Journal of Earth Sciences* 12:28-43.
- Zona, D., W. Oechel, K. Peterson, R. Clements, K. PAW U, and S. Ustin. 2010. Characterization of the carbon fluxes of a vegetated drained lake basin chronosequence on the Alaskan Arctic Coastal Plain. *Global Change Biology* 16:1870-1882.
- Zwieback, S., Q. Y. Chang, P. Marsh, and A. Berg. 2019. Shrub tundra ecohydrology: rainfall interception is a major component of the water balance. *Environmental Research Letters* 14:055005.

References



10.

Summaries & End Matter



Summary

The fate of the Arctic affects us all

Arctic regions are considered the canaries in the coalmine of global change. They are now warming three times faster than the planet on average and show evidence of rapid and drastic changes in structure and functioning. Changes include loss of sea ice and snow cover, increasing disturbances of ecosystems due to wildfire and permafrost thaw and changes to hydrology (e.g. precipitation, river discharge). Beside global impacts on sea levels and local impacts on livelihoods, these disturbances can cause additional emissions of greenhouse gasses to the atmosphere, reinforcing global warming. Hence, the development of Arctic ecosystems may also have a critical role in determining our future climate. Widespread degradation of permafrost (frozen ground of which only the top layer thaws in summer) strongly contributes to this reinforcement of warming. As permafrost soils thaw, previously frozen carbon in the soil can decompose and be emitted as greenhouse gas. This warming effect may, however, be partly offset by atmospheric cooling through enhanced uptake of atmospheric carbon in plant biomass. Field observations and satellite images of the Earth's surface show that warmer conditions in the Arctic promote plant growth and especially that of shrubs. This thesis focuses on the balance between these two opposing drivers of global change.

Teasing out the web of interactions between permafrost, vegetation and climate

It is challenging to predict exactly to what extent the response of permafrost and vegetation growth in Arctic regions will affect our future climate. Although permafrost degradation and vegetation change are evident throughout the Arctic, they are also influenced by local conditions and interactions. Permafrost provides the foundation for Arctic tundra vegetation and determines essential properties of the ground surface. Especially ice-rich permafrost tends to lose structure once it thaws and melting ice leaves depressions in the terrain, which affects wetness and other growth conditions for vegetation. At the same time, vegetation regulates the amount of heat and water from the atmosphere that can penetrate into frozen Arctic soils. With this thesis, I addressed three specific knowledge gaps on the interface of climate, vegetation and permafrost to help understand the influence of rapid changes in Arctic ecosystems on our global climate. I focused particularly on the lowland tundra ecosystem in North-eastern Siberia near the remote settlement of Chokurdakh. The Siberian lowland tundra region occupies a large proportion of the world's tundra area. Due to its continental climate with warm summers and soils rich in ice and carbon, this region has high potential for permafrost degradation and greenhouse gas emissions. Yet, this region has been studied very little in Western scientific literature. I assessed (1) to what extent this Siberian tundra ecosystem shows expansion of shrub vegetation and “greening” of the land surface or “browning” due to shrub drowning in thaw ponds, (2) how this permafrost ecosystem reacts to predicted increases in extreme rainfall events in summer and, lastly, (3) how areas affected by local degradation of ice-rich permafrost evolve over time and whether the permafrost and shrub vegetation can recover again. I answered these three questions using a combination of field experiments, field monitoring, modeling, remote sensing and tree ring analyses of shrubs.

Vegetation succession can aid recovery of degraded permafrost and thus partly offset greenhouse gas emissions, but degradation outpaces recovery on the landscape scale

Small tundra ponds (< 100 m²) are a common feature in our study area. These ponds form when ice rich permafrost thaws and ground ice melts, and emit substantial amounts of the greenhouse gas methane (a greenhouse gas approximately thirty times stronger than carbon dioxide over a timespan of 100 years). In Chapter 2 I assess how these ponds form and evolve over time, to help estimate their contribution to permafrost degradation and greenhouse gas emissions. From high resolution satellite images taken during different summers since 2010 I identified older and younger ponds. I found that thaw ponds form and expand laterally at approximately half a meter per year over the course of about two decades. Afterwards, these ponds fill in with aquatic vegetation over a similar time frame and at a similar rate.

Sedges (grass-like plants commonly found in wetlands) are early colonizers, while *Sphagnum* (peat moss) becomes dominant in a later stage. This “succession trajectory” is associated with reduction of thaw depths and elevation of the ground surface, which strongly suggests that permafrost can recover, aided by the insulating properties of colonizing vegetation. Chapter 3 studies changes in vegetation cover over a larger area over the period 2010 to 2019, using a similar time series of high resolution satellite images. I classified satellite images into different groups of plant species using field reference data. Changes in the cover of these species groups show that ponds generally form in shrub-dominated vegetation, and that the succession trajectory is evident on a landscape scale. Supporting data on methane emissions (fig 7.3) show that open water and sedge dominated vegetation are substantial methane sources. *Sphagnum* vegetation emits less methane, but still more than shrub vegetation. Occasionally, *Sphagnum* carpets that form in thaw ponds and other water features show sparse cover of shrubs, indicating that recovery towards previously dominant shrub vegetation may occur. My results align with findings from other Arctic and boreal ecosystems, suggesting that vegetation succession is a key factor in the recovery of permafrost and the greenhouse gas balance across permafrost regions. However, data from Chapter 2 & 3 suggest that recovery to shrub-dominated conditions requires longer timescales than the rapid processes of permafrost degradation and initial succession. This results in a net increase in the area of tundra ponds and aquatic vegetation at the expense of shrub vegetation. This provides a contrast to the general greening trend and shrub expansion reported in a warming Arctic.

Extreme rainfall can enhance permafrost thaw for multiple years in a row, especially under warm summer conditions

Future changes in the Arctic climate may well result in changes in the rates of permafrost degradation and vegetation succession and thereby also affect thaw pond dynamics. Beside temperature, heavy rainfall events in summer are expected to increase in the Arctic. To assess how this might affect permafrost degradation and tundra vegetation, I describe the results of an irrigation experiment in Chapter 4. We supplied 100mm of extra rain to 10 representative sites dominated by shrub vegetation, and left another 10 untouched. 100mm is approximately 120% of the average total summer rainfall at the site. We found that under this extreme rainfall addition, thaw depths were increased by up to 6cm (or 35% relative to the untouched sites). This increase was observed again in the two years after, likely because added water accumulated above the permafrost, froze over in autumn and caused wetter soil conditions again in the following year. Supporting model-analysis indicates that permafrost thaw is increased by rainfall especially in warm years. In a warming climate, extreme summer rainfall events will occur more frequently in the Arctic. Combined with a general warming trend such extremely wet summers may cause unexpectedly rapid permafrost degradation.

Vegetation, however, seems to benefit from summers with high rainfall in this relatively dry tundra ecosystem

I used climate data series, tree ring records (Chapter 5) and satellite images (Chapter 6) to assess relationships between summer rainfall and vegetation growth. A time series of satellite-derived vegetation greenness (NDVI) shows a decreasing trend (“browning”) for the study area and larger surrounding region over the past two decades, suggesting that vegetation productivity has decreased. NDVI is positively associated with summer rainfall and negatively with winter snow height, making recent drought, extreme snowfall and flooding of the Indigirka river likely causes for browning. The relations between NDVI and precipitation additionally varied with elevation and among landforms. Such differences in topography cause contrasts in water availability as a result of water flow, differences in snow accumulation and flooding. Floodplain areas for instance showed extremely low NDVI after high snowfall and resulting flooding in the early summer season. High elevation sites showed a stronger positive response to rainfall and soil moisture availability. Lastly, the small scale succession dynamics described in Chapters 2 - 3 explained some additional variability in NDVI changes, as different plant functional groups are associated with higher or lower NDVI. However, on the short timescales

considered here (one to two decades), vegetation shifts are too small and locally variable to be evident from coarser resolution (e.g. Landsat satellites, with an average spatial resolution of 30m) satellite products such as NDVI. This implies that improved remote monitoring of permafrost degradation processes and shrub dynamics in heterogeneous, ice-rich tundra ecosystems would require satellite data with spatial resolution that better reflect the scale of permafrost and vegetation processes relevant for such ecosystems (spatial resolution of several meters or less). At coarser resolution, the large-scale effects of climate predominate, and local hotspots of greenhouse gas emission related to small-scale permafrost degradation and shrub decline are easily overlooked.

As precipitation variability becomes more extreme, future growth of Arctic shrubs may become increasingly unpredictable and locally variable

In Chapter 5 I used a 45-year record of tree rings of the Arctic shrub *Betula nana* to quantify the association between shrub growth and weather conditions over a (micro)topographical gradient. While summer temperature remained the main climatic driver of shrub growth across the study area, my results confirm that shrubs respond to temperatures more strongly under higher rainfall. Relations between rainfall and shrub growth also changed over time and developed differently among higher and lower elevation sites. This variability in response should be studied in more detail to identify how variability in the terrain and climate relate to physiological processes in the plant. However, my results indicate that the response of *Betula nana* to rain and snow is regulated by the distribution of water through the landscape over elevation gradients. This redistribution is also affected by thawing of ice-rich permafrost, which alters elevation on very local scales. Growth of *Betula nana* seems to become more rain-dependent under prolonged periods of drought. Finally, the response of shrub growth to moisture availability was often non-linear; while higher rainfall resulted in better growth, completely water-saturated soils led to mortality of shrubs. This fits findings from other ecosystems that indicate reduced benefits of warming under increasing drought and moisture limitation. With increasing variability in Arctic precipitation, plant growth in Arctic ecosystems may as a result start showing stronger local ups and downs over time.

Future research: better quantification of degradation - recovery dynamics across various permafrost ecosystems in a more extreme future climate

My research has highlighted that the response of permafrost and vegetation to climate extremes are highly interconnected, often non-linear and dependent on the landscape context. This sets a challenge for prediction of the future greenhouse gas balance of tundra ecosystems based on current data. In ice-rich, poorly drained ecosystems such as the Siberian lowland tundra, degradation of permafrost results in local disturbance and waterlogging of the terrain, to which permafrost and vegetation respond in a highly synchronized manner. Through successional processes, recovery of this degraded permafrost seems possible at least to some extent. Longer-term monitoring is necessary to assess the timescales required for potential full recovery of permafrost and vegetation and the net greenhouse gas contribution of such disturbances over their lifespan. Such monitoring should be extended to various permafrost ecosystems and various types and magnitudes of permafrost disturbance. An important challenge will be to assess how degradation and recovery rates may change in a warming climate. This way, improved estimates of the potential recovery of degraded permafrost features and lifetime trajectories of greenhouse gas emissions could add to improved estimates of carbon emissions from a warming Arctic.

Our results on the potential impact of future increases in heavy rainfall events suggest that the impact of climate variability and extremes varies over landscape gradients, and may be felt for multiple years. Even small elevation differences of at most several meters cause differences in the occurrence of permafrost degradation and waterlogging and in the response of vegetation to weather patterns. Apart from that, the presence of ice-rich permafrost means that the terrain itself is subject to very local scale changes in water flow and growth conditions for vegetation. Ideally, future studies should seek

to understand the degree to which this small-scale landscape variability (e.g. in topography, wetness and permafrost ice content) mediates the response of permafrost degradation and plant growth to climatic change across a range of Arctic regions. These studies should - beside monitoring - ideally rely on experimental simulation of future climatic change, as the response to unprecedented climate extremes may not follow logically from responses to current climatic variability and may last multiple years. Identified patterns of permafrost- and vegetation response to climatic changes across small-scale gradients in, for instance, topography and permafrost ice content may then be used to improve panarctic prediction of permafrost carbon emissions and plant growth.

Samenvatting

De opwarming van Arctische gebieden treft ons allemaal

Arctische ecosystemen zijn de “kanaries in de kolenmijn” van een opwarmende aarde. Op dit moment warmen de poolregio’s drie keer zo snel als de gemiddelde temperatuurstijging op aarde, waardoor zich snelle en drastische veranderingen in ecosystemen voltrekken. Voorbeelden van zulke veranderingen zijn verlies van bedekking door sneeuw en zee-ijs, toename in het aantal bos- en toendra branden, dooi van permafrost en veranderingen in neerslagpatronen en de watercyclus. Deze verstoringen van het ecosysteem hebben grote gevolgen voor wereldwijde zeespiegelstijging en lokale leefomstandigheden en kunnen door toename van lokale broeikasgasemissies de opwarming van de aarde versterken. Arctische gebieden spelen daarmee dus een belangrijke rol in ons toekomstige klimaat. Wijdverspreide degradatie van permafrost (permanent bevroren grond waarvan alleen de bovenste laag dooit in de zomer) draagt sterk bij aan versterkte opwarming van de aarde. Wanneer een permafrostbodem ontdooit kan de koolstof die daar in opgeslagen zit worden afgebroken door micro-organismen en uitgestoten als broeikasgas. Dit opwarmende effect zou echter deels kunnen worden gecompenseerd door een toename in plantengroei in een warmer Arctisch milieu. Veldobservaties en satellietbeelden laten een algemene “vergroening” (toename van levende biomassa) zien in Arctische regio’s onder warmere omstandigheden. Vooral struikvegetatie groeit beter in warmere zomers. Dit proefschrift richt zich op de balans tussen twee contrasterende drijvende krachten in ons klimaat: de dooi van de permafrost enerzijds, en de vermeende extra groei van struikvegetatie anderzijds.

Patronen ontdekken in complexe interacties tussen permafrost, vegetatie en klimaat

Het inschatten van de netto uitstoot en opname van koolstof door permafrost degradatie en plantengroei in Arctische ecosystemen is een lastige taak. Beide processen vinden weliswaar plaats op grote schaal, maar worden behalve door de temperatuur ook beïnvloed door hele lokale omgevingsfactoren en interacties. Permafrost biedt de fundering en bepaalt essentiële condities voor groei van toendravegetatie. Vooral dooi van ijsrijke permafrost leidt tot verlies van bodemstructuur en vormt verzakkingen in het terrein, wat de vochtigheid van het terrein en andere groeicondities verder beïnvloedt. Tegelijkertijd beïnvloedt vegetatie de mate waarin warmte en neerslag uit de atmosfeer kunnen doordringen in de ondergrond. Met dit proefschrift draag ik bij aan het beantwoorden van drie belangrijke kennisvragen op het snijvlak van permafrost en vegetatie in een veranderend klimaat, om een beter beeld te vormen van de rol van Arctische toendra-ecosystemen in het mondiale klimaat. De focus van dit onderzoek ligt op de laaglandtoendra van Noord-Oost Siberië, op basis van onderzoek bij de afgelegen nederzetting Chokurdakh. Deze Siberische laaglandtoendras beslaan een aanzienlijk deel van het mondiale toendraoppervlak, hebben een sterk continentaal klimaat met warme zomers, en bodems rijk aan ijs en koolstof. Daarmee hebben ze een hoog potentieel voor permafrost-degradatie en broeikasgasemissies. Toch zijn deze gebieden weinig beschreven in de Westerse wetenschappelijke literatuur. Ik heb onderzocht (1) in welke mate ons studiegebied een uitbreiding van struikvegetatie en “vergroening” laat zien, of juist een afname van struikvegetatie door vorming van dooimeertjes, (2) hoe dit permafrostecosysteem reageert op voorspelde toekomstige extreme zomerbuien en (3) hoe permafrost en struikvegetatie zich ontwikkelen na lokale degradatie van ijsrijke permafrost en of deze weer kunnen herstellen van een dergelijke verstoring. Ik heb deze vragen beantwoord met combinaties van veldexperimenten, monitoring van permafrost en vegetatie op de toendra, modelanalyse, satellietbeelden en analyse van jaarringen van Arctische dwergstruiken.

Vegetatiesuccessie lijkt het herstel van gedegradeerde permafrost te bevorderen en methaanemissies te verminderen, maar degradatie domineert het landschap

Ons studiegebied bevat een groot aantal kleine (< 100m²) dooimeertjes. Deze lokale depressies ontstaan wanneer ijsrijke permafrost ontdooit (thermokarst) en ijs in de bodem smelt en zijn sterke lokale bronnen van het broeikasgas methaan. Over een tijdschaal van 100 jaar is methaan een 30 keer sterker broeikasgas

dan koolstofdioxide. In Hoofdstuk 2 heb ik onderzocht hoe deze dooimeertjes zich ontwikkelen over de tijd, om beter te kunnen beoordelen wat hun netto bijdrage aan permafrostdegradatie en methaanuitstoot is. Met behulp van een serie hoge resolutie satellietbeelden, die sinds 2010 regelmatig zijn opgenomen in het zomerseizoen, heb ik recent en minder recent gevormde dooimeertjes geïdentificeerd. Jonge dooimeertjes bleken zich met ongeveer een halve meter per jaar lateraal uit te breiden, over een typische tijdsperiode van rond de twintig jaar. Oudere meertjes kunnen met vergelijkbare snelheid weer krimpen doordat ze dichtgroeien met vegetatie. Vooral veenpluis en zegges (grasachtige soorten die veel voorkomen in natte gebieden) vestigen zich vaak al binnen tien jaar in dooimeertjes, waarna later *Sphagnum* (veenmos) de dominante vegetatie wordt. Dit “successietraject” is geassocieerd met een afname van de dooidiepte van de permafrost en ophoging van het ingezakte terrein, wat suggereert dat vegetatiesuccessie het herstel van permafrost lokaal bevordert. In Hoofdstuk 3 heb ik met behulp van dezelfde satellietbeelden veranderingen in de vegetatiesamenstelling van een groter studiegebied onderzocht over de periode 2010 tot 2019. Deze beelden heb ik met behulp van referentiedata uit het veld geïdentificeerd in verschillende functionele vegetatiegroepen. Veranderingen in het areaal van deze groepen laten zien dat dooimeertjes zich vooral vormen in door struiken gedomineerde vegetatie, en dat het successietraject van open water naar veenpluis, zegges en later veenmos ook op grotere schaal optreedt. Een inventarisatie van methaanemissie over dit successietraject (fig. 7.3) laat zien dat open water, veenpluis en zegges geassocieerd zijn met hogere methaanuitstoot, veenmos met lagere uitstoot en dat struikvegetatie over het algemeen netto geen methaan uitstoot. Veenmostapipen bieden daarnaast een groeibodem voor jonge struikjes, wat suggereert dat de dooimeertjes op termijn wellicht kunnen herstellen naar methaan-neutrale struikvegetatie met mogelijk verder herstel van permafrost. Deze resultaten zijn in overeenstemming met bevindingen uit andere Arctische en boreale regio’s, wat suggereert dat vegetatiesuccessie een cruciaal proces is in het herstel van de permafrost en de broeikasgasbalans na lokale verstoring. Echter, resultaten uit Hoofdstuk 2 & 3 laten zien dat mogelijk herstel van struikgedomineerde vegetatie veel langzamer gaat dan de abrupte verstoringen veroorzaakt door permafrostdooi. Dit resulteert in een netto toename van dooimeertjes en aquatische plantensoorten en afname van struikvegetatie. Dit biedt een kanttekening bij de algemene trend van uitbreiding van vergroening en uitbreiding van struikvegetatie in een opwarmende Arctisch gebied.

Extreme regenval in de zomer kan de dooi van permafrost meerdere jaren versterken, zeker in warme zomers

Een extremer Arctisch klimaat heeft mogelijk ook gevolgen voor de degradatie- en herstel dynamiek van permafrost en toendravegetatie, en daarmee op de ontwikkeling van dooimeertjes en struikvegetatie. Naast temperatuur is de verwachting dat ook extreme zomerbuien gaan toenemen in de Arctische regio’s. Om te beoordelen of dit effect heeft op permafrost en toendravegetatie heb ik een irrigatie-experiment uitgevoerd waarin een natte zomer werd gesimuleerd (Hoofdstuk 4). We creëerden ongeveer 100mm extra regen door middel van irrigatie op 10 representatieve, door struikvegetatie gedomineerde locaties, en lieten 10 vergelijkbare locaties ongemoeid. 100mm regen is een toevoeging van 120% ten opzichte van een gemiddelde zomer. Deze toename van regenval leidde tot een toename van 6cm in de dooidiepte van de permafrost (of 35% ten opzichte van de controle sites). Ook in de twee jaren na de irrigatie bleef de permafrost in de geïrrigeerde sites sneller dooien, waarschijnlijk als gevolg van accumulatie van water in de bodem, die na bevriezen in de herfst opnieuw beschikbaar kwam in de volgende zomer. Modelanalyse op basis van de gegevens uit dit veldexperiment laat zien dat het negatieve effect van regenval op permafrostdooi waarschijnlijk sterker is in warme zomers. Door opwarming van het klimaat zullen extreme zomerbuien vaker gaan voorkomen in Arctische gebieden. In combinatie met een trend van stijgende temperaturen zouden zulke extreem natte zomers onverwachts snelle degradatie van permafrost kunnen veroorzaken.

In dit relatief droge toendra gebied lijkt hoge regenval echter ook plantengroei te bevorderen

Om het effect van zomerbuien op toendravegetatie te beoordelen heb ik klimaatgegevens, jaarringanalyse van dwergstruikjes (Hoofdstuk 5) satellietbeelden (Hoofdstuk 6) gebruikt. Een op satellietdata gebaseerde index van “groenheid” van het terrein (NDVI) laat in de afgelopen 20 jaar een afname zien (“verbruining”) voor het studiegebied en de omliggende regio, wat impliceert dat de productiviteit van toendravegetatie hier is afgenomen. NDVI was positief geassocieerd met zomerregen, maar negatief met de sneeuwhoogte in de winter. Daarmee zijn droge condities en extreme sneeuwval en resulterende overstromingen in recente jaren logische verklaringen voor deze verbruining. De mate van associatie tussen NDVI, regen en sneeuw varieerde over een hoogtegradiënt in het landschap, wat verklaard kan worden door herverdeling van water en sneeuw in het landschap op basis van topografische verschillen. NDVI in de overstromingsvlakten van rivieren toonde bijvoorbeeld een sterke negatieve associatie met sneeuwhoogte als gevolg van overstroming na het smelten van grote hoeveelheden sneeuw. Hogere landschapsposities toonden juist een sterkere positieve associatie van NDVI met zomerregen en bodemvocht, mogelijk vanwege snelle afwatering. Als laatste verklaarde de vegetatiesuccessiedynamiek beschreven in Hoofdstuk 2 en 3 een hele kleine mate van variatie in de verbruining van het studiegebied, omdat verschillende vegetatiegroepen ook geassocieerd zijn met verschillende typische NDVI waarden. Echter, over de korte tijdsspanne van deze datareeksen (10 tot 20 jaar) hadden lokale successies nauwelijks invloed op de gebruikte NDVI beelden omdat ze daarvoor te kleinschalig en ruimtelijk variabel zijn. Om de dynamiek van vegetatie en permafrost in het heterogene en ijsrijke Noord-Oost Siberische toendraecosysteem op representatieve wijze in kaart te brengen door middel van satellietmonitoring, zou een ruimtelijke resolutie van enkele meters of minder vereist zijn. Met een grovere ruimtelijk resolutie domineren de grootschalige effecten van klimaat waarschijnlijk het NDVI signaal en worden lokale hotspots van broeikasgasuitstoot door kleinschalige permafrostdegradatie en vegetatieveranderingen gemakkelijk over het hoofd wordt gezien.

Onder extremere neerslagpatronen wordt de toekomstige groei van struikvegetatie minder voorspelbaar en lokaal variabel

In Hoofdstuk 5 heb ik gemiddelde jaarringcurves voor 45 jaar aan groei van de Arctische dwergstruik *Betula nana* gebruikt om associaties tussen struikgroei en klimaat te beoordelen over een hoogtegradiënt in het landschap. Zomertemperatuur bleef de voornaamste klimaatinvloed op de groei van *Betula nana*, maar de invloed van temperatuur is over het algemeen sterker in zomers met meer regen. De associatie van groei met regenval was niet even sterk over de tijd en tussen hogere en lagere landschapsposities. Betere kwantificatie van fysiologische processen binnen de individuele plant zouden helpen om deze non-uniforme respons te verklaren. Echter, mijn resultaten suggereren dat de respons van *Betula nana* op regen en sneeuw sterk wordt bepaald door de herverdeling van water over het landschap door kleinschalige hoogteverschillen. Deze herverdeling wordt ook bepaald door dooi van ijsrijke permafrost, wat leidt tot lokale verzakkingen in het landschap. Daarnaast werd de associatie van groei van *Betula nana* met regen sterker gedurende de afgelopen twee decennia met over het algemeen droge condities. Tenslotte was de respons van *Betula nana* op vochtbeschikbaarheid niet lineair. Hoewel meer regen over het algemeen resulteerde in betere groei, leidt een té natte bodem juist tot sterfte van struikjes. Deze bevindingen passen binnen recente trends van struikgroei over het Arctische gebied, waaruit blijkt dat de positieve respons van Arctische dwergstruiken op zomertemperatuur afneemt naarmate groei sterker wordt gelimiteerd door droogte. Met toenemende variabiliteit in jaarlijkse hoeveelheden regen in de toekomst zouden Arctische gebieden dus sterkere lokale ups en downs in struikgroei kunnen gaan laten zien.

Toekomstig onderzoek: degradatie- en herstel dynamiek in verschillende Arctische ecosystemen onder een extremer klimaat

Mijn onderzoek heeft aangetoond dat de respons van vegetatie en permafrost op een veranderend klimaat vaak sterk door elkaar worden beïnvloed. Daarnaast zijn relaties tussen klimaat, struikgroei en permafrostdegradatie vaak non-lineair en afhankelijk van de landschapscontext. Dat maakt het lastig om toekomstige veranderingen te voorspellen op basis van huidige data. In ijsrijke, relatief vlakke ecosystemen zoals de Noord-Oost Siberische laaglandtoendra veroorzaakt het dooien van permafrost lokale verstoringen in het terrein, die leiden tot een lappendeken van verschillende stadia van degradatie en herstel van permafrost en vegetatie binnen het landschap. Door vegetatiesuccessie kan permafrost weer in bepaalde mate herstellen van degradatie. Veldmonitoring over lange termijn is cruciaal om de tijdschaal van het degradatieproces en met name het langzamere herstelproces beter af te bakenen, en zo een inschatting te kunnen maken van de netto bijdrage van deze landschapsverstoring aan lokale koolstofemissies. Dergelijke monitoring is nodig over een brede representatie van Arctische ecosystemen en vormen en maten van landschapsverstoring als gevolg van permafrostdegradatie. Een belangrijke openstaande vraag is de mate waarin degradatie- en hersteldynamiek den tijdschalen waarop deze zich afspelen zullen veranderen in een steeds extremer Arctisch klimaat.

Onze resultaten suggereren dat de effecten van klimaatverandering en klimaatextremen op de dynamiek van permafrostdegradatie meerdere jaren kunnen duren. Daarnaast veroorzaakten hoogtegradiënten van enkele meters al verschillen in de vatbaarheid van het landschap voor permafrostdegradatie en vorming van dooimeertjes. Ook de mate waarin plantengroei reageerde op klimaatextremen en weerpatronen varieerde met hoogteverschillen in het landschap. Als laatste is door de aanwezigheid van ijsrijke permafrost het terrein zelf onderhevig aan kleinschalige veranderingen in hoogte en natheid, wat weer invloed heeft op de verdeling van plantensoorten en hun respons op het toekomstige klimaat. De mate waarin deze kleinschalige variatie in het landschap (bijvoorbeeld in hoogte, natheid en ijsgehalte van de permafrost) de respons van permafrost en plantengroei op een veranderend klimaat bemiddelt zou moeten worden bestudeerd in een groter aantal contrasterende Arctische regio's. Idealiter zou naast monitoring ook gebruik worden gemaakt van geïnformeerde experimentele simulatie van toekomstige klimaatverandering, omdat de impact van een extreme weerscondities niet altijd logisch volgt uit huidige relaties tussen klimaat, permafrost en plantengroei, en zo'n impact meerdere jaren kan duren. Zo zou kunnen worden beoordeeld of er opschaalbare relaties bestaan tussen de respons van permafrost en vegetatie op een veranderend klimaat aan de ene kant, en kleinschalige landschapsvariabiliteit in bijvoorbeeld hoogte, natheid en ijsgehalte van de permafrost aan de andere kant. Deze informatie zou kunnen worden ingezet voor verbeterde projecties van koolstofemissies als gevolg van permafrostdegradatie en vegetatieveranderingen.

Affiliations of Co-authors

Dr Juul Limpens

Plant Ecology & Nature Conservation Group
Wageningen University & Research
Wageningen, the Netherlands

Dr Ko van Huissteden

Earth & Climate Cluster, Department of Earth Sciences
Vrije Universiteit
Amsterdam, The Netherlands

Prof. Dr David Kleijn

Plant Ecology & Nature Conservation Group
Wageningen University & Research
Wageningen, the Netherlands

Prof. Dr Trofim C. Maximov

Institute for Biological Problems of the Cryolithozone
Siberian Branch Russian Academy of Sciences
North-Eastern Federal University
Yakutsk, Russia

Ronny Rotbarth

Plant Ecology & Nature Conservation Group
Wageningen University & Research
Wageningen, the Netherlands

Dr Ute Sass-Klaassen

Forest Ecology and Management Group
Wageningen University & Research
Wageningen, The Netherlands

Dr Monique M. P. D. Heijmans

Plant Ecology & Nature Conservation Group
Wageningen University & Research
Wageningen, the Netherlands

Dr Sylvain Lobry

Geoinformation Science and Remote Sensing Group
Wageningen University & Research
Wageningen, The Netherlands

Alexandra Hamm

Department of Physical Geography
Bolin Centre for Climate Research
Stockholm University
Stockholm, Sweden

Sergey V. Karsanaev

Institute for Biological Problems of the Cryolithozone
Siberian Branch Russian Academy of Sciences
Yakutsk, Russia

Dr Andrew Frampton

Department of Physical Geography
Bolin Centre for Climate Research
Stockholm University
Stockholm, Sweden

Susan Ras

Plant Ecology & Nature Conservation Group
Wageningen University & Research
Wageningen, the Netherlands

Dr Daan Blok

Netherlands Polar Programm
Dutch Research Council
the Hague, the Netherlands

Finn Groten

Plant Ecology & Nature Conservation Group
Wageningen University & Research
Wageningen, the Netherlands

Dr Harm Bartholomeus

Geoinformation Science and Remote Sensing Group
Wageningen University & Research
Wageningen, The Netherlands

About the Author

Curriculum Vitae

Rúna Íris Magnússon was born in Amsterdam on January 17th, 1992. As a child she wanted to work in a zoo or be a stuntwoman. She studied Future Planet Studies (an interdisciplinary bachelor programme focused on future sustainability) with a specialisation in Earth Science, at the University of Amsterdam (UvA), and took additional courses in Forest and Nature Conservation (Wageningen University) and Computer Programming (UvA). Combining her interests in these various fields, her BSc thesis assessed canopy structures of different types of forest stands in the Netherlands using high resolution LiDAR point cloud data. She continued her exploration of landscapes and their dynamics in the master Earth Science at the UvA, with a specialization in Geo-Ecological Dynamics. Both her literature thesis on the role of dead wood in the forest carbon cycle and her MSc thesis on the influence of glacial sediments on the chemical quality of surface water in the Peruvian Andes were published in peer-reviewed journals. After a brief appointment as laboratory technician at the Institute for Biodiversity and Ecosystem Dynamics of the UvA, she applied for a PhD that matched her interests in landscape dynamics, the future of our planet and remote, cold environments. Zoo? Not exactly... Stunts? Sometimes... Best decision ever? Absolutely! Particular highlights were lying down between the dwarf shrubs on the Siberian tundra and discovering a whole new micro-universe, a plenary talk at the Dutch Polar Symposium, teaching field ecology on the sunny island of Terschelling and nerve-wracking snow scooter trips on Svalbard. In her free time, she enjoys longsword fencing, yoga, concerts, being outdoors, playing bass, photography and printmaking.



Publications

This thesis:

Magnússon, R.Í., Limpens, J., van Huissteden, J., Kleijn, D., Maximov, T.C., Rotbarth, R., Sass-Klaassen, U. & Heijmans, M.M.P.D. (2020). Rapid vegetation succession and coupled permafrost dynamics in Arctic thaw ponds in the Siberian lowland tundra. *Journal of Geophysical Research: Biogeosciences*, 125(7), e2019JG005618.

Magnússon , R.Í., Limpens, J., Kleijn, D., van Huissteden, J., Maximov, T. C., Lobry, S. & Heijmans, M.M.P.D. (2021). Shrub decline and expansion of wetland vegetation revealed by very high resolution land cover change detection in the Siberian lowland tundra. *Science of the Total Environment*, 782, 146877.

Magnússon, R.Í., Hamm, A., Karsanaev, Limpens, J. Kleijn, D., Frampton, A., Maximov, T.C. & Heijmans, M.M.P.D. (2022). Extremely wet summer events enhance permafrost thaw for multiple years in Siberian tundra. *Nature Communications*, 13, 1556.

Other:

Magnússon, R.Í., Tietema, A., Cornelissen, J.H.C., Hefting, M.M., & Kalbitz, K. (2016). Tamm Review: Sequestration of carbon from coarse woody debris in forest soils. *Forest Ecology and Management*, 377, 1-15.

Magnússon, R.Í., Cammeraat, E., Lücke, A., Jansen, B., Zimmer, A., & Recharte, J. (2020). Influence of glacial sediments on the chemical quality of surface water in the Ulta valley, Cordillera Blanca, Peru. *Journal of Hydrology*, 125027.

Van Huissteden, J., Teshebaeva, K., Cheung, Y., Magnússon, R.Í., Noorbergen, H., Karsanaev, S. V., Maximov, T.C., & Dolman, A. J. (2021). Geomorphology and InSAR-Tracked Surface Displacements in an Ice-Rich Yedoma Landscape. *Frontiers in Earth Science*, 9.

Heijmans, M. M. P. D., Magnússon, R. Í., Lara, M. J., Frost, G. V., Myers-Smith, I. H., van Huissteden, J., Jorgenson, M. T., Fedorov, A. N., Epstein, H. E., Lawrence, D. M., & Limpens, J. (2022). Tundra vegetation change and impacts on permafrost. *Nature Reviews Earth & Environment*, 3(1), 68-84.

Vuorinen, K., Austrheim, G., Tremblay, J. P., Myers-Smith, I. H., Hortman, H. I., Frank, P., ... Magnússon, R. Í., ... & Speed, J. D. M. (2022). Growth rings show limited evidence for ungulates' potential to suppress shrubs across the Arctic. *Environmental Research Letters*, 17, 034013.

Acknowledgements

Monique. First of all I am so grateful that you put your confidence in me to take on this amazing and challenging PhD. People who, like you, travel to the strangest edges of the world to resolve environmental puzzles will always have my deepest respect and I am happy that I got to carry on this tradition. From the very first day in my PhD you have trusted me to make my own decisions and bring challenging fieldwork to a good end, and enabled me to become a leader in my own project. This has helped me grow enormously and I appreciate it a lot. I hope we will sit together around the kitchen table in Kytalyk some day again in the future.

Juul. Going on fieldwork with you is always an amazing and colourful adventure and I am so glad we got to work in beautiful places like Siberia, Svalbard and Terschelling. There was always room for humour, chocolate moments and creative side quests. I've always found it very inspiring to see how you approach landscapes with a scientific as well as an intuitive approach. And perhaps one day I will figure out the secret to your seemingly endless source of energy. I hope to work with you on many more adventures, because it is truly a joy.

David. As you have said yourself on occasion, you are a fairly direct communicator. But you also combine this with empathy, clarity and a little bit of humour here and there, which I think makes you a wonderful promotor. It has often helped me to see the bigger perspective in moments where I felt a little lost or overwhelmed, or moments where I was about to go down another statistics rabbit hole. It also means a lot to me that you and the institute supported my efforts to set up new field research on Svalbard. I look forward to working in your group the coming years and sharing the magic of the Arctic with our students.

A big thank you to all the students that I had the pleasure to work with. Ron, Katrien, Daniël, Qays, Els, Finn, Susan, Bart, Mirthe, Christian and many others. Through your work, questions, perspectives and characters I got to discover so many additional things that enriched my PhD experience. Tundra research really does attract the finest people!

Ute and Ellen, I loved working with you in the DendroLab. You've set up something truly exciting there and you lead WUR's dendrochronological research with such amazing passion. I would love to continue working on Arctic shrubs with you and help spread the passion.

Большое Вам спасибо to prof. Trofim Maximov and the staff of IBPC Yakutsk: Trofim, Roman, Sergey, Egor and Alya. You've enabled essential collaboration between Russian and international scientists from all over the world, and enabled them to visit some of the most remote corners of the world. This is not only important to us researchers, but it is crucial for our understanding of the future condition of our planet. In recent times, we're also finding out how important it is to protect these scientific collaborations in a polarized world. I sincerely hope we get to meet and work together again in the future. Of the IBPC staff, I want to give extra special thanks to Sergey. You were there on my first fieldwork campaign to help me, severely jet-lagged, sleep deprived and confused young researcher that I was, to get started at the field station. Your help and hard work have been incredibly valuable, whether it was in a scientific sense or just heating up the banya after a long day of work. Thank you also for sharing my absurd sense of humour. I hope one day we get to implement our ridiculous plans for upgrading the station with a pool, a karaoke bar and a laser shield to keep out the mosquitoes.

Thanks to all the other people that I have met, worked with and learned from at the station in Kytalyk. Special thanks to Gabriela and Ko, whose experience and advice was so supportive for this tundra newbie. The staff of the nature inspection of the Allaikhovsky region also deserve a special mention.

Summaries & End Matter

You were the caretakers of a very unique hidden treasure of nature that has inspired me deeply. Thanks for running day-to-day maintenance of the station so that we were free to play with our little devices and count plants. Thank you for understanding my piss-poor Russian when I really needed to pee in the middle of a 2.5hrs speedboat trip. And thanks for cooking. During my accidental 1-day career as station chef I got to experience the challenge of feeding a team of hungry researchers using only a wood stove, canned and dried food items and river water. I haven't had any complaints, luckily, but you have my respect.

A big, warm and fuzzy thanks to the staff of the PEN group. PEN is a group where everyone is appreciated and equal, and where all staff mingle naturally. I've always felt very supported and accepted, despite my skepticism about beloved lunch conversation topics like birdwatching or sport. After 4.5 years in PEN I now sometimes catch myself stepping off my bicycle to look at a bird. I even bought binoculars. What the #&\$% have you done to me?! Special thanks to my office mates Eline, Sasja and Jan-Markus for tolerating my sudden outbursts of rage against bureaucracy and my big clumsy bag of fencing gear that was often in your way. Thanks to all the other PEN PhDs, postdocs and staff for the shared moments, lessons learned about bees, grasses and birds, exciting PEN trips and spontaneous orchid hunts in the Lumen garden. And finally, my heartfelt thanks for all the administrative and logistic support and slap geouwehoer at the coffee machine.

Two colleagues from outside WUR deserve special mention. Fabian, I am really happy that I met “the only other PhD in the Netherlands working with *Betula nana*”. Of course with such an occupation you have to be a pretty amazing person and you are. Thank you for your fresh perspectives, deep thoughts and phonecalls during tough moments. Stay haunted, shred 'til your dead and keep seizing the means of production! Alex, it has been great to work together with you, even if it was mostly online until recently. I think we managed to create a $1 + 1 = 3$ situation when we started working on rainfall impacts on permafrost together. Or maybe even $1 + 1 = 10$, as new projects continue to grow from our collaboration. I'm grateful that both of you were my peers and sources of support for the past years.

Other dear friends; Evi, Youval, Peter, Bart, Judith, Berend, Martin, the whole gang from de Keu. All the other constellations I got to be part of; the UvA Earth Science people, the Zwaard & Steen army, my Roadburn team, the UNIS CCB group 2022, and so many more. Thank you all for sharing the good stuff and listening when there was bad stuff. As I crawl out of my PhD cave and the world crawls out of a pandemic, I hope to go on many nice adventures with you soon!!

Mom. Even though you raised me in a city, you didn't raise a city kid. Almost every weekend of my youth we spent poking sticks in decomposing logs, sculpting castles out of mud, gathering insects and leaves with interesting colours, eating blueberries in the wood and learning which flowers were okay for picking and which were rare. You made sure that never, ever, under no circumstances my supplies of paper, paint, crayons and such ran out. You showed me that everything starts with observation. So I basically did exactly all that. I went outdoors, I poked sticks in the ground, I observed and I illustrated. I look forward to many more beautiful days outside with packed lunch, lots of observing and guerilla plant reintroduction experiments in the garden.

Vera. You are one of the strongest characters that I know and I have seen you achieve so much in the past years. Who cares what other people think that adult life and a career should like like. I have complete faith in your journey and so should you. Before you know you will be an amazing literary translator and write a fantastic book about the history of Polar exploration. You're also a living example of kindness and the best vegan baker I know. Thank you for always making me feel at peace when I visited you, mom and Findus.

Chapter 10

Pabbi. When I was with you in Iceland as a kid, you often had to stop me from wanting to walk further and climb higher to see whether a beautiful glacier might be hiding behind that next rocky ridge. Maybe it shouldn't be a surprise then that I chose to study the Arctic. I found a photo of six year old me sitting down in a patch of *Betula nana* close to Kónsstaðir with a frowning look on my face and thought, ah, that's probably where it began. It's always so nice to come to Iceland and escape to the family cabin with you, drive the car through rivers, wander and explore or just drive around town all day on a series of strange errands.

My favourite bearded, bodybuilding guitar wizard Thijmen, who I have the honour of calling my boyfriend. You always understood my victories and struggles so well, and I think I understand yours too. Perhaps the music business and science are quite similar; not landing a record deal = having your manuscript rejected, being approached for shit gigs = weird emails from predatory journals, bandmates = co-authors, no production budget for next album = lack of funding for field campaign, I could continue... And through all this I feel we could always just unconditionally love each other as the overly ambitious obstacle-fighting weirdos that we are. I hate to think about what my whole PhD experience would have been like without you.

Overview of Artwork

Cover (Front)	<i>Betula nana</i> ; greening or drowning? Linocut.
Cover (Back)	<i>Eriophorum angustifolium</i> . Linocut.
p. 7	The Chokurdakh Scientific Tundra Station. Linocut and watercolour.
p. 25	Leaves of <i>Betula nana</i> . Dotwork with fineliner. Don't the veins of the leaves look just like a polygonal tundra landscape..?
p. 47	Stylized Markov Chain diagram representing vegetation succession observed at the Kytalyk site (as described in Chapters 2 & 3). Linocut and ink.
p. 69	Raindrops. Linocut.
p. 85	Microthin cross-section of a <i>Betula nana</i> stem. Acetone transfer print and dotwork with fineliner.
p. 108-109	Tundra landscape in the Kytalyk reserve. Acetone transfer print.
p. 130-131 (bottom)	A lake in the Kytalyk reserve. Acetone transfer print.
p. 131 (top)	<i>Eriophorum vaginatum</i> . Linocut.
p. 146-147 (bottom)	Tundra landscape in the Kytalyk reserve. Acetone transfer print.
p. 147 (top)	<i>Sphagnum</i> moss. Linocut.
p. 174-175 (bottom)	Lakes in the Kytalyk reserve. Acetone transfer print.
p. 175 (top)	<i>Flavocetraria cucullata</i> . Linocut.
p. 200-201 (bottom)	Tundra landscape in the Kytalyk reserve. Acetone transfer print.
p. 201 (top)	An abandoned reindeer coral in the Kytalyk reserve. Linocut.

All artwork by Rína Magnússon



*Netherlands Research School for the
Socio-Economic and Natural Sciences of the Environment*

D I P L O M A

for specialised PhD training

The Netherlands research school for the
Socio-Economic and Natural Sciences of the Environment
(SENSE) declares that

Rúna Íris Magnússon

born on 17 January 1992 in Amsterdam, the Netherlands

has successfully fulfilled all requirements of the
educational PhD programme of SENSE.

Wageningen, 28-09-2022

Chair of the SENSE board

Prof. dr. Martin Wassen

The SENSE Director

Prof. Philipp Pattberg

The SENSE Research School has been accredited by the Royal Netherlands Academy of Arts and Sciences (KNAW)



K O N I N K L I J K E N E D E R L A N D S E
A K A D E M I E V A N W E T E N S C H A P P E N



The SENSE Research School declares that **Rúna Íris Magnússon** has successfully fulfilled all requirements of the educational PhD programme of SENSE with a work load of 59.4 EC, including the following activities:

SENSE PhD Courses

- o Environmental research in context (2018)
- o Research in context activity: 'Co-organizing the Dutch Annual Polar Symposium and setting up an educational outreach activity for elementary school children with APECS Netherlands' (2018)

Selection of other PhD and Advanced MSc Courses

- o Machine Learning for Spatial Data, PE&RC and WIMEK (2018)
- o Mixed Effects Models, PE&RC and WIMEK (2018)
- o Structural Equation Models, PE&RC (2020)
- o Communication with Media & General Public, Wageningen Graduate Schools (2020)
- o Climate Change Biology, UNIS (2022)
- o Transformative Research for Sustainable Change, WIMEK / SRC (2021)

Selection of Outreach and Communication activities

- o Eight media interviews (live radio and for news articles), the Netherlands (2020-2022)
- o Guest lecture for KNNV Nijmegen, the Netherlands (2021)
- o Field Blog for the EU Interact TA programme, Russia (2019)

Selection of Management and Didactic Skills Training

- o Board member Dutch National Committee of the Association of Polar Early Career Scientists (2018-2022)
- o Member of the WIMEK Education Committee (2018-2020)
- o Organization of session 'Permafrost in Transition', EGU 2020
- o Supervising seven MSc students and two BSc students with thesis (2019-2021)
- o Teaching in the courses 'Ecology I', 'Trends in forest and nature conservation', 'Models for ecological systems' and 'Management Planning and tools' (2020-2021)

Selection of Oral Presentations

- o *Coupled Vegetation Succession and Thermokarst Development in a lowland tundra site.* Netherlands Earth Scientific Congress, 14-15 March 2019, Utrecht, The Netherlands
- o *Extreme Summer Precipitation Increases Permafrost Thawing Depth over Multiple Years.* The Xth International Symposium on C/H₂O/Energy balance and climate over the boreal and Arctic regions with special emphasis on Eastern Eurasia, 4-7 October 2019, Sapporo, Japan

SENSE coordinator PhD education

Dr. ir. Peter Vermeulen

Funding

The research described in this thesis was financially supported by the Netherlands Polar Programme of the Dutch Research Council (NWO) under grant agreement number ALWPP.2016.008

The research described in this thesis would not have been possible without travel grants for fieldwork for dr. Monique Heijmans, dr. Juul Limpens, Ronny Rotbarth and Daniël Kollen provided by the European Union's Horizon 2020 project INTERACT under grant agreement 730938.

Financial support from Wageningen University for printing this thesis is gratefully acknowledged.

Printed by Digiforce | www.proefschriftmaken.nl